NASA SP-311

AIRCRAFT ENGINE NOISE REDUCTION

A conference held at
LEWIS RESEARCH CENTER
CLEVELAND, OHIO
MAY 16–17, 1972

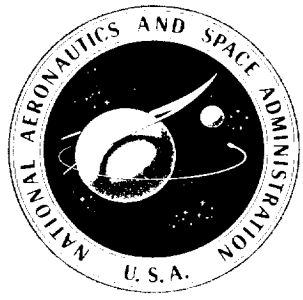

NATIONAL AERONAUTICS AND SPACE ADMINISTRATION

NASA SP-311

AIRCRAFT ENGINE NOISE REDUCTION

The proceedings of a conference held May 16–17, 1972,
at the NASA Lewis Research Center, Cleveland, Ohio

Prepared at Lewis Research Center

Scientific and Technical Information Office 1972
NATIONAL AERONAUTICS AND SPACE ADMINISTRATION
Washington, D.C.

For sale by the National Technical Information Service
Springfield, Virginia 22151 Price $6.00

FOREWORD

The Lewis Research Center is the National Aeronautics and Space Administration's principal field installation for research and development of advanced aerospace-propulsion and power-generating systems. More specifically, a substantial part of the Center's activities is devoted to progress in the technology of aircraft propulsion. Work includes such diverse areas as components, controls and other aspects of installation, V/STOL and low-cost engine designs, and - in particular - noise reduction.

The results of our work are published as NASA reports and as articles in the technical journals. In addition, an occasional technical conference assists us in communicating more directly with others in the engineering fraternity. Accordingly, this conference - in which we are joined by NASA Headquarters, NASA Langley and Flight Research Centers, General Electric Company, Boeing Aircraft Company, and Pratt & Whitney Aircraft Division - is held to present to you the results of recent and current work.

Bruce T. Lundin
Director

CONTENTS

I. INTRODUCTION

Newell D. Sanders

This conference is a progress report on some of the principal NASA programs for the reduction of aircraft engine noise. A major emphasis of the conference is focused on the Quiet Engine project.

The first portion of the conference is devoted to noise technology: fan noise and performance, fan noise suppression, and jet noise. This technology applies to a broad spectrum of airplanes including new subsonic airplanes, the older subsonic airplanes in service today, STOL airplanes of the future, and future supersonic transports.

The second portion of the conference reports on the Quiet Engine program and demonstrates the noise reductions achieved. The Quiet Engine is an experimental engine incorporating many low-noise features. It was assembled for NASA by the General Electric Company. The engine experiment has three purposes: (1) to demonstrate the effectiveness of noise reduction techniques in a full-sized engine, a proof of concept approach; (2) to measure the performance penalties accompanying the use of noise-reduction techniques and to find methods of reducing these penalties; (3) to uncover obstacles to still further reductions of engine noise. Also as part of the Quiet Engine program, the Boeing Company, under NASA contract, designed and built experimental sound-absorbing mufflers to surround the engine and reduce the noise even more.

Following the Quiet Engine portion of the conference, possible applications of low-noise technology to future airplanes and to the airplanes of today are discussed. Finally, a brief progress report on research for quiet STOL airplanes is given.

Historically, the British pioneered in research for the reduction of jet engine noise in the early 1950's. Later, the aircraft and engine industry in the United States together with the NACA (predecessor of NASA) engaged in an intensive program with the same objective. These programs resulted in the multitubed nozzles as shown in figure I-1. This photograph shows one of the nozzles that was tested in the Lewis wind tunnel. Nozzles

like this were used on many airliners. More complicated nozzles (fig. I-2) in combination with ejector shrouds were also used. The moderate noise suppression from these nozzles did not stem the rising tide of public objection to aircraft noise. With the advent of Sputnik and the Space Age, research on noise declined. The Lewis Research Center dropped noise research entirely.

The phenomenal growth of air traffic in the early 1960's intensified the noise problem. Recognizing the seriousness of the situation, President Johnson in 1966 directed appropriate Government agencies to plan programs for noise abatement. At that time, NASA began formulating new programs directed at the noise problem.

The first major new program was the Acoustically Treated Nacelle Program managed by the Langley Research Center. In that program, Douglas and Boeing built experimental mufflers to silence the fans on DC-8 and 707 airplanes. The program demonstrated significant noise reductions for airplanes approaching an airport, but noise reductions on takeoff were small. Results of that program were fully reported in a conference in 1969 at the NASA Langley Research Center.

Some of the sources of engine noise are shown in figure I-3. The noise which is emitted from the inlet and from the fan discharge duct is generated principally by the fan and, to a lesser extent, by the compressor. The noise emitted by the primary jet at the rear of the engine is generated by the turbulent mixing of the jet with the surrounding air. This turbulent-mixing noise is responsible for the tremendous roar associated with jet airplanes. Less important but not insignificant are turbine noises which are emitted at the rear of the engine.

A tape-slide demonstration of these noises has been prepared to show the basic elements that make up the noise from fan and jet engines. It is obvious from this demonstration that an aircraft noise reduction of only 3 decibels is barely noticeable. A 10-decibel improvement is clearly noticeable. A 20-decibel reduction is a large improvement, and the public would applaud the aviation community for such a reduction. Even a 30-decibel reduction may be sought in special cases as, for example, the STOL airplane.

Goals for airplane noise research were stated approximately 1 year ago

in the joint DOT-NASA Civil Aviation Research and Development Study report (the CARD study). The recommended goal was a 10-decibel noise reduction per decade. Figure I-4 shows some noise levels related to this goal. The noise level for the DC-8 at the FAR-36 (Federal Air Regulation 36) takeoff point is approximately 116 PNdB (perceived noise decibels). The certification limit for new airplanes of the same gross weight is 104 EPNdB (effective PNdB). The new wide-bodied jet airplanes equal or better this value. Thus, the first 10-decibel reduction has been achieved. As you will hear later in this conference, the Quiet Engine is close to 90 EPNdB, which is below FAR-36 minus 10 decibels. The next level, FAR-36 minus 20 decibels, is below demonstrated noise levels for airplanes of this class at takeoff.

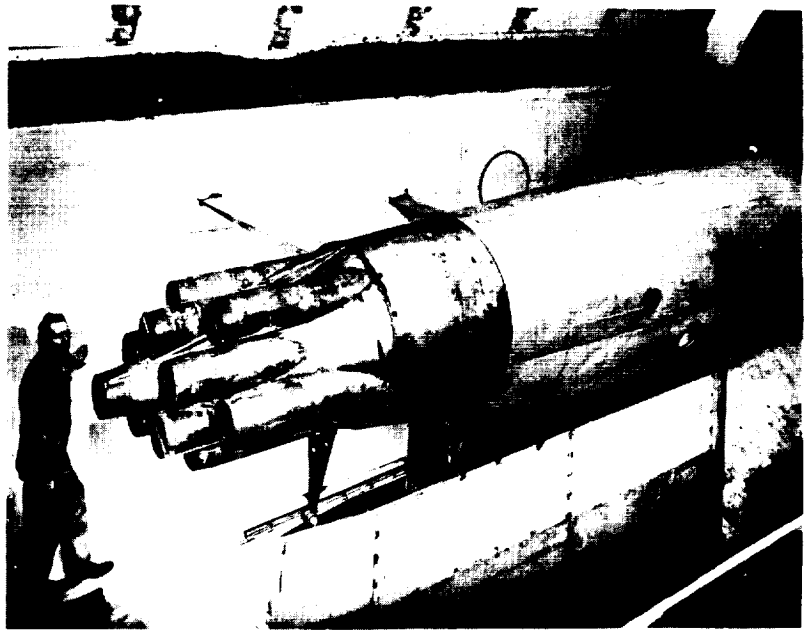

Figure I-1

8-LOBE SUPPRESSOR AND EJECTOR ON AIRCRAFT

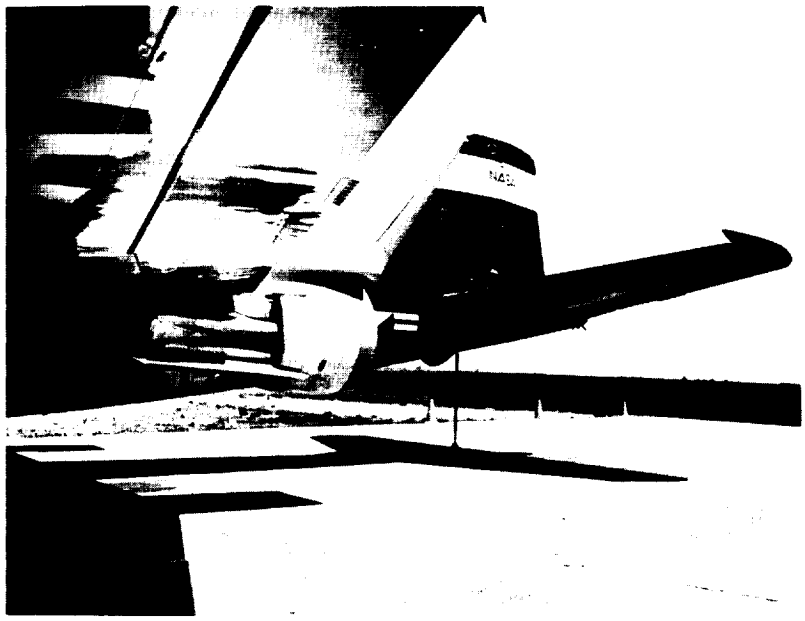

Figure I-2

TURBOFAN–ENGINE NOISE EMISSION

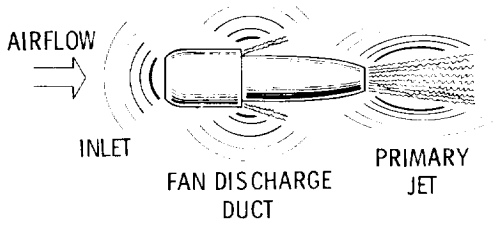

Figure I-3

CS-63207

NOISE REDUCTION GOALS

TAKEOFF; FOUR ENGINES

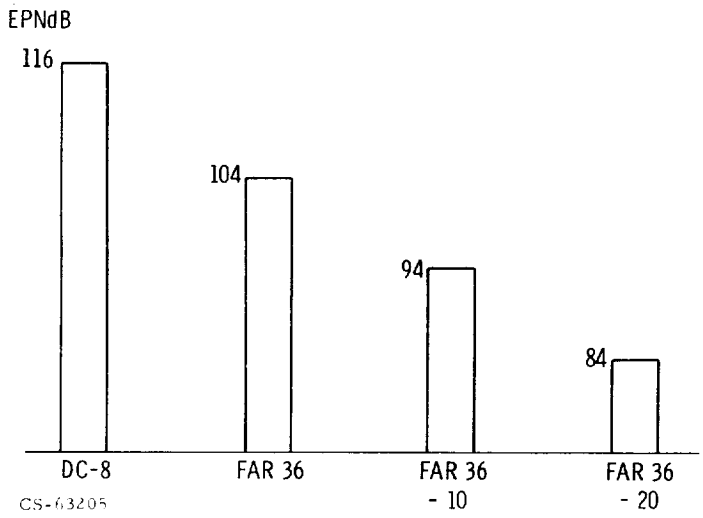

CS-63205

Figure I-4

II. FAN NOISE AND PERFORMANCE

James J. Kramer, Melvin J. Hartmann, Bruce R. Leonard,
Jack F. Klapproth*, and Thomas G. Sofrin**

For an engine like the Quiet Engine, which is designed for long-range subsonic cruise at conventional takeoff and landing, the fan noise controls the engine noise. This discussion includes the generation process of fan noise and what can be done to control it by design changes in the fan.

In discussing the interplay between the aerodynamics and acoustics of fans, a family of fans are referred to which were tested as part of the Quiet Engine Program. The design characteristics of these fans are tabulated in table II-1. For simplicity in terminology, the fans are lettered A to G.

TABLE II-1. - FAN DESIGN

CHARACTERISTICS

Fan	Tip speed, ft/sec	Pressure ratio	Number of stages
A	1160	1.5	1
B	1160	1.5	
C	1550	1.6	
D	1107	1.4	
E	1107	1.5	
F	1090	1.6	
G	1000	1.45	2

Fans A, B, and C were furnished by the General Electric Company as part of the Quiet Engine Program. They were designed and built by General

*General Electric Company.

**Pratt & Whitney Aircraft Company.

Electric, tested for aerodynamic performance, and then tested for acoustic performance at Lewis Research Center. Fans A and B are single-stage, low-speed fans designed for a pressure ratio of 1.5. Fan C is a single-stage, relatively high-speed fan designed for a slightly higher pressure ratio. Fans D and E were designed, built, and tested at Lewis. They were designed as single-stage fans with pressure ratios of 1.4 and 1.5. Fan F was designed and built by Pratt & Whitney. That fan is now installed in the Lewis fan noise test facility, and data are being generated with it at this time. Fan G is the only two-stage fan that was tested as part of the Quiet Engine Program. It was designed for low speed at 1000 feet per second and a pressure ratio of 1.45. It is a modified version of the inner panel of the fan used on the TF-39 engine.

The first and most important thing a fan must do in order for it to be an integral part of a useful, viable engine system is to produce pressure rise. The fan requirements necessary for a quiet engine are discussed in the next section.

FAN REQUIREMENTS

The Quiet Engine Program is directed toward providing a fan engine for long-range CTOL aircraft. These engines must be economical, quiet, and clean and must provide good operating margins and growth potential. The aerodynamic requirements of the fans are established by the engine cycle conditions. It is necessary to determine the optimum fan flow, pressure ratio, and operating characteristics for the particular thrust, cycle pressure ratio, and temperature of interest. Some of the considerations and areas of interest can be shown by the following trend curves.

In figure II-1 the trends of specific fuel consumption and fan pressure ratio with bypass ratio are indicated at two levels of cruise Mach number. For a cruise Mach number of 0.80, the specific fuel consumption continues to decrease with increasing bypass ratio. For this cruise Mach number, fan pressure ratios of 1.4 to 1.6 are considered (crosshatched area). This is the range of fan pressure ratios studied in the Quiet Engine Program. To indicate the effect of cruise Mach number on these parameters similar curves are shown for a cruise Mach number of 0.95. At this higher cruise

Mach number, fan pressure ratios of 1.9 to 2.1 would be of interest (cross-hatched area).

It would appear that even higher bypass ratios may be desirable for lower fuel consumption; however, the engines become very large. This is illustrated in figure II-2; the lower-pressure-ratio fan engines are associated with lower fan jet velocities and, as shown in the sketch, are very large. At the higher pressure ratios, substantially higher fan jet velocities occur but the fans are relatively smaller and of lower bypass ratios. The higher-pressure-ratio fans may require two or more stages. The low-pressure-ratio fans can be single stage, but they require a large nacelle and installation drag becomes a large fraction of the thrust. The large fans must be driven by the relatively small-diameter turbine. This may require increasing the number of turbine stages to achieve the necessary power from the small core flow. This increased engine weight must be considered as a penalty for the very-high-bypass-ratio engine system.

The fan must also be suitable to meet all the required engine operating conditions. This can be illustrated by referring to a fan performance map such as shown in figure II-3. Flow curves are given for three rotational speeds. The highest speed line shown includes the cruise operating point. Above the cruise operating point, the fan encounters stall and becomes unstable. Similar pressure ratio flow curves are indicated at the speed required for takeoff and at a lower speed. The fan must produce the desired pressure and flow along the cruise and takeoff operating conditions The positions of the takeoff and cruise operating points depend on the cruise Mach number and the engine cycle. These operating conditions should be in the region of high fan efficiency. They must also be sufficiently removed from the stall line to allow engine acceleration and transient operation. The margin between the operating lines and the fan stall must be sufficiently large to take into account inlet flow distortions, as shown schematically in figure II-4. Crosswinds and inlet flow distortion cause the stall line to be moved toward the operating lines. There are a number of additional reasons for building or selecting the fan design to have a high stall margin. These include the eventual performance degradation which results from blade foreign object damage and provision of a thrust growth potential. Engine thrust growth requires an increase in either fan flow or pressure ratio. Fans de-

signed with large stall margins can be more easily uprated with minor hardware changes.

Having established the overall requirements, the fan must be selected to meet the requirements of pressure ratio, efficiency, and operating margins. Fan pressure ratio is established primarily by the rotational speed and aerodynamic loading, as shown in figure II-5. On this calculated graph the rotational speed is given as rotor blade tip speed. Increasing the blade tip speed at a given aerodynamic loading results in a substantial increase in fan pressure ratio. However, at the high speeds the rotor blades must operate at a higher relative Mach number, as indicated on the lower scale. The blade shape must be selected to be suitable for the flow Mach number level used. Increasing the aerodynamic loading, or the lift of the airfoil sections, results in increasing the fan pressure ratio at any given speed. However, at some level of loading, the airfoils reach a "stalling condition" and the machinery cannot operate. The limit region is shown by the "shading" and is not a clearly defined limit as it depends on details of blade design. The levels of aerodynamic loading parameter indicated are for the rotor blade tip region, which usually becomes the critical airfoil section. Rotor tip elements usually initiate fan stall. Thus, to achieve a high stall margin, it is necessary that the rotor blade tip aerodynamic loading be held somewhat below the limit region shown.

Fan pressure ratios from 1.4 to 1.6 are considered for the Quiet Engine Program. This would indicate that blade tip speeds of 1000 to 1600 feet per second should be considered. The higher speeds would be at lower aerodynamic loading and potentially should lead to a larger stall margin. The relative flow Mach number to the blading for the high-speed fan would approach 1.6. The fans designed for the Quiet Engine Program incorporated low-noise features, as shown in figure II-6. These fan performance points are shown on the background plot as solid symbols. Fans A and B were designed for about 1150-foot-per-second tip speed, and fan C was designed for 1550-foot-per-second tip speed. The open symbols represent a number of experimental fans designed primarily to investigate aerodynamic performance over a range of rotor tip speeds from 1000 to 1800 feet per second. These experimental fans are of relatively high aerodynamic loading, with pressure ratios ranging from 1.5 to about 2.2. Fan C and one experimental

fan are at substantially lower levels of aerodynamic loading.

Peak efficiency for these fans is indicated in the upper portion of figure II-6. The band of data indicates that efficiencies of 0.88 to 0.84 can be achieved over this range of designs. The blade shapes were selected for the blade Mach number and loading level of the design. Fans A, B, and C of the Quiet Engine Program are included in this efficiency band. Fan A has a slightly higher efficiency than fan B.

Measured stall margins for fans A and B are shown on the bar chart in figure II-7; the bars are located at about the design speed. The stall margin for fan C was not measured above 90-percent speed. The stall margin for fan B was estimated to be at least 22 percent, as shown. Stall margins for some of the experimental stages are shown. The aerodynamic loading of the experimental fans is generally somewhat higher than that of the Quiet Engine Program, and the stall margins are generally slightly less. Most of these fan stall margins were measured with initially built hardware, and some stall margin improvement may be available through small blading changes. For example, two low-speed highly loaded stages, as indicated by the solid bars, were improved to 16- and 17-percent stall margin by stator reset and redesign. No particular trend of stall margin is intended by this figure. In long-range CTOL aircraft, it is probably desirable to have a fan stall margin of the order of 20 percent. In the range between 1100- and 1600-foot-per-second blade tip speed, where most of the fans have been investigated, a 20-percent stall margin appears feasible.

The fan requirements are determined by the engine cycle and application. The fan rotational speed and aerodynamic loading level must be selected to meet the performance and operational requirements of the engine and the application. Fans A, B, and C of the Quiet Engine Program, which incorporate low-noise features, are shown to have efficiency and stall margin trends comparable to a rather wide range of experimental fans.

FAN NOISE FUNDAMENTALS

Fan noise is a prominent component of aircraft powerplant noise. As shown in figure II-8, it is generated internally by the fan components, prop-

agates through the inlet and fan discharge ducts, and propagates to the ground from both inlet and discharge duct planes. Additional important engine noise sources are indicated and include jet mixing noise from fan and primary streams, turbine noise, and core compressor noise radiated forward through the fan.

During an airplane flyover, noises from these engine sources peak at different instants and contribute to a complicated history of the flyover noise event. Since all engine noise sources are also present during static ground noise tests, special means must be used to separate fan noise so that its characteristics can be studied. Some of the special test rigs used in fan noise programs will be described. Through their use, supplemented by analytical methods, a fairly clear picture of fan noise has emerged.

Fan noise radiates in a complicated directivity pattern from the inlet and discharge ducts. At each angular position in the far field the noise is conveniently described by means of its spectrum, or frequency distribution of acoustic energy. Figure II-9 gives two illustrative spectra of forward-radiated fan noise. In the top half of this figure, which is typical of subsonic-blade-tip-speed single-stage fan operation, a broad base of continuous sound, called broadband noise, exists over a wide frequency range. This noise is generated by random pressure fluctuations in the fan and sounds, generally, like jet mixing noise. Prominent features of the spectrum are the two sharp peaks or "spikes" at fan blade passage frequency and its harmonic. These discrete tones correspond to fan whine and are generated by periodic pressure fluctuations on the fan airfoil surfaces.

At supersonic fan blade tip speeds, noise of a different character appears. It is exhibited in figure II-9 as a closely spaced series of discrete frequency spikes separated by shaft rotation frequency and has a distinctive sound described variously as deep, rich, raspy, or buzz saw. Multiple-pure-tone (MPT) noise, combination-tone noise, and buzz saw are the usual descriptive terms. In brief, it results from the rotating pattern of shock waves from the fan blades when their tip speed is supersonic. Because of the nonlinear propagation behavior of shock waves, slight variations in the shock structure from blade to blade, caused initially by small manufacturing deviations, are amplified with distance from the fan into a pattern having marked irregularities. Since this irregular pattern turns with the rotor, its

frequency is that of shaft rotation speed and all multiples thereof rather than being restricted to blade passage frequencies, which would result from theoretically identical blading.

These noise spectral features may be incorporated in a subjective rating of the noise exposure by means of units such as PNdB in a manner described previously. But a better understanding of fan noise details for purposes of noise reduction can only be reached if the processes that produce the spectral components are looked into still more closely.

Three processes are involved in fan noise, as illustrated in figure II-10: generation, duct propagation, and radiation. Understanding of fan noise is facilitated by examining the features of these processes, and noise reduction concepts are made more feasible to develop by separating the overall problem into these areas.

Basically, fan noise is generated at the rotating blades and stationary vanes. Both broadband and discrete blade passage noise result from fluctuating blade surface pressures. These fluctuations arise from inflow velocity variations into a stage due to the turbulent flow structure and to airfoil wakes from upstream stages. At supersonic fan blade tip speeds, additional noise is produced by the blade shock wave patterns. These generation processes are more fully reviewed in this section. It will serve to point out here that the essential generation problems are aerodynamic rather than acoustic in nature. While the basic performance of a fan is understood, analytical description of the flow details is far from complete. And it is exactly these details, in particular the unsteady features, that are responsible for the infinitesimal fraction of the mechanical power converted to acoustic energy. Several theories for unsteady blade airloads exist, but to date they have not been critically compared in the context of fan geometry. More importantly, no comprehensive measurements of the airfoil fluctuating surface pressure distributions have yet been made in a fan to check theory. A rich and important field of aerodynamic research is here awaiting much needed analytical and experimental exploration.

As will presently be described, both discrete-frequency blade passage noise and multiple-pure-tone noise generated by the fan aerodynamic loads take the form of coherent, periodic acoustic wave patterns in the fan inlet and exit ducts. These patterns propagate in spiral paths to the free ends,

from which they then spread out and radiate to free space. The process of duct propagation has received a great deal of attention because it is subject to control both by sound-absorbing duct lining and by the selection of fan rotor and stator geometry. Duct lining is the subject of a subsequent paper and will not be reviewed here. Propagation in a hard-wall duct also has features which can be exploited for noise reduction. It is well known that a pipe, as exemplified by a "speaking tube," is a good conductor of sound. These tubes usually involve the equivalent of a pulsating piston or diaphragm at the transmitting end, which vibrates to and fro in a synchronous manner. In a fan or compressor the excitation or driving force on the duct is fundamentally different. The sound does not pulse back and forth in an umbrella fashion; instead there is a rotating pattern of circumferentially alternating high- and low-pressure ridges extending radially from the centerline to the walls. This spinning excitation pattern may be visualized by recognizing qualitatively that the pressure very near the face of the rotor alternates periodically as the blades spin by a fixed point. This spinning pattern, containing B (where B is the blade number) cycles of pressure variation around the circumference, provides the excitation and differs markedly from the pattern of a synchronous piston-like structure.

Whereas a synchronously pulsing pattern always propagates axially in a duct, a rotating pattern behaves in a more complex manner. It has been learned that the circumferential velocity component with which the pattern sweeps the wall must actually be supersonic to allow it to propagate in a spiral path along and out the duct. If the pattern spins more slowly, such that its circumferential wall speed is subsonic, it will not truly propagate. Instead, the magnitude of the pressure fluctuations will decay exponentially with axial distance from the source plane. Thus, the rotating pressure field of a subsonic-tip-speed fan rotor decays inside the inlet and the discharge duct and does not contribute to the noise heard from the powerplant. However, the interactions between rotor blades and stator vanes or other circumferential disturbances produce other patterns of noise at blade passage frequencies. It will be shown that in many cases interaction noise is produced in patterns that spin at high supersonic speeds. These patterns spiral easily through the fan ducting and are responsible for the noticeable discrete frequencies present in the spectra of fan noise. Controlling the blade-vane

number ratio makes possible bringing the circumferential wall speed of the interaction patterns below sonic speed, causing them to decay inside the powerplant, and thus effectively eliminating this source of noise. Unfortunately, there is sufficient flow distortion due to other influences affecting the fan so that there remains a considerable level of blade passage noise after blade-vane interaction has been eliminated. Many details of duct propagation remain to be explored. These include primarily the effects of varying duct contours and airflow gradients. Methods for analyzing the propagation of fan broadband noise are considerably more involved since the processes are basically random and statistical considerations must be employed.

The last stage in fan noise transmission involves radiation into the far field of the patterns spinning at the duct faces. Comparatively little control of this part of the noise chain is possible, but studies of radiation from the spinning duct patterns have led to understanding of the complex directivity patterns of fan noise. On the axis there is a minimum level, which rises and falls in a series of lobes in an arc around the engine. Angular locations of these peaks and valleys have been linked to the details of the pattern shapes at the engine inlet and exit ducts. Since the radiation directivity patterns govern both far-field peak levels and duration in an overflight, consideration of this phase of fan noise emission completes the tracing of the important fan noise processes from their source to the ground observer.

Special facilities have proved indispensable in fan noise studies. These include both rigs for running isolated components and special instrumentation systems for recording and processing test information. Figure II-11 presents representative examples of the variety of equipment used.

Figure II-11 shows the inlet to a 52-inch-diameter single-stage research fan in an outdoor noise test facility that allows far-field surveys to be made of inlet and discharge noise. Prominent in the foreground is a probe microphone system with axial, radial, and circumferential traversing capability. It is by means of such traverse equipment that the complicated spinning patterns of fan interaction and combination-tone noise are mapped.

Anechoic chambers play an important part in all major noise studies, and fan noise programs have been no exception. The NASA Langley Research Center anechoic chamber is also shown in figure II-11, with a small-scale compressor installed. In addition to allowing weather-free

operation the echo-free environment has proved instrumental in permitting accurate fan noise directivity patterns to be measured without contamination by wind or thermal and ground reflection influences.

Studies of multiple-pure-tone noise involve details of the blade shock wave patterns at supersonic speeds. To visualize these patterns, optical methods such as schlieren photography have been employed in supersonic cascade wind tunnels, as shown in figure II-11. Work is underway to conduct similar optical programs in special rotating fan rigs.

The effects of forward flight speed upon fan noise generation, propagation, and radiation are being explored (fig. II-11) in an acoustic wind tunnel in the open throat of which is installed a miniature working model of a fan-powered nacelle driven by a high-pressure air turbine. Again, anechoic construction of the working section enables free field effects to be reliably measured. In spite of its size the small (4.2 in. diam) fan can be driven at supersonic tip speeds, and multiple pure tones are clearly produced.

Discrete frequency noise at blade passage frequency and its harmonics was one of the most conspicuous noise characteristics of early turbofan powerplants. These fans employed inlet guide vanes, and it was found that the cutting of the vane wakes by the rotor blades was a major noise source. Current high-bypass-ratio engines dispense with inlet vanes, but the shedding of wakes from the rotor blades into the downsteam exit stators can be a similar source of blade passage interaction noise. How these interaction patterns are generated is described in the following paragraphs.

Figure II-12 portrays in a developed view a row of moving blades shedding wakes into the vanes of a downstream stator. As a wake passes by a stator vane the effective angle of attack and the velocity change, producing a fluctuating lift distributed over the vane surface. The life fluctuates with a base frequency equal to the blade passage rate and constitutes what is called a dipole source of sound. In the illustration, equal numbers of blades and vanes are employed, so that when one vane is about to receive a blade wake all the other vanes are at the identical point in their cycles. As shown, the stator vanes would thus produce an array of sources pulsating in unison. In practice, however, the numbers of blades and vanes are different, so that while one vane would be on the verge of intercepting a blade wake, another vane might just have recovered from a wake passage. Generally, there is a

sequential phasing of the wake interaction events around the stator assembly. This phasing forms a pattern that sweeps circumferentially around the vane array rather than in a synchronous, umbrella-like oscillation. The number of complete cycles in the pattern has been derived analytically in terms of blade and vane numbers, and the existence of such patterns has been frequently confirmed on a variety of rigs and engines.

However, the plausibility of this interaction pattern effect is most directly perceived by use of a simple optical analogue called the Moiré effect. If the stator assembly is represented by an array of radial spokes drawn on stationary background and the rotor blading is similarly represented on a clear sheet of plastic, when the two patterns are overlaid the interference of light and dark regions will produce a pattern of resultant intensity that suggests the blade-vane interaction effect. Consider now two such arrays, one containing 46 spokes and the other having 48. The resulting two cycles (48 - 46 = 2) of intensity variation are conspicuous when photographed. In a live demonstration, one wheel can be turned slowly about a common concentric axis. The interference pattern will be observed to spin comparatively rapidly. In fact, if the 46-spoke pattern is turned, the interference pattern will turn 23 times (46/(46 - 48) = 23) as fast as the simulated rotor in the opposite direction. The number of lobes or cycles of variation in the interference pattern and its rotational speed can be changed by changing the number of vanes in the stator. Parenthetically, this does not change the blade passage frequency, just the associated acoustic mode structure. Consider now the Moiré pattern for 46 rotor blades in conjunction with 60 simulated stator vanes. Although the pattern is not as well defined as the first case, 14 interference cycles can be counted from photographs. When the plastic 46-spoke rotor overlay is turned, the interference pattern will be observed to turn more slowly than in the first example. In fact, it turns at a multiple of rotor speed given by the expression $46/(46 - 60) \approx -3$, the minus sign indicating a backward motion.

It will be recalled that the requirement for a spinning acoustic pattern to propagate in a duct is that its tip speed at the wall be supersonic. These optical diagrams make it quite clear that supersonic interference patterns can be generated by interaction effects when the rotor itself is subsonic. They also show how the pattern can be slowed down by increasing the number

of stator vanes without changing rotor speed. When the interference pattern itself drops below sonic speed, it no longer propagates axially from the generating zone, and noise due to this interaction is essentially eliminated. These features of interaction noise have been exploited in the design of modern turbofan powerplants. While major interaction noise sources have been eliminated, discrete frequency noise still exists because of nonuniform inflow. However, there has been a marked improvement over early turbojet and turbofan discrete frequency noise.

Sources of fan broadband noise are suggested in figure II-13. As with discrete interaction noise, it is generated by airload fluctuations on the blade and vane surfaces. In this case, these fluctuations are random in time instead of periodic. Turbulence in the air entering the rotor, turbulence from the rotor impacting the stator, and boundary-layer turbulent fluctuations all constitute random broadband noise sources. Quantitative understanding of this category of noise is in a primitive stage compared with the discrete frequency case because of the inherently greater complexity associated with turbulence and random processes generally.

Simplified analyses of one part of the problem, the interaction of a rotor with incoming turbulence, have provided insight into the shape of the broadband spectrum. If the scale of the turbulence is small compared with the blade chord, the correlation between lift fluctuations occurring on neighboring blades will be low, and the resulting noise-against-frequency distribution will be relatively flat. On the other hand, if the axial scale of inflow turbulence is large, corresponding to long streaks, several blades will successively cut through each such nonuniformity, generating bursts of noise at the blade passage frequency. The resulting spectrum will contain peaks centered around blade passage frequencies, and the peaks will become progressively sharper as the axial scale of the turbulence is increased. Consequently, in controlling broadband noise, it is clearly important to ensure that the flow passages are designed to produce the smoothest possible flows.

As described previously, combination-tone or multiple-pure-tone noise is associated with the shock waves produced by rotors operating at supersonic tip speeds. It is helpful to consider two cases: first, an ideal rotor containing perfectly spaced identical blades; and second, an actual rotor

assembly incorporating small blade-to-blade deviations in shape and orientation.

Figure II-14 portrays the shock wave structure attached to the leading edges of an ideal supersonic rotor. On the right side of the figure is a representation of the pressure-time history that would be detected by a probe microphone in the inlet duct. A repetitive sawtooth pattern results as the succession of shock waves passes by. In a relatively short distance from the rotor the amplitude of these shocks will have attenuated, because of nonlinear effects, to what is called an acoustic disturbance or Mach wave. This symmetric wave pattern propagates in a spiral path out the inlet since its circumferential wall speed is supersonic. It would be detected in the far field as a sharp discrete noise at blade passage frequency and its harmonics.

In practice, what happens is significantly different. Actual rotors contain small blade-to-blade differences due to manufacturing deviations and service wear. These variations are usually small; this has been confirmed by moving an inlet duct probe microphone close to the blade leading-edge plane of test rotors. In this very close location the shock wave structure of a normal production rotor is extremely uniform. Correspondingly, the spectrum of the noise is clearly dominated by blade passage harmonics. However, there are small variations in shock strength from one blade to another. The importance of these normally negligible deviations is that shock wave behavior is nonlinear: the higher amplitude shocks propagate a little faster than their lower amplitude neighbors. Consequently, the uniform pattern existing very close to the rotor becomes warped as distance from the rotor is increased. Despite the small magnitude of the initial shock amplitudes, there is sufficient difference in their nonlinear behavior to produce a marked nonuniformity in amplitude and spacing of the pattern within a short axial distance of the rotor.

Figure II-15 portrays the phenomenon just described. To the right of the figure is shown the pressure-time trace recorded by a probe microphone placed a few chord lengths ahead of the rotor. Here, the pressure irregularities are conspicuous; in many cases there is no visible evidence of blade periodicity. The pattern repeats faithfully with every turn of the rotor, so that the spectrum of the resulting sound will have a fundamental frequency of

shaft rotation speed rather than blade passage frequency. Since the pattern contains many sharp irregularities, a large number of harmonics result, giving rise to the multiple-pure-tone (MPT) noise descriptive term.

It might be supposed that it would be relatively simple to eliminate MPT noise by sufficiently close control of rotor construction, but this has not proved possible. Even if a sufficiently perfect rotor could somehow be produced, unequal blade wear in service would soon cause enough irregularity to develop MPT noise. Nor would it be desirable to have such a perfect rotor; its sound would be the shrill whine of blade passage frequency, which is much more disturbing than the distributed tonal quality of MPT or combination-tone noise. Reduction of this noise component is being explored by designing blading to reduce the strength of all the blade shocks and by means of sound-absorbing wall liner constructions. Wall lining has proved quite successful in reducing multiple-pure-tone noise.

An understanding of these basic principles of fan noise has been used to improve significantly the characteristics of modern turbofan engines now entering service and planned for future use. Inlet guide vanes have been eliminated and the spacing between rotating and stationary blade rows has been increased. The well-known effect of increased rotor-stator spacing is shown in figure II-16. Figure II-17 compares the fan geometry of a modern high-bypass-ratio single-stage fan with an earlier generation low-bypass-ratio two-stage turbofan engine. The noise reduction features include removal of inlet guide vanes, reduced fan tip speed, elimination of the second-stage fan and its interstage stator, increased rotor-stator spacing, and selection of stator vane number to eliminate interaction effects.

This review of fan noise fundamentals has identified the sources of the several types of fan noise and has indicated measures that can be taken to reduce noise in powerplant design. However, the problem of predicting actual levels of noise produced by a specific design configuration contains many uncertain elements. Two general methods are available. Noise levels may be calculated from the results of theoretical analyses of the generation, duct propagation, and radiation phases; or they may be obtained empirically from scale-model test data. The latter method is usually more reliable. There are so many steps in the theoretical calculations and these involve unconfirmed or doubtful assumptions at several stages that the reliability of the

calculated end product is questionable. This argument does not indicate that the theoretical aspects of noise generation should be ignored. Theory has suggested many useful concepts for experimental evaluation, several of which are currently in use. But a great deal of theoretical work and experimental verification remains to be done before reliable noise level predictions can be calculated on a purely theoretical basis.

Figure II-18 portrays the alternative theoretical and empirical methods used to predict one type of fan noise - blade-vane interaction noise at blade passage frequency. Both processes start with given information about the fan geometry and operating conditions. The van and blade numbers and the rotor speed are such that interaction noise propagates. On the left part of the diagram are shown three sources of this noise: impacting of velocity defects from the rotor into the stator, perturbation of the stator vane loads by the passage of the rotor blade potential fields, and the effect upon the rotor blade loading due to its cutting the upstream potential field of the stator vanes. These load fluctuations must be calculated at several spanwise locations. From the rotor fluctuations can be calculated the acoustic field generated in the duct, and its propagation through the duct can be determined. The acoustic field generated by the stator has to pass upstream through the rotor before reaching the inlet ducting. Calculation of the transmission process through the rotor is a highly involved, completely unchecked procedure. The rotor and transmitted stator fields combine in the inlet to produce a resulting pattern at the inlet face. This pattern involves significant radial variations that add to the complexity of the far-field directivity pattern, which is the final stage of the calculation. The outcome of such calculation procedures is subject to considerable uncertainty.

On the other hand, test results from an appropriate model of the fan geometry are relatively straightforward to obtain. Normalizing the data yields fairly reliable predictions of blade passage noise as a function of operating parameters. Eventually, as more data on a greater variety of configurations are compiled and as theoretical aspects of the processes are confirmed, it will be possible to combine both theoretical and empirical methods to establish reliable prediction methods for new fan configurations.

FAN AERODYNAMIC-ACOUSTIC DESIGN INTERACTIONS

So far the fan component aerodynamic requirements and the acoustic characteristics have been considered separately. Quite often, the features desirable for acoustics are not compatible with best aerodynamic performance.

Detailed design trade studies must be made in order to obtain a fan and engine configuration which best balances the conflicting requirements. To be meaningful, these trades must be assessed on the basis of the total system aspects. Not only the fan component, but also the acoustic performance must be evaluated by the subjective reaction of the ground observer to the aircraft flyover. The engine performance should be measured by the overall aircraft economics. The evaluation requires consideration of all the elements which contribute - with the problem being complicated by strong interactions between these elements. For example, the appropriate noise evaluation requires an accounting of

(1) The noise source, such as the fan

(2) Propagation of the noise through the acoustically treated ducts

(3) Radiation from the engine to the ground observer

(4) The subjective response of the observer

The interactions between these elements can be strong enough that a lower fan source noise, for example, does not necessarily mean a lower noise as measured by the observer.

In order to establish the proper overall perspective, it is necessary to consider all the successive elements, including the interaction between the elements. The design compromises between some of the more important aerodynamic and acoustic fan design parameters are considered herein - in particular,

(1) Rotor-stator spacing

(2) Number of rotor blades

(3) Vane-blade ratio

(4) Fan tip speed

(5) Blade design

Rotor-Stator Spacing

The first item of rotor-stator spacing is illustrated in figure II-19. The spacing is defined as the separation between the trailing edge of the rotor and the leading edge of the stator. This separation is measured as a fraction of the rotor blade chord. The acoustic effect of this spacing is obtained by testing at several different spacings with the resultant impact on the noise shown in the right part of the figure. The maximum aft tone-corrected perceived noise level (PNLT) is plotted as a function of spacing-to-chord ratio for takeoff and approach. A continuing reduction in noise with increased spacing is shown, with the effect being more important to the approach condition than to the takeoff. In this case, increasing the spacing from approximately 1/4 chord, which would be usual for normal turbomachinery design practice, to two chords reduces the aft PNLT by 6 to 8 dB.

Large spacings between the rotor and stator obviously tend to increase the engine length and weight. However, by adjusting the engine design such that some of the core compression stages are moved from the high-pressure spool to the low-pressure spool and placed ahead of the frame, the penalty associated with the large spacing can be minimized.

The aerodynamic effects of increased spacings can be illustrated by using results of recent NASA fan component tests as shown in figure II-20. Generally, aerodynamic studies are conducted in separate facilities from noise tests; so the aerodynamic effects of blade row spacing on the same fan on which these acoustic data were obtained cannot be shown. Spacing has been investigated in a fan designed for a pressure ratio of 1.5 at about 1100-foot-per-second rotor blade tip speed. This places it in the range of a moderately high aerodynamic loading. The 53 rotor blades are of high aspect ratio. The spacing shown in the upper half of the figure is $3\frac{1}{2}$ rotor blade chord lengths; 112 stators were used. Considerable wall curvature is required in the region of the blades to achieve the desired area change or annulus area contraction over this stage. The stage was also tested with other reduced stator spacings. The blading is shown at a spacing of 1 rotor chord in the lower part of the figure.

The trend of measured peak fan efficiency with blade row spacing is shown in figure II-21. In the range from 1 to $3\frac{1}{2}$ blade chord spacings,

about 2 percentage points in efficiency are lost. This aerodynamic penalty may be somewhat different for various blade designs. But the general trend and penalty must be traded off against the indicated noise reduction for increased blade row spacing.

To summarize, increasing the spacing between the rotor and the stator permits a significant reduction in the source noise of about 6 to 8 PNdB for an aerodynamic penalty of slightly less than 1 percent in fan efficiency. Experience has shown that low-noise designs cannot be achieved without some penalties, and this trade must be considered a relative bargain. Consequently, all advanced Quiet Engines incorporate a wide spacing between the rotor and the stator.

Rotor Blade Number

The second parameter influencing the aerodynamic-acoustic fan characteristics is the number of rotor blades. In the Quiet Engine Program, two low-speed fans with similar aerodynamic characteristics such as tip speeds, solidities, and pressure ratios but differing primarily in the number of blades were tested. These fans are shown schematically in figures II-22 and II-23. Both of these fans were built and tested aerodynamically and acoustically in full size. The advantages of fan A, with the large number of blades, were a lower noise over the full-speed range; higher efficiency; a shorter fan which still satisfied the blade spacing ratios discussed previously; and a lighter weight - particularly when considering the total weight of the fan blade, the disk, and the fan containment.

Fan B, with fewer blades, has advantages from the standpoint of fewer parts, potentially lower manufacturing costs, and a higher stall margin for a given tip speed. When confronted with the problem of choosing between the two fans, the better performance and lower noise of fan A more than offset the cost advantages of the low-speed fan. Adequate stall margin can be obtained with the high number of blades by proper choice of fan tip speed and aerodynamic design.

Vane-Blade Ratio

The third parameter is described as the ratio of the number of stator vanes to the number of rotor blades, or the vane-blade ratio. (The effect of this ratio on the rotor-stator interference patterns and the desirability of maintaining an appropriate relation between the number of stator vanes and rotor blades has been discussed in a previous section of this paper.)

Noise characteristics of a typical fan were measured by using two different stators aerodynamically matched to the rotor discharge conditions, as shown in figure II-24. The acoustic characteristics shown in the figure illustrate the increase in noise that can occur when the number of stator vanes is reduced from 108 - which satisfies the desirable acoustic relation - to 76. Increases in noise of more than 5 PNLT are observed at the low speeds where the cutoff phenomenon occurs, with the penalty reducing to about 2 PNLT at the takeoff condition.

The combinations of the desirability for a large number of rotor blades along with the desirability of a vane-blade ratio of about 2 leads to a large number of thin, narrow stator vanes, which impacts on both the aerodynamic performance and the aeromechanical characteristics of the vane.

Keeping the ratio of stator to rotor blades high has resulted in critical stator range problems. A fan which was designed for a pressure ratio of 1.5 at a rotor blade tip speed of 1000 feet per second is shown in figure II-25. In this case, 24 rotor blades were used. The gap corresponds to 2 rotor blade chords, and 64 stators were used. Thus the stator vanes are rather high-aspect-ratio (4.1) blades. The performance of this fan is shown by the dashed lines in figure II-26. Stage pressure ratio increases to about 1.5 and then is flat as the flow rate is decreased. Fan peak efficiency is slightly above 87 percent. However, reducing the flow rate only a small amount resulted in stall. The stall margin is less than 7 percent. It was also necessary to remove a small amount of flow from the stator corner to achieve this performance and stall margin.

A redesigned stator with 50 vanes, an aspect ratio slightly below 3, and a slight change in wall curvature at the hub was also tested (fig. II-25). The performance for the redesigned stator is shown as the solid lines in figure II-26. Pressure ratio and efficiency levels are about the same as for the

previous design. However, the flow could be reduced a good deal more before fan stall was observed. And in this case, slit suction from the stator hub was not necessary. The stall margin has been increased 9 percent by this stator redesign. In this fan the stator must operate with high aerodynamic loading and is responsible for stall. Small changes in vane number and aspect ratio and the local wall curvature had a relatively large effect on stall margin. However, even the reduced number of stators is over twice the number of rotor blades.

The increase in stator chord as the number is decreased also is beneficial in providing a structurally desirable stator. Even though stator vanes are supported at both the inner and outer walls, midspan dampers could be required to avoid serious vane flutter, particularly if a very large number of short-chord stators were considered necessary from a fan noise standpoint.

The combination of the aerodynamic and acoustic design requirements forces the fan towards the aerodynamic loading limits on the stator as well as pushing the design towards the aeromechanical limits.

Fan Tip Speed

The fourth parameter to be discussed is fan tip speed. From the standpoint of the unsuppressed fan component, the data shown previously indicated the lowest noise fans are generally the subsonic fans. However, the best untreated fan component does not imply the best low-noise engine system. For example, use of low fan speeds introduces the need for more stages on the low-pressure spool - leading to larger, heavier, and costlier engines. A portion of the weight and cost advantage of a high-speed engine can be used to introduce more sound-absorbing panels to reduce the noise measured by the observer to the same level as that of the subsonic fan. Consequently, the best low-noise propulsion system cannot be a priori assumed to be the lowest noise untreated fan component. The choice can be made only after a total system evaluation is completed.

The effects of tip speed on noise were evaluated in the Quiet Engine Program by designing a fan with a 1550-foot-per-second tip speed. The acoustic comparisons are shown in figure II-27. Tip speed effects are obtained by

comparing fans B and C - each with 26 blades. The fan noise levels are of concern essentially at two points - approach and takeoff. For approach power settings, the fan operates at about 60-percent speed in the region of 1.2 pressure ratio. The noise levels at approach are essentially identical. The takeoff power settings are at the highest pressure ratio points shown. The difference in maximum perceived noise level at this condition between fans B and C is about $3\frac{1}{2}$ PNdB. A portion of this difference is due to the fact that fan B is operating at a lower pressure ratio. The acoustic challenge is essentially that of reducing the noise penalty due to tip speed at this takeoff point.

Of particular interest on the high-speed fan is the trend at takeoff of a reduction in maximum perceived noise level as speed and pressure ratio are increased - which is contrary to the usual correlations. The maximum noise is associated with a partial-speed, or off-design, operating condition. In fact, even at takeoff the fan is operating at an aerodynamic off-design - usually at about 90 percent of the aerodynamic design speed. A natural hypothesis is that the noise-generating phenomena are related to the aerodynamic flow fields illustrated in figure II-28. The design condition has the shock at the entrance to the blade channel with a relatively weak bow shock propagating upstream. At off-design, the passage shock is forced out of the channel, resulting in a strong shock pattern propagating upstream of the rotor. The reduction in noise as the design speed is approached occurs concurrently with the reduction in strength of the upstream shock pattern.

To explore the potential of reducing the noise associated with supersonic operation of the blading, a modification was made to a scale-model version of fan C. The blade channel area was opened to permit the shock to move back toward the channel entrance at the takeoff speed and reduce the strength of the upstream propagating wave patterns.

The acoustic impact of this modification is shown in figure II-29. The basic fan C characteristic shows the strong multiple pure tones (MPT) in the 500- to 1500-hertz region. The modified blade substantially reduced the MPT noise, by as much as 10 decibels over the entire MPT spectrum. However, the blade passing tone was increased by about 5 decibels.

The acoustic energy obtained by integrating around the forward angles of the fan showed an 8-decibel reduction, or a reduction to about 20 percent of

its original value. When the blade passing tone (BPT) is adjusted for its greater annoyance, the subjective evaluation decreases this to a 3-PNdB reduction.

Associated with the increase in blade channel area was an increase in the effective blade camber. The effect on aerodynamic performance of this change was to raise the pressure ratio at which peak efficiency occurs to a region well above the engine operating line. Although the peak efficiency levels were actually increased at all speeds, the efficiency on the engine operating line was improved only to 90 percent - or takeoff speed. Above this speed, and in particular at the critical altitude cruise, an unacceptable efficiency penalty of about 4 percent was observed.

Studies of blade shapes particularly suited to minimize the aerodynamic penalties and operated with a weak forward shock pattern have been initiated. These blade shapes would be particulary useful where relatively high blade speeds are utilized to achieve a rather low pressure ratio, that is, at low aerodynamic loading. Blade shapes with strong passage shocks have been repeated in figure II-30 along with blades designed to achieve a weaker forward shock configuration. In this case the blade is shaped so that the first passage shock is a weak oblique shock. This is followed by a second oblique shock near the blade trailing edge when the first shock is essentially attached to the blade leading edge and the forward shock configuration is very weak.

Blades for this shock configuration were designed into a fan with a pressure ratio of 1.5 at 1600 feet per second. This is a somewhat higher speed than used in fan C. The initial model of this fan resulted in a design speed efficiency of nearly 85 percent, as shown in figure II-31. The peak efficiency region and operating line would be well away from the stall line. The measured stall margin was at least 17 percent. It would appear the low blade losses were achieved by this blade design. However, the rotor had blade corner vibrations. This indicates than in addition to aerodynamic and noise considerations the new fan blade designs must also consider the aeroelastic effects.

The noise generated by this fan was not evaluated, but the aerodynamic data obtained indicate that the desired shock configuration was obtained.

In summary, a number of design parameters are being evolved which impact on both acoustic and aerodynamic performance. This work has already led to significant reductions in noise levels for the new high-bypass-ratio engines now being introduced into service.

A few of these parameters have been discussed in some detail. These, as well as others, need to be further exploited - not only to assure that much quieter configurations are obtained, but also to obtain the data for engine tradeoff studies. These studies are necessary to permit selection of the total systems which achieve the desired noise suppression at a mininum economic penalty.

PERFORMANCE RESULTS WITH LARGE-SCALE FAN FACILITY

A quiet fan is needed in order to have a quiet engine. As discussed previously, the fan must meet certain aerodynamic requirements. However, it is also a noise generator. Although much theoretical acoustic analysis has been done, fan designs are heavily dependent on empirical data.

Consider now what an inefficient noise generator a quiet fan really is. Shown in figure II-32 are data points for various low-speed and high-speed fans that have been tested. The percentage of fan shaft horsepower that radiates as noise, or sound power, is plotted against fan pressure ratio. For the lowest noise fans that are of interest, less than 0.005 percent of the shaft horsepower radiates as noise. This means that for a 20 000-horsepower fan, less than 1 horsepower radiates as noise.

In order to obtain the necessary large-scale fan acoustic data for empirical correlations and extrapolation, NASA built the test facility shown in figure II-33. Initially, the research fan was located 50 feet from the building wall and 19 feet above grade to minimize ground reflections and the effects of the ground on inlet flow. The 10- by 10-Foot Supersonic Wind Tunnel drive motors were utilized to power the fan. Fortunately, when the tunnel drive system was designed, the motors were double-ended, to provide for a time when another facility might be added. This resulted in a costs saving by eliminating the need for drive motors in the fan test facility.

The motors in the building drive the fan through a speed increaser and a 50-foot-long drive shaft. A portion of the building wall was treated with 6 inches of polyurethane foam to minimize acoustic reflections that the microphones might pick up. An open area as free of reflecting surfaces as possible was chosen for the test site, as shown in figure II-34.

The microphones were placed at 10° intervals, generally, on 100-foot radii centered on the fan. The forward microphones were located closer to the fan to clear the drive motor building, and the data from these microphones are corrected to a 100-foot radius. The microphones are at 19-foot elevation: the same elevation as the fan centerline. The fan inlet (fig. II-35) is free of obstructions such as bearings, struts, guide vanes, and instrumentation, in order to minimize inlet flow distortion. However, some of the inlet air flows over the support structure and causes some inlet flow distortion.

Inlet flow distortion causes fluctuating forces on the rotor blades as they pass through the distorted flow region. This, in turn, results in an increase in the noise generated by the fan, which manifests itself primarily in the blade passage tone (BPT). A narrow-band spectrum is shown in figure II-36 to illustrate the effect of inlet flow distortion, in terms of BPT, on the sound pressure level. The maximum sound pressure level of the discrete tone at blade passage frequency for takeoff speed is very pronounced. An analysis of the noise revealed that the discrete tone was higher than expected.

A decision was made to move the fan farther from the building to provide relief from the inlet flow problem. The shaft was extended so that the fan was 100 feet from the building. The fan was turned around so that the inlet extended well beyond the support structure in order to obtain an unobstructed, or clean, inlet (fig. II-37). The fan was now driven from the rear and flow was discharged toward the building wall. The clean inlet with less inlet flow distortion resulted in a considerable reduction in the blade passage tone (fig. II-38). However, the low-frequency broadband noise was greatly increased. This was caused by the discharge airflow scrubbing over the bearings and shaft supports and being turned by the wall of the drive building. This low-frequency noise was unacceptable; and since it was impractical to move the fan farther from the building wall and there was no

readily apparent way to reduce the scrubbing noise, it was necessary to accept the best compromise available. Consequently, the fan was turned around to the final version - 100 feet from the building wall and discharging away from the building wall, as shown in figure II-39. The inlet obstructions were also minimized. In order to do this, the pedestal was separated to allow undisturbed flow from below and the support structure was streamlined (fig. II-40). This reduced the broadband noise, as shown in figure II-41. The blade passage tone is not as low as desired. However, it is the best that can reasonably be done with the facility and no further changes are contemplated.

The family of fans described early in this paper has been tested in support of the Quiet Engine Program. Some of the more interesting aspects of the basic data that have been obtained during the evaluation and selection process of these fans are discussed in the following paragraphs.

In figure II-42, some of the data from fan D are shown in terms of narrow-band spectra. The data are shown as sound pressure level as a function of frequency at 50^{o} from the inlet at takeoff and approach speeds. Illustrated in the figure are broadband noise, some evidence of multiple pure tones (MPT), and blade passage tones (BPT) with harmonics.

In figure II-43, the same fan D data are shown in terms of 1/3-octave frequency bands instead of narrow bands. At the takeoff speed (square symbols) the broadband, MPT, and BPT are apparent. The overall power levels can be integrated and the noise components separated as a function of speed. Total noise (fig. II-44) is a summation of the components of broadband, BPT, and MPT. The total noise increases with increasing speed; and MPT comes in at a tip speed of just below 900 feet per second and climbs fast, while the BPT peaks and drops off. This represents an interchange of energy from BPT to MPT with increasing speed.

To obtain subjective noise ratings of fans, 1/3-octave plots are used and weighted levels of human response in the various frequency bands are factored in to get the perceived noise level expressed in terms of PNdB. For fan D this resulted in a maximum level of 95.5 PNdB at takeoff speed at a 1000-foot altitude and at 50^{o} from the inlet (fig. II-43).

This procedure can be applied for every angle with a resultant plot of perceived noise as a function of angular position, as shown in figure II-45

for fan D. The noise reaches a maximum at 50° from the inlet and then peaks again at 110°. The level for fan D is essentially the same for front and rear.

From data such as have been presented, the various types of subjective noise ratings which are used to evaluate the relative quietness of engines can be calculated. Three of these are perceived noise level (PNL); tone-corrected PNL, or PNLT, which penalizes the engine for excessive BPT; and effective perceived noise level (EPNL), which takes into account the duration of the noise as the plane passes overhead. EPNL is the value used in FAR-36. The results of these calculations are shown in table II-2. The

TABLE II-2. - FAN D NOISE RATING

[Pressure ratio, 1.4; tip speed, 1107 ft/sec.]

Noise rating	Takeoff power	Approach power
Maximum perceived noise level, PNdB	104.4	107.1
Maximum tone-corrected perceived noise level, PNdB	105.1	108.6
Effective perceived noise level, PNdB	102.6	103.1

values in the table are the maximum noise that a person on the ground would hear during takeoff of a four-engine airplane 3.5 nautical miles from brake release and, for the same airplane, on approach 1 nautical mile from touchdown.

On the basis of the basic data for all the fans, one was selected for the Quiet Engine. A plot of the data for the low-speed, single-stage fans is

shown in figure II-46 in terms of maximum noise levels as a function of fan pressure ratio. It is apparent that fan A is the lowest noise fan. Fortunately, fan A is also the best from aerodynamic and mechanical standpoints.

When the single-stage, high-speed fan data are included, it is apparent that the noise level for the supersonic fan is considerably higher than that for low-speed fans (fig. II-47). However, this may not be as bad as it first appears. (It is discussed in another paper.)

Another way to look at the difference between low- and high-speed fans is how the noise varies with angle from the inlet. Figure II-48 shows a noise directivity plot for fans A and C similar to that previously shown for fan D. The noise level peaks at 50°, falls off, and then reaches another peak at 120° (similar to fan D). Both front and rear peaks are essentially equal. High-speed fan C differs from low-speed fan A primarily in the higher front-end noise level.

Examination of narrow-band spectra of sound pressure level as a function of frequency at 50° from the inlet for takeoff (fig. II-49) shows that fan A is similar to fan D with broadband, BPT, and harmonics noise evident. Fan C, however, is dominated by MPT, which masks the BPT. This phenomenon is caused by nonuniform shocks emanating from the leading edge of the rotor blades at high speeds.

CONCLUDING REMARKS

The fact that there are tradeoffs between the aerodynamics and acoustics in the fans is not surprising. The design of every engine component involves some compromise. The basic knowledge of fan noise generation is not sufficiently precise to permit quantitative estimates or predictions of fan noise. Consequently, a largely empirical approach is used. The facilities which are used to obtain fan noise empirical data have been discussed and some of the results shown.

The empirical work can be summarized through the use of several charts, the first of which (fig. II-50(a)) shows the data that have been obtained on several single-stage, low-speed fans. The maximum perceived noise level (in PNdB) is shown plotted against fan pressure ratio for fans of

Quiet Engine size which would produce a total of 90 000 pounds of takeoff thrust (four engines). The measured noise is extrapolated to a simulated 1000-foot flyover.

The data group together well for the single-stage, low-speed fans which cover the pressure ratio range of 1.4 to 1.6. Before deciding on a single-stage fan for the Quiet Engine, two-stage-fan data were also examined (fig. II-50(b)). These data include, on the extreme left, that from a modified TF-39 engine which was run as part of the Quiet Engine Program and also two-stage fan data collected from various low-bypass-ratio engines now in common service on narrow-bodies jet transports. The data from these operational, two-stage, low-bypass ratio engines were obtained with fans that were running at fairly high speeds and had closely spaced inlet guide vanes, as opposed to the data point on the extreme left, which represents a widely spaced, two-stage fan operating at low speed. Consequently, the correlation band around these data points probably is to a great extent fortuitous, although the fans have some relation to each other when plotted against pressure ratio.

In figure II-50(c) are shown some data points for single-stage, high-speed fans and again these data points tend to group together. The data are somewhat higher than for the single-stage, low-speed fans and somewhat lower than for the two-stage fans.

The collection of data points in figure II-50(c) represents the basis from which to work in the Quiet Engine Program for subsonic cruise, CTOL airplanes. Other applications of propulsion systems with low-noise technology built into them are of interest and are being examined. In order to do that effectively, our knowledge has to be extended in two directions: to the higher pressure ratios and the lower pressure ratios. In figure II-50(d), some open squares have been added which represent planned tests of single-stage, high-speed fans. Obviously, their actual noise output is estimated because the tests are just now being planned; however, the hardware is being built. The noise estimates shown are based on empirical correlations so that it should come as no surprise that they fall right in the data band.

Work in the low-pressure-ratio range is also being extended and is shown in figure II-50(e) by the open squares. These fans are designed for various pressure ratios that are a part of the technology program in support

of externally blown flap STOL airplanes. Again, the noise levels are estimated and may be different from those shown in the figure.

In general, from the data shown in figure II-50(e) for 90 000 pounds of thrust (four engines), a variety of fans can be selected which produce noise levels in the range of 100 to 120 PNdB. Selection of a particular fan depends on the fan configuration and the design pressure ratio required for a specific operation and that, in part, depends on the type of mission to be performed.

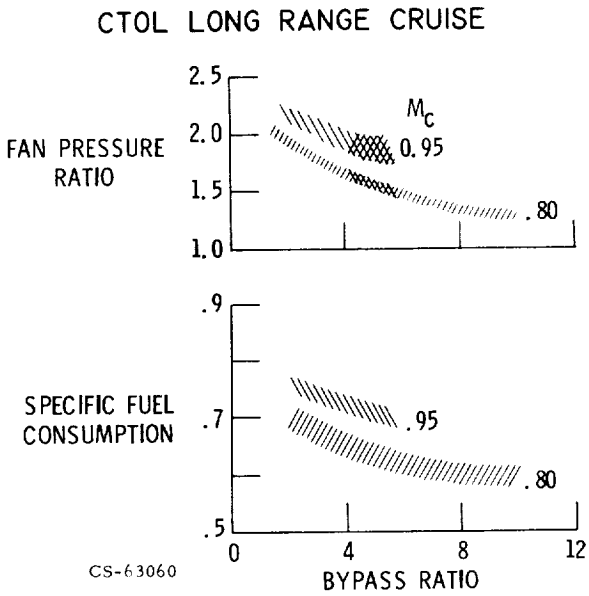

Figure II-1

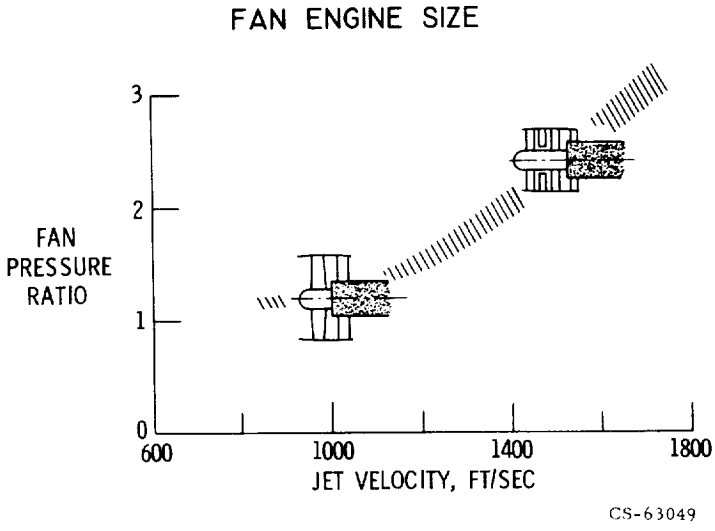

Figure II-2

FAN PERFORMANCE MAP

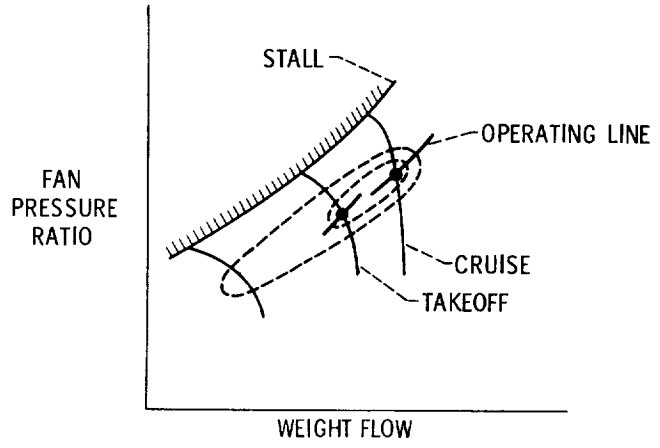

CS-63050

Figure II-3

DISTORTION PERFORMANCE

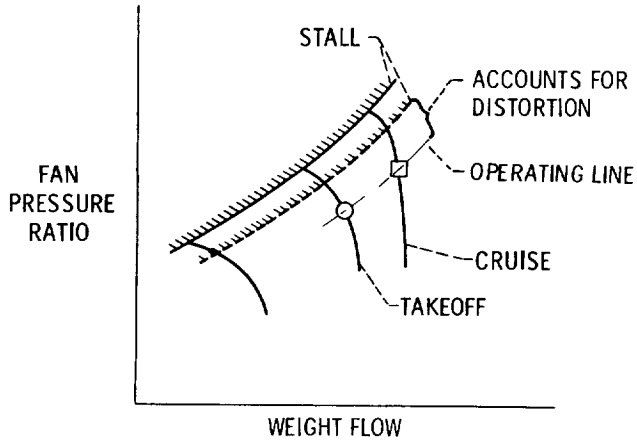

CS-63051

Figure II-4

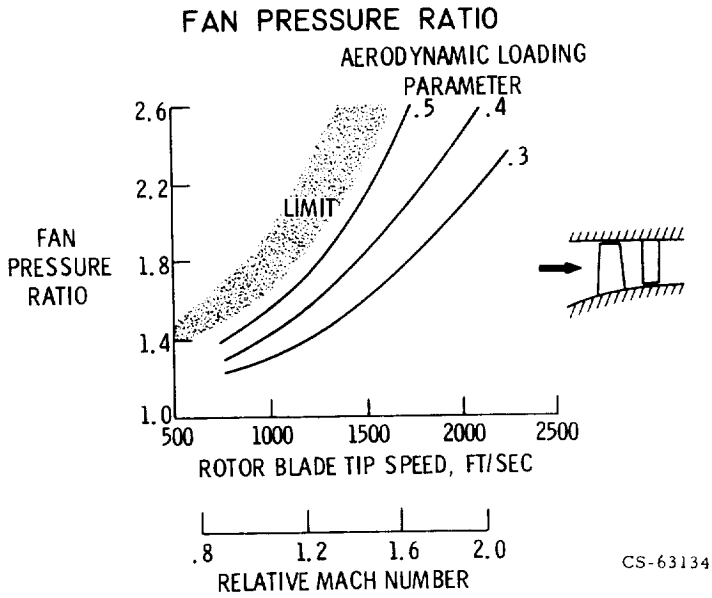

Figure II-5

COMPARATIVE PERFORMANCE OF LOW-NOISE FANS

DESIGN SPEED

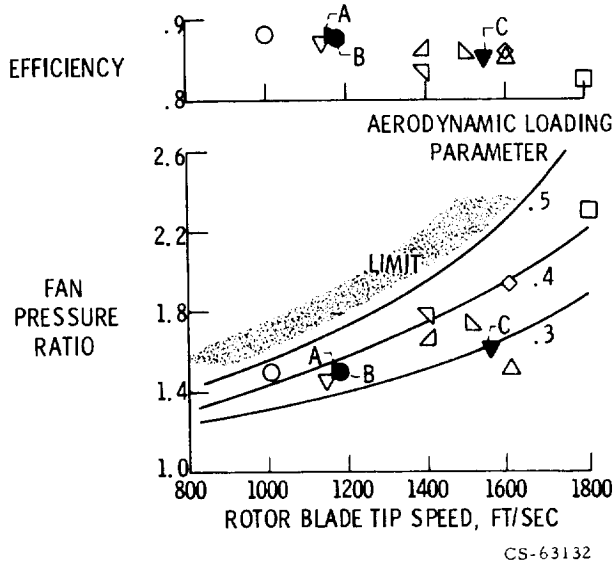

Figure II-6

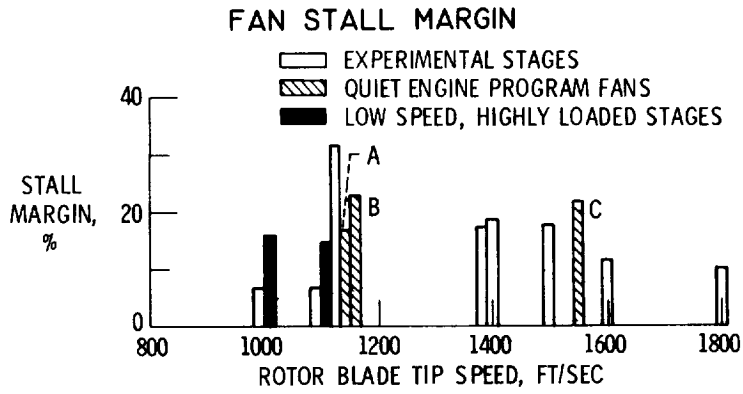

Figure II-7

CS-63053

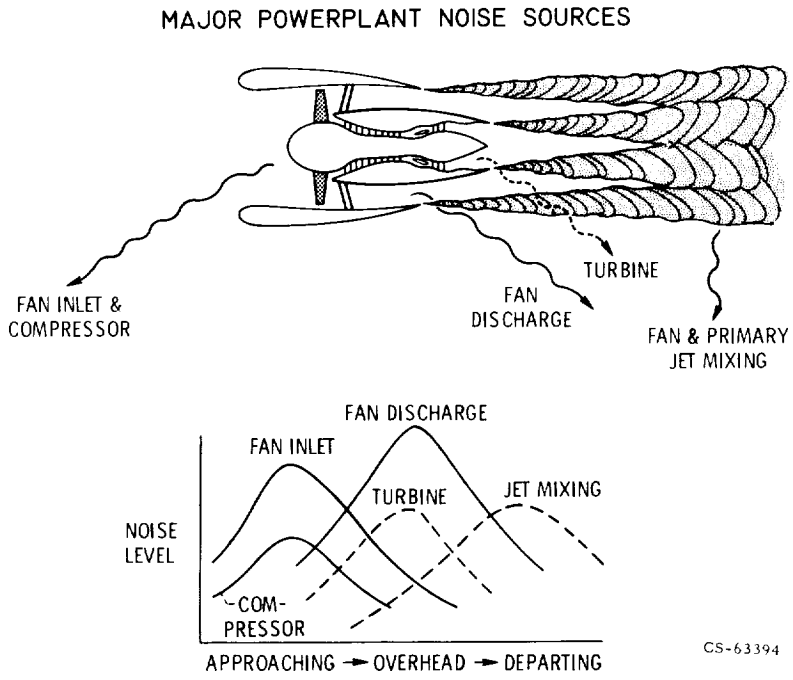

Figure II-8

FAN NOISE SPECTRA AT SUB- AND SUPERSONIC TIP SPEEDS

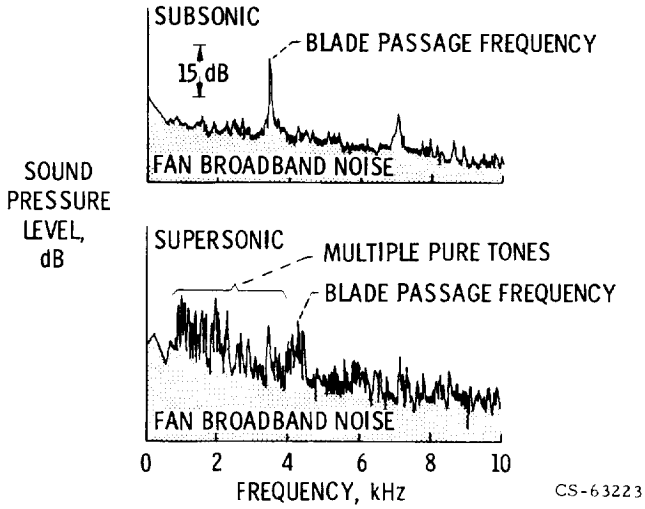

Figure II-9

PHASES IN EMISSION OF FAN NOISE

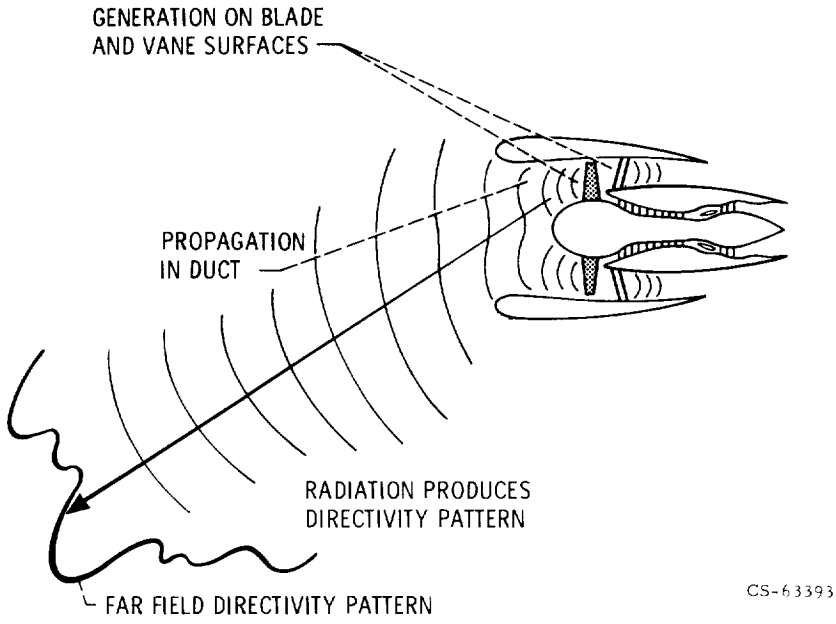

Figure II-10

FAN NOISE RESEARCH FACILITIES

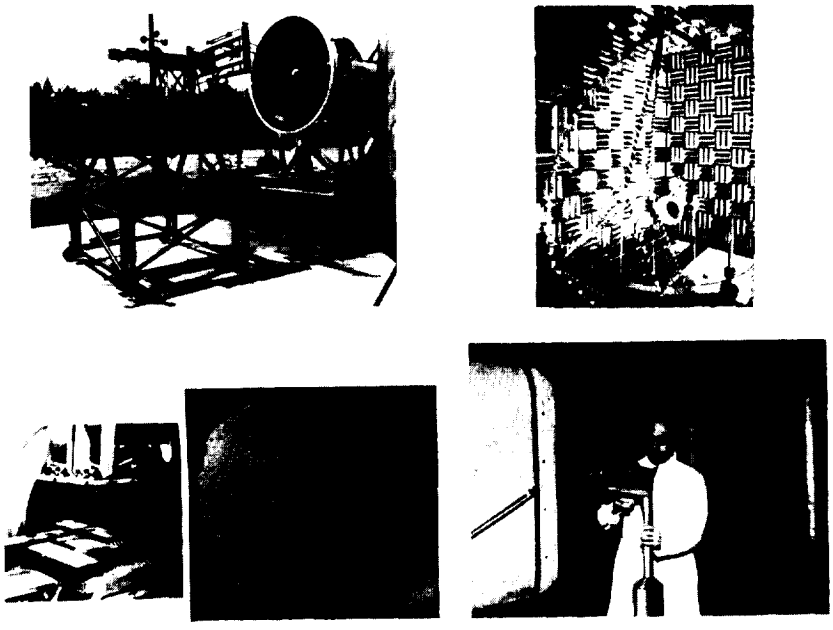

CS-63212

Figure II-11

GENERATION OF DISCRETE BLADE PASSAGE NOISE BY PERIODIC WAKE CUTTING

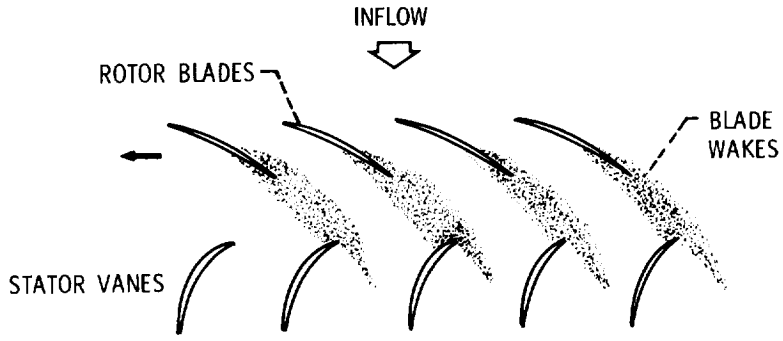

VELOCITY DEFICIT IN WAKES PRODUCES PERIODICALLY FLUCTUATING AIR ANGLE TO VANES

↓

INDUCING LIFT FLUCTUATIONS ON VANES

↓

FORMING MOVING PRESSURE PATTERNS IN DUCT

↓

AND RADIATING TO FAR FIELD AS NOISE

CS-63231

Figure II-12

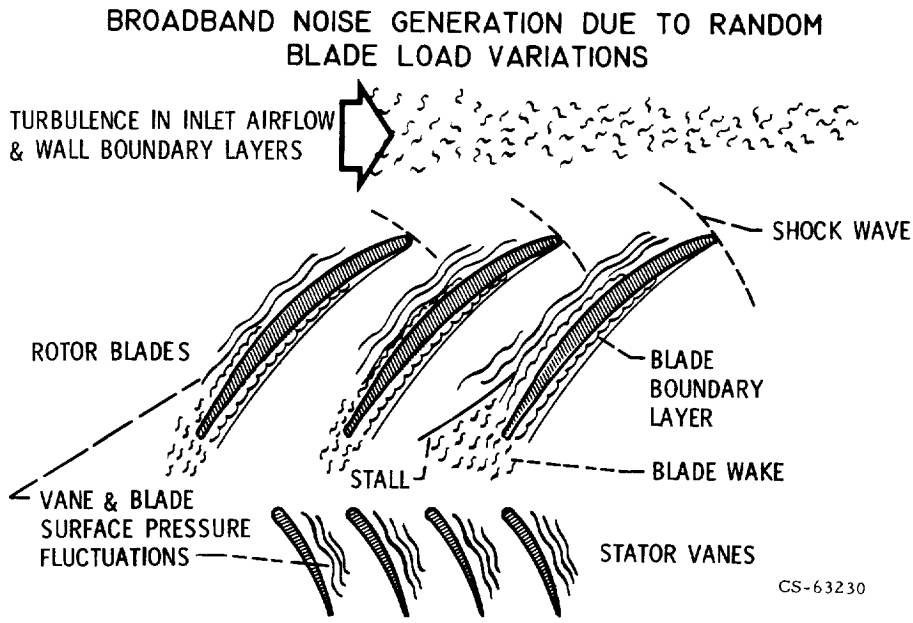

Figure II-13

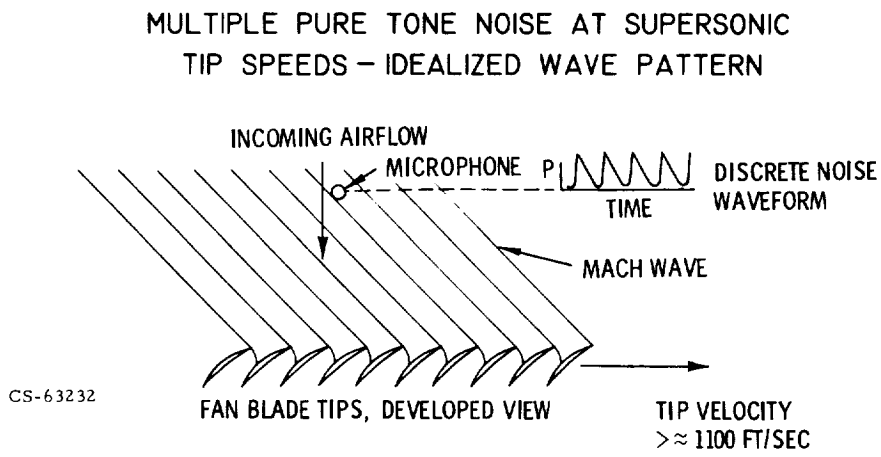

Figure II-14

MULTIPLE PURE TONE NOISE AT SUPERSONIC TIP SPEEDS – ACTUAL WAVE PATTERN

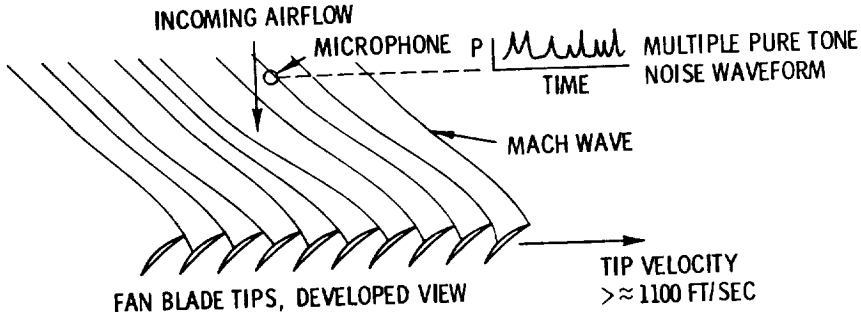

Figure II-15

EFFECT OF FAN EXIT GUIDE VANE SPACING ON FAN DISCRETE NOISE

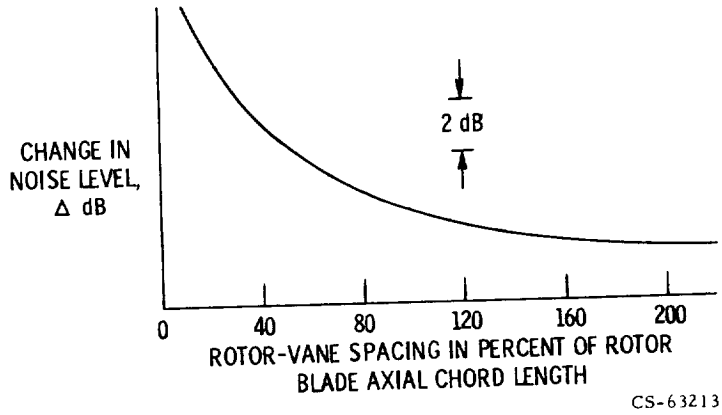

Figure II-16

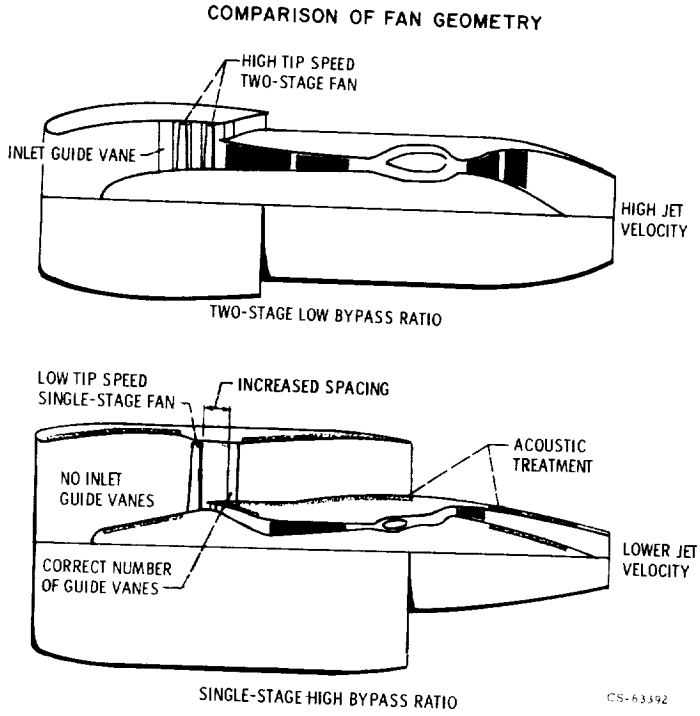

Figure II-17

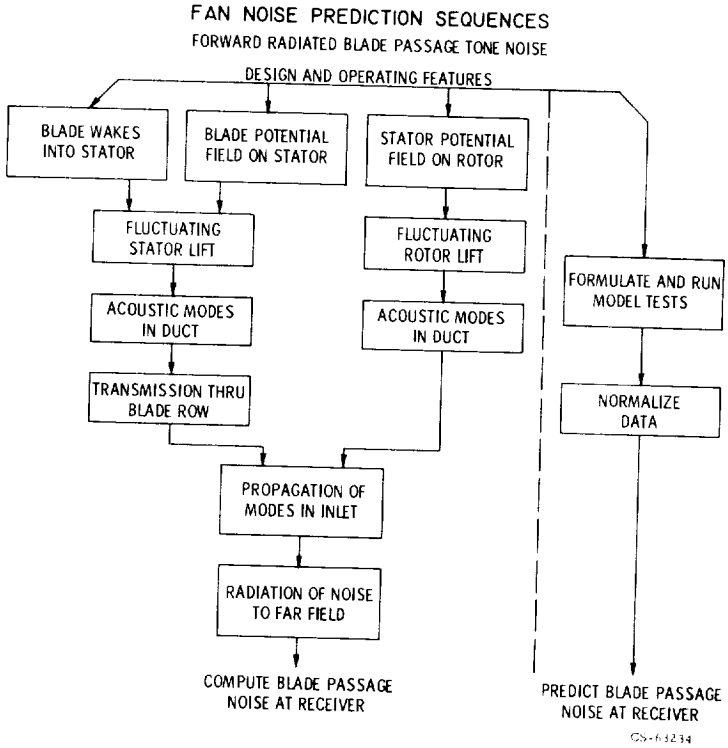

Figure II-18

SPACING EFFECTS ON NOISE

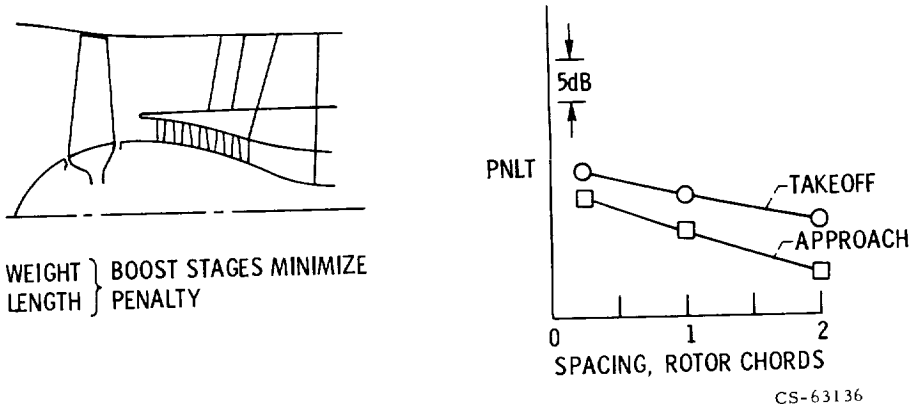

Figure II-19

LOW NOISE FANS – STATOR SPACING

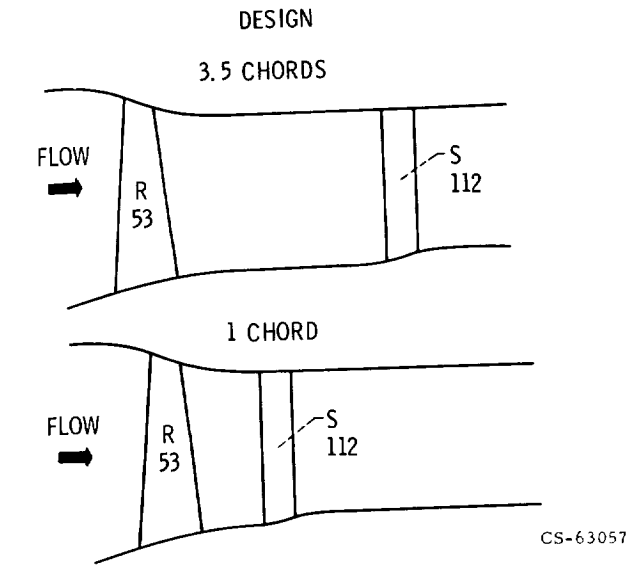

Figure II-20

SPACING EFFECTS ON EFFICIENCY

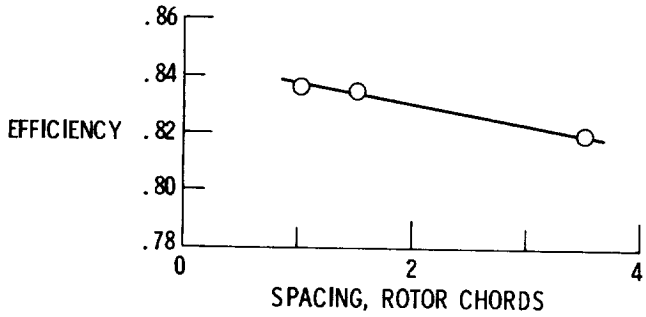

Figure II-21

CS-63047

ROTOR BLADE NUMBERS – FAN A

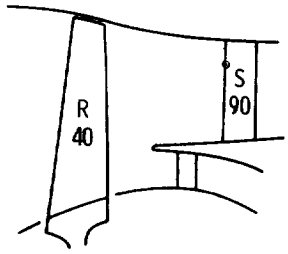

ADVANTAGES
LIGHTER
HIGHER EFFICIENCY
SHORTER
LOWER NOISE

CS-63056

Figure II-22

ROTOR BLADE NUMBERS – FAN B

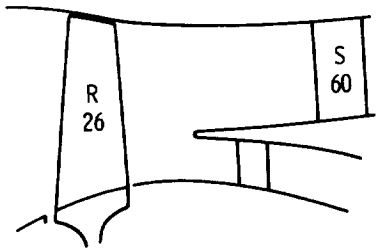

ADVANTAGES
FEWER PARTS
HIGHER STALL MARGIN

CS-63048

Figure II-23

VANE/BLADE RATIO EFFECTS

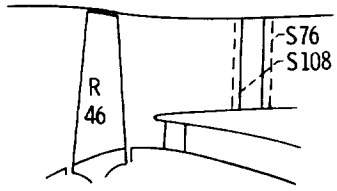

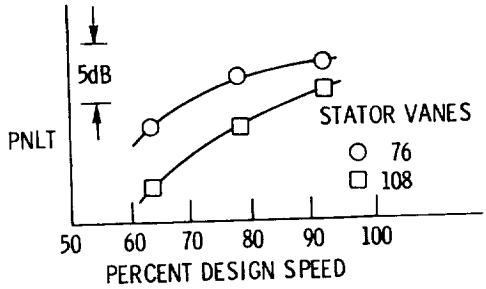

INCREASED NUMBER OF STATOR VANES

- REDUCES STALL MARGIN
- INCREASES VANE VIBRATION

CS-63137

Figure II-24

DESIGN OF LOW-NOISE FANS - NUMBER OF STATOR VANES

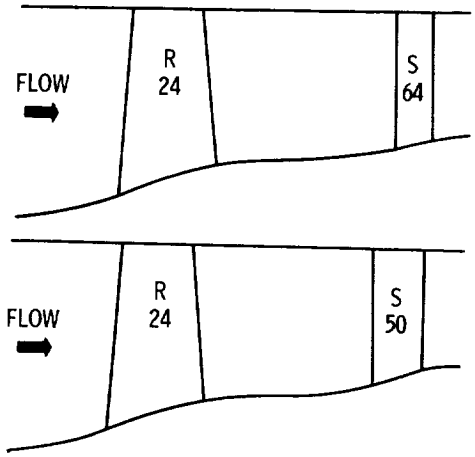

Figure II-25

AERODYNAMIC PERFORMANCE OF LOW NOISE FANS - NUMBER OF STATOR VANES

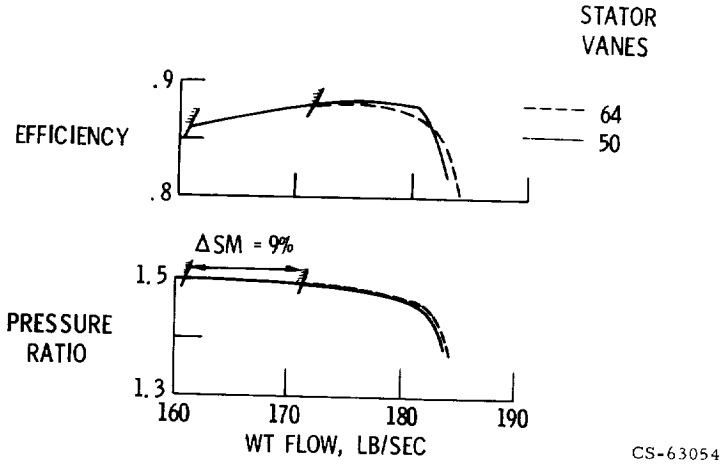

Figure II-26

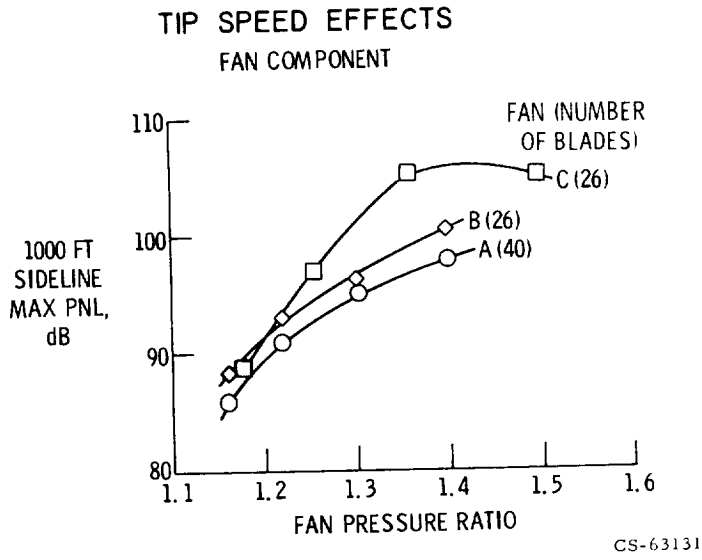

Figure II-27

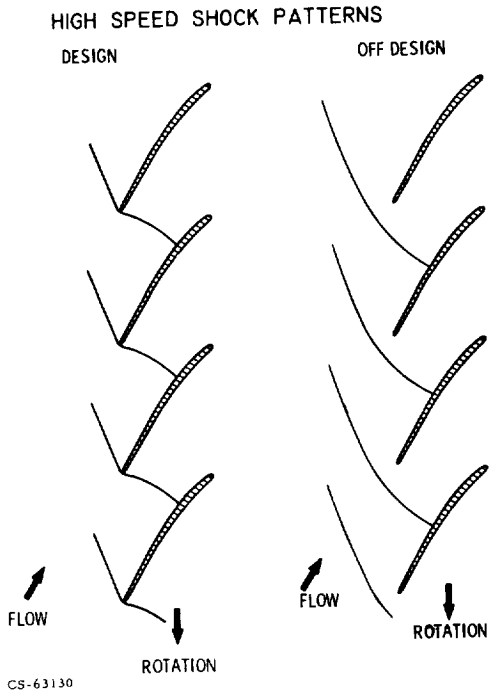

Figure II-28

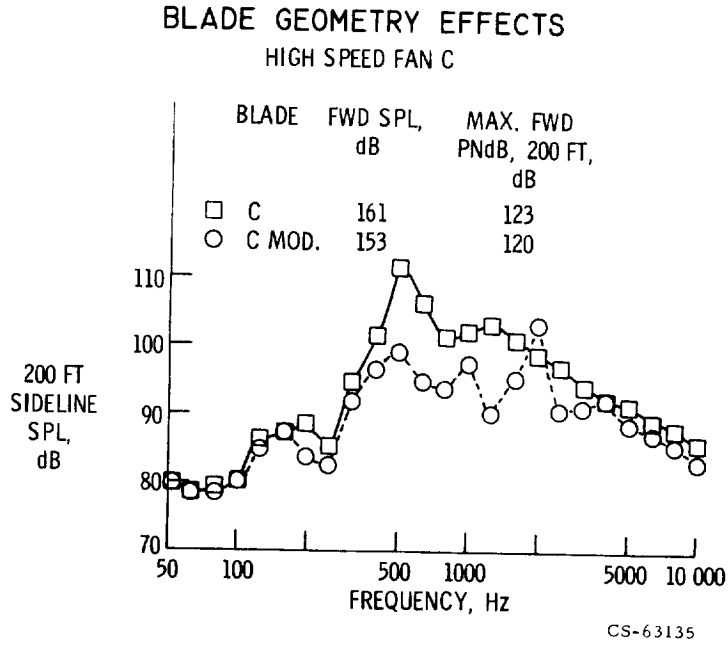

Figure II-29

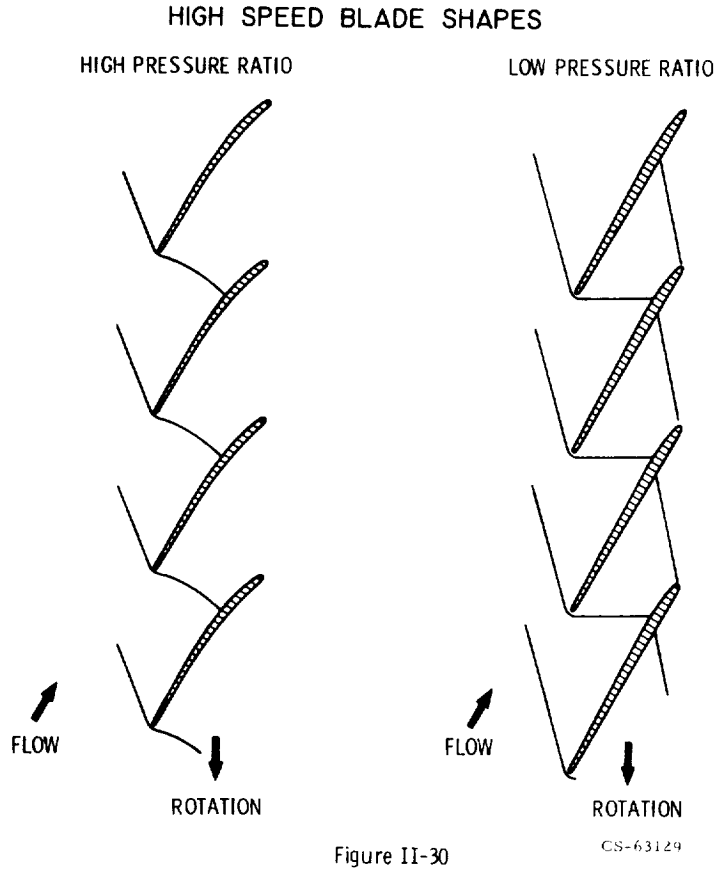

Figure II-30

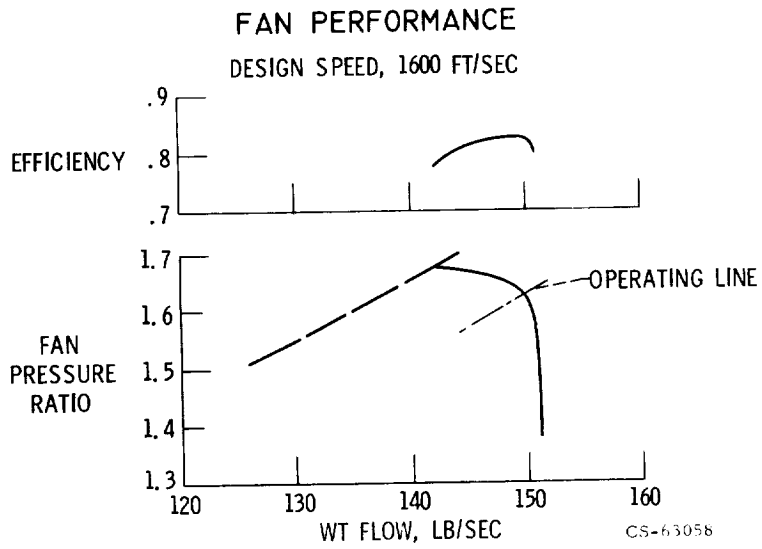

Figure II-31

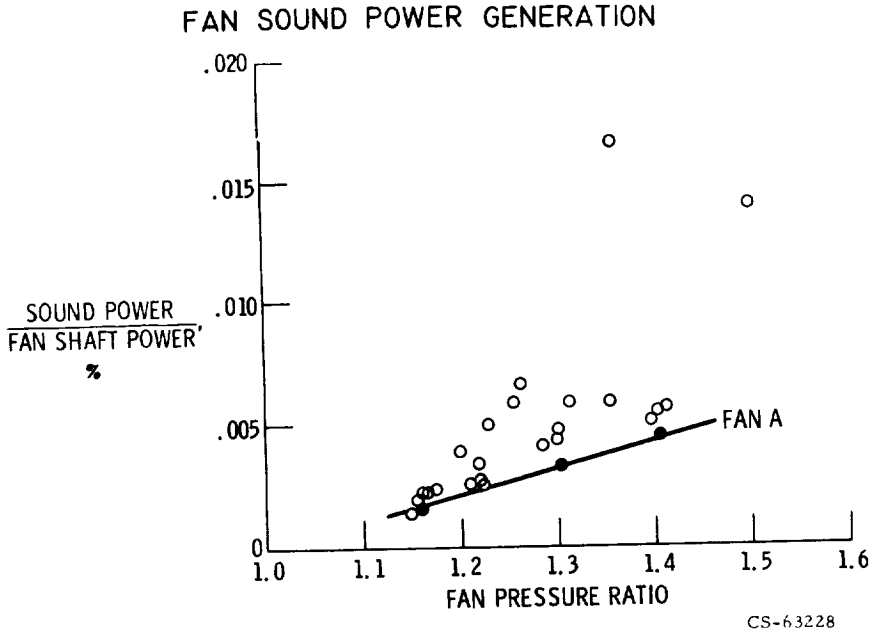

Figure II-32

FAN NOISE TEST FACILITY

SHORT SHAFT – FRONT DRIVE

Figure II-33

CS-63211

FAN NOISE TEST AREA

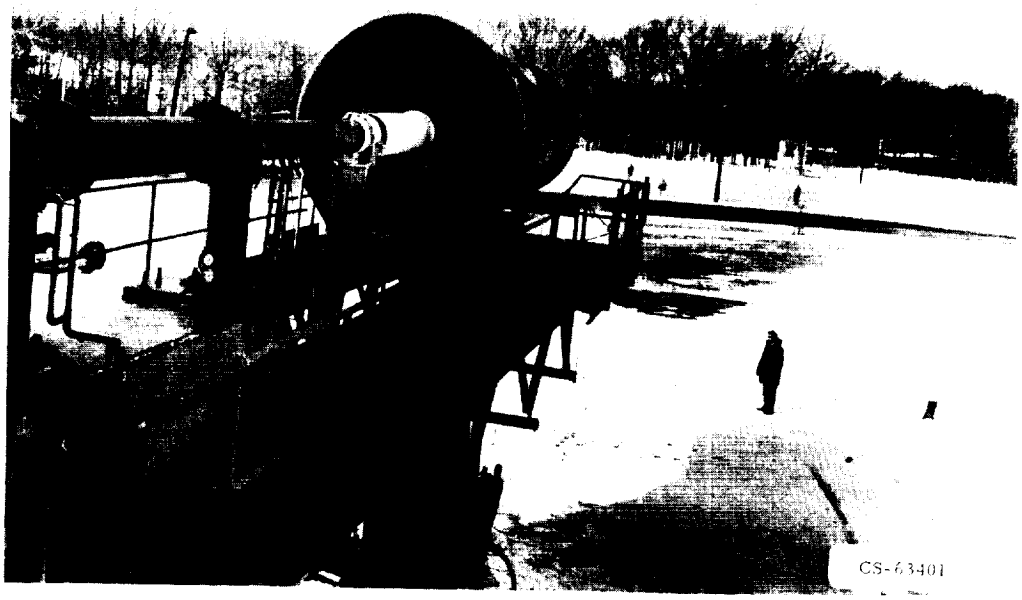

Figure II-34

FAN INLET

Figure II-35

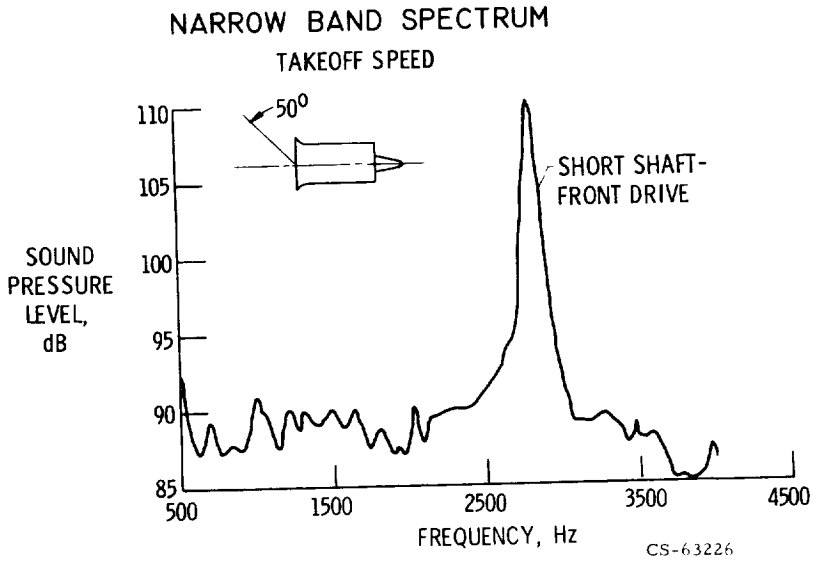

Figure II-36

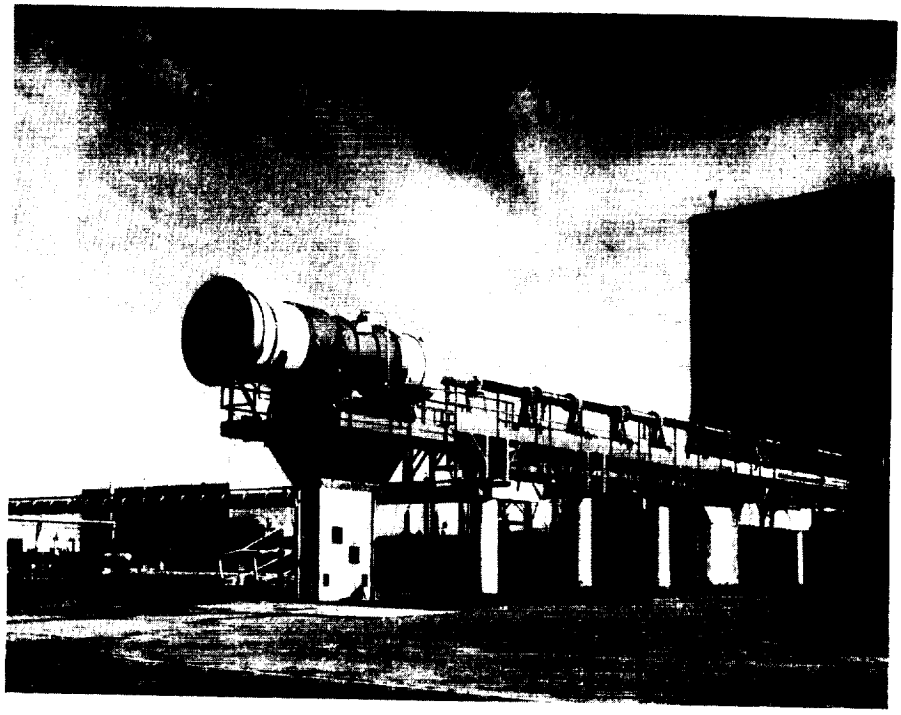

Figure II-37

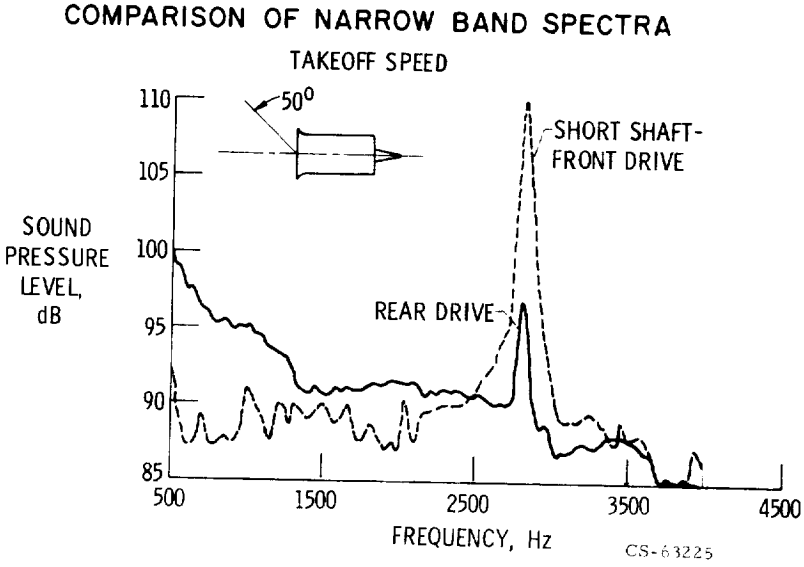

Figure II-38

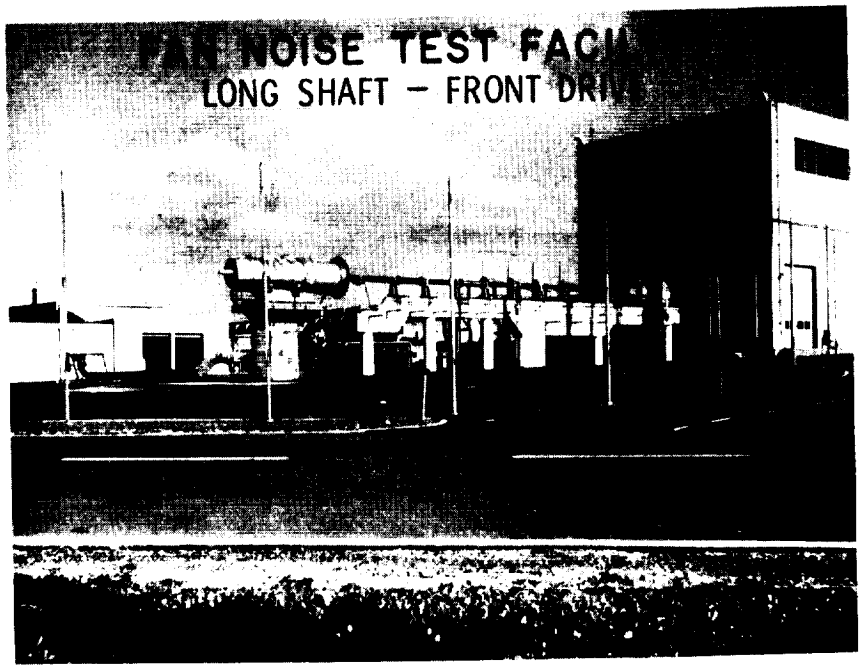

Figure II-39

FAN SUPPORT PEDESTAL

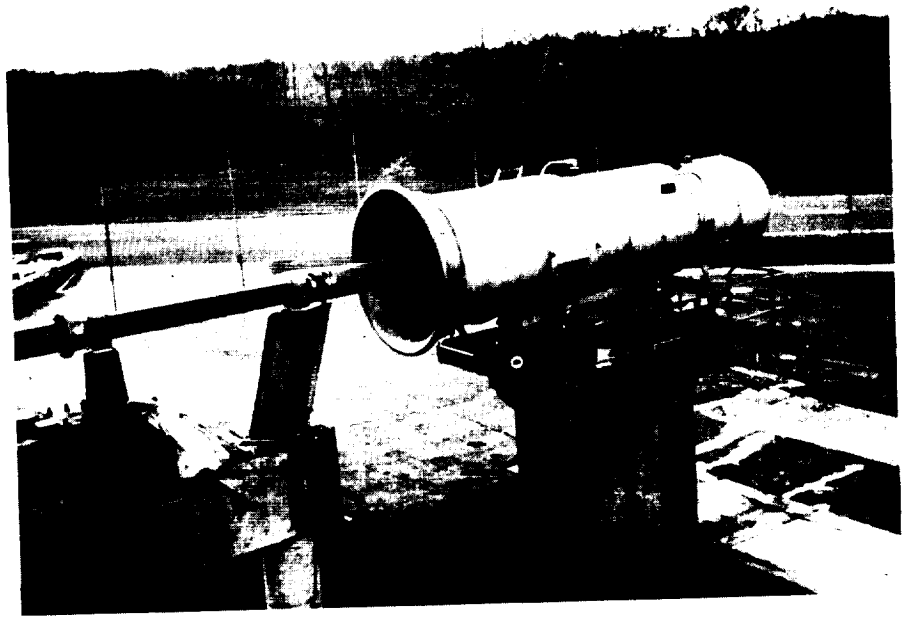

Figure II-40

NARROW BAND SPECTRA WITH SEPARATED PEDESTAL

TAKEOFF SPEED

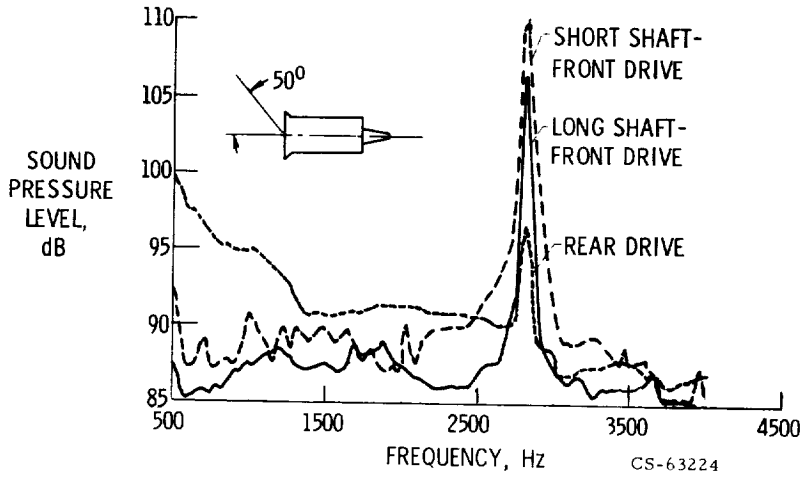

Figure II-41

FAN D NARROW BAND SPECTRA

1.4 PRESSURE RATIO; 1107 FT/SEC TIP SPEED

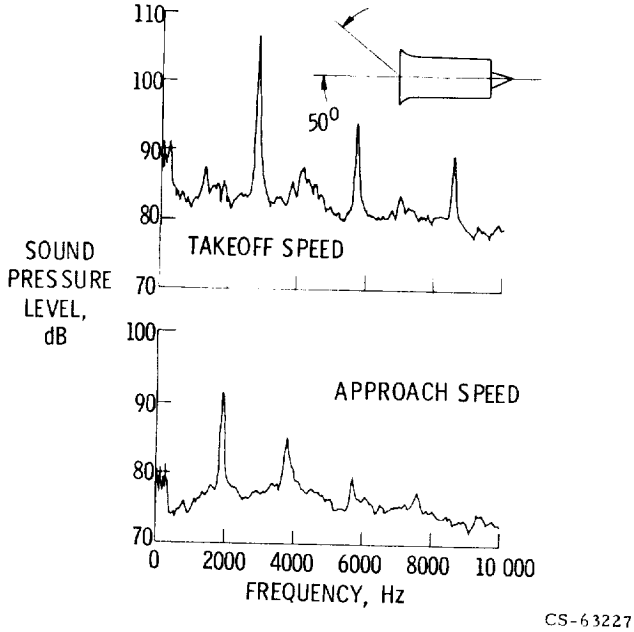

Figure II-42

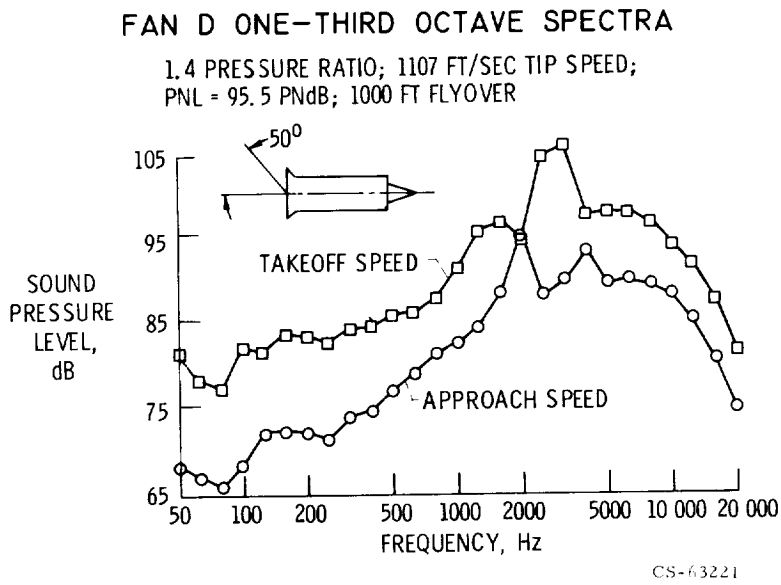

Figure II-43

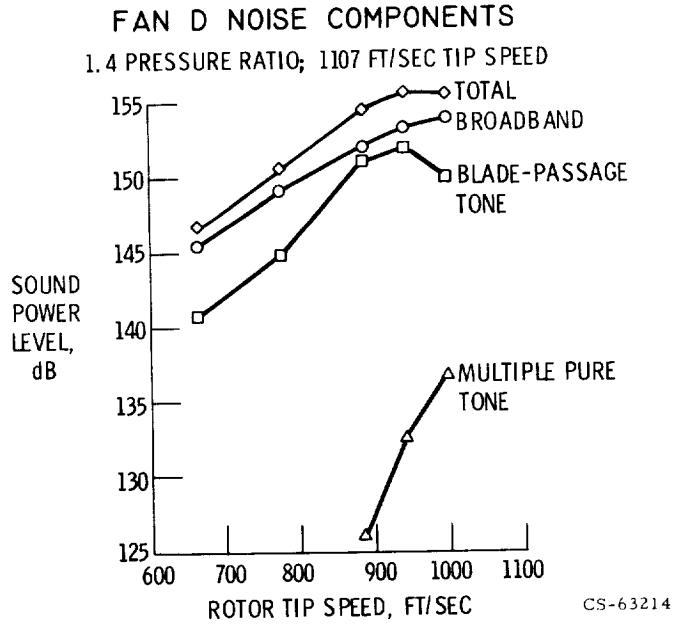

Figure II-44

FAN D PERCEIVED NOISE LEVEL AT TAKEOFF

1.4 PRESSURE RATIO; 1107 FT/SEC TIP SPEED; 1000 FT FLYOVER

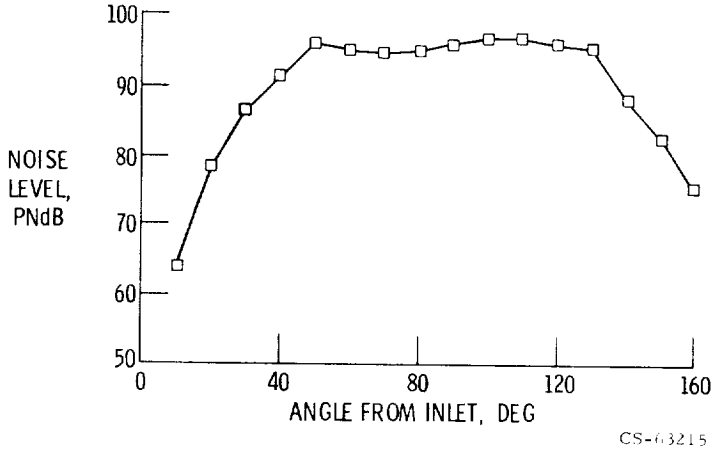

Figure II-45

COMPARISON OF NOISE LEVELS – LOW SPEED FANS

1000 FT FLYOVER

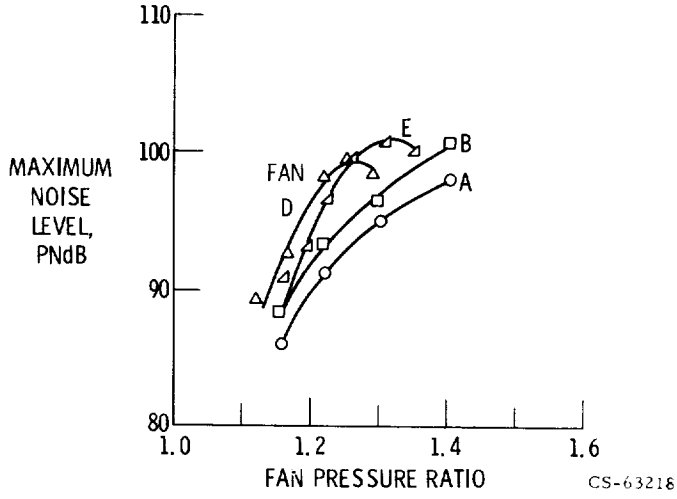

Figure II-46

COMPARISON OF NOISE LEVELS – LOW– AND HIGH–SPEED FANS

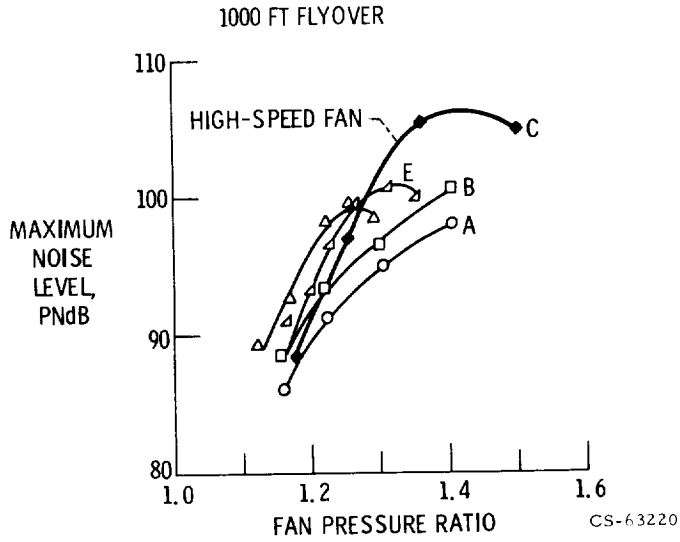

Figure II-47

FAN PERCEIVED NOISE DIRECTIVITY

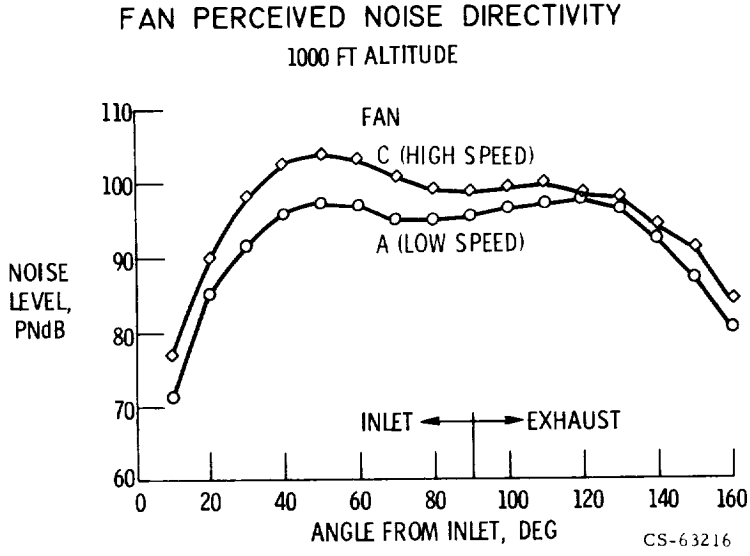

Figure II-48

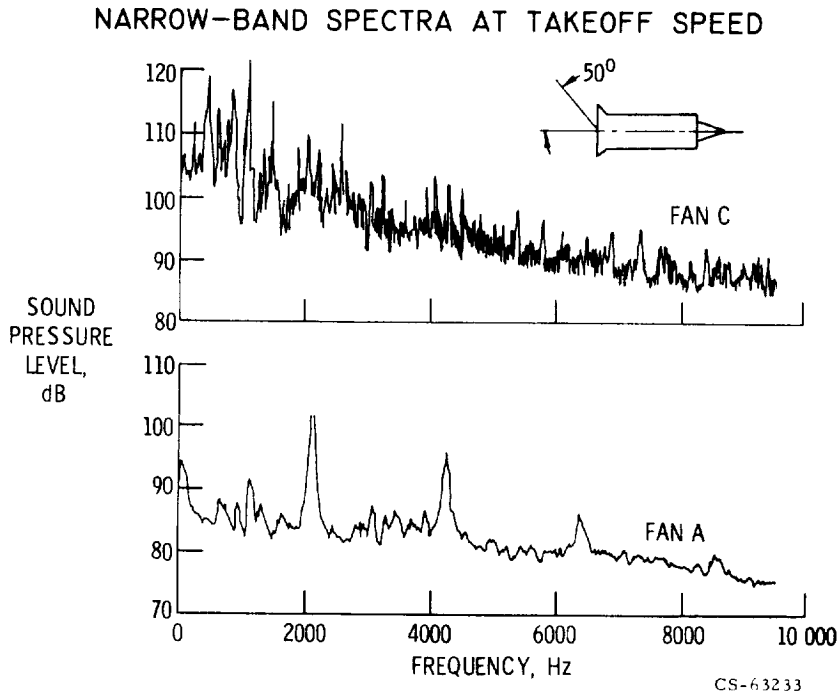
NARROW–BAND SPECTRA AT TAKEOFF SPEED
50°
FAN C
FAN A
SOUND PRESSURE LEVEL, dB
120
110
100
90
80
110
100
90
80
70
0
2000
4000
6000
8000
10 000
FREQUENCY, Hz
CS-63233

Figure II-49

FAN NOISE

90 000 POUND TAKEOFF THRUST; 1000 FOOT FLYOVER

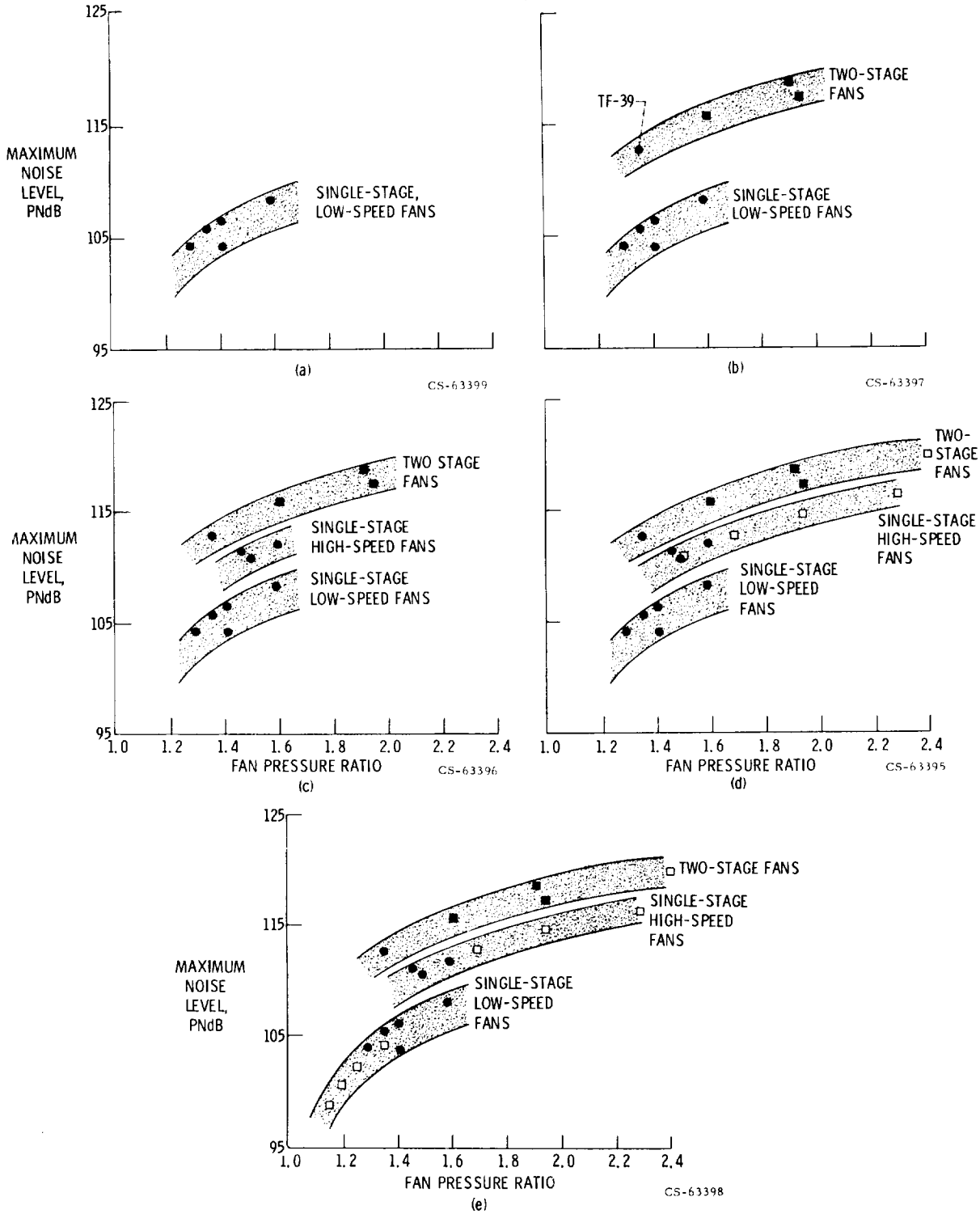

Figure II-50

III. FAN NOISE SUPPRESSION

Charles E. Feiler, John F. Groeneweg, Edward J. Rice,
Edward B. Smith,* and Roger H. Tucker**

A significant reduction in noise can be achieved, even for low-noise fans, by the use of acoustic suppression. Acoustic suppression may be attained by using sonic inlets or acoustically treated surfaces, which are discussed in this paper. Acoustically treated surfaces suppress noise by converting acoustic energy to heat through friction and turbulent dissipation.

Suppression requirements and the limits to suppression are treated first. Then the important suppressor parameters and how they influence suppressor design are shown by drawing on theoretical studies and laboratory experiments. Finally, data from full-scale fan suppressors are presented, and estimates of the performance penalties associated with suppression are made.

The internal noise sources of a turbofan engine are shown in figure III-1. It is important to recognize that acoustic linings (suppressors) can affect only noise originating within the engine and not that originating outside the engine. The important sources to consider are the fan, the turbine, and the compressor. Noise from these rotating elements propagates out the engine inlet and the fan and core exhaust nozzles. The relative level of noise from these sources in an unsuppressed engine is shown in figure III-2. The exact relation of these levels will depend on the particular engine cycle; but, in general, fan noise is the dominant source for turbofan engines and, as shown in this figure, it determines the total engine noise. At an appreciably lower level is the core engine noise, dominated by the turbine noise, and then perhaps at a still lower level is the external jet noise.

The same engine with internal noise suppression might appear as shown in figure III-3. The inlet has treatment on three splitter rings and on the

*General Electric Company.
**The Boeing Company.

outer cowl wall and an extended centerbody. The fan exhaust duct has treatment on the inner and outer cowl walls and on a single splitter ring. Similarly, treatment is located in the inlet of the compressor and in the core exhaust duct.

With this suppression added, the relative noise levels might be as shown in figure III-4. The fan and core noise levels are shown reduced to the jet noise level, and the total noise is therefore equally determined by the three sources shown. It is important to recognize here that the total noise can be reduced about 5 PNdB more by further reducing fan and core engine noise. At that point the total noise is solely determined by jet noise and no benefits can be obtained by more acoustic suppression. The jet noise thus determines, or limits, the amount of suppression that can usefully be employed. It is a noise floor that is ultimately reached. In practice, there are other noise sources or noise paths that may set floors to limit the useful suppression at levels above the jet noise floor. For example, a possible floor might be set by the scrubbing noise of the high-velocity air over the suppressor and cowl surfaces, or by radiation of noise through the engine casing. In any case, it is important to note that there is a finite amount of suppression to be achieved by acoustic treatment.

NOISE SPECTRUM CHARACTERISTICS

In order to determine the suppression design requirements, the fan noise spectrum characteristics must be known. These are examined for a low-speed fan in figure III-5. At a far-field measurement position the typical 1/3-octave-band sound pressure level spectrum shown in this figure is composed of fan noise and jet noise. The fan noise consists of a broadband spectrum with superimposed tones which are equal to the blade passing frequency (and multiples) of the fan rotor. Fan noise suppression can be attained in the frequency range from about 400 hertz to 10 kilohertz since the fan noise is higher than the jet noise in this range.

In figure III-6, the far-field sound pressure level spectrum produced by a high-speed fan is compared to the previously shown low-speed fan noise spectrum. This spectrum is typical for high-speed fans at the "takeoff"

power setting in the front quadrant of the fan. At low power settings and in the aft quadrant at takeoff power, the spectra produced by the high- and low-speed fans are very similar. The noise component added by the high-speed rotor in the forward quadrant ranges from 100 hertz to the blade passing frequency fundamental and is the result of a series of "tones" which are multiples of the rotor shaft rotational frequency. These tones, commonly referred to as multiple pure tones (MPT) or "buzz saw" noise, are an additional fan noise element requiring suppression. The suppression of this noise is discussed in the section FULL-SCALE FAN SUPPRESSION TESTS.

The primary concern of noise suppression is to reduce the annoyance of fan noise. The typical forward-radiated spectra are plotted in figure III-7 as the annoyance in NOY units as a function of frequency. The NOY weighting tends to emphasize the energy in the 3150- to 4000-hertz range, which consequently emphasizes this frequency in terms of required suppression. The weighted jet noise spectrum is now a very flat "floor."

Required attenuation spectra are plotted in figure III-8. These were obtained by determining the sound attenuation necessary at each frequency to bring the attenuated spectra down to a constant annoyance level. This annoyance level was set by the peak in the weighted jet noise spectrum shown in figure III-7. Again, the larger low-frequency fan noise produced by the high-speed fan is peculiar to the forward quadrant at "takeoff" power settings only. The conclusion from this figure is that the acoustic treatment designed and placed both in the fan inlet and the exhaust must cover a very wide frequency range and produce peak suppressions in far-field sound pressure levels close to 30 decibels.

In order to accomplish maximum suppression in terms of ΔPNdB, three important acoustic treatment design parameters must be considered. These are shown in figure III-9. The level of peak sound pressure level attenuation is important and is determined by the maximum required attenuation of curves such as those shown in figure III-8. The frequency where peak suppression is obtained is important since the maximum contribution to the NOY-weighted spectrum usually requires the maximum attenuation (fig. III-7). Finally, the bandwidth of the attenuation spectrum should be made as wide as possible in order to attenuate effectively the very wide fan spectrum shown in figure III-8. The important treatment design parameters

which are used to design acoustic treatment which achieves these established fan noise suppression requirements are discussed in the next section.

SUPPRESSION PARAMETERS

An enlarged view of a section of the exhaust suppressor of an engine is shown in figure III-10. Some of the more important parameters are shown: the duct height H is the distance between lined walls; L is the liner length. The wall impedance is an important parameter which is treated in some detail later in this section. The environmental parameters include the steady-flow Mach number M and the incoming noise spectrum.

Sound propagation theory is available for such a lined duct, but the details of this theory cannot be covered here. However, some of the more important results of the theory are presented. The theoretical parameters are listed at the bottom of the figure. These include the frequency parameter fH/c in which f is the sound frequency, H is the height between the lined surfaces, and c is the speed of sound.

The frequency parameter can be related to the duct height in sound wave lengths H/λ. Other important parameters are the treated-duct length-height ratio L/H, the steady-flow Mach number M, and the wall impedance. The initial sound pressure profile at the duct entrance is a very strong parameter in determining the sound attenuation since it determines the modal content within the duct. The various modes are attenuated at different rates, and the overall attenuation is thus governed by the modal content. Of all the possible modes, one is of particular interest since it damps slower than the rest. This is referred to as the least-attenuated mode. In fairly long ducts, this will be the only remaining mode and the attenuation will be determined primarily by this mode.

Another initial condition is a plane pressure wave at the lined duct entrance. This will excite several modes within the lined duct.

Spinning modes were mentioned in the preceding paper. With these, several pressure maxima and minima occur around the circumference of the duct. This entire pressure pattern may be spinning around the duct axis.

This pressure pattern may be produced by the spinning rotor or by the rotor-stator interaction. In general, these modes will damp more rapidly than the axisymmetric modes.

The first result to be considered is the effect of the frequency parameter on the peak sound attenuation (fig. III-11(a)). The ordinate of this figure is the peak attenuation normalized by the duct length-height ratio. This normalization collapses all the various curves for different L/H ratios onto one curve. The abscissa is the frequency parameter fH/c. The peak attenuation is the maximum possible attenuation obtainable with a particular geometry (L and H) at a given sound frequency. This sound attenuation is obtained at a unique wall impedance called the optimum impedance, which is discussed later in this section.

In the typical attenuation spectrum presented in figure III-8, the peak attenuation and the frequency at which the peak occurs can be associated with the parameters shown here.

The important point in figure III-11(a) is that at high values of the frequency parameter only small attenuations can be obtained unless very large duct L/H values are used. To increase the attenuation, the duct height H must be made smaller, which leads to splitters in large ducts. A reduction in duct height decreases the frequency parameter and increases the attenuation. A practical range of operation for a turbofan engine might be in the frequency parameter range of 0.75 to 2.

For a better picture of what the frequency parameter really means we can select several sample points along this curve and show some specific examples. This is done in figure III-11(b). For these sample inlets, the duct diameter is 6 feet, the frequency for peak attenuation is 2000 hertz, and a peak attenuation of 20 decibels is considered.

The frequency parameter with a single splitter ring is quite large due to the large distance between treated surfaces. To get the 20-decibel attenuation, a large duct length must be used. If two splitter rings are used, the duct height and frequency parameter are decreased. A considerable reduction in suppressor length is achieved over the single splitter case.

As three and four splitter rings are used, the length of treatment is progressively shortened; however, more and more of the inlet area is blocked with these splitter rings. The Mach number will be increased, and

thus the losses increased, unless the outer cowl is expanded to accommodate the flow.

As the treated length is shortened in these examples, more rings are required. It is interesting to see the relative area of suppression required for this variety of inlets. This is shown in figure III-12. In this figure, the relative suppressor area is plotted against the number of splitter rings. All areas are normalized by the area required with wall treatment only. As the number of splitter rings is increased, the total suppressor area is substantially reduced. Again it should be recognized that as the wetted area of suppression is reduced the inlet area blockage is increased and thus the Mach number is increased. Also as the number of splitter rings is increased, the inactive area is increased due to leading and trailing edges. In any real case the number of splitter rings should be selected so that the necessary attenuation is obtained with the minimum pressure loss.

In figure III-13, the effect of Mach number on peak attenuation is shown. The zero Mach number curve is the same as on figure III-11(a); however, two additional curves are shown. The top curve is for a Mach number of -0.4. The negative sign implies that the sound is propagating in a direction opposing the steady flow. This is the case found in the fan inlet. The bottom curve is for a Mach number of 0.4. Here the sound propagates in the same direction as the steady flow. Positive Mach numbers thus imply the case found in the exhaust duct.

The most important point in figure III-13 is that the peak attenuation is a function of Mach number only for values of frequency parameter below about 1.5. Low values of frequency parameter, of course, imply very low frequencies or small duct heights. In this case the sound will attenuate faster in the inlet than in the exhaust duct.

For values of frequency parameter above 1.5, the peak attenuation is not a function of Mach number and the approximate equation shown in the figure can be used. The attenuation is proportional to duct length divided by duct height squared. This emphasizes the strong effect of duct height on attenuation. Doubling the length only doubles the attenuation, while decreasing the height by a factor of 2 increases the attenuation by a factor of 4.

In this section, theoretical results have been discussed to show trends and relationships between the several variables. The theory has been kept

as simple as possible so as not to complicate the picture any more than necessary. In figure III-14, some data are compared with theoretical results. The peak sound attenuation normalized by duct length-height ratio is plotted against frequency parameter. The limits of plane wave theory are indicated by the dashed lines. This plane wave description implies that the initial pressure wave at the duct entrance is uniform across the duct. The plane wave excites several modes within the lined portion of the duct. The normalization by L/H does not collapse all of the peak attenuation curves for various values of L/H onto a single curve. Instead several curves are obtained, and the band indicated encloses these curves over a wide range of duct length-height ratios.

Superimposed upon these theoretical results are experimental peak attenuations from several sources. These include engine, fan, and duct data. The important point is that the experimental data and the theoretical curves follow the same trend with frequency parameter. The attenuation magnitudes agree fairly well with the theory also.

Important ingredients in the propagation analysis are the properties of the soft walls of the passage. A schematic cross section through a soft wall is shown in figure III-15. The wall structure consists of a porous face sheet, shown with just one opening for simplicity. Behind the porous face sheet are resonant cavities. Pressure fluctuations, including acoustic disturbances, near the wall cause gas to flow in and out of the opening with velocity V. During the process, energy in acoustic form is removed from the duct by transforming it into disordered gas motion which eventually results in heating of the gas.

For purposes of analysis, the response of the soft wall to sound is characterized by impedance, which is the ratio of the pressure to velocity (fig. III-16). Impedance has two components. The part corresponding to pressure and velocity variations which are in phase is termed resistance. This is related to the dissipation of acoustic energy by flow through the porous wall. Resistance is inversely proportional to porosity.

The part of impedance which corresponds to pressure and velocity variations which are out of phase is termed reactance. Two mechanisms contribute to reactance. One is the inertia of the gas moving in and out of the wall. The other is the compliance of the gas in the cavity as compression

and expansion occur during inflow and outflow. This compressibility is a large factor in the reactance and is inversely proportional to cavity volume or depth.

In addition to geometric parameters such as porosity and cavity volume which influence impedance, environmental conditions also affect the acoustic response of the wall. The spectral levels and frequencies are important along with the steady-flow field as indicated by the mean velocity profile at the wall. Models have been developed, at least for simpler wall constructions, which relate impedance to both geometric and environmental parameters. Experimental methods of measuring impedance under realistic environmental conditions are also being developed and applied.

In the following figures these two components of impedance are referred to in nondimensional form arrived at by dividing by the impedance of free air.

Now consider what analysis indicates about the values of resistance and reactance which will maximize the dissipation of acoustic energy, that is, maximize the attenuation of sound as it propagates down the duct. In figure III-17, the desired, or optimum, impedances are shown versus the frequency parameter fH/c. For a fixed passage height, theory indicates that as the frequency at which we want to maximize attenuation is increased, resistance should be increased and reactance decreased. In physical terms this means that at low frequencies, wall structures must be thicker and more porous, while for high-frequency tuning they must be thinner and less porous.

The situation shown in figure III-17 is for no steady flow in the duct, $M = 0$. Fixing the frequency parameter at a particular value, for example $fH/c = 1$, and varying the passage Mach number leads to the optimum impedance shown in figure III-18. As before, negative Mach numbers refer to inlet cases and positive Mach numbers to exhaust cases. Maximizing inlet attenuation requires thinner, less porous wall constructions. As the exhaust Mach number increases, optimum resistance and reactance tend toward zero, which leads to the specification of thicker, more open structures. Thus, the propagation theory specifies desired wall impedance values. Models and experiments must be used to translate these wall impedances into actual geometric constructions.

ACOUSTIC LINER DESIGN

In figure III-19 four types of lining construction are illustrated. The lining in the upper left position is a single-layer lining formed with a perforated plate bonded to a honeycomb cellular structure. The perforated plate is the resistive impedance element, while reactive impedance is due to both the perforated plate and the air volume in the honeycomb cells.

The lining in the upper right position is also a single-layer lining; however, the facing sheet is a layer of porous material. This material may be woven or fibrous, metallic or nonmetallic. The lining in the Quiet Engine nacelle is an example of this type of construction. In this application, the porous facing sheet is laminated from glass cloth impregnated with polyimide resin.

Both the perforated plate and porous layer lining construction can be designed for equivalent acoustic performance.

A bulk absorber is shown in the lower left corner. Both resistive and reactive impedance results from the porous material under the perforated facing sheet. The porous material may be either metallic or nonmetallic fibers or foams. The facing sheet generally has high porosity and is normally used as a protective cover rather than as a significant contributor to lining impedance.

The last example is a double-layer lining formed with porous outer and inner facing sheets and two honeycomb structures. With this construction, the two layers are designed to attenuate noise at two frequencies. Two segments of this type of lining construction are located in the Quiet Engine nacelle fan duct.

A multilayer lining is shown in figure III-20. Like double-layer acoustic linings, the purpose of this construction is to provide peak attenuations at multiple frequencies. This example shows a perforated sheet covering an X-shaped core structure. The walls of the core are perforated to form resistive elements between the adjacent cells. This construction is used in the Quiet Engine fan frame and compressor inlet duct.

In the next three figures, the merits of particular lining constructions with regard to their impedance properties and acoustic performance are compared. In figure III-21, calculated impedance properties of single- and

double-layer linings are compared with the optimum impedance. The example is based on designing for the least attenuated acoustic mode. The upper group of curves shows that the optimum normalized resistance increases with increased frequency parameter fH/c. The dot-dash curve shows the resistance of a single-layer lining designed for optimum attenuation at an fH/c of 0.75. Its resistance also increases with frequency parameter but at a slower rate. The dashed line is the resistance of a double-layer lining. This lining has been designed to be optimum at fH/c values of 0.75 and 1.5, which is illustrated by the intersection of the double-layer resistance curve with the optimum at these two points.

The lower group of curves shows that optimum reactance decreases with increasing frequency parameter. The single-layer lining has the opposite trend and is near optimum only in the region of the design point. The reactance of the double-layer lining is similar to the single layer at values of fH/c below the design point. Above the design fH/c the reactance increases and then decreases to the optimum value at an fH/c of 1.5.

In figure III-22 the calculated acoustic performances of these two linings are compared. No difference is noted in 1/3-octave attenuation between the single- and double-layer linings below the peak at a fH/c of 0.75. Above this point, the single-layer lining attenuation decreases continuously. The double-layer lining attenuation also decreases after the first peak and then increases to peak at its second design point at an fH/c of 1.5.

In this example, the increased bandwidth of the double-layer lining over the single layer is achieved with no increase in lining wetted area and only a 16-percent increase in lining thickness.

Double-layer acoustic linings can broaden the attenuation spectrum over that of a single-layer lining. However, in low-noise applications, use of only one double-layer construction may still not provide satisfactory attenuation over an adequate frequency range. An alternate is to combine several lining constructions to provide sufficient bandwidth, as shown in figure III-23. The curve shows sound attenuation versus frequency for three single-layer linings marked A, B, and C, with peaks at three different frequencies. Note that the total attenuation spectrum is much broader than any of the individual components.

This combination of different wall constructions can be done in two

ways, as shown in the inserts on the figure. The first sketch illustrates a series combination with similar linings opposing each other on the two walls. The second method is parallel construction, as illustrated in the second sketch. In this case, the opposite walls have different lining constructions. This parallel combination is desirable when a single splitter is used since the thinner high-frequency linings can be located on this splitter to minimize ring thickness and to reduce aerodynamic losses. The thicker low-frequency linings are then located on the duct walls. Current propagation models are based on ducts with the same lining construction on opposite walls; consequently, series combination of linings is better understood. However, it is anticipated that the parallel combination can be an effective design option after propagation models are established for optimizing linings with dissimilar construction on opposite walls.

EXPERIMENTAL METHODS

One method of evaluating the performance of acoustic treatment in a fan duct is to measure the noise reduction in a test which simulates the conditions in the fan passages as closely as possible. The airflow through the duct, the incident sound pressure level spectrum, and the duct geometry are readily simulated. Simulation of mode structure is also desirable but difficult to achieve without the use of a fan. Figure III-24 shows a schematic of such an acoustic flow duct that provides this simulation except for mode structure. Two reverberation chambers are connected by a rectangular test duct which can be treated selectively on each of the duct walls. Splitters can be tested also. A high-intensity noise source is located in one chamber with a microphone which measures the input spectrum level. A microphone in the other chamber detects the acoustic signal with and without the acoustic treatment in place in the duct. Airflow direction can be reversed to simulate both inlet and exhaust configurations. By varying the airflow rate and input frequency the performance of the acoustic treatment configurations can be measured at Mach numbers and sound pressure levels typical of a full-scale fan.

An alternate approach to this measurement scheme is shown in figure III-25. As before, a steady airflow can be passed through the duct with

Mach numbers equivalent to those found in typical engine flow passages. The height between treated walls can be varied to simulate engine duct geometry. For the case shown here, the noise source is downstream of the treatment test section and therefore simulates the inlet mode. By moving the source downstream of the facility noise muffler and upstream of the treatment section, the exhaust mode is set up. The noise reduction produced by the treatment is measured by traversing acoustic probes which measure the sound pressure level distribution between the treated walls and permit the calculation of sound energy reduction by the treatment.

These facilities provide a means to evaluate treatment effects such as duct geometry and wall impedance that can be correlated to give design procedures or used to guide theoretical studies. They can also be used to evaluate novel wall treatment constructions that are not amenable to any theory.

COMPARISONS BETWEEN THEORY AND EXPERIMENT

An example of a measured and calculated sound attenuation spectrum is shown in figure III-26. The measurements were obtained as described previously in the reverberation chamber facility at a Mach number of 0.28, and it can be seen that the theoretical curve predicts the main features of the measured attenuation spectrum.

Another example of experimental duct data is shown in figure III-27. These data were taken in the acoustic flow duct facility (fig. III-25). These data, with repeat points, were acquired with pure tones and consequently exhibit more experimental scatter than in the previous example. Again the main features of the experimental data are reflected by the theoretical prediction.

In order to calculate the theoretical duct attenuation accurately, the acoustic impedance components are a required input. The effects of sound pressure level and grazing flow must be incorporated in the impedance model. In order to determine the accuracy of the theoretical impedance model, measurements of the impedance components of a single-layer treatment in the presence of grazing flow have been made in a flow duct similar to

the one shown in figure III-25. A comparison of the calculated impedance (for a particular impedance model) with the measured impedance at a Mach number of 0.35 is shown in figure III-28. The acoustic resistance with flow is seen to be very flat with frequency and agrees well with the calculations. The calculated reactance agrees with the measured data at low frequencies but not at high frequencies. Measurements will be relied on in this case and can become the basis for modifying the impedance model.

These comparisons indicate that the acoustic impedance components can be calculated and measured under simulated engine flow conditions, and that the noise reduction capability of acoustic treatment can be effectively tested in laboratory flow duct tests.

FULL-SCALE FAN SUPPRESSION TESTS

Duct test facilities provide a useful tool for screening suppressor materials; however, the noise environment cannot truly simulate that found in the turbofan engine ducts. The Lewis full-scale fan test facility was used to test full-scale suppressors.

Figure III-29 shows a cutaway view of this facility. Shown are the 6-foot-diameter rotor and the stators. The inlet suppressor shown has three splitter rings. The fan is driven by the shaft passing through the inlet. The exhaust duct suppressor has a lined inner and outer cowl with one lined splitter ring.

An inlet which was tested in this facility is shown in figure III-30. This suppressor is 6 feet in diameter and is made up of cylindrical sections. The outer cowl is lined, as are both sides of the three splitter rings. A parallel combination of wall constructions are used for the rings. The outer side of each splitter ring is tuned for high frequency, while the inner sides are tuned for a lower frequency.

Typical noise data obtained with this inlet suppressor on fan A are shown in figure III-31. The sound pressure level spectra at 50° to the inlet for both the unsuppressed and suppressed cases are shown. The dominant blade passage tones are reduced to levels which are barely distinguishable in the suppressed spectrum. The difference between the suppressed and un-

suppressed spectra, that is, the attenuation spectrum, is shown at the bottom of the figure. A maximum attenuation of about 18 decibels occurs at blade passage frequency.

For comparison, the same inlet suppressor was put on high-speed fan C and the results are shown in figure III-32. The unsuppressed spectrum is characterized by strong multiple pure tones which are roughly the same level as the blade passage tone at 2000 hertz. The blade passage tone is nearly indistinguishable in the suppressed spectrum. Since the suppressor was designed for a low-speed fan with a spectrum similar to fan A, its bandwidth was not wide enough to realize uniform attenuation throughout the multiple pure tone range. Although substantial attenuation (about 19 dB) was observed at 800 hertz, the multiple pure tone content at 500 hertz was not reduced as much. Another section of suppressor tuned in that range would have been desirable.

The variation of perceived noise levels with angle is shown in figure III-33 for low-speed fan A. As before, open symbols are for unsuppressed data, while solid symbols refer to the suppressed case. The fan was operating at takeoff speed and the levels correspond to a 1000-foot flyover. About 12 PNdB of suppression was realized in the inlet and about 6 PNdB in the exhaust. For comparison we can superimpose the same type of data for fan C, as shown in figure III-34. It can be seen that the magnitudes of the perceived noise reductions (unsuppressed minus suppressed) were about the same both in the inlet and exhaust as they were for fan A. However, treatment acting over a greater bandwidth is required to bring fan C noise down to levels approaching those of suppressed fan A.

There is some evidence that cowl treatment alone can be very effective in reducing the multiple pure tone noise of high-speed fans like fan C. The results of such a test on fan C are shown in figure III-35. Two attenuation spectra corresponding to the cases with and without splitters are given. Attenuations in the multiple pure tone range, 500 to 1600 hertz, were essentially the same whether or not the splitters were present. This result is not predicted by the analyses discussed previously. Planned suppressor tests on fan C will further explore the characteristics of multiple pure tone attenuation.

Our experience with suppressors on five full-scale fans is summarized

in figure III-36. The maximum perceived noise levels shown are for 90 000 pounds thrust generated at takeoff speed for a 1000-foot flyover. Inlet levels are shown on the left and exhaust levels are on the right. Unshaded bars are unsuppressed levels, shaded regions represent suppressed levels, and the heavy black line is the estimate of fan jet noise. Reductions of 12 to 18 PNdB were realized in the inlet with jet noise a limiting factor only for fan E. On the exhaust side, reductions range from 4 to 10 PNdB. Jet noise was clearly limiting fan E levels. The overall suppressor performance in the exhaust was generally less satisfactory than in the inlet. The possibility of noise being generated by flow through lined exhaust passages operating at higher Mach numbers may be a factor limiting exhaust suppressor performance.

In this connection, some effects of passage geometry on suppressor performance in the aft direction are shown in figure III-37. These data, which were obtained from tests on full-scale fan D, show how splitters can affect noise. Aft sound power spectra are shown for three configurations. The configurations are represented schematically by a cross section through the fan axis. The base case, shown with triangular symbols, is the hard cowl with no splitters. When hard splitters are added, as shown by the open circular symbols, the noise is raised over a broad frequency range. With all passage surfaces soft, the solid circular symbols, the levels are reduced to the lowest values measured except in the small frequency range around 600 hertz where the suppressed levels are not quite as low as those existing without suppression. This result suggests that noise generation processes occur in the lined passages, especially in the fan exhaust. While suppression reduces the noise, it may not remove enough acoustic energy at all frequencies to overcome generation effects.

CORE NOISE SUPPRESSION

In the late 1960's, a program was sponsored by NASA Langley Research Center to reduce fan noise from the Pratt & Whitney JT3D engine. Flight tests with the engine in a quiet nacelle (fig. III-38) reduced fan noise to the point where noise from other sources became significant. For exam-

ple, at approach power settings, fan noise was reduced below the level of turbine noise. A subsequent program was established by NASA Langley to design, fabricate, and demonstrate acoustic treatment of the turbine noise. The tailpipe lining shown in the schematic consisted of brazed stainless-steel perforated sheet/honeycomb linings installed on the tailpipe wall and both sides of a ring installed in the tailpipe. The lining was tested on a JT3D engine housed in a quiet nacelle from the 1969 program.

Figure III-39 shows the treated tailpipe. The tailpipe lining shown in the photograph was analytically designed based on aerodynamic and acoustic measurements obtained within a production tailpipe. The 19-inch-long lining was designed for maximum attenuation of the fourth-stage turbine tone at 5500 hertz at an approach power setting. The linings required for this application had low open areas and thin core thicknesses. For example, the lining on the tailpipe wall and the opposing ring was a 3.44-percent perforated plate with a honeycomb core depth of 0.18 inch. The ring inner lining was a 1.85-percent perforated sheet with a 0.10-inch core depth.

Test results for the lining installed in a JT3D engine are shown in figure III-40. In this figure is shown the 1/3-octave spectrum measured for the treated and untreated tailpipe at a 200-foot radius at a polar angle of 120^{o} from the inlet centerline at the design speed. This is the angle at which the fourth-stage turbine tone has maximum sound pressure level. The shaded area represents the attenuation accomplished by the treated tailpipe. Approximately 11 decibels of suppression were obtained in the 5000-hertz 1/3-octave band containing the fourth-stage turbine tone. The second- and third-stage turbine tones, located in the 8000-hertz band, were attenuated 7 decibels at this angle. The reduction in perceived noise at this angle was 3.9 PNdB.

This program demonstrated that the same lining design and analysis techniques described previously for fan noise suppression can be successfully applied to reducing turbine noise.

INSTALLATION CONSIDERATIONS

To complete the discussion, there are several other aspects of a suppressor that should be mentioned. These are shown in figure

III-41 and categorized as installation considerations. In the inlet, there is concern about anti-icing of the splitter ring leading edges and their support struts and about the ability of these members to withstand foreign object damage.

In the core exhaust, materials and bonding methods must be suitable for the high temperatures that are present. There are also several more general factors that enter into treatment selection. For example, materials and bonding techniques must be selected with a view to their sonic fatigue life. The construction technique must provide a way for water and other contaminants to drain from the backing cavities of the treatment. Still another factor is the pressure loss associated with splitters and with porous or perforated surface materials.

For this purpose, splitters are located by potential flow analysis so that they follow streamlines, and care is taken in the shaping of leading- and trailing-edge surfaces. Some of these considerations are discussed in another paper, which describes the nacelle for the Quiet Engine.

Finally, three standard factors - maintainability, cost, and weight - must be considered.

One question of obvious interest is the performance penalty associated with acoustic treatment. In figure III-42, we have made an estimate of the pressure loss as a function of noise reduction. The estimated total pressure loss in percent is plotted against the estimated reduction in perceived noise level. The estimates are for a value of the frequency parameter between 1 and 2. Curves are shown for three values of the flow Mach number over the surfaces. It can be seen that the losses increase with flow Mach number.

For small noise attenuation the losses are also small; however, as the amount of attenuation increases above about 10 PNdB, the losses increase sharply. This is due to the decrease in treatment effectiveness as treatment length is increased to give the large attenuation required.

The data points shown on the curves are Boeing estimates for the Quiet Engine nacelle. At the cruise and takeoff conditions the Mach numbers in the engine are about 0.6 and 0.48, respectively. This suppressor was designed for about 15 PNdB of attenuation so that these estimates are in reasonable agreement with the curves shown.

It should be emphasized that these curves are only estimates and should not be applied in any general sense. Improvements in suppressor

technology should lead to a reduction in these losses.

SUMMARY

To summarize this discussion, significant noise reductions can be realized by acoustic treatment for all the engines currently under consideration. The amount of reduction will depend on the particular engine cycle and its use. A floor is set to suppression by the jet noise; however, in some practical cases, noise sources other than jet noise seem to limit the benefits of treatment. Work is needed to identify these sources.

The principal suppressor parameters and their relationships have been discussed. These relationships have been used to formulate a suppressor design methodology which has been applied to the design of several full-scale suppressors.

Tests of these suppressors on several full-scale fans have demonstrated noise reductions of the order of 10 PNdB. The amount of suppression in several instances seems to have been limited by reaching noise floors that are not clearly at the estimated jet noise level but are not far above it. It should also be remembered that the fans involved in these tests were designed for as low a noise output as currently possible and therefore the noise to be suppressed is not as far above the jet noise floor as it might be in some other fan stages.

In addition to identifying noise floors, two other areas need attention. The first is attenuation by the fan exhaust suppressors, which seems in most cases to be less than that of the inlet. This, as suggested, may be related to noise generation by the higher velocity air in the fan exhaust duct scrubbing over the splitter and cowl surfaces. The second is the effectiveness of the outer cowl treatment alone on multiple pure tones. We need to understand why this treatment alone is as effective as it is. This question relates to whether a high-speed fan can become as quiet as a low-speed fan without a substantial increase in the amount of treatment.

In the future, substantial improvements in suppressor efficiency should occur as understanding of the mechanisms of suppression improves. In this way, reduced amounts of treatment may be possible with no loss in noise reduction.

INTERNAL NOISE SOURCES

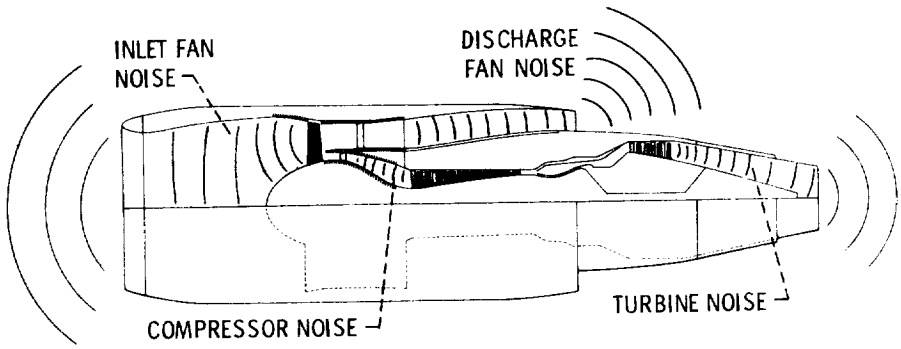

Figure III-1 CS-63268

TYPICAL UNSUPPRESSED SOURCE NOISE

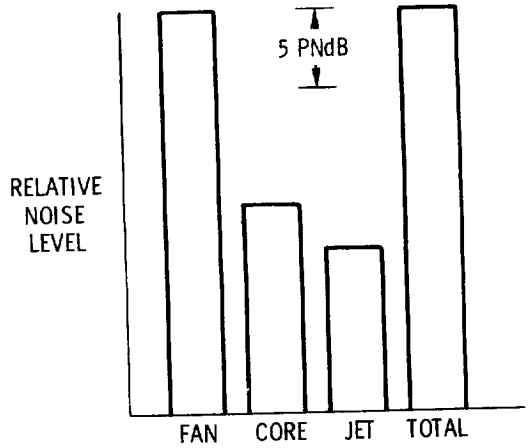

Figure III-2 CS-63190

ENGINE WITH SUPPRESSION

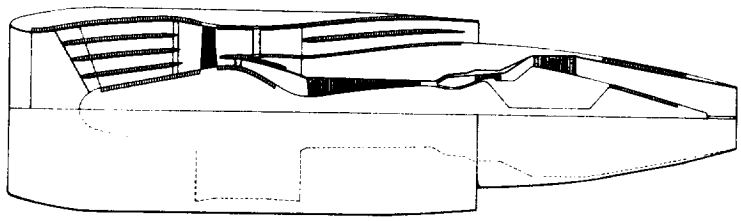

Figure III-3

CS-63329

TYPICAL SUPPRESSED SOURCE NOISE

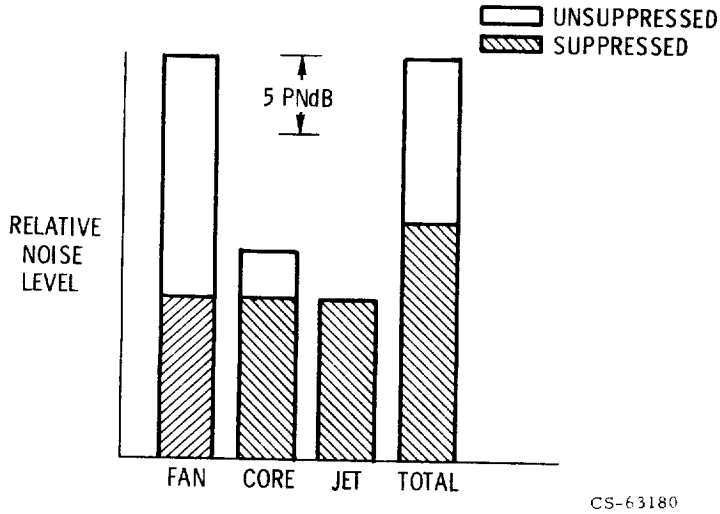

CS-63180

Figure III-4

NOISE SPECTRUM REQUIRING SUPPRESSION - LOW SPEED FAN

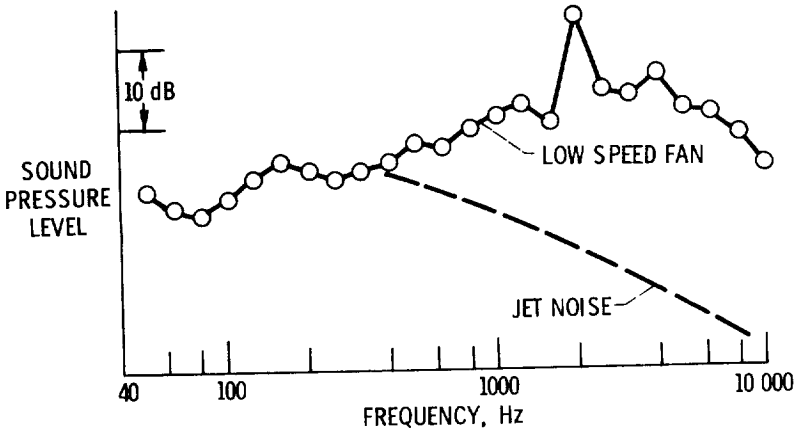

Figure III-5

CS-63186

NOISE SPECTRA REQUIRING SUPPRESSION - LOW AND HIGH SPEED FANS

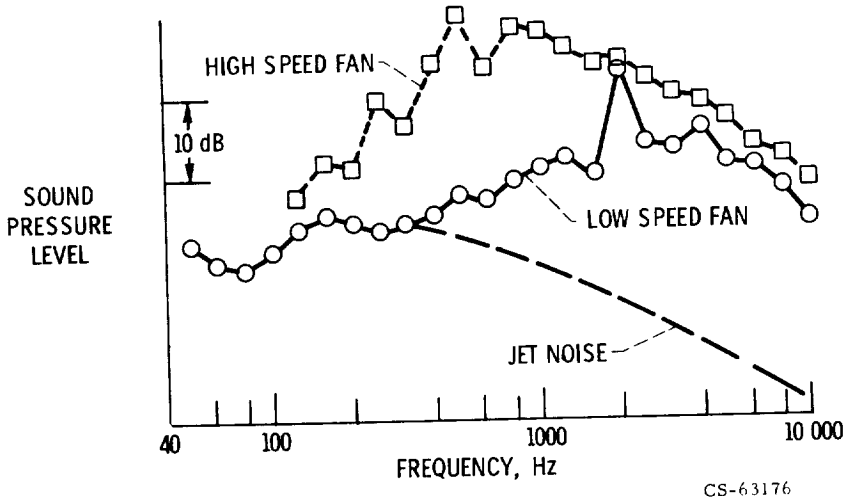

CS-63176

Figure III-6

SUBJECTIVE INFLUENCE ON SUPPRESSOR ATTENUATION GOAL

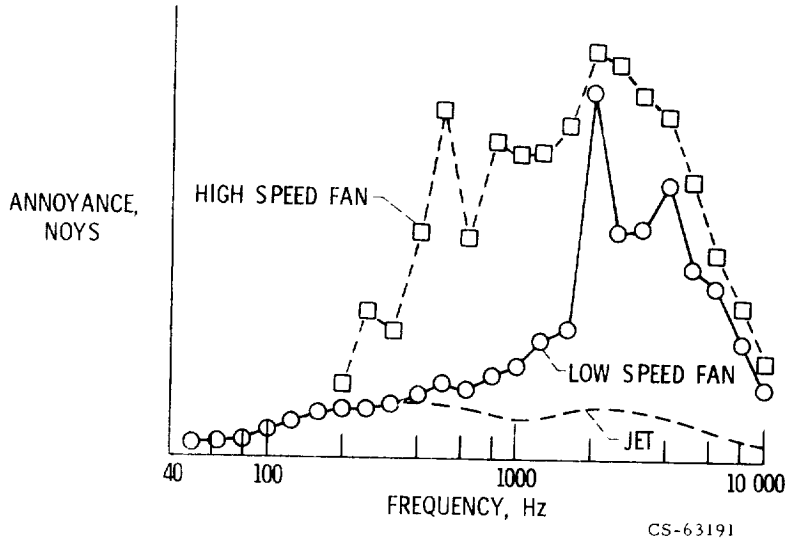

Figure III-7

REQUIRED ATTENUATION SPECTRA - LOW AND HIGH SPEED FANS

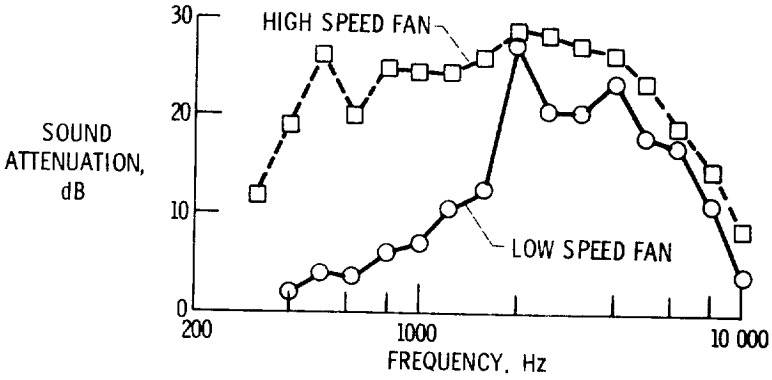

Figure III-8

CS-63181

PARAMETERS FOR TYPICAL ATTENUATION SPECTRUM

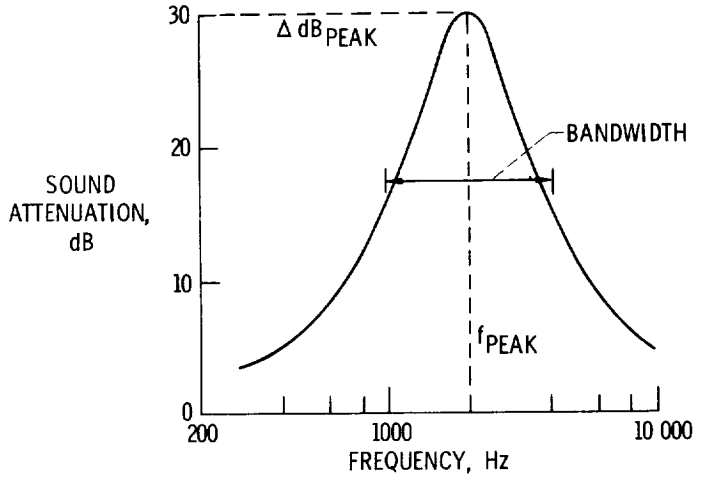

Figure III-9

SUPPRESSION PARAMETERS

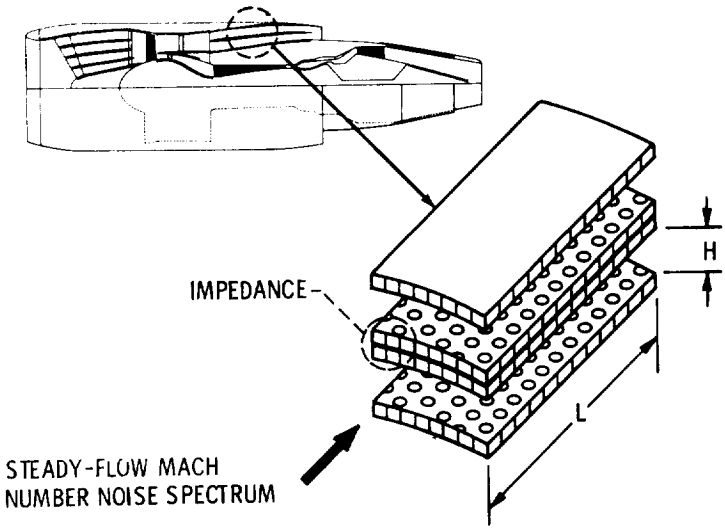

IMPORTANT PARAMETERS: $fH/c \approx H/\lambda$, L/H, M, WALL IMPEDANCE, INITIAL SOUND PRESSURE PROFILE

CS-63332

Figure III-10

EFFECT OF FREQUENCY PARAMETER ON PEAK ATTENUATION

(a) LEAST ATTENUATED MODE THEORY

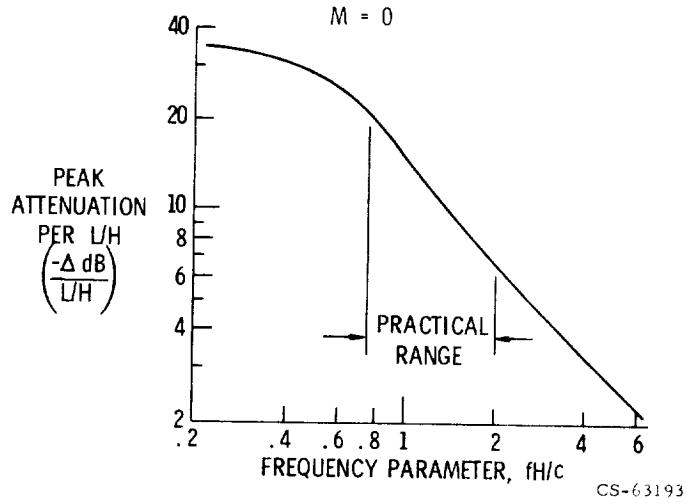

(b) FOR SAMPLE INLETS: D = 6 FT, f = 2000 Hz, ΔdB = -20

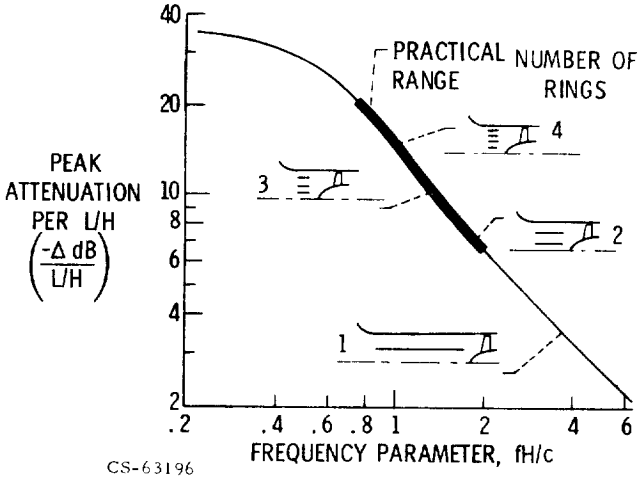

Figure III-11

EFFECT OF SPLITTER RING NUMBER ON REQUIRED SUPPRESSOR AREA

DUCT DIAMETER = 6 FT, f = 2000 Hz

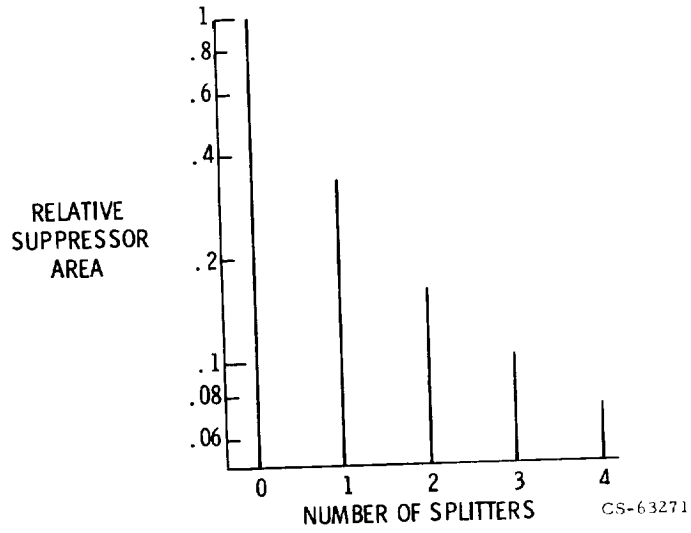

Figure III-12

MACH NUMBER EFFECT ON PEAK ATTENUATION

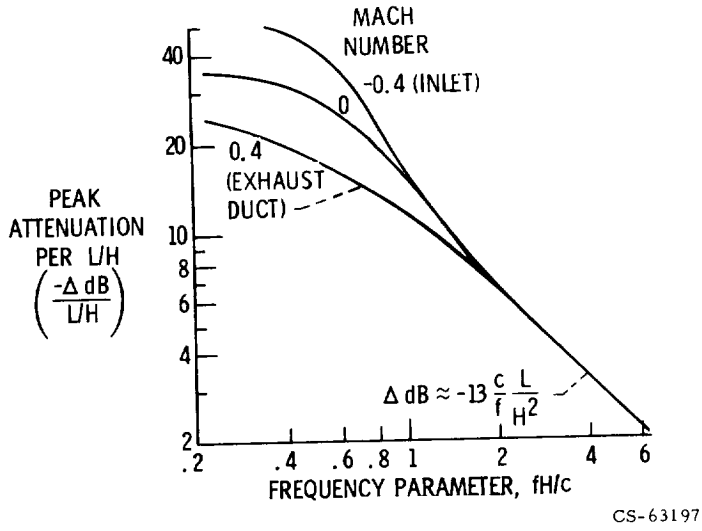

Figure III-13

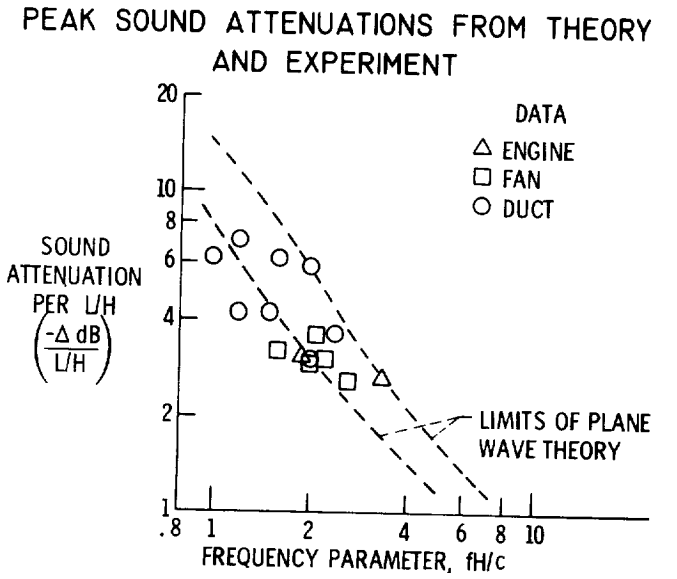

Figure III-14

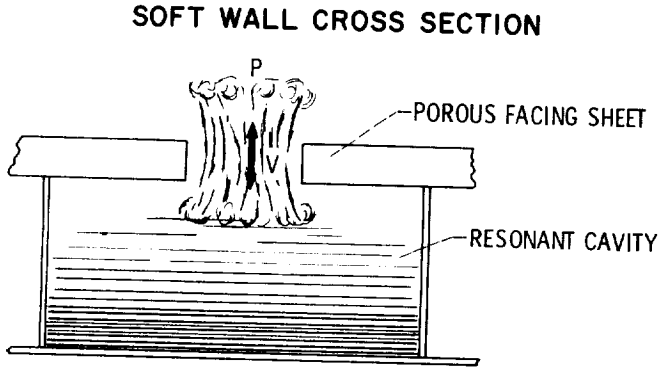

Figure III-15

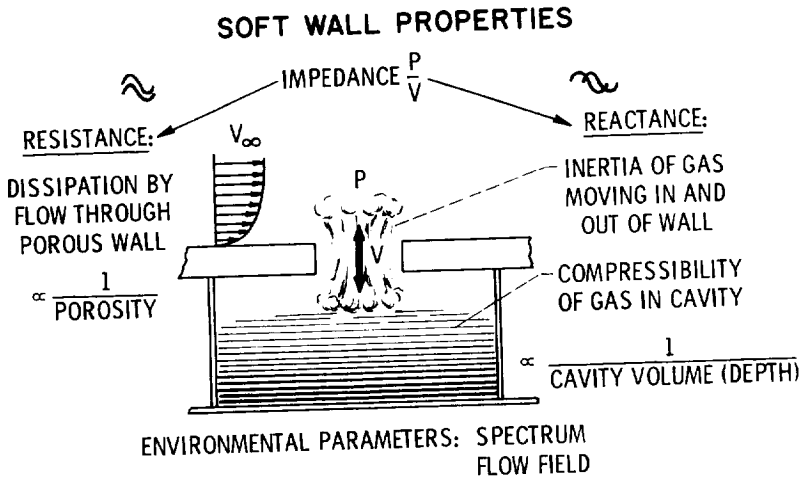

Figure III-16

CS-63266

THEORETICAL IMPEDANCE FOR MAXIMUM ATTENUATION

M = 0

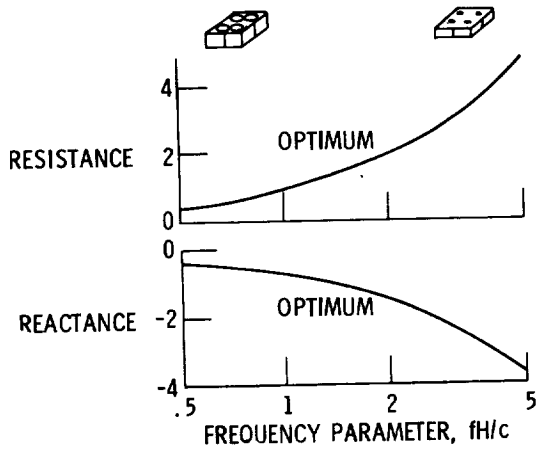

CS-63264

Figure III-17

MACH NUMBER EFFECTS ON OPTIMUM IMPEDANCE

fH/c = 1

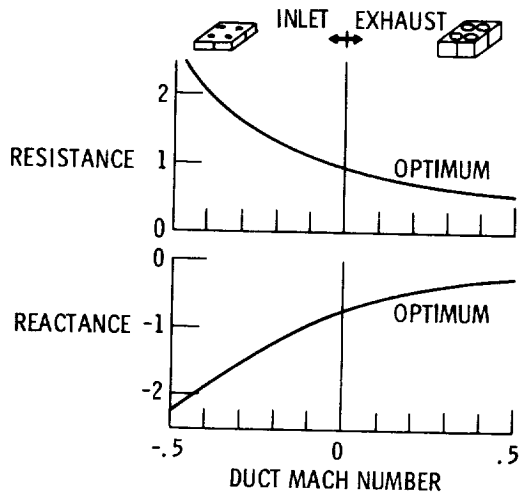

CS-63265

Figure III-18

LINING MATERIALS AND CONSTRUCTION

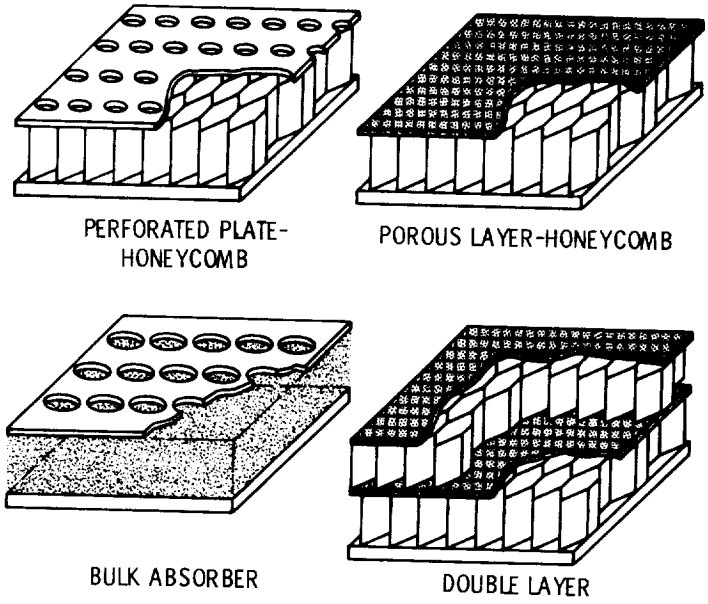

Figure III-19

CS-63330

MULTILAYER WALL CONSTRUCTION

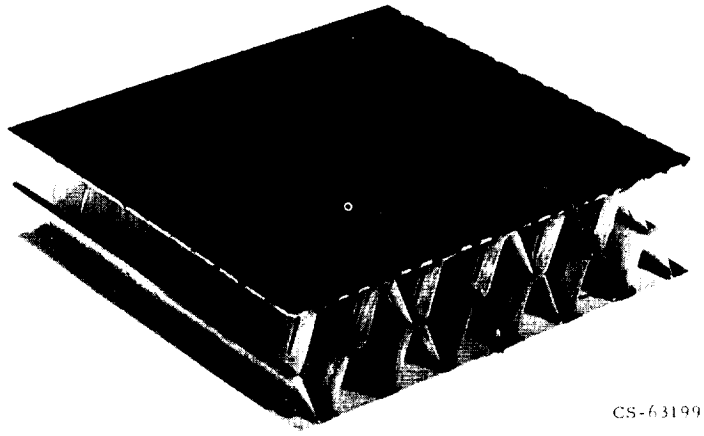

Figure III-20

IMPEDANCE CONTROL BY CONSTRUCTION

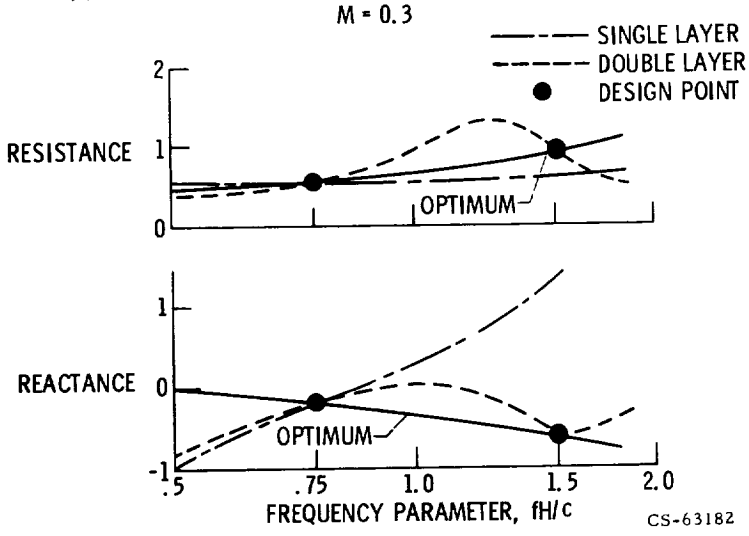

Figure III-21

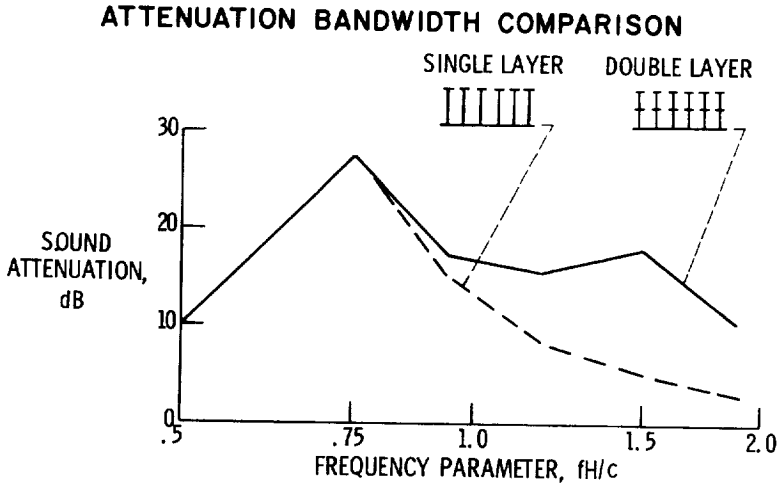

Figure III-22 CS-63183

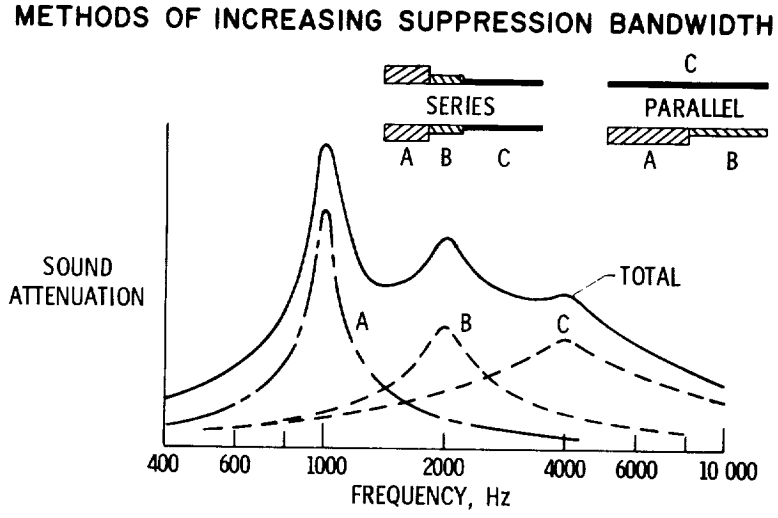

Figure III-23 CS-63178

FLOW DUCT TESTS USING REVERBERATION CHAMBERS

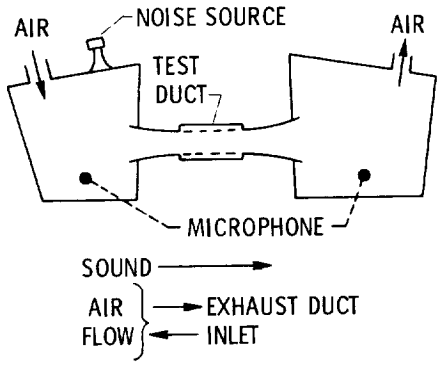

Figure III-24

CS-63177

FLOW DUCT TEST USING SOUND MEASUREMENTS IN THE DUCT

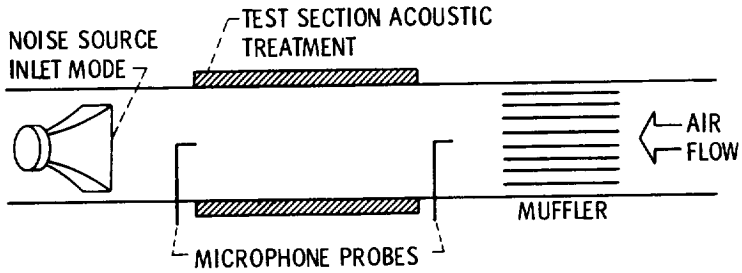

Figure III-25

CS-63272

FLOW DUCT ATTENUATION SPECTRUM
USING REVERBERATION CHAMBER

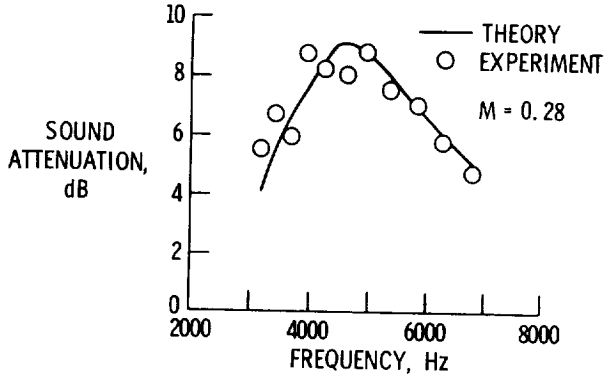

Figure III-26

CS-63198

FLOW DUCT ATTENUATION SPECTRUM
USING SOUND MEASUREMENTS IN DUCT

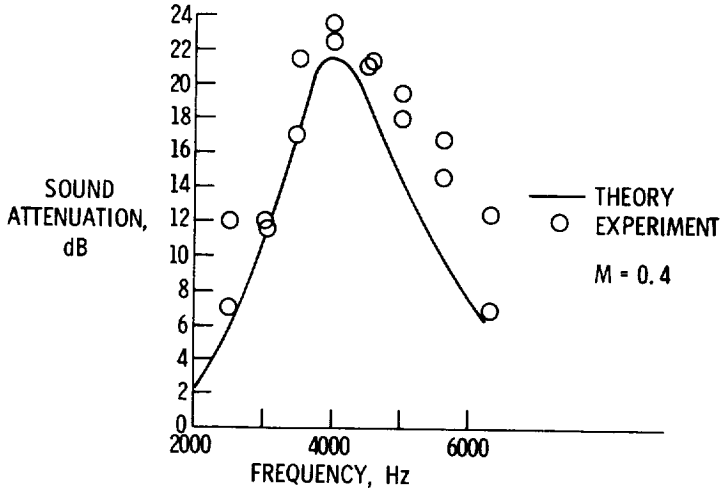

CS-63194

Figure III-27

IMPEDANCE MEASUREMENTS WITH GRAZING FLOW

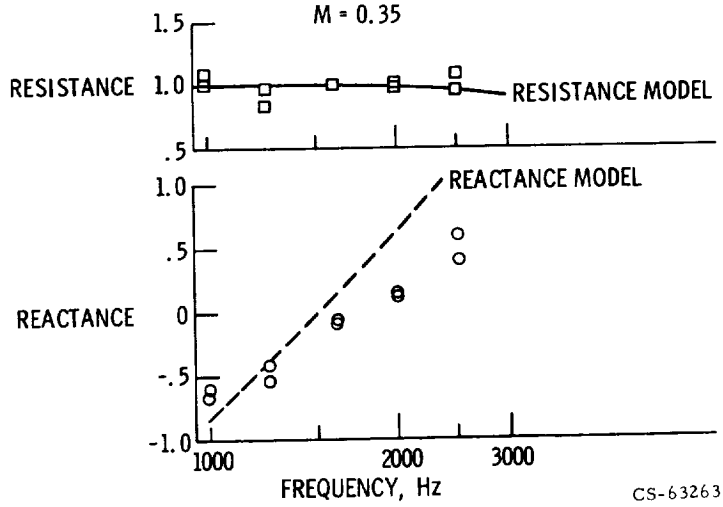

Figure III-28

FULL-SCALE FAN WITH SUPPRESSION

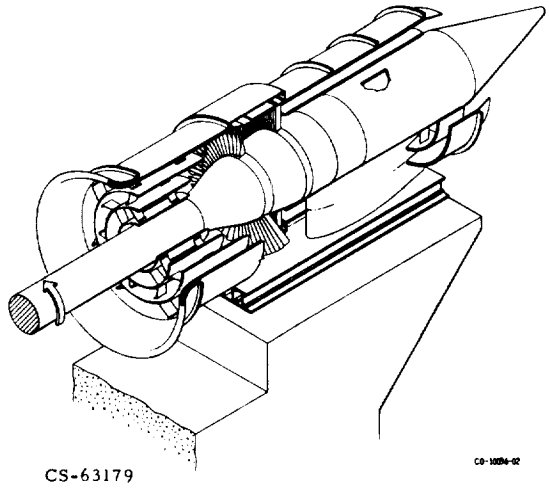

Figure III-29

INLET DUCT WITH ACOUSTIC TREATMENT

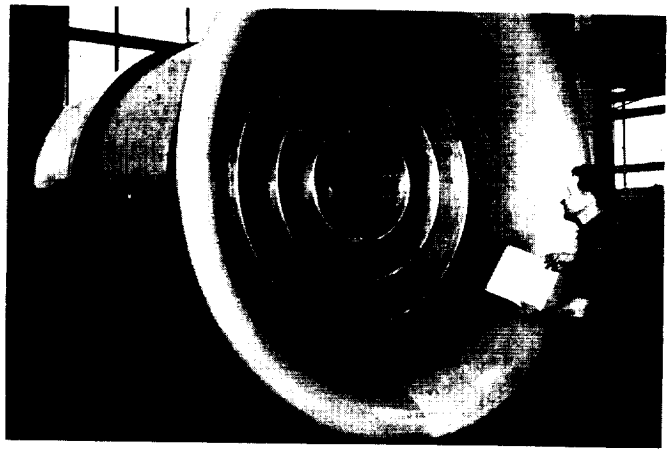

CS-63200

Figure III-30

SUPPRESSOR PERFORMANCE ON LOW SPEED FAN A

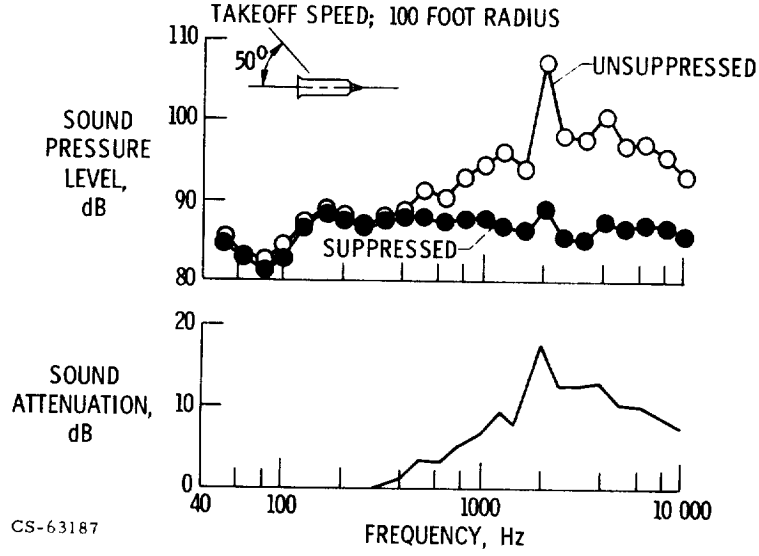

Figure III-31

SUPPRESSOR PERFORMANCE ON HIGH SPEED FAN C

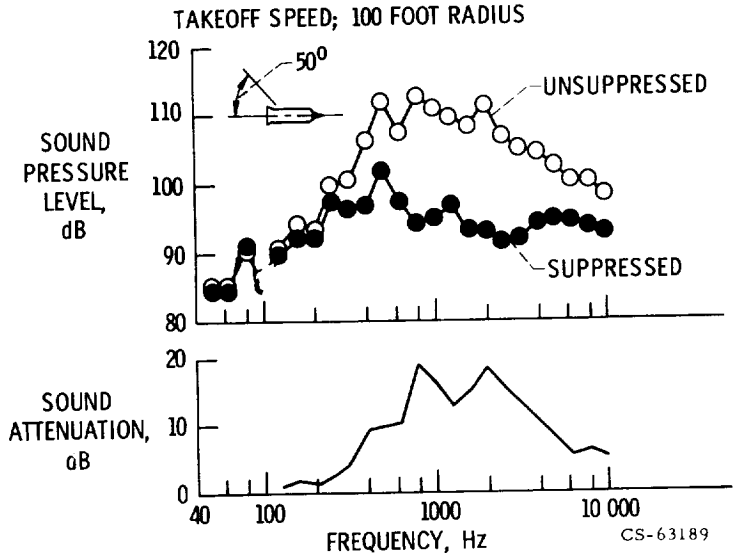

Figure III-32

FAN PERCEIVED NOISE DIRECTIVITY - LOW SPEED FAN A

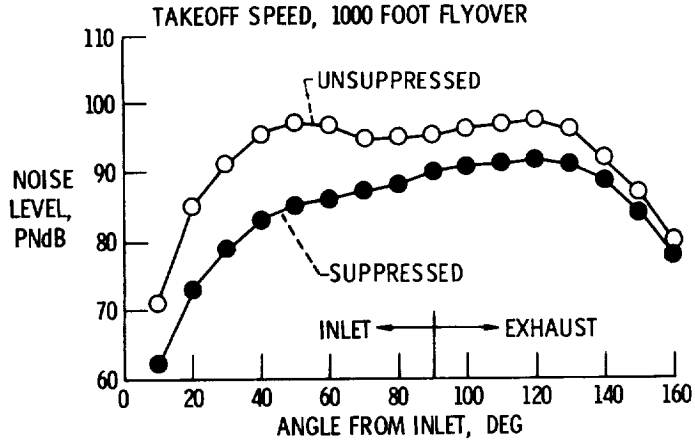

Figure III-33

CS-63184

FAN PERCEIVED NOISE DIRECTIVITY - FANS A AND C

TAKEOFF SPEED, 1000 FOOT FLYOVER

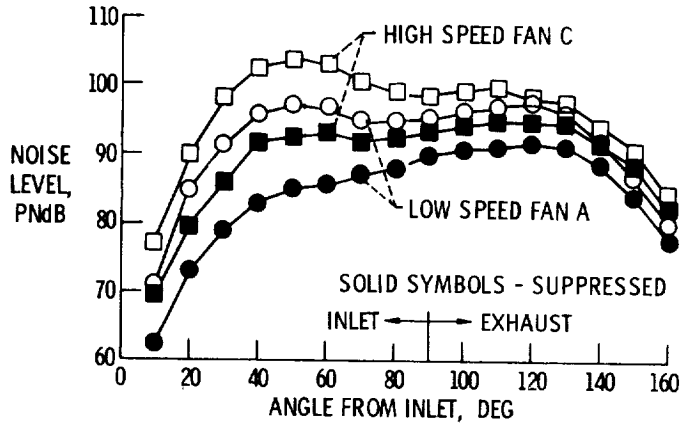

CS-63192

Figure III-34

SUPPRESSOR PERFORMANCE ON HIGH SPEED FAN C

TAKEOFF SPEED; 100 FT RADIUS

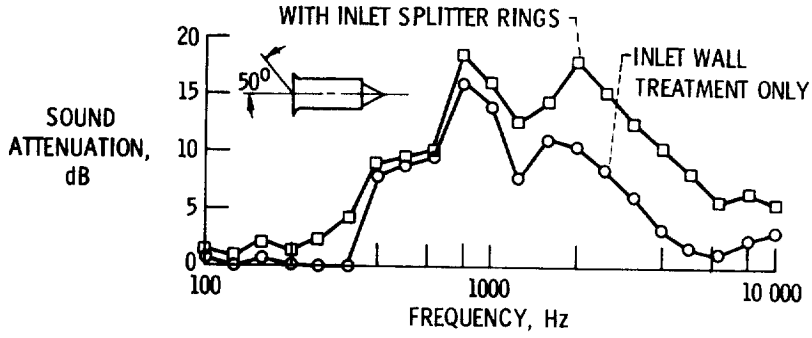

Figure III-35

CS-63445

SUPPRESSOR PERFORMANCE ON FULL-SCALE FANS

TAKEOFF SPEED; 90 000 LB THRUST; 1000 FOOT FLYOVER

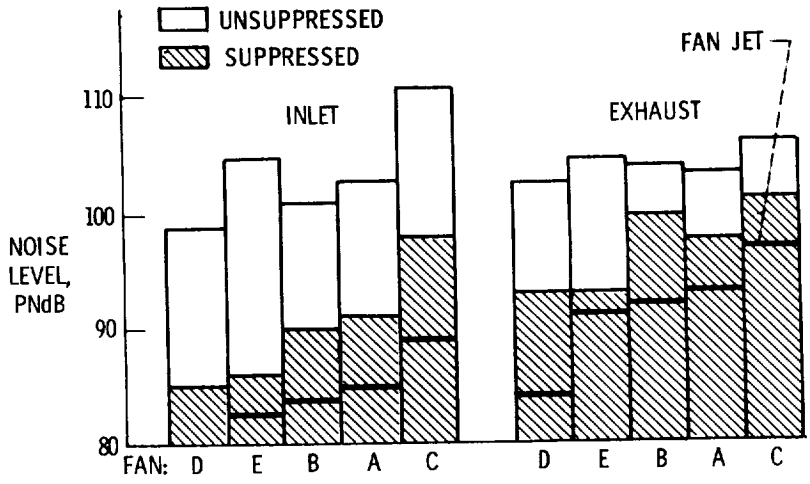

Figure III-36 CS-63174

EFFECTS OF PASSAGE GEOMETRY ON SUPPRESSOR PERFORMANCE

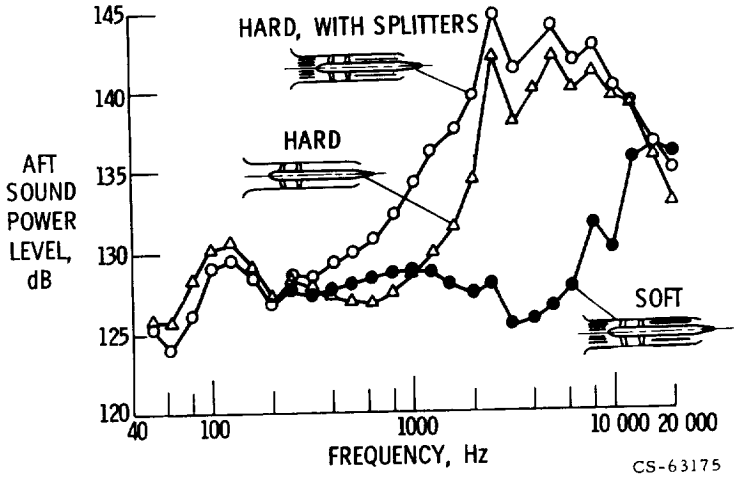

Figure III-37

JT3D TURBINE SUPPRESSOR

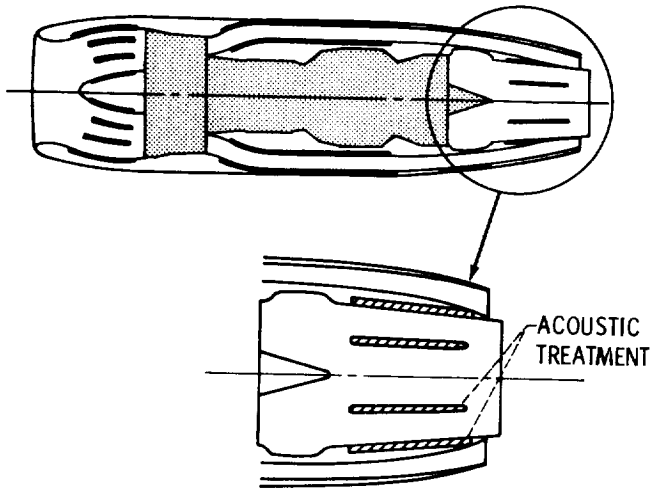

Figure III-38

TURBINE NOISE SUPPRESSOR

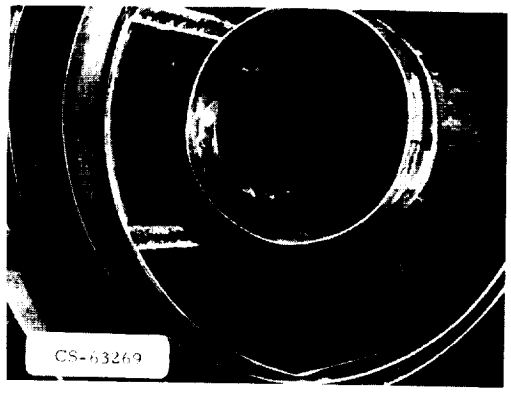

Figure III-39

JT3D TURBINE NOISE SUPPRESSION

APPROACH SPEED; 200 FOOT RADIUS

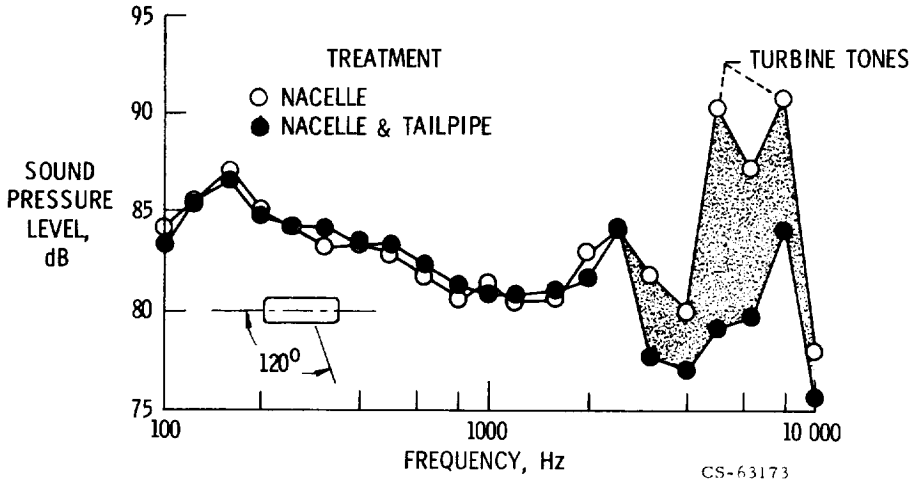

Figure III-40

TREATMENT INSTALLATION CONSIDERATIONS

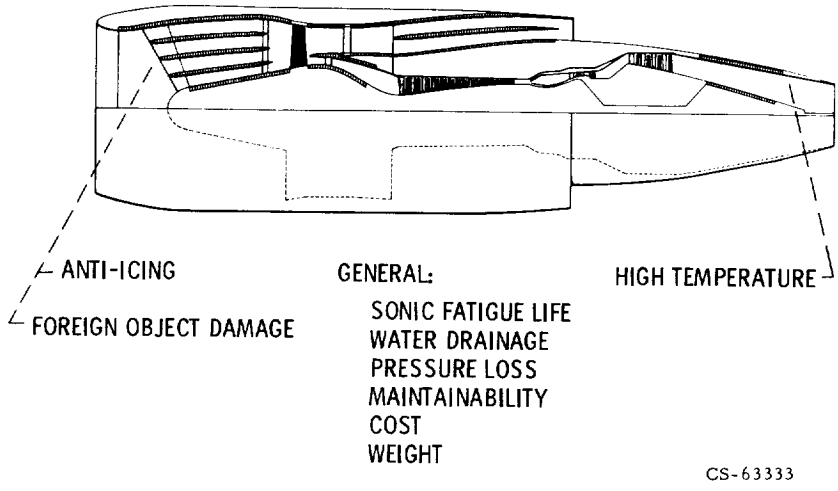

Figure III-41

ESTIMATED PRESSURE LOSS DUE TO SUPPRESSION

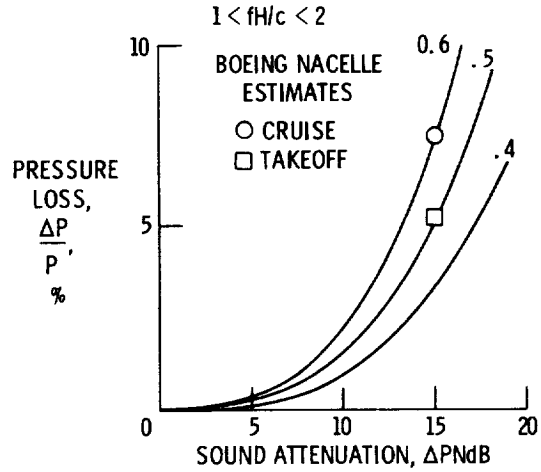

CS-63424

Figure III-42

IV. JET NOISE

Uwe H. von Glahn, Vernon H. Gray, Eugene A. Krejsa,
Robert Lee,* and Gene L. Minner

Jet noise can be the critical factor in establishing the noise factor for an engine. The jet-noise floor is determined primarily by the jet exhaust velocity. At the high exhaust velocities of an SST engine, the ability to meet the noise standards in Federal Air Regulation 36 (FAR-36) is difficult even with the best available exhaust noise suppressors. If the noise level requirement is lowered 10 or 20 decibels below FAR-36, as has been advocated in the Civil Aviation Research and Development Policy Study, a major breakthrough in noise suppression must occur or a variable-cycle engine must be used. Operation of many older conventional CTOL aircraft, such as the DC-8, also present noise problems because their noise levels, due to their high exhaust velocities, are near the present FAR-36 sideline requirement at takeoff. On the other hand, advanced CTOL engines, because of their low exhaust velocities, can achieve noise levels at least 15 decibels below FAR-36 without noise suppressors. For further reductions the jet noise level could be lowered by the use of exhaust noise suppressors. It should be noted, however, that experience has shown that jet noise suppression becomes increasingly more difficult with low jet velocities.

For practical applications, the jet noise must be predictable together with a means of assessing attainable suppression levels.

The specific problem areas and progress made in understanding jet noise and its suppression discussed in this paper are

(1) Subsonic velocity power law

(2) Jet density effect

(3) Supersonic jet noise

(4) Jet noise correlation

(5) Quiet engine noise measurements and prediction

(6) Jet noise suppressors

---

* General Electric Company.

(7) Flight effects on suppressors

(8) Thrust reverser noise

The validity of the Lighthill eight-power law with respect to the variation of noise level for low subsonic velocities will be examined. The effect of jet density on subsonic jet noise is then considered. Having examined the major problem areas of subsonic jets, the noise of supersonic jets is briefly discussed. Then a NASA correlation for the peak sideline overall sound pressure level (OASPL) is presented. The available noise prediction techniques as applied to NASA's Quiet Engine is then considered.

The acoustic and aerodynamic performance of a number of jet noise suppressors then is discussed. This discussion will also include the effect of flight velocity on the performance of jet noise suppressors.

The last item concerns an aspect of jet noise that has been largely ignored to date, namely, thrust reverser noise.

STATUS OF JET NOISE

With the introduction of turbojet powered aircraft, jet noise became a major problem. More current turbofan engines, having larger flow areas and lower exhaust velocities, had less jet noise, and internally generated noise was the major problem. Much effort at present, notably in the Quiet Engine and STOL Programs, is devoted to reducing internal noise by fan design and acoustic absorbers. The effectiveness of these measures has been limited by a jet-noise floor, even at exhaust speeds below 1000 feet per second, which are characteristic of turbofan engines. As future noise regulations become more restrictive, the jet-noise problem will become even more important. It is therefore necessary to have a basic understanding of low-velocity jet noise.

The main concern with noise disturbance has been with peak levels for a fixed observer. It has been standard practice (fig. IV-1) to present jet noise correlations in terms of the maximum 200-foot sideline overall sound pressure level (OASPL). The noise level is normalized on jet density ρ_j^2 and area A. Jet exit velocity V is the primary determinant of the noise and is used as the abscissa.

A standard procedure for prediction of jet noise of engines at exhaust speeds above 1000 feet per second was established by the Society of Automotive Engineers Aerospace Information Report-876. The curve (representing sound pressure squared) in the range of 1000 to 2000 feet per second varies with about the eighth power of velocity. This result compares favorably with the classical Lighthill theory, which predicts that the jet noise total sound power varies as V^8.

It was expected that one should be able to extend the SAE correlation curve to lower jet velocities. However, a large amount of the early engine data exhibited higher noise levels and lower velocity dependence. It was suspected that this different behavior might be caused by noises from sources other than the jet, increasing in relative importance as jet velocity was reduced. This suspicion was supported by jet noise data from NASA's first quiet fan rig. The fan had noise suppressors that eliminated some noise from internal sources. The results (circle symbols in fig. IV-1) show the same trend as the SAE curve, although the level is shifted downward a few decibels. This shift probably results from overcorrection for ρ_j and will be discussed later.

The General Electric Company has provided jet noise data (fig. IV-2) taken for fans A, B, and C in full-scale and B and C in scale-model versions. These data are in satisfactory agreement with the curve fit of the quiet fan (QF 1) results (fig. IV-1), which are approximately an eighth power curve. The deviation at low velocity is believed due to internal noise.

Small scale model jets have long been used to study jet noise, assuming that these studies were representative of full-scale engine jet-noise behavior. Experience with model jets (fig. IV-1) showed the data lying in a broad uncertainty band from slightly above the engine experience band down to somewhat below the extrapolated SAE curve. It is believed that jet noise in this velocity range varies directly with V^8 and that internal suppressible noises have caused the deviations.

In order to determine if an engine shows results similar to those for fans, the effect of muffling a J-65 turbojet engine was studied (fig. IV-3). A long acoustically treated inlet was placed on the engine in order to reduce the inlet-radiated noise to a negligible level. An exhaust duct liner (fig. IV-4) was designed to remove noise in the frequency range of interest for jet noise, with peak attenuation at 250 hertz (large holed surface) and

1000 hertz (small holed surface). The liner shown served as the inner surface of the annular exhaust muffler. The outer boundary of the annular flow passage was covered with the same type of liner. This was a research tool and not flightworthy hardware.

The engine was run with both hard-wall and lined-wall exhaust ducts. Typical 1/3-octave frequency spectra of sound power at 50 percent of design speed are shown in figure IV-5. Comparison of the lined- and hard-wall spectral results shows a significant noise reduction by the liner over the frequency range of interest for jet noise. As can be seen the maximum attenuation occurred near the design points of 250 and 1000 hertz.

The peak-sideline OASPL as a function of velocity (fig. IV-6) is also higher for the hard configuration than for the lined configuration. The data for the lined configuration follow the V^8 curve down to about 700 feet per second. These data indicate that there is a significant amount of low-frequency internally generated noise in an engine. With adequate internal noise suppression the pure jet noise obeys the V^8 law.

Some insight into the effect of jet density on jet noise can be obtained from data taken at different temperature levels since jet density is inversely proportional to jet temperature. The data used in this presentation cover a temperature range from ambient to about 2500° R. These data are taken from reports published by NACA-NASA and Boeing. In addition, some recent unpublished data from the NASA Lewis hot-jet facility (fig. IV-7) is used. In this facility pressurized air is supplied from the Center's central air supply. A muffler is located downstream of the supply line valve to remove any valve and upstream noise. Just downstream of the muffler is a preheater. This preheater is made up of five annular combustors that can heat the air to 1400° F. The final section of the rig is a J-85 afterburner that can heat the air an additional 2000° F. The nozzle is an adjustable convergent nozzle. For the data used herein, the nozzle was set at 11 inches.

The data from this facility and the published data will be presented in terms of the peak sideline overall sound pressure level, referenced to 200 feet. As indicated in figure IV-8, the peak-sideline OASPL is normalized by the exit nozzle area times the jet density squared. Lines representing data at several temperature levels are shown. The jet density is largest for the lower temperature data and decreases as the temperature increases. Also shown is the curve of jet noise from SAE AIR 876. The data segregate

by jet temperature level with the higher temperature data coinciding with the SAE curve.

A similar plot is shown in figure IV-9, except that only the nozzle area is used to normalize the OASPL. On this plot the data fall together, and no trend with temperature or density is apparent. The data in figures IV-8 and IV-9 indicate that normalizing by density squared overcorrects for density effects. At the lower velocities the relation between OASPL and velocity is about an eight-power law. At higher jet velocities (greater than 1500 ft/sec) the curve bends over, and a three-power law is approached. At these higher velocities, the flow is still subsonic.

The measured peak-sideline OASPL for supersonic jets is shown in figure IV-10 together with the subsonic curve. As the jet Mach number increases above 1.0, the OASPL for the supersonic jets increases to values above the subsonic jet curve. This increase is probably due to shock-turbulence interaction or the fact that for supersonic jets the mixing region becomes much longer than that of a subsonic jet. The data taken are at several temperatures, and as the temperature increases the difference between the supersonic and subsonic jet decreases. It is evident that supersonic jet noise is influenced by both jet temperature and jet exhaust Mach number.

Correlation parameters have been developed that include these preceding factors in what otherwise can be classed as a modified Lighthill correlation. The correlated data are shown in figure IV-11. The ordinate consists of the peak-sideline OASPL normalized by the expanded-flow area, jet Mach number, and shock parameter F', which is a function of the jet velocity, Mach number, and the ambient speed of sound as follows:

$$F' = 1 + \left\{ \frac{7.5(M - 1)^3}{\left[0.0135 + (M - 1)^3\right]\left[1 + 2(M - 1)^4\right]\left[1 + 0.05\left(\frac{V}{a}\right)^8 M^{-3}\right]} \right\}$$

where M is the jet Mach number, V is the jet velocity, and a is the ambient speed of sound. The abscissa is a dimensionless velocity and Mach number parameter. Also shown in this figure is the subsonic jet noise curve. It is apparent that good correlation between the subsonic jet noise data

(shown by the plain symbols) and that for supersonic jets (tailed symbols) has been achieved over the entire range of conditions noted. It should be pointed out that the proposed correlation was developed without including the jet density as a parameter. It remains to be seen if other convergent-nozzle data from worldwide sources also correlate after being properly screened for internal noise effects.

In order to account for changes in the ambient speed of sound a and in the ambient density ρ, the ordinate in this figure should be expanded to include these parameters. Thus, the ordinate should include the additional term $-10 \log \rho a^3$. The ordinate can be normalized to avoid negative values. Inclusion of these terms does not alter the basic correlation, but it does change the absolute value of the ordinate.

Because the peak-sideline OASPL is closely related to the sound power, a similar correlation can be developed for total sound power data.

The preceding OASPL correlation applies to simple nozzles, so the question arises as to how well the noise for fan-jet engines that have both core and bypass jet exhausts can be predicted. The NASA Quiet Engine falls in this class.

Some of the noise characteristics of the Quiet Engine are shown in figure IV-12. Typical 1/3-octave band frequency spectra are shown of the sound pressure level measured at takeoff speed at 120° to the fan inlet direction for the engine and the fan. At this angle, both internal and external sources are strong noise contributors.

Typically for an engine of this size, the jet noise is primarily contained in the low-frequency part of the spectrum (up to 1000 Hz). The internally generated noise dominates the spectrum at higher frequencies, notably at the blade passing frequency and its harmonics. There is also some internally generated noise that contributes to the low-frequency part of the spectrum. By internally generated noise is meant all sound propagating from inside the engine.

A significant difference at low frequency between the data taken for the quiet fan and the Quiet Engine is shown in figure IV-12. This difference is a result of added jet noise generated by the high-speed core flow, which was not present in the fan, and there may be some additional contribution from internal sources.

In general, jet noise is not a limiting item to the Quiet Engine systems noise at takeoff power while the aircraft is in flight. There are several things that have been learned about jet noise as a result of the Quiet Engine Program. It was found that, when the fan ducts are fully suppressed, the exhaust jet noise from the fan stream does behave like any pure jet noise ought to behave, namely, the acoustic power and velocity relation obeys the classic eighth power law.

In figure IV-13 the 200-foot sideline maximum OASPL is plotted as a function of exhaust jet velocity. The data are based on all the full-scale and scale-model fans that have been tested at Lewis and at General Electric under the Quiet Engine Program. No engine data are included in this plot. The OASPL is taken from 50 to about 1000 hertz.

The data correlate quite well with velocity raised to the eighth power. An empirical equation developed by General Electric for the straight line is shown. Both the velocity exponent and the proportionality constant agree well with previous results on this subject reported by Lewis, and also with other scale-model jet data. The data shown are for fan jets discharging at essentially ambient jet density. Whether the density term used in the empirical equation is indeed a significant correlating parameter cannot be tested. At General Electric the retention of the density term to the first power for jet correlation work is still favored.

Correlation procedures adequate for predicting a single-stream pure jet noise may not be adequate for predicting the exhaust noise of a turbofan engine. This is illustrated in figure IV-14 in which a comparison of the measured and predicted sideline OASPL is made as a function of engine thrust for engine A. The prediction method follows that developed in the previous figure and again is shown in equation form in figure IV-14. Both the fan exhaust and core jet noise are predicted and summed, assuming no interaction effect between the two exhaust streams.

At high power settings, the measured noise level appears to be somewhat lower than the predicted value, due probably to a favorable interaction effect between the fan and core streams. At low power settings, the measured exhaust noise exceeds that predicted using the eighth power law. This suggests that the exhaust noise from the core engine must have included noise sources other than the externally generated jet noise and that these are low-frequency noise sources. The J-65 engine core noise suppressor

experiment described earlier supports this hypothesis.

Internally generated low-frequency noise, without flight effect, can add several perceived noise decibels (PNdB) to the total systems noise on engine A at approach power when the fan noise is fully suppressed.

It is apparent that jet noise prediction based on single-stream pure jet noise data is not fully workable for predicting turbofan engine exhaust noise because of internal noise considerations. A strictly empirical method based on correlation of exhaust noise from several turbofan engines has been devised at General Electric. Empirical fits of spectral and directivity data obtained from the CF-6, CJ-805, and TF-39 engines led to the formulation of a set of prediction equations that appears to apply quite well also to the NASA Quiet Engine. A comparison of predicted and measured spectra for engine A at the 200-foot sideline, 120^{o} takeoff power is shown in figure IV-15. The spectral contents above 100 hertz are accurately predicted. Below 100 hertz strong ground-reflection nulls in the test data appear to cause some discrepancy, but the impact on the PNdB unit is insignificant.

Predicted spectrum based on the SAE method is also shown. The SAE procedure tends to overpredict the exhaust noise of turbofan engines at takeoff power.

It should be emphasized that these empirical correlation methods are appropriate for engines whose internal noise, including low-frequency sources, has not been suppressed. Such internal noise can and should be suppressed for a certain application (e.g., quiet STOL engines). Low frequency core noise suppression represents an area requiring further effort.

The difference between the predictions using SAE procedures and the data for the Quiet Engine is probably due, in part, to the coannular-bypass engine flow. The effect of the fan flow is to reduce the noise generated by the core flow.

The precise means of quantifying the noise reduction due to the relative velocity is not completely known. The noise of several coannular jets was measured, and the noise attenuation effect due to the bypass flow was indicated. As shown in figure IV-16, as the bypass velocity approaches about six-tenths of the core velocity, the noise attenuation reaches a maximum. Beyond this value, the total noise production increases and eventually becomes greater for the combined jet than for the single jet, the attenuation then being negative. This figure is applicable only to the specified area

ratio. Further work is being done here at Lewis and by industry in order to obtain a basic understanding of this effect.

Jet Noise Suppression

A common type of experimental jet noise suppressor is shown schematically in figure IV-17 and consists of a multielement or mixer nozzle combined with an ejector. The mixer nozzle serves the function of breaking up a single large jet into many small jets. These multiple jets provide a mutual shielding effect on each other, thus reducing the noise level. The mixing of the small jets with the surrounding air results in a rapid jet velocity decay so that the ejector exhaust velocity is reduced with a consequent reduction in noise level. Finally, the center frequency of the noise spectrum of the individual small jet is much higher than that for a single large jet, making it much easier to attenuate the jet mixing noise with a relatively thin acoustic liner.

The ejector serves as a surface to which the liner can be attached as well as providing thrust augmentation during takeoff. In order to minimize performance losses in cruise, the ejector can be retracted and the mixer nozzle elements stored within the confines of the engine nacelle. Development of a variable-geometry ejector to minimize thrust losses for cruise can also be considered.

Several types of mixer nozzles that could be used with an ejector for noise suppressors are shown in figure IV-18. These nozzles include arrays of multitubes, trapezoids, and lobes among other shapes. Similar multielement nozzles have been investigated in the past, and more recently in the SST noise-reduction program by General Electric and Boeing.

In order to evaluate further the benefits derivable from ejector-mixer nozzle suppressors, a current Lewis program in which a Boeing multitube nozzle is being tested under contract with and without acoustically lined ejectors.

In this program one multitube suppressor nozzle design is being tested at both small- and full-scale; in both cases an ejector is added, first with hard walls and then with a variety of acoustically lined walls. In addition, the same series of tests are being made with single-tube elements of the

large- and small-scale nozzles. This should help to establish better scaling relations and to optimize the design of linings.

The full-scale J-75 engine static test rig is shown in figure IV-19. Part of the concrete pad and some of the microphone stations shown. The arrangement of the 37 tubes in the suppressor nozzle is also shown in the figure. These tubes are each 4.3 inches in diameter. The outside line was added to indicate the walls of a hexagonal ejector.

One sampling of preliminary data from the J-75 tests is shown in figure IV-20. The top curve shows the sound pressure level spectrum for a standard conical nozzle at a pressure ratio of 2.4 and at the directivity angle of maximum noise (140^{o} from the inlet axis). The peak sound pressure level of 119 decibels occurs at low frequencies because of the large nozzle diameter of 28 inches. The lower curve shows the results when the suppressor nozzle with 37 tubes is used in place of the standard nozzle. In some of the lower frequency bands, as much as a 21-decibel reduction in sound pressure level is obtained, and the remaining peak is shifted to frequencies above 1000 hertz.

In figure IV-21 the two previous curves are repeated and, in addition, the results obtained for the 37-tube suppressor nozzle with a hard-wall ejector are shown. The effect of the hard-wall ejector on sound pressure level is minor except for a slight attenuation at the high frequencies.

Sound pressure level values after application of an acoustically soft liner to the ejector are shown in figure IV-22. This liner is made of stainless-steel honeycomb sandwich panels with perforated facing sheets. The sound pressure level was attenuated as much as 11 decibels at the design center frequency of 1600 hertz. This higher range of frequencies was not affected appreciably by the suppressor nozzle alone, as was shown by the previous curves.

To interpret the performance of these suppression devices, comparisons should be made on the basis of perceived noise levels which account for the human annoyance factors at the various frequencies. These 200-foot-radius noise measurements are extrapolated to the 0.35-nautical-mile sideline distance of FAR-36, and the perceived noise suppression values are given at the right end of the various curves in ΔPNdB. The values are referenced to the standard nozzle as zero and are for the 140^{o} angle.

The suppression of 19 PNdB for the softwall ejector is not the minimum sideline suppression, however, as shown in figure IV-23. The suppression, at 140^{o} from the inlet axis, corresponds to the peak perceived noise level for the standard nozzle, but the softwall ejector peaks at about 110^{o}. The difference between the two peaks is the minimum sideline suppression that an observer would experience, or about 12 PNdB in this case. Effective perceived noise levels (EPNdB) penalize for the time duration of peak noise and will be worse for the standard nozzle than with the ejector, by another 1 to 2 decibels.

This minimum sideline suppression is shown in figure IV-24 in ΔPNdB as a function of jet velocity, or pressure ratio. The suppressions are less at the lower jet velocities, but the improvement due to the lined ejector is evident down to quite low velocities, as is seen by the difference between the top curve and the other two. Jet velocities below 2000 feet per second are of interest because advanced transports will likely be operating in this jet velocity range, in order to achieve low overall noise levels.

In figure IV-25 the changes in thrust from the standard nozzle are shown as a function of jet velocity and pressure ratio. The 37-tube suppressor nozzle had about a 5-percent thrust loss, while, due to thrust augmentation of the ejector, the combination of suppressor and ejector resulted in a 2- to 6-percent gain in thrust. It should be emphasized that these data are not for flight hardware nor for flight speed conditions and are preliminary.

NASA is also conducting research on jet noise suppressors. Shown in figure IV-26 is a nozzle design that shows some promise for noise reduction at supersonic exhaust conditions. The nozzle is a convergent-divergent nozzle that operates in an overexpanded condition. The design of the nozzle is such that the jet is divided into lobes. An ejector is placed around the nozzle. The convergent portion is a standard conical nozzle. The divergent portion consist of eight plates separated by V-gutters. A step area increase exists at the throat. A low pressure exists in the base cavity formed by this area step. This low pressure causes the flow to overexpand. The flow attaches to the plates and is divided among the plates by the V-gutters. A strong shock structure results, and the velocity rapidly decreases.

Some of these effects can be seen in figure IV-27, which shows the axial Mach number distribution along the jet centerline and along the plates. The Mach number is higher along the plate region, which indicates that the flow

has expanded into this region and, in fact, is even concentrated in this region. Shocks exist just upstream of the end of the V-gutters. Downstream of these shocks, the Mach number decreases and the flow becomes subsonic in about 3 or 4 diameters, and the normally long supersonic mixing region has been eliminated.

The noise reduction characteristics of this nozzle are shown in figure IV-28. The decibel reduction per percent thrust loss is plotted against nozzle pressure ratio. The particular nozzle tested was optimized for supersonic exhaust conditions, and no noise reduction was obtained at subsonic velocities. At t typical operating point and at a pressure ratio of 3.5, a 12-decibel noise reduction and a 9-percent thrust loss were obtained. The initial tests on this nozzle were made using a small-scale cold facility. Recently, the nozzle has been tested on the Lewis hot jet facility, and the results are similar to those from the cold tests.

Jet noise from high velocity jets is of interest because of possible applications to advanced supersonic transport engine designs. One important question is how aircraft forward velocity influences the noise suppression characteristics. Flight tests have been conducted by NASA on the F-106 airplane (fig. IV-29), which was modified to be powered by the J-85 engines for the noise test. Various types of multielement suppressors were tested both under static and flight conditions. Some of these are shown in the figures IV-30 and IV-31. The cylindrical ejector nozzle is used as the reference baseline nozzle for the suppressor nozzles. The suppressor nozzles consist of a plug nozzle, 12-chute, 32-spoke, and 64-spoke suppressor nozzles. General Electric participated in the flight program and in the data reduction.

In figure IV-32 is a comparison of PNdB suppression as a function of jet exhaust velocity under static and under flight conditions for three suppressor nozzles (12 chute, 32 spoke, and 64 spoke). The solid line is the peak-to-peak suppression in PNdB under static condition on a 300-foot sideline between the suppressor and the baseline nozzle. The dashed line is the suppression achieved in flight (altitude, 300-foot; aircraft speed, approx. 220 knots).

Several observations may be drawn from the data in figure IV-32:

(1) Multielement suppressors generally have an increasing amount of suppression as the number of elements in the design increases. Thus, the

64 spoke is better than the 32 spoke, which in turn is better than the 12 chute. This fact is fairly well known. Unfortunately the suppressor performance loss also increases with increasing number of elements.

(2) The amount of suppression decreases with decreasing velocity. This holds true for both static and flight conditions. The probable reason for this is that reduction in mean shear, which is responsible for noise reduction, is dependent on the effectiveness of the flow induction process that takes place between adjacent elements in the multielement suppressor. As the velocity is reduced, the pumping capability is reduced, and hence suppression is less. However, the tendency for lowered noise reduction with drop in velocity might have also been partly due to the presence of internal noise in the engine as external jet noise is lowered by the suppressor.

(3) In the higher velocity range, the amount of suppression under flight conditions is about comparable with that obtained under static conditions. At the lower velocities (<1500 ft/sec), noise suppression in flight appears to be significantly poorer than that obtained under static conditions when compared on the basis of equal jet exhaust velocity. No satisfactory explanation for this trend exists at present.

In figure IV-33 a typical comparison of the measured flyover PNdB as a function of time characteristics between the baseline nozzle and a 32-spoke suppressor nozzle is shown. Time duration characteristics essentially reflect the noise directivity characteristics of the noise source as well as the airplane speed and the observer's distance. The top is the baseline nozzle, and the bottom is the 32 spoke. It is seen that the noise characteristics of the suppressor nozzle appear to rise and fall more rapidly relative to time than those of the baseline nozzle whose noise seems to linger over a longer duration. From the standpoint of effective perceived noise computation, the longer duration noise is more annoying and therefore less favorable. The duration corrections for the two nozzles are calculated and shown on the right side of the plot. On the baseline nozzle 6 PNdB is subtracted to change from PNdB to EPNdB; on the 32-spoke nozzle, 9 PNdB would be subtracted. This particular comparison suggests, of course, that the ΔEPNdB associated with suppression is greater than the ΔPNdB number.

The observations made with reference to figures IV-30 and IV-31 should not be taken to represent complete generalization of the problem. Both at Lewis and at General Electric data have been obtained that do not always

conform to the trend just described, suggesting that the problem is really more complex. Nevertheless, the results shown in the last two figures, although fragmentary in nature, indicate that flight effect may have a substantial impact on the suppressor acoustical performance, perhaps in a way that cannot be predicted without considerable additional experience from flight-test results. The conclusion drawn is that development of jet noise suppressors for future supersonic transport engines must require flight tests of the suppressor designs during the early stage of the development cycle.

Thrust Reverser Noise

Thrust reversing (fig. IV-34) is used to shorten the landing distance for both conventional and STOL aircraft. In addition, reversing the core jets may be used in flight to steepen the approach flight path.

Lewis recently initiated studies of thrust reverser noise. Target-type reversers have so far been used because of their simplicity, and because they can reverse both circular-nozzle and slot-nozzle flows. Shown in figure IV-35 are types that have been tested, namely, a V-gutter target and a semicylindrical target.

The noise directivity of a semicylindrical reverser is shown in figure IV-36 as a polar plot of the OASPL as a function of the angular position θ. Looking first at the jet noise from the 2-inch circular nozzle alone, it is apparent that the jet has a pronounced directivity. The maximum OASPL is 107 decibels at an angle of 160°. The minimum, toward the upstream direction, is 12 decibels less than the maximum. The reverser noise, in contrast, is nearly uniform in all directions and is everywhere louder than the bare jet maximum by 1 to 6 decibels. Toward the upstream direction, the reverser is about 17 decibels louder.

Study of the noise spectra for the nozzle and reversed jets (fig. IV-37) shows that the SPL for the cylindrical reverser peaks over a broad band at higher frequencies than the bare nozzle. This peaking at higher frequencies adds to the effective perceived noise penalty, but these high frequencies attenuate in the atmosphere faster than those of the bare nozzle.

From the preceding discussion, it is obvious that thrust reversers generate more noise than nozzles and direct it more strongly toward the critical

sideline and flyover points. To present this problem in more specific terms, the experimental data have been scaled up to the case of a CTOL aircraft of 300 000 pounds gross weight using fan-jet reversers on four Quiet Engines. Figure IV-38 shows the perceived noise level distribution along the 0.35-nautical mile sideline, not including extra ground attenuation. It is apparent that achieving noise levels below about 100 PNdB for this example will be difficult.

Other methods for reducing noise from reversers are being studied. For example, cascade reversers may be quieter than target reversers and perhaps can make use of acoustically treated surfaces. In addition, the use of acoustical doors or shields to redirect reverser noise away from the sidelines may be feasible.

CONCLUDING REMARKS

The main conclusions reached by this discussion may be summarized as follows:

1. At low subsonic jet exhaust velocities, jet noise varies as the velocity to the eighth power.

2. At high subsonic exhaust velocities (above 2000 ft/sec), we reaffirm that jet noise approaches a variation with velocity to the third power.

3. Use of the jet density squared, as in SAE AIR 876, overcorrects density effects on jet noise.

4. Subsonic and supersonic jet noise levels can be predicted from a simple empirical correlation.

5. Although the present Quiet Engine jet noise can be estimated within its geometry constraints, the understanding of such details as noise mechanisms and geometry considerations for fan-jet engines continues to require further work.

6. Use of multielement nozzles and acoustically lined ejectors can significantly suppress jet noise at intermediate jet exhaust velocities. Further work is required at both low exhaust velocities (less than 1000 ft/sec) and high exhaust velocities (greater than 3000 ft/sec) to achieve needed suppression levels.

7. Forward velocity effects in flight can cause some attenuation reductions with suppressors. Thus, wind tunnel or flight tests should be made before committing suppressor configurations to the hardware stage.

8. In view of proposed reductions in the FAR-36 noise levels, thrust reversers can present new noise problem areas, particularly for advanced CTOL and STOL aircraft.

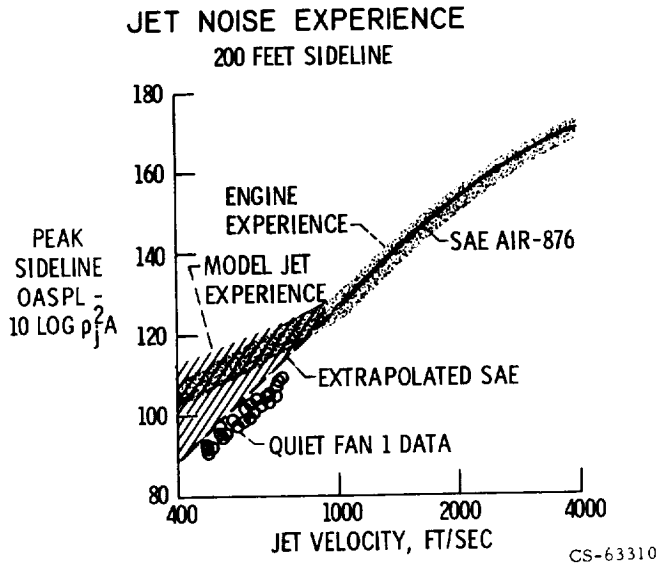

Figure IV-1

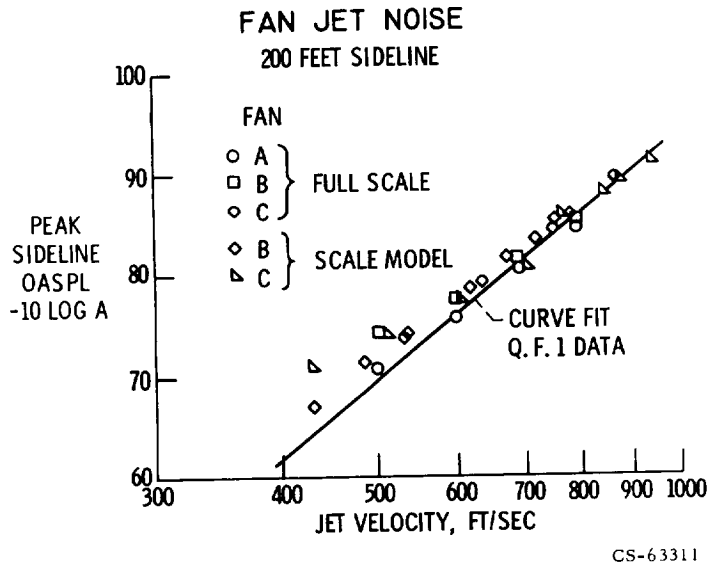

Figure IV-2

J-65 ENGINE WITH SUPPRESSORS INSTALLED

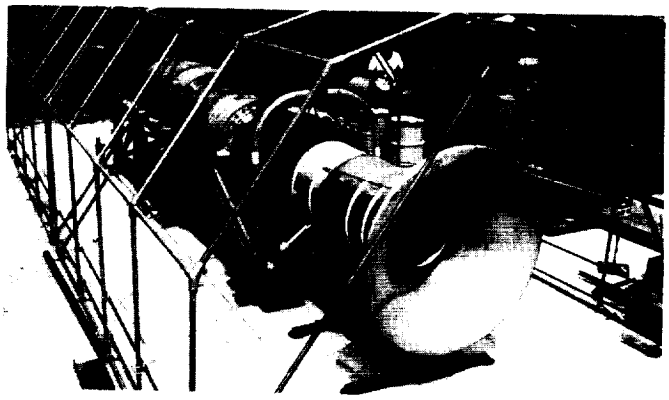

Figure IV-3

CS-63261

J-65 EXHAUST SUPPRESSOR

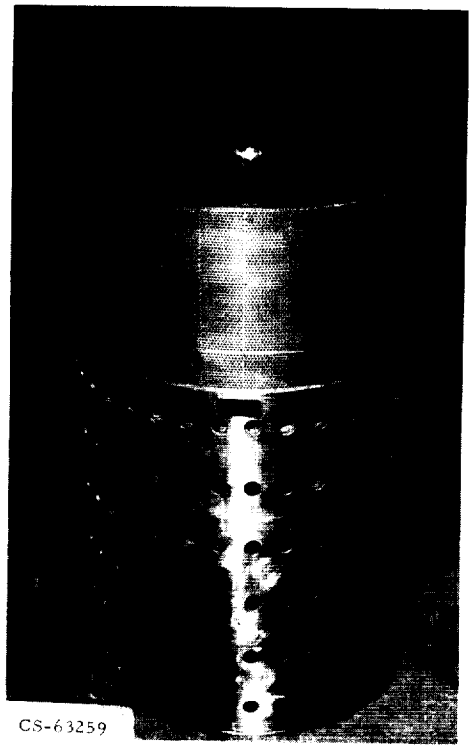

CS-63259

Figure IV-4

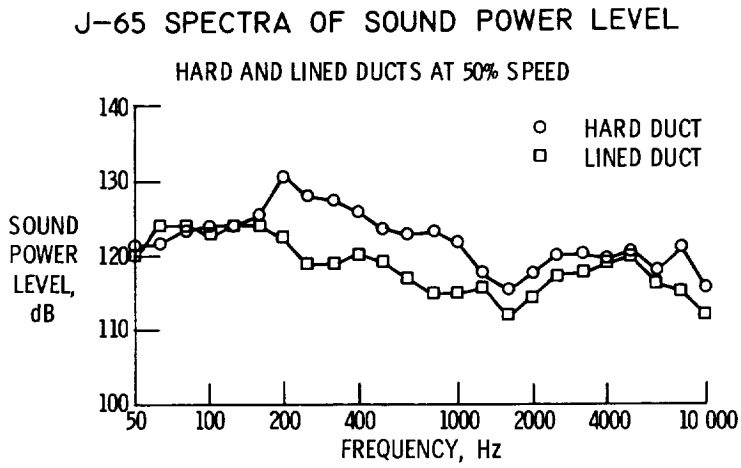

Figure IV-5

CS-63247

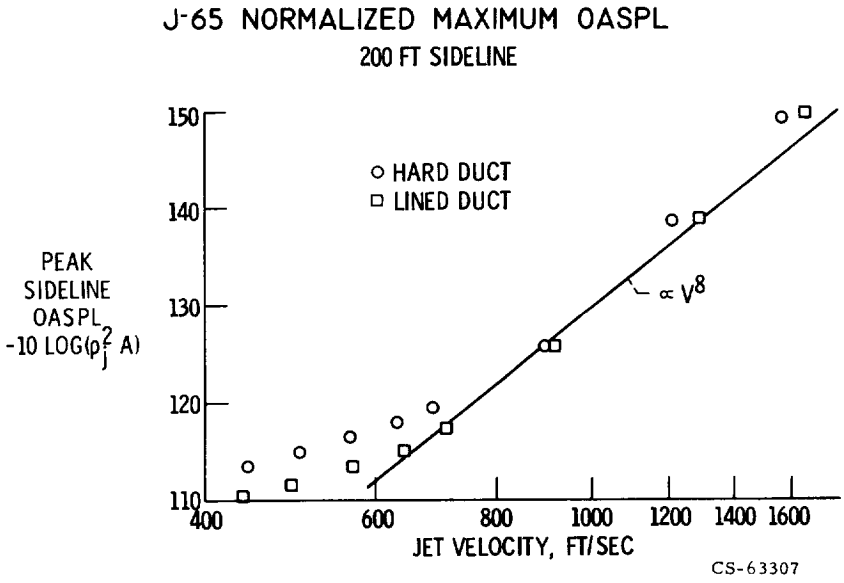

Figure IV-6

HOT JET FACILITY

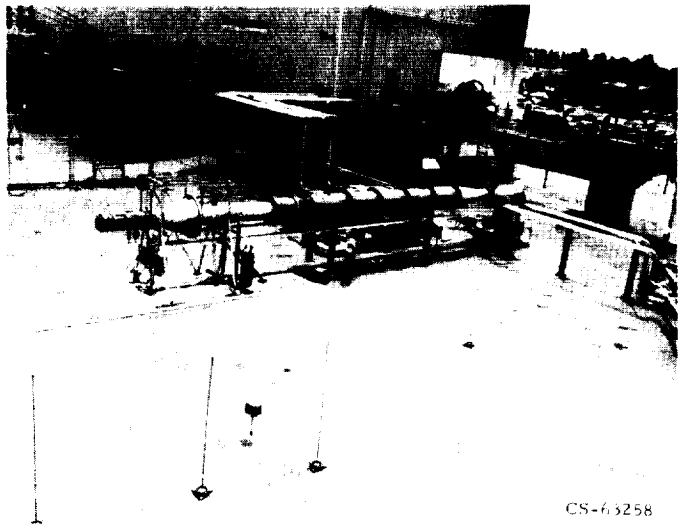

Figure IV-7

COMPARISON OF SUBSONIC JET NOISE DATA WITH SAE PREDICTION

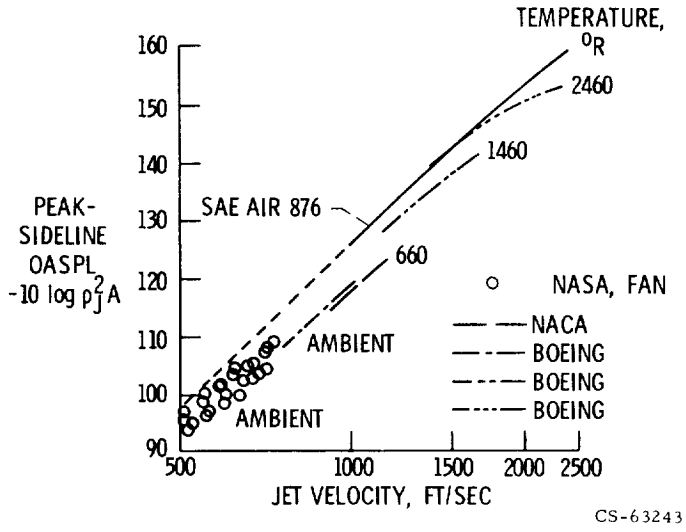

Figure IV-8

SUBSONIC JET PEAK–SIDELINE OASPL VARIATION WITH JET VELOCITY

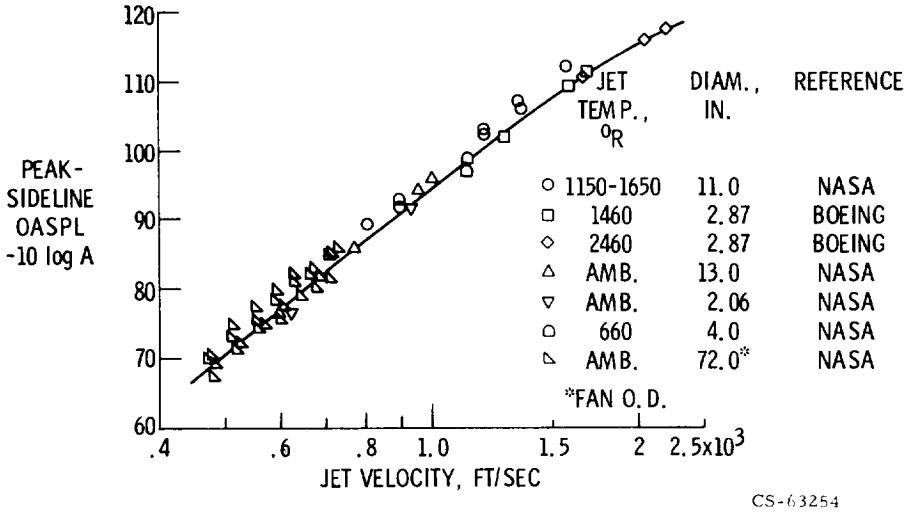

CS-63254

Figure IV-9

COMPARISON OF SUPERSONIC JET NOISE WITH SUBSONIC JET NOISE

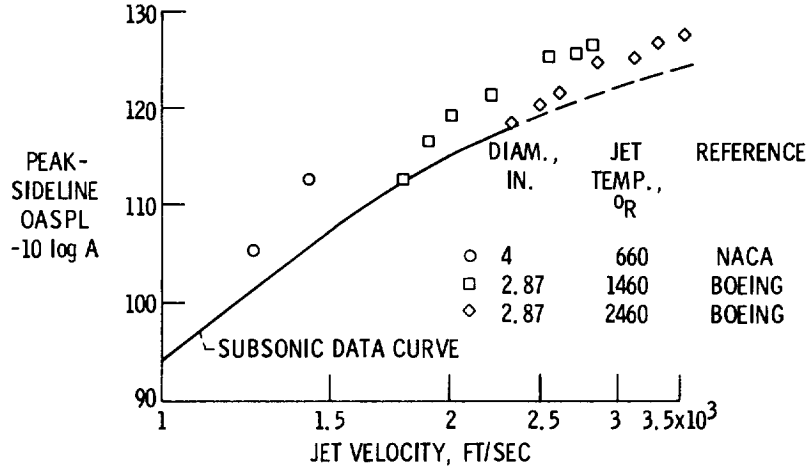

CS-63306

Figure IV-10

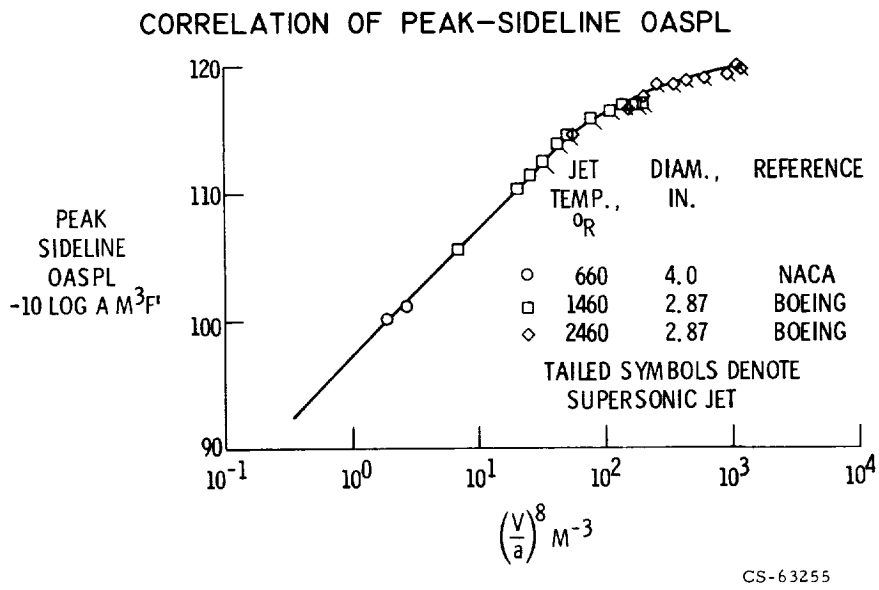

Figure IV-11

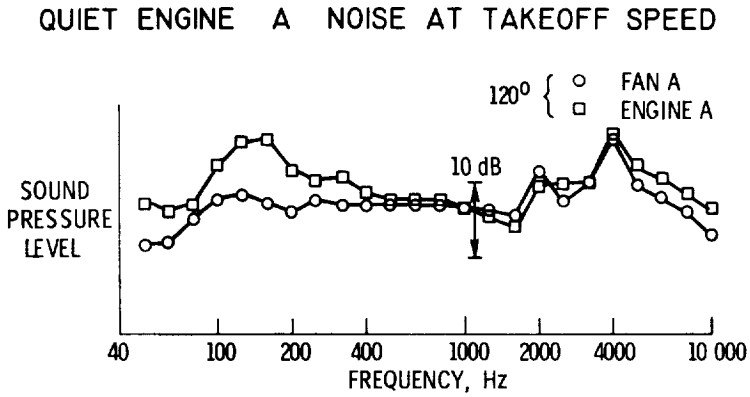

Figure IV-12

CS-63248

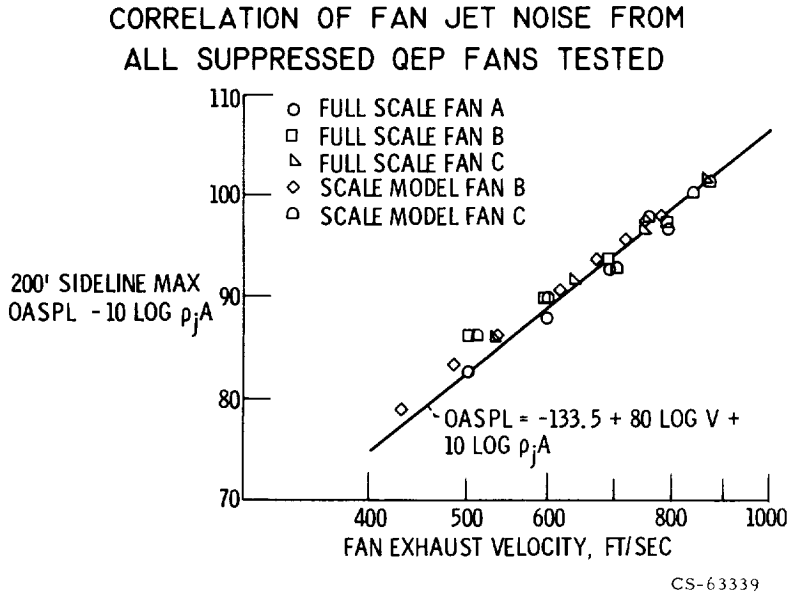

Figure IV-13

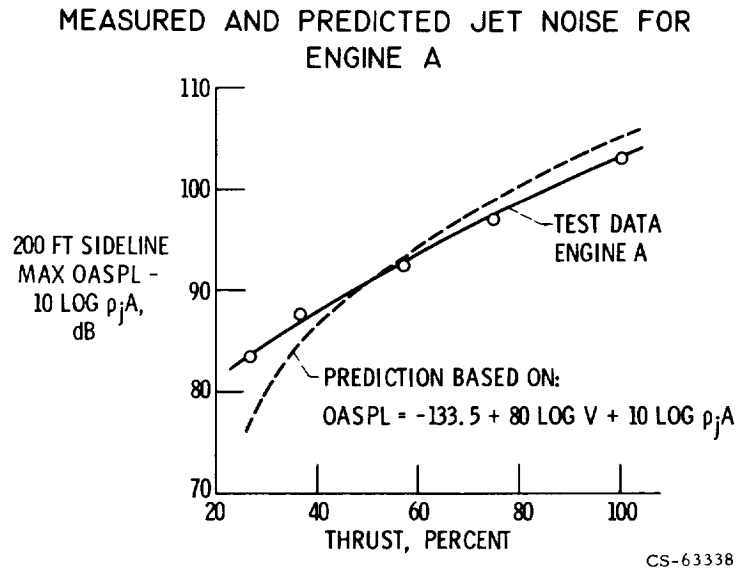

Figure IV-14

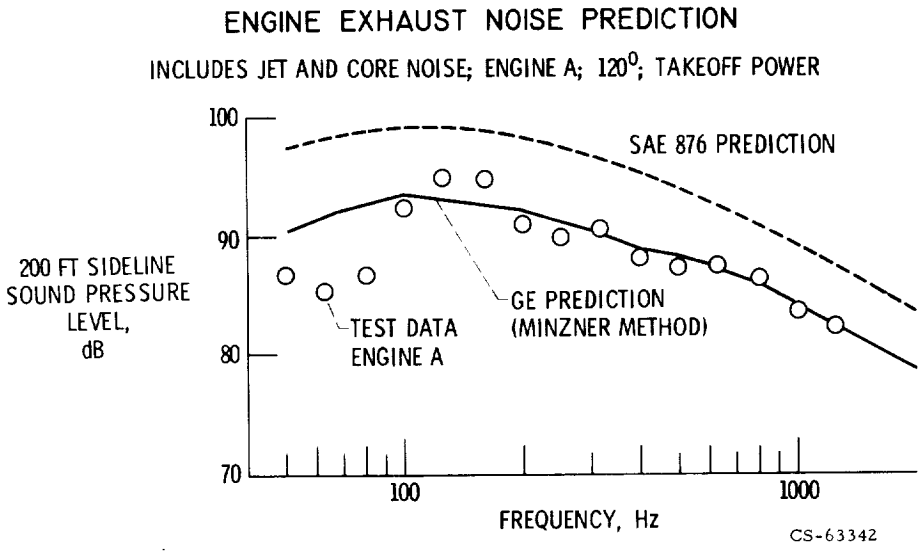

Figure IV-15

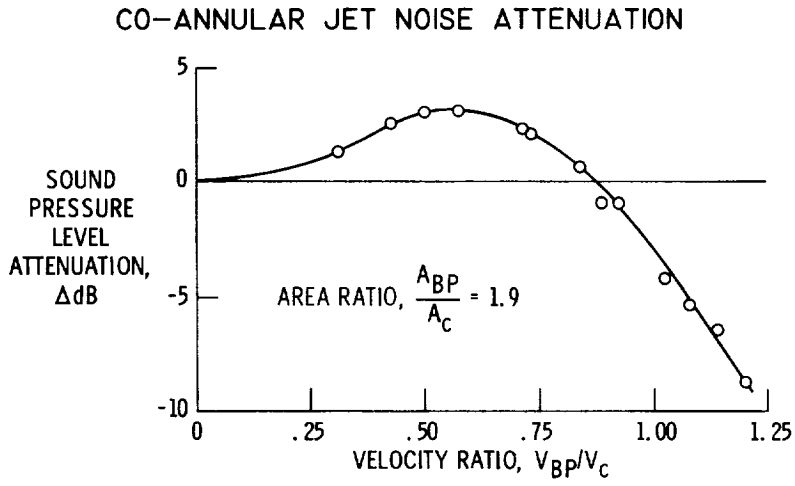

Figure IV-16

CS-63309

MIXER–TYPE SUPPRESSOR NOZZLE
WITH EJECTOR

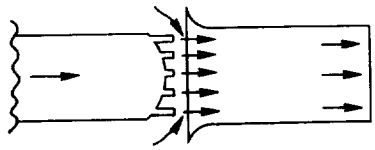

CS-63337

Figure IV-17

TYPICAL MULTIELEMENT NOZZLES

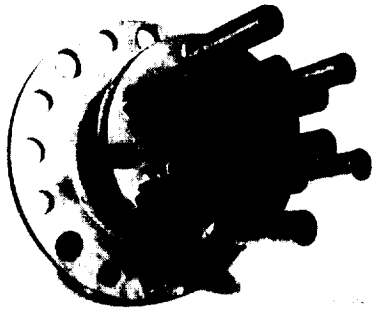

MULTITUBE NOZZLE

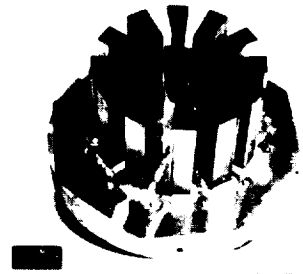

SQUARE-ENDED TRAPEZOIDAL NOZZLE

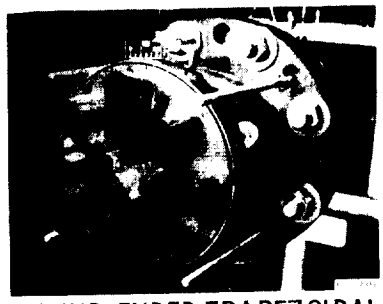

ROUND-ENDED TRAPEZOIDAL NOZZLE. ALTERNATE LOBES CANTED 10^{0} OUTWARD FROM NOZZLE CENTERLINE.

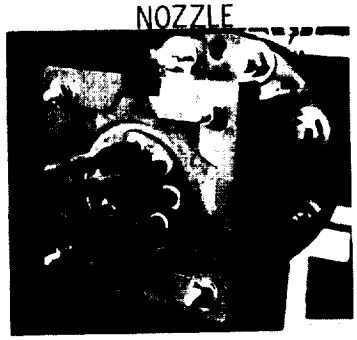

ANNULAR BYPASS-TYPE NOZZLE WITH 8 CORE TUBES

CS-63313

Figure IV-18

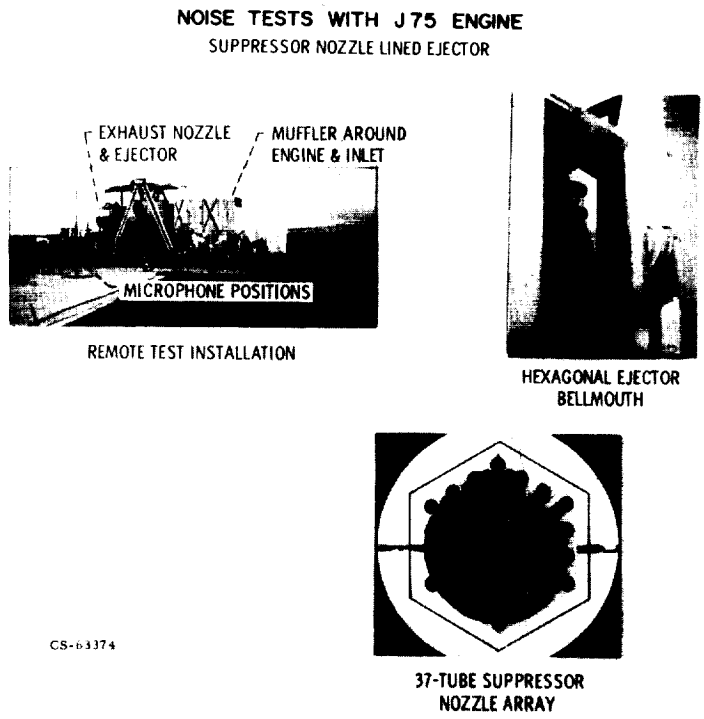

Figure IV-19

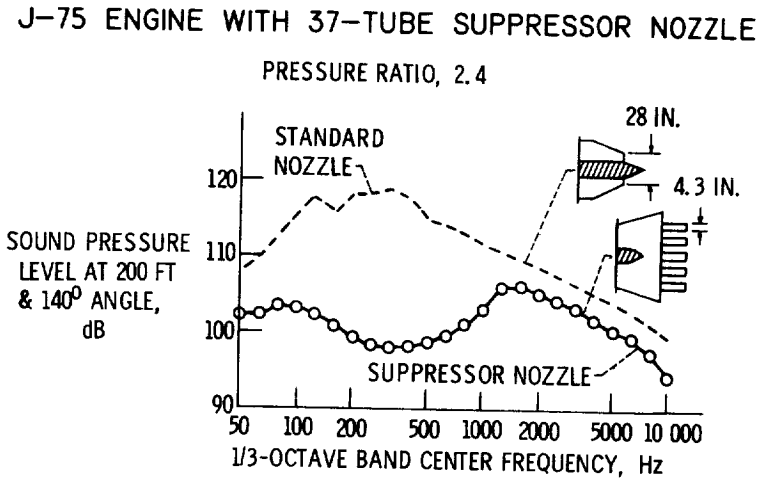

Figure IV-20 CS-63246

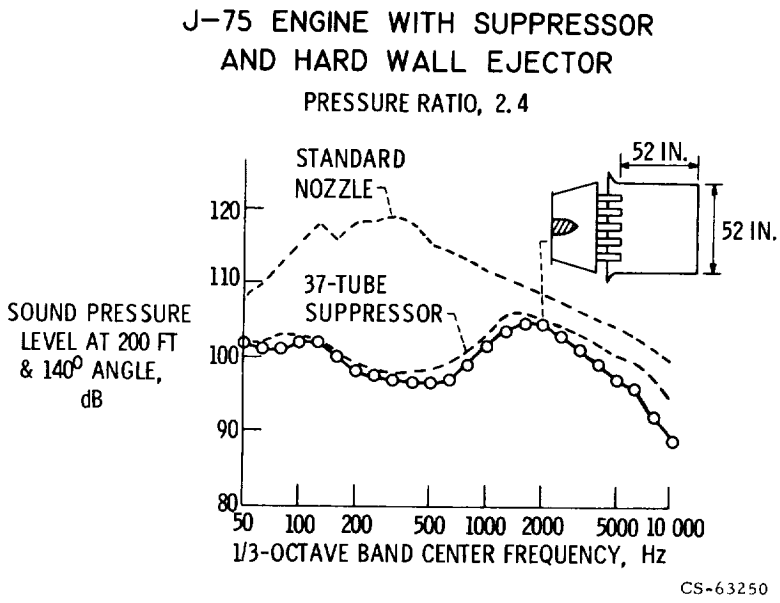

Figure IV-21

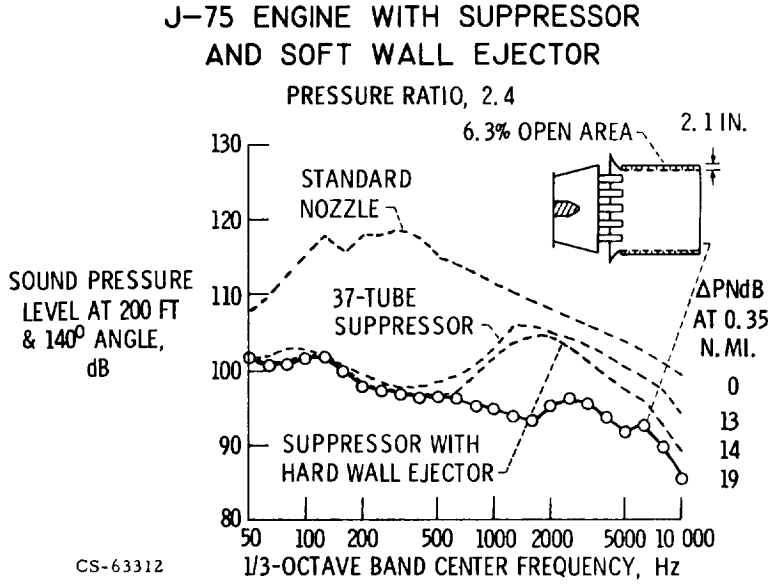

Figure IV-22

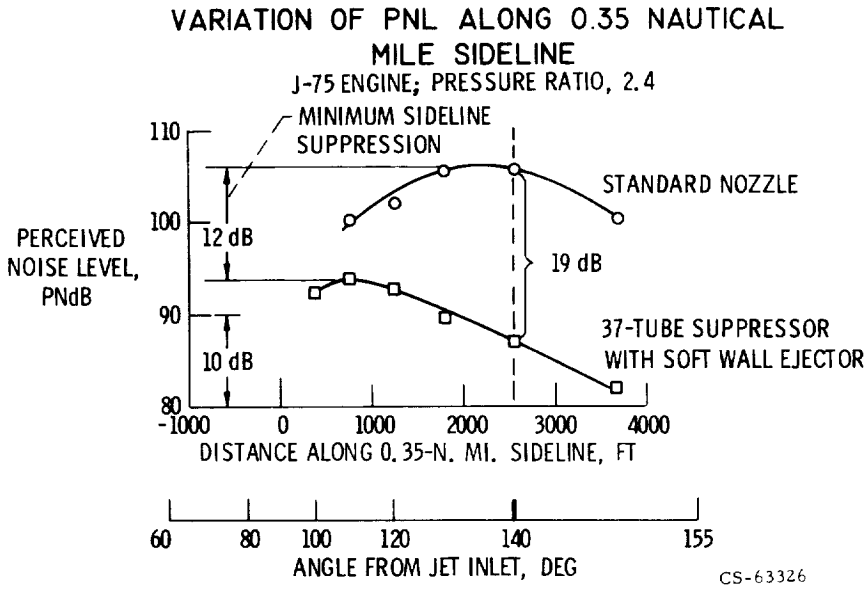

Figure IV-23

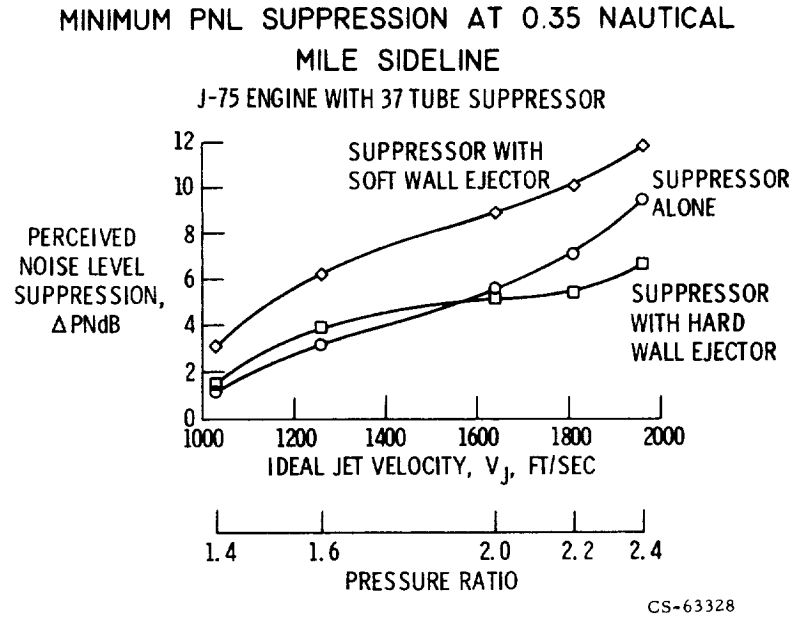

Figure IV-24

CHANGES IN THRUST ON J-75 ENGINE RELATED TO STANDARD NOZZLE

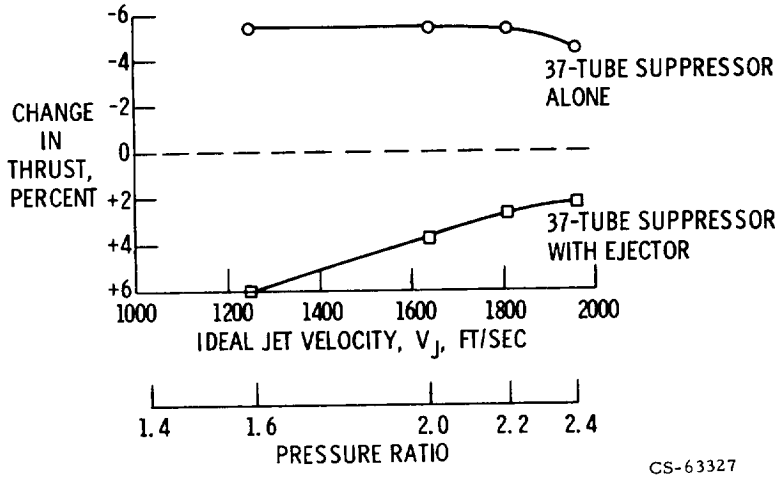

Figure IV-25

OVEREXPANDED MULTILOBED CONVERGENT DIVERGENT NOZZLE

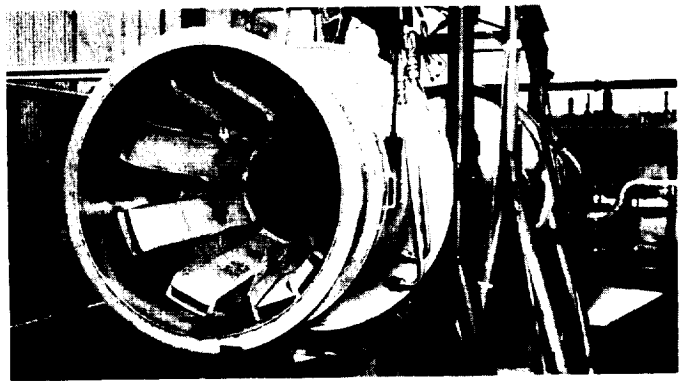

Figure IV-26 CS-63260

MACH NUMBER DISTRIBUTION
ALONG PRIMARY PLATE AND NOZZLE CENTERLINE

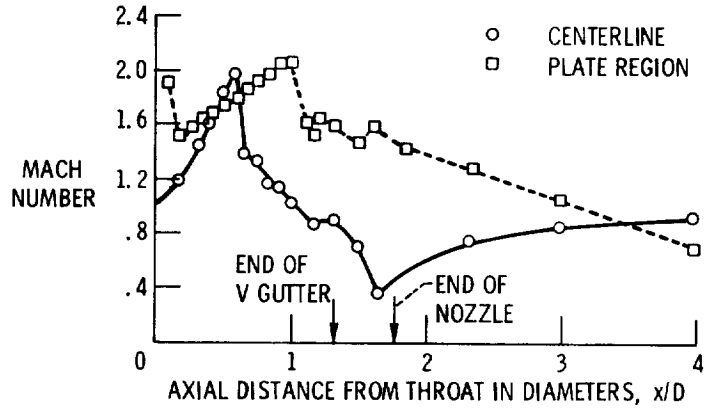

Figure IV-27

CS-63237

PERFORMANCE CHARACTERISTICS OF OVEREXPANDED
MULTILOBED CONVERGENT–DIVERGENT NOZZLE

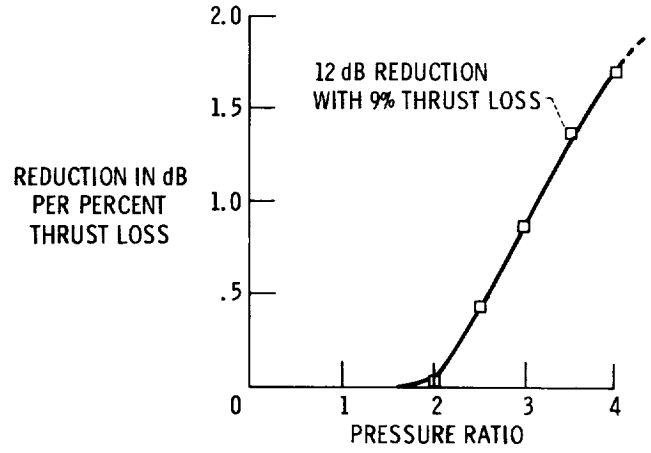

Figure IV-28

CS-63239

FLIGHT JET-NOISE RESEARCH

CS-63257

Figure IV-29

F-106 NOISE SUPPRESSION NOZZLES

CS-63344

Figure IV-30

CYLINDRICAL EJECTOR NOZZLE

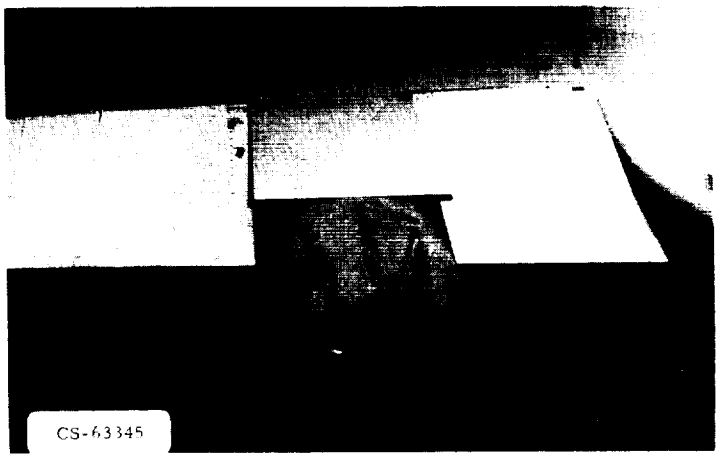

Figure IV-31

JET NOISE SUPPRESSION—STATIC AND FLIGHT

REFERENCED TO CYLINDRICAL EJECTOR NOZZLE, 300 FT SIDELINE OR ALTITUDE

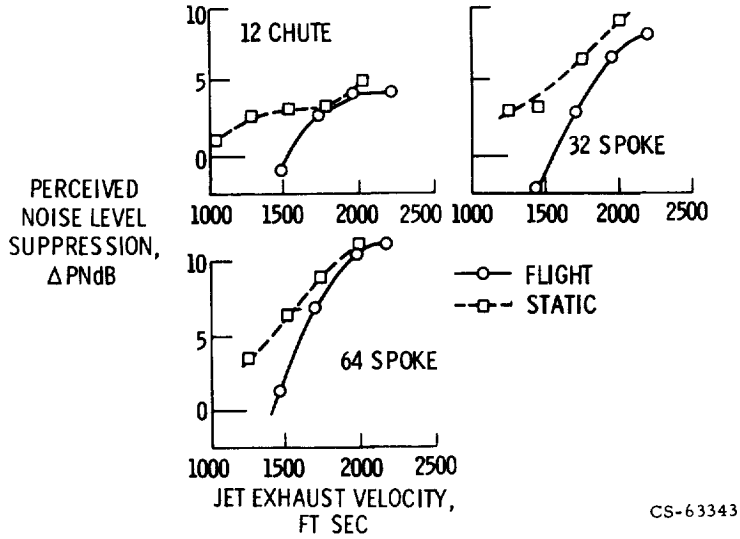

Figure IV-32

TIME DURATION CHARACTERISTICS

300 FT ALTITUDE FLYOVER; MAXIMUM THRUST

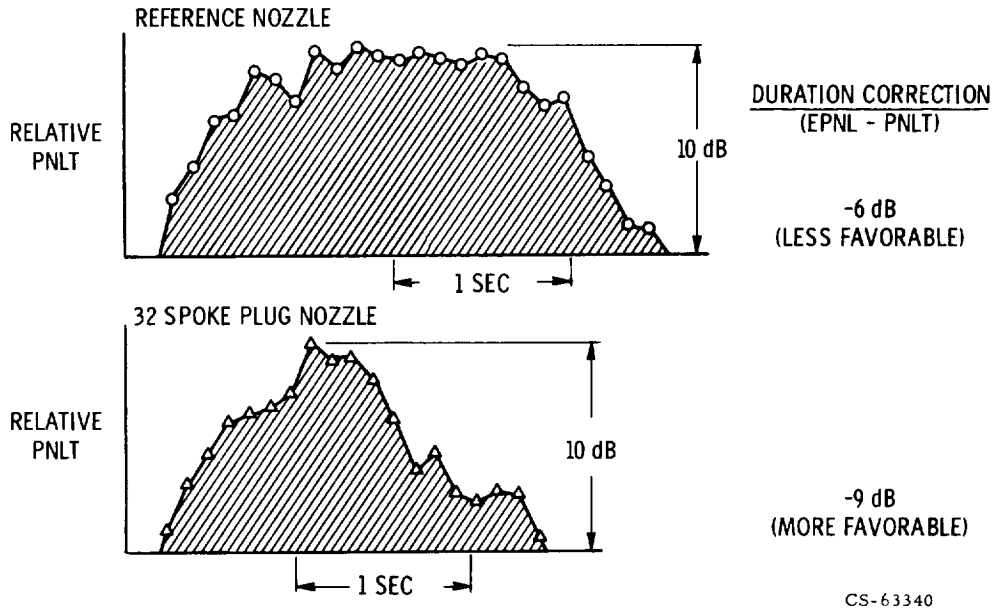

Figure IV-33

THRUST REVERSERS

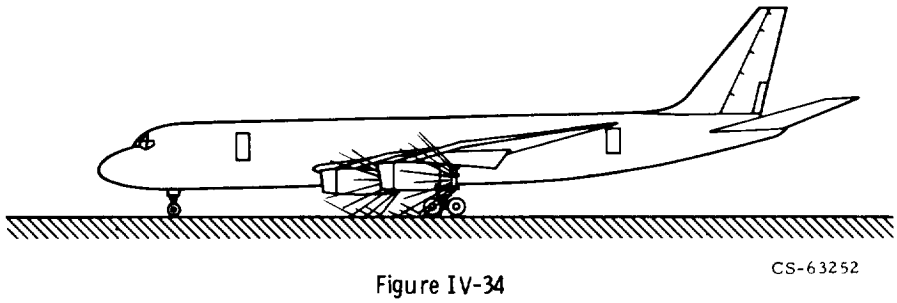

Figure IV-34

TARGET–TYPE THRUST REVERSERS

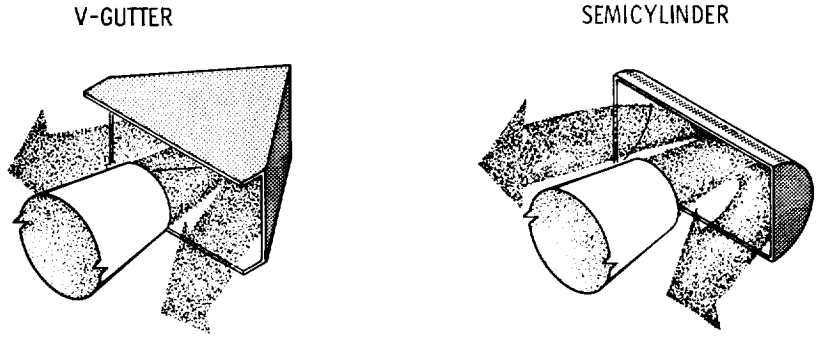

Figure IV-35

THRUST REVERSAL NOISE DIRECTIVITY

2-INCH NOZZLE AND CYLINDRICAL REVERSER;
JET VELOCITY, 960 FT/SEC

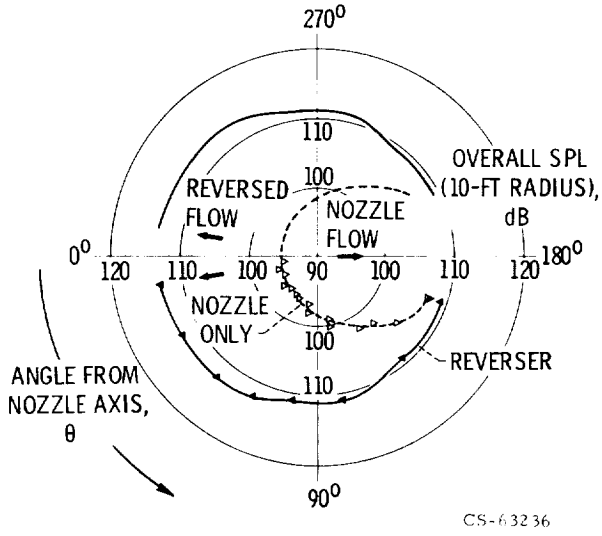

Figure IV-36

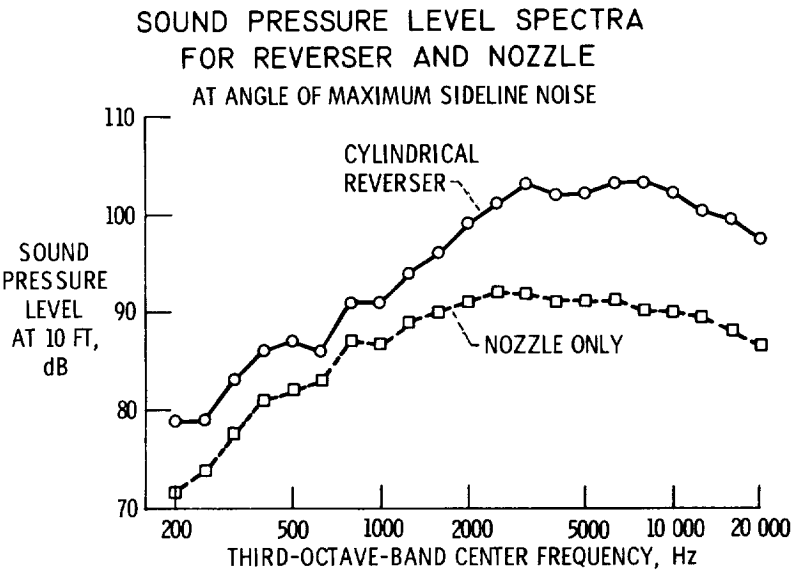

Figure IV-37

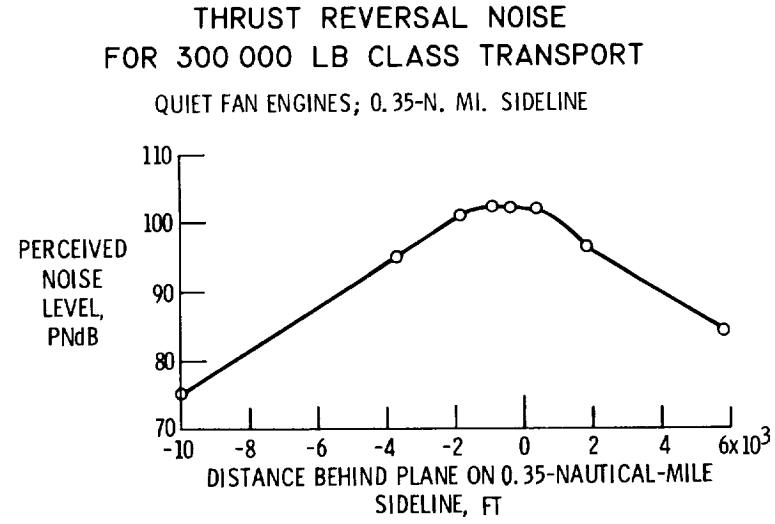

Figure IV-38

V. THE QUIET ENGINE PROGRAM

Newell D. Sanders

The first objective of the Quiet Engine program is to demonstrate noise reduction technology in an engine. At the inception of the program, in the mid-1960's, the goal was a 15- to 20-decibel reduction relative to the noises produced by the DC-8 and 707 airplane engines.

The first obstacle to reaching that goal was the high jet noise at takeoff. Recall that the Acoustically Treated Nacelle Program with DC-8 and 707 airplanes produced only minor noise gains at takeoff because of the jet noise. The most effective way of obtaining very low jet noise is to choose an engine with low jet velocity. And low jet velocity is achieved with a high-bypass-ratio engine.

Estimates of noise reductions accompanying increased bypass ratios are shown in figure V-1. This figure was first prepared by NACA in 1954 and was used to advocate the development of low-noise bypass engines in the United States. At that time the only bypass engine was the British Conway. These early calculations were confirmed and extended to higher bypass ratios by Pratt & Whitney as shown in figure V-2. The JT3D, which powers 707 and DC-8 airplanes, the JT9D, and an experimental engine are shown on the graph. At that time the JT9D design was not firm. This graph indicates that a bypass ratio of 5 is required to bring the noise level 15 decibels below that of the JT3D fan technology curve.

The fan noise (fig. V-2) increases with increasing bypass ratio and dominates above a bypass ratio of approximately 1.0. The reduction of fan noise to the level of the jet noise requires the application of several techniques, some of which are discussed in papers II and III. One of the techniques is to reduce fan speed as shown here (fig. V-2). Much of this decrease resulted from other fan changes such as the elimination of inlet guide vanes, the elimination of the second fan stage, and increased spacing between the rotor and the stator. Reducing fan speed is beneficial, however, and if the tip speed is lowered below sonic speed, shock noises can be avoided.

In 1967, under NASA contract, Allison and Pratt & Whitney studied quiet engine designs incorporating high bypass ratios for low jet noise and low-speed, low-noise fans. These studies indicated that, at bypass ratios near 5 or 6 and with low noise fans, noise reductions in the order of 15 to 20 decibels relative to DC-8 and 707 airplane engines were possible.

Concurrently, under NASA contract, the Douglas Aircraft Company studied the application of these engine designs to the DC-8 airplane. The engine characteristics resulting from the study are shown in table V-1.

TABLE V-1. - RESULTS OF ENGINE AND AIRPLANE STUDIES

	New engine	JT3D
Bypass ratio	5.0	1.41
Cruise thrust, (35 000 ft, M = 0.82), lb	4900	4450
Takeoff thrust, lb	23 350	18 000
Nacelle weight, lb	8403	6930
Thrust specific fuel consumption, lb/hr-lb	0.61	0.830
Retrofit cost, $/airplane	5 000 000	------

The JT3D characteristics are shown for comparison. The study showed that, although the Quiet Engine nacelle was nearly 1500 pounds heavier than the JT3D nacelle, the improved fuel consumption more than offset the effects of the weight increase, and the airplane range was extended. In addition, the payload was not changed, the takeoff roll was shortened, and the initial cruise altitude was raised. Everything looked favorable except the cost. The estimated retrofit cost was $5 million per airplane. For new airplanes, the situation is different. The cost of the quiet engine is favorable in competition with other potential new high-bypass engines.

Following the Douglas, Pratt & Whitney, and Allison studies the Quiet Engine project was initiated.

The General Electric Company in 1968 entered into a fixed-price contract to build two experimental Quiet Engines using derated CF6 cores. One engine has a low-speed fan running at a tip speed of 1160 feet per second,

and the other engine has a fan running at the high speed of 1550 feet per second. The two engines are expected to show the relative advantages of fans operating at low tip speeds with high lift coefficients in comparison with fans operating at high tip speeds with low lift coefficients.

The low-speed engine has been completed, tested by General Electric, delivered to Lewis, and tested at Lewis. The high-speed engine has been assembled and is now being tested by General Electric.

Sound absorbing ducts for the fan inlet and outlet along with other nacelle parts have been built by the Boeing Company for the Quiet Engine. This nacelle has been assembled with the engine and is now being tested at Lewis.

Design details of the Quiet Engine and its performance are described in subsequent papers.

NOISE REDUCTION FOR A BYPASS ENGINE

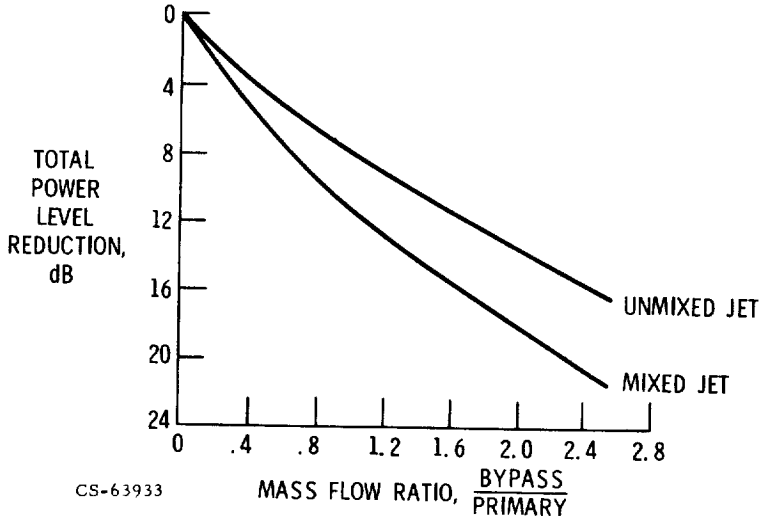

Figure V-1

EFFECT OF BYPASS RATIO ON TAKEOFF NOISE

EQUAL TAKEOFF THRUST

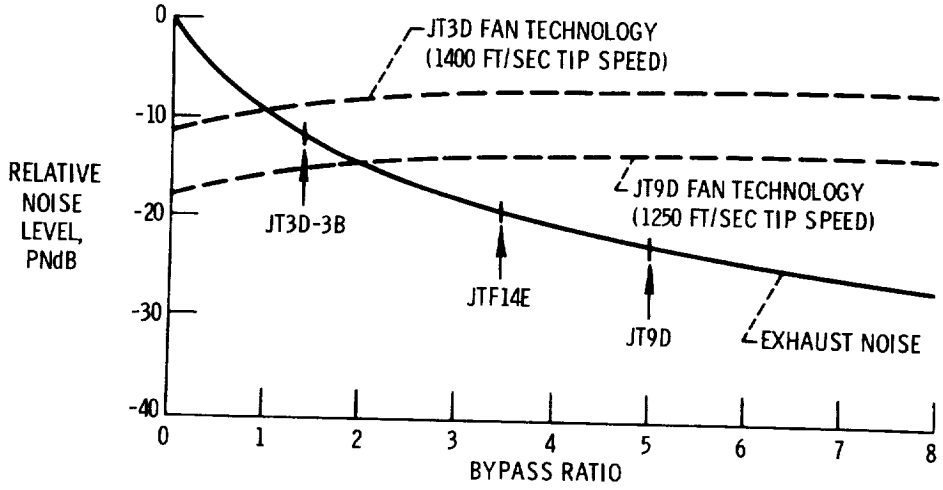

Figure V-2

VI. QUIET ENGINE DESIGN HIGHLIGHTS

Bernard L. Koff*

This discussion highlights both components and engines designed, built, and tested by General Electric for the Quiet Engine Program. Figure VI-1 shows the overall development plan from component to turbofan engine testing. Two low-speed fans (cruise tip speed, 1160 ft/sec) and one higher speed fan (cruise tip speed, 1550 ft/sec) with lower aerodynamic loading were designed and manufactured. All three fans were built, instrumented, and tested in a component vehicle at the General Electric Large Fan Test Facility at Lynn, Massachusetts. Aerodynamic performance and operating characteristics, such as blade vibration, were evaluated with and without inlet distortion. Three screen patterns were used to simulate inlet-pressure distortion resulting from flow separation experienced in typical aircraft installations. After aerodynamic performance evaluation, all three fans were shipped to NASA-Lewis for acoustic testing. After testing fans A and B, fan A was selected for the low-speed turbofan engine.

Two turbofan engines (low-speed A and high-speed C) were built and shipped to Peebles, Ohio, for both acoustic and performance testing. Flight-type inlet configurations, such as the thick lip DC-10 and the thin lip with blow-in doors, were evaluated against the standard bellmouth. The effect of acoustic treated splitters, as well as wall treatment, was evaluated for both the fan inlet and exhaust duct. The discharge of the core engine was also treated to suppress the turbine noise. After evaluation, engine A was shipped to NASA-Lewis for further acoustic testing. Engine C is currently undergoing performance and acoustic testing at Peebles, Ohio.

In figure VI-2 the turbofan demonstrators (low-speed A and high-speed C), both using the proven CF6 core engine operating at reduced speed and turbine temperature, are illustrated and compared.

Both fans are titanium, with fan C designed for lower aspect ratio to utilize advanced lightweight composites. As a result, fan C has longer

*General Electric Company.

chord blading and is also slightly longer than fan A because of the two-chord spacing between the rotor and bypass outlet guide vanes.

Engine A has a four-stage low-pressure turbine straddle-mounted between the turbine midframe and rearframe. Engine C has a close coupled, highly loaded two-stage turbine, which is cantilever-mounted on the low-pressure shaft. This mounting substantially reduces the amount of surface area requiring cooling and also eliminates the need for a rear sump.

Figure VI-3 shows a typical performance map of bypass pressure ratio against fan corrected flow obtained in the Lynn Test Facility. The performance of fan A in this case is shown at the design point at 100 percent corrected speed, including the stall line and efficiency islands. The pressure ratio, airflow, efficiency, and stall margin are tabulated and show excellent performance for this fan at high specific flow (88.3 percent efficiency at 42.5 lb/sec-ft^2 of annulus area).

A comparison of the three fans (two low speed and one high speed) is shown in figure VI-4. The fan A rotor has 40 tip shrouded titanium blades with two seals in the tip shroud and has the higher aspect ratio.

Fans B and C both have 26 titanium blades without shrouds. Fan C rotor blades are longer and also have the highest specific flow based on frontal area, as a result of having a lower radius ratio (0.36 compared with 0.47). The higher blade speed permits using a lower radius ratio without excessive aerodynamic loading. Fan C also has a higher bypass pressure ratio, which results in greater specific thrust (lb thrust/lb airflow) and therefore requires a smaller fan tip diameter and lower flow to produce the same engine thrust (68.3 in. against 73.4 in. and 915 lb/sec against 980 lb/sec for the other fans).

All three fans have approximately the same vane-blade ratio ($\sim 2\frac{1}{4}$) and identical rotor to stator spacing in both bypass and core flow paths.

CORE ENGINE DESCRIPTION

The single-spool 16-stage core compressor with variable inlet guide vanes and six variable stators is shown in figure VI-5. The design airflow is 139 pounds per second at 16.8 pressure ratio. The compressor operates

at 104 pounds per second flow and pressure ratio of 12.0 in the Quiet Engine demonstrators. The horizontal split casing permits individual blade replacement in the rotor spool. The eighth, ninth, and thirteenth stage bleed manifolds are shown and used for cabin, sump, and turbine cooling.

Figure VI-6 shows the annular stacked ring combustor and combined rear frame and outer casing. Thirty high-pressure atomizing dual-fuel nozzles are used for high- and low-range operation. High dome flow is also used for low smoke. The combustor has a design temperature rise of 1600° F and operates at a temperature rise of 1380° F in the Quiet Engine.

The two-stage high-pressure turbine is shown in figure VI-7. This turbine has moderate aerodynamic loading, a work extraction of approximately 90 Btu per pound per stage and high efficiency (91.5 percent). The first-stage blade is cooled by convection with impingement and film cooling on the leading edge. The design turbine rotor inlet temperature is 2370° F and runs derated to 1970° F in the Quiet Engine demonstrators.

Figure VI-8 shows the core engine assembly prior to going horizontal at main engine buildup.

LOW-PRESSURE COMPONENTS - ENGINE A

The low-pressure components for engine A use the tip shrouded fan and a four-stage modified CF6 turbine with the last-stage removed. The turbine was rematched by closing the stage 1 nozzle diaphragm area 6 percent.

The 40-blade-tip shrouded rotor assembly is shown in figure VI-9 and is a proven design concept introduced at General Electric in 1965. This fan configuration has high efficiency and rugged blading with excellent aeroelastic stability and low overall vibratory characteristics. The interlocks are located as shown and hold the blade tip sections in the design position during unsteady flow conditions. Individual replacement is made by removing a shim below the dovetail and displacing the blade radially inward to disengage the shroud interlocks.

Figure VI-10 shows the fan A stator with bypass and core outlet guide vanes and splitter. The flow path surfaces are lined with acoustic panels using an aluminum perforated sheet and multiple degree-of-freedom diamond

core treatment. The required porosity of the double diamond core is provided by slots rather than holes to allow flexibility for compound forming. This also eliminates the need for individual core tooling on each panel. Drainage of condensate or fuel is also provided by circumferentially oriented channels formed by the core material combined with these forming slots and panel edge holes. An abradable material is used over the rotor tip shroud seals to allow the seals to wear in without overheating.

The tip shrounded four-stage low-pressure turbine rotor is shown in figure VI-11. This turbine is lightly loaded with a work extraction of 90 Btu per pound and a design point efficiency of 91.8 percent.

Figure VI-12 shows the main engine buildup with core, variable compressor stator actuation system, piping, and low-pressure fan and fan turbine components. The engine is shown in figure VI-13, mounted in the overhead thrust stand with the bellmouth inlet. An aft end view showing the separated fan and core exhaust is shown in figure VI-14 with two radial traversing acoustic probes at the entrance and the exit of the fan exhaust duct.

Figure VI-15 shows the performance test setup with the inlet rakes ahead of the fan and the traversing core smoke probe. The core smoke was measured at an SAE smoke number of 7 and well below the threshold of visibility, which is approximately an SAE smoke number of 25.

Figure VI-16 shows the engine in the test stand and the far field microphone test setup. There are sixteen 40-foot microphone towers in a 150^{o} arc. The engine is shown in figure VI-17 with the thick-lip DC-10 type inlet and the acoustic probes in the fan exhaust duct; figure VI-18 shows the thin lip inlet with simulated blow-in doors. This inlet is 12 percent smaller in frontal area and 11 percent shorter than the thick lip inlet. The recovery at takeoff for this inlet was approximately 2 percent lower and at a somewhat higher radial distortion than the thick lip inlet.

LOW-PRESSURE COMPONENTS - ENGINE C

The high-speed C engine was also built up for testing at Peebles and uses fan C with the new highly loaded two-stage low-pressure turbine. Figure VI-19 shows the low radius ratio fan C assembly. This fan demonstrated

good vibration characteristics with various kinds of inlet distortion without shrouds. The treated stator and frame incorporating acoustic panels is shown in figure VI-20 with bypass and tandem core outlet guide vanes to accommodate the high aerodynamic loading. Figure VI-21 shows the low-pressure combination turbine stator and frame that close couples the low-pressure and high-pressure turbines.

Figure VI-22 shows the two-stage highly loaded low-pressure turbine with 90- to 91-percent efficiency based on recent engine test data. This turbine has equivalent efficiency to the four-stage turbine with less than one-half the number of airfoils. The first stage of this two-stage turbine demonstrated a high pitchline loading ($2Jg\Delta h/Up^2$) of 1.6 and did most of the work extraction, while the second stage was lightly loaded to reduce discharge swirl.

The main engine C buildup is shown in figure VI-23 before shipment to test, and figure VI-24 shows the high-speed engine in the test stand during performance testing.

SUPPERSUPPRESSED INSTALLATIONS

In addition to the basic performance and acoustic evaluation of the engines, a number of tests are being made with configurations to further suppress engine noise.

Figure VI-25 illustrates the suppressed configurations that have been run on engine A and those planned for evaluation on engine C. The base configuration incorporates acoustic treatment extending from ahead of the rotor through the frame. The supersuppressed configuration tested includes an extended inlet with full-length treatment, a three-ring treated splitter in the inlet, extended aft treatment in the fan exhaust duct (inner and outer flow path), and a treated exhaust duct splitter. Treatment in both inner- and outer-core engine exhaust nozzles is also used to suppress the turbine noise. A number of tests with various combinations of treatment were made to identify the effectiveness of the separate sections of the treatment. Some of these data will be discussed in following papers.

The hardware for the engine C supersuppressed configuration will be

evaluated this summer. A contoured bellmouth more representative of a flight-type inlet will be used. A four-ring acoustic splitter will also be evaluated separately. A specially designed wall treatment to suppress the multiple pure tones characteristic of the high-speed fan will also be evaluated. The aft treatment will include a contoured splitter with the duct Mach number reduced to improve the effectiveness of the treatment and to minimize flow scrubbing noise. Core engine exhaust nozzle treatment to suppress turbine noise is also used.

Planned engine tests will include a number of combinations that will permit evaluation of the effectiveness of the separate elements. Figure VI-26 shows the engine A on test with the acoustic treated splitters and outer casing. Figure VI-27 shows the aft acoustic treated splitter in the fan exhaust duct including the inner and outer flow path. The two rows of double-layer sheet/honeycomb acoustic panels for both inner and outer flow paths used in the core engine exhaust nozzle are shown in figure VI-28.

The acoustic and engine performance results of these engine configurations will be presented in subsequent papers.

SUMMARY

Summarizing the component and engine testing: Three high performance fans were designed, built, and tested, accumulating 444 hours. All three fans are both aerodynamically and mechanically suitable for direct incorporation into engine applications. Two turbofan demonstrators to evaluate both low- and high-speed fan systems were also designed, built, and tested (accumulating 158 hr). All components and engine systems are demonstrating high reliability.

These components have demonstrated advanced state-of-the-art in acoustics, aerodynamics, and mechanical design. The next step is to incorporate this demonstrated technology and additional improvements into advanced flight systems with even lower noise and better performance.

NASA-GE QUIET ENGINE PROGRAM TURBOFAN ENGINE DEVELOPMENT

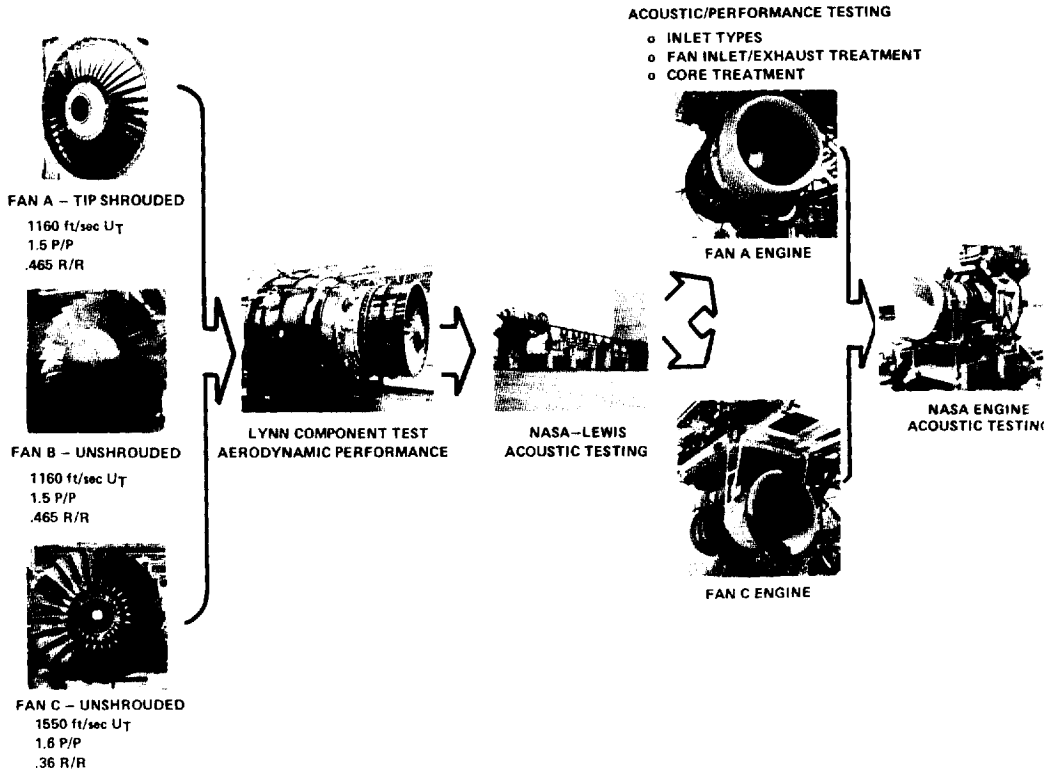

Figure VI-1

NASA-GE QUIET ENGINES

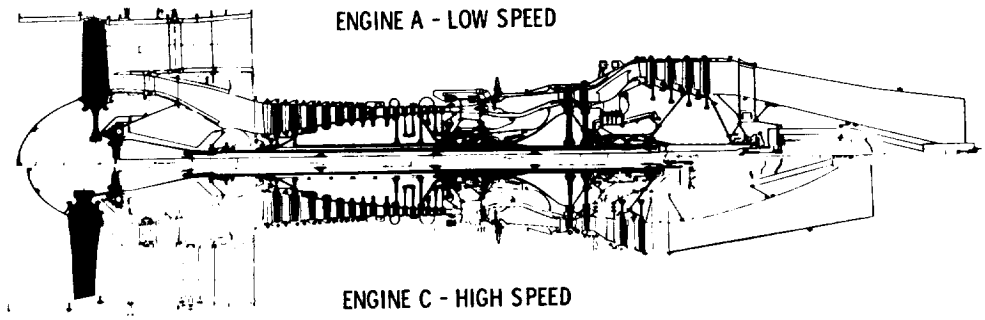

Figure VI-2

FAN A AERODYNAMIC PERFORMANCE

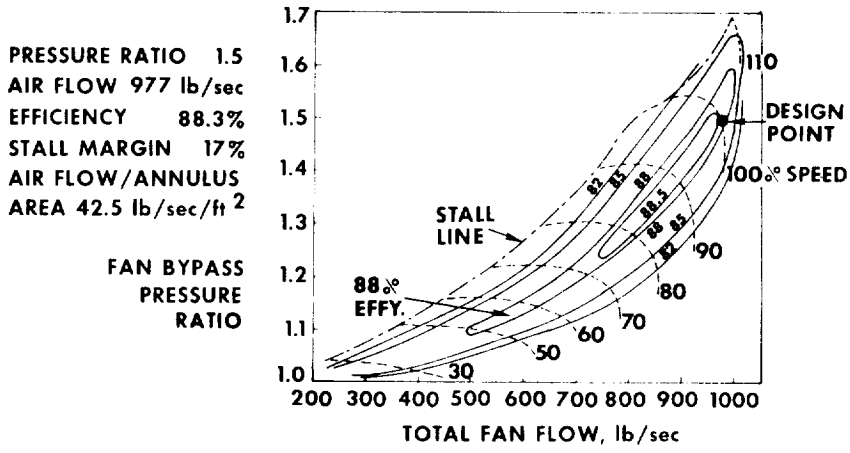

Figure VI-3

QUIET ENGINE FAN DESIGN

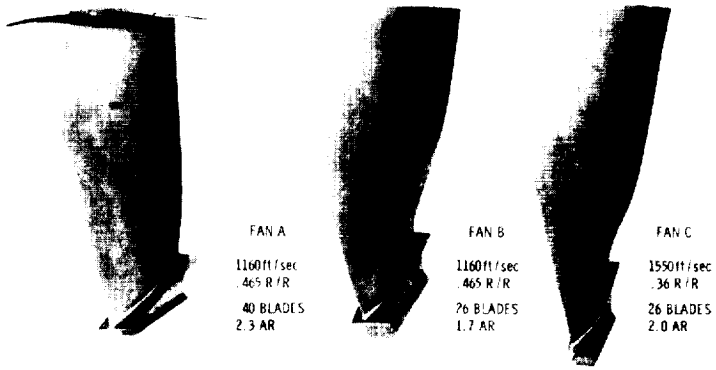

FANS		A	B	C
• AIRFLOW, lb/sec	100% $N/\sqrt{\theta}$	977	983	915
• BYPASS - PRESSURE RATIO		1.5	1.5	1.6
- EFFICIENCY, %		88.3	87.0	84.0
• $W\sqrt{\theta}/\delta/A_F$ lb/sec-ft^2		33.3	33.5	36.0
• ROTOR TIP DIA, in.		73.4	73.4	68.3
• BLADE/VANE RATIO		40/90	26/60	26/60
• ROTOR - STATOR SPACING				
- BYPASS			2 ROTOR CHORDS	
- CORE			1-1/4 ROTOR CHORDS	

Figure VI-4

COMPRESSOR

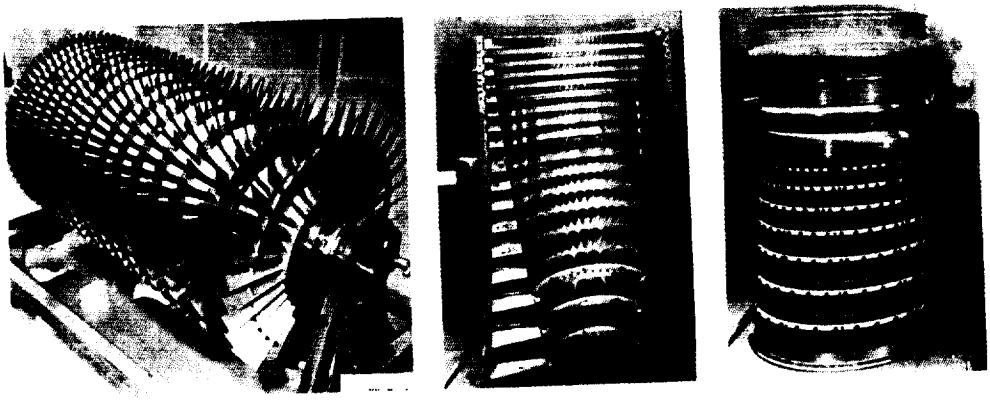

16 STG COMPRESSOR ROTOR

STATOR ASSEMBLY

Figure VI-5

COMBUSTION SECTION

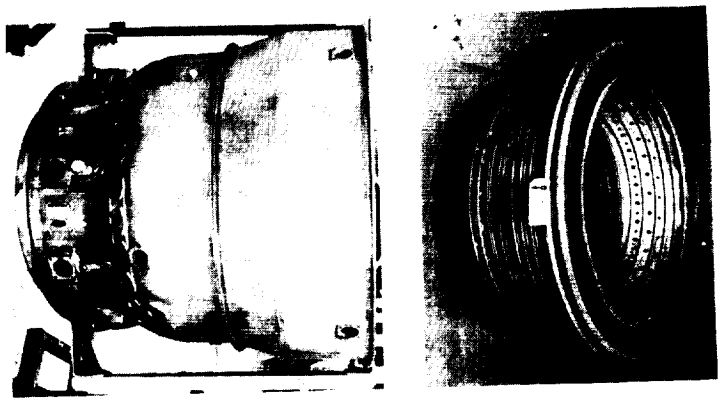

REAR FRAME AND OUTER CASING

COMBUSTOR

Figure VI-6

TWO-STAGE HIGH-PRESSURE TURBINE

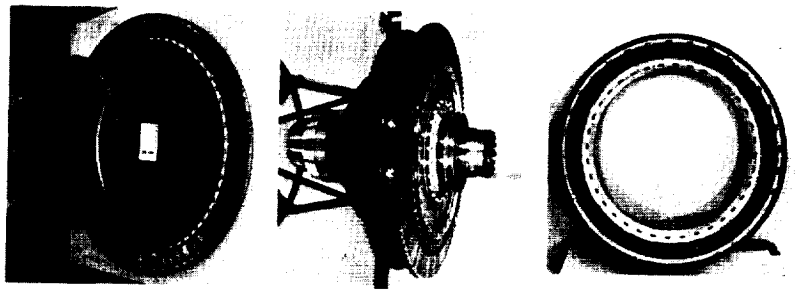

1ST STAGE NOZZLE DIAPHRAGM ROTOR ASSEMBLY 2ND STAGE NOZZLE DIAPHRAGM

Figure VI-7

CORE ENGINE ASSEMBLY

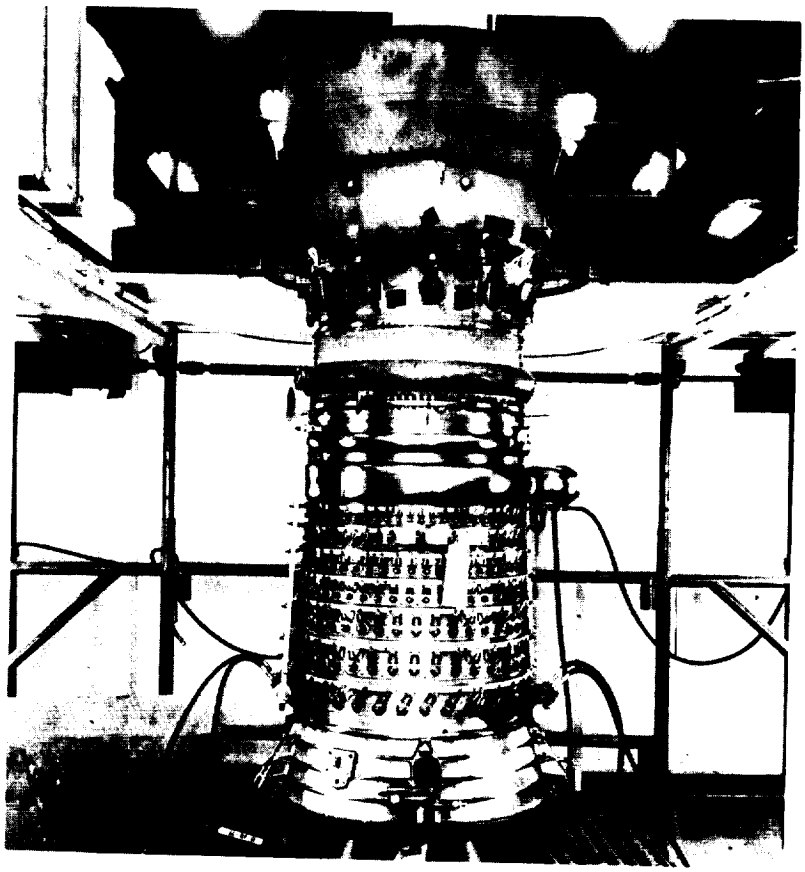

Figure VI-8

TIP SHROUDED FAN A ROTOR ASSEMBLY

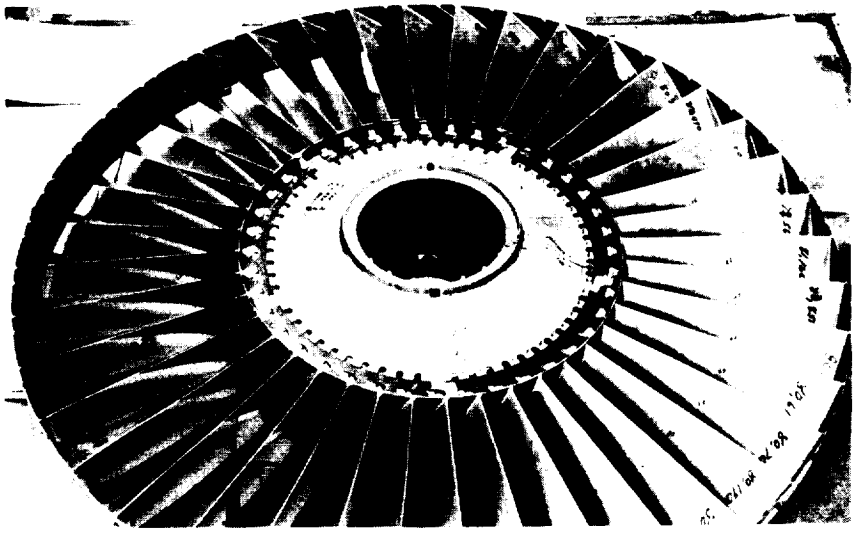

Figure VI-9

ACOUSTIC TREATED FAN A STATOR WITH BYPASS AND CORE OUTLET GUIDE VANES

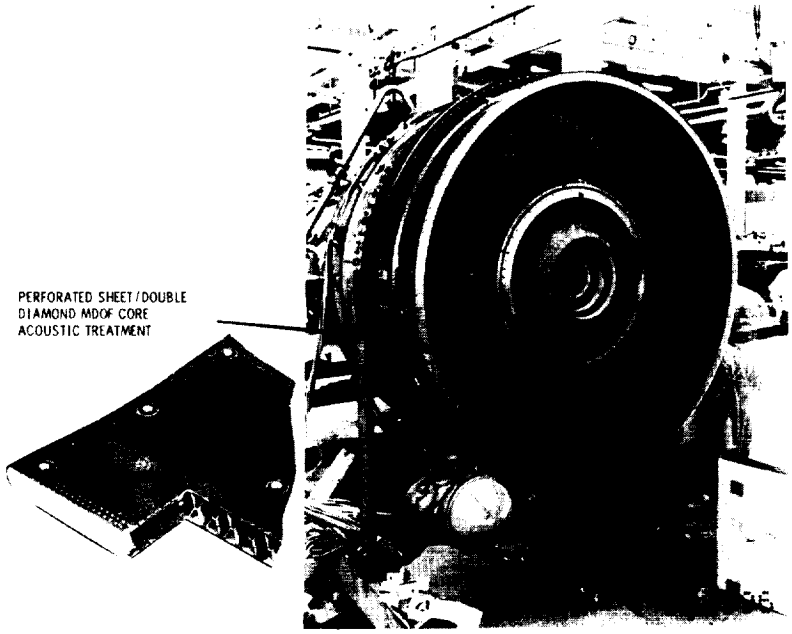

Figure VI-10

FOUR-STAGE LOW-PRESSURE TURBINE
ROTOR ASSEMBLY

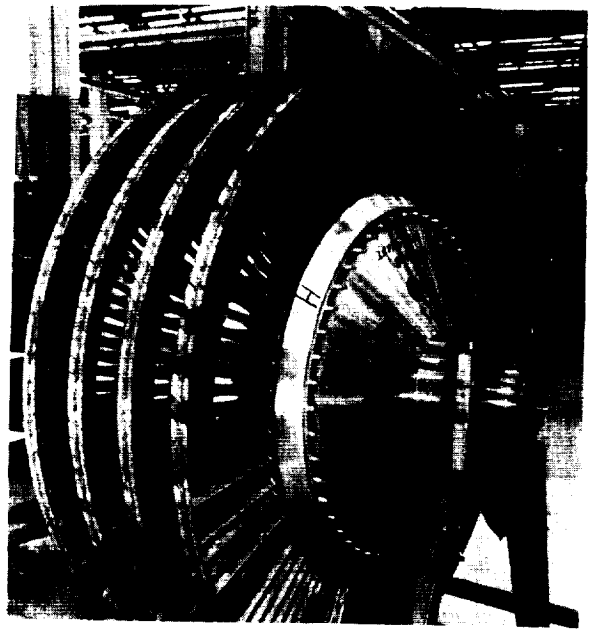

Figure VI-11

MAIN ENGINE A ASSEMBLY

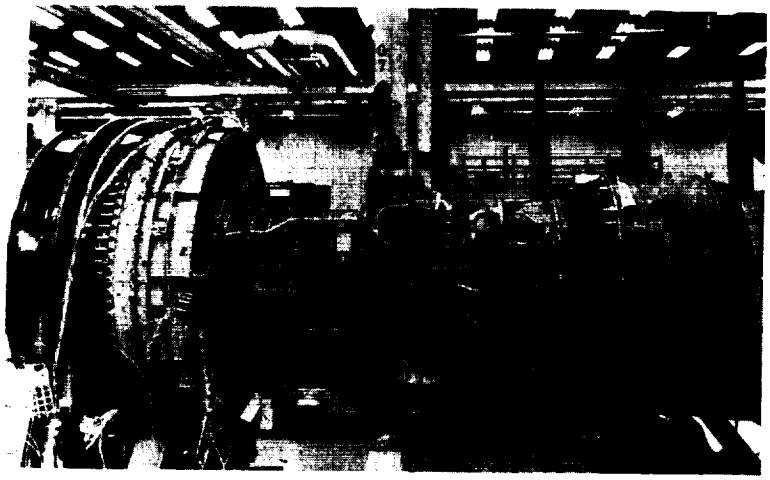

Figure VI-12

FRONT END OF ENGINE A IN TEST STAND AT PEEBLES, OHIO

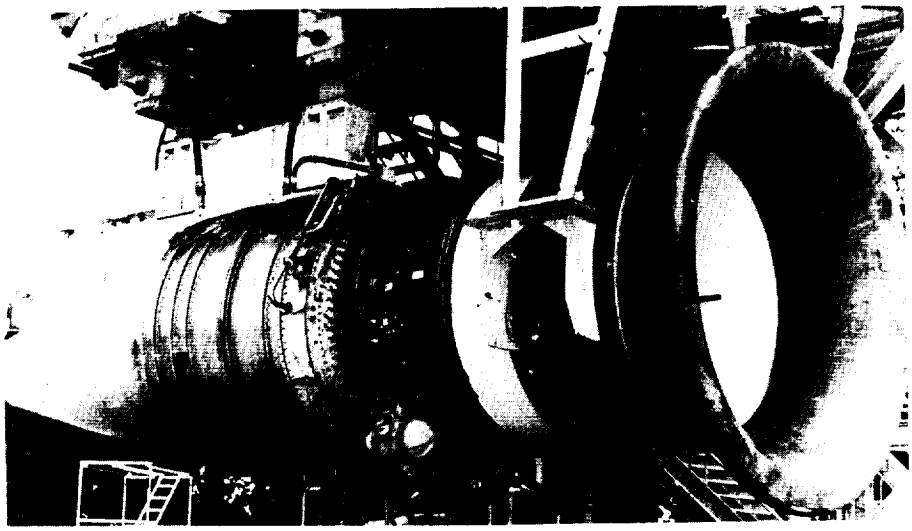

Figure VI-13

AFT END VIEW OF ENGINE A IN TEST STAND AT PEEBLES, OHIO

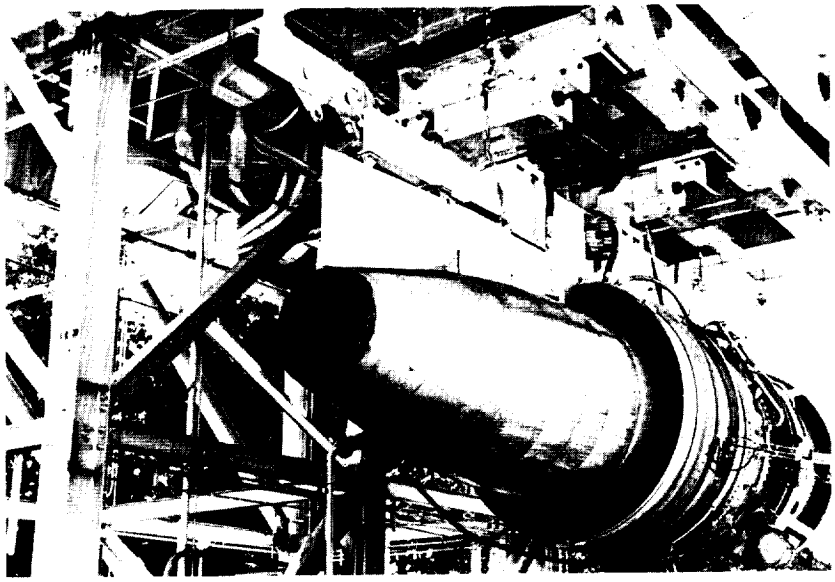

Figure VI-14

ENGINE A PERFORMANCE TEST SETUP INCLUDING TRAVERSING CORE SMOKE PROBE

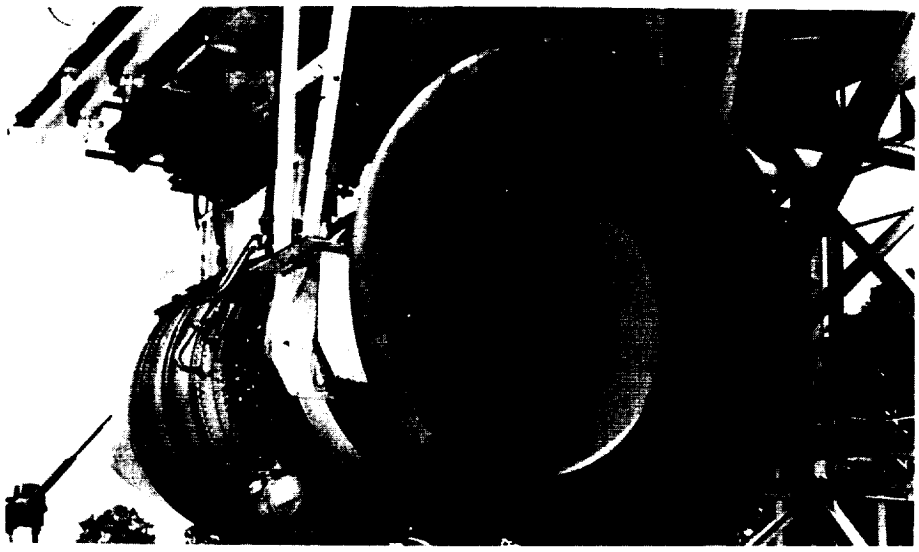

Figure VI-15

FAR FIELD ACOUSTIC MICROPHONE SETUP

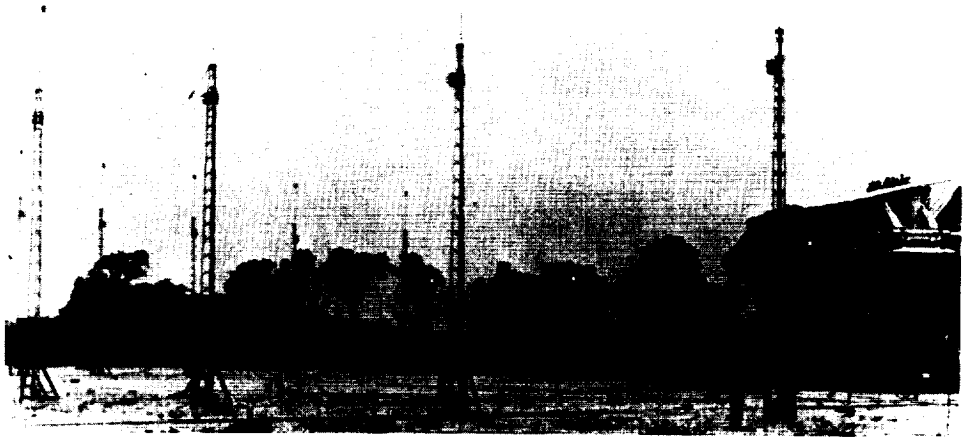

Figure VI-16

ENGINE A THICK LIP INLET CONFIGURATION

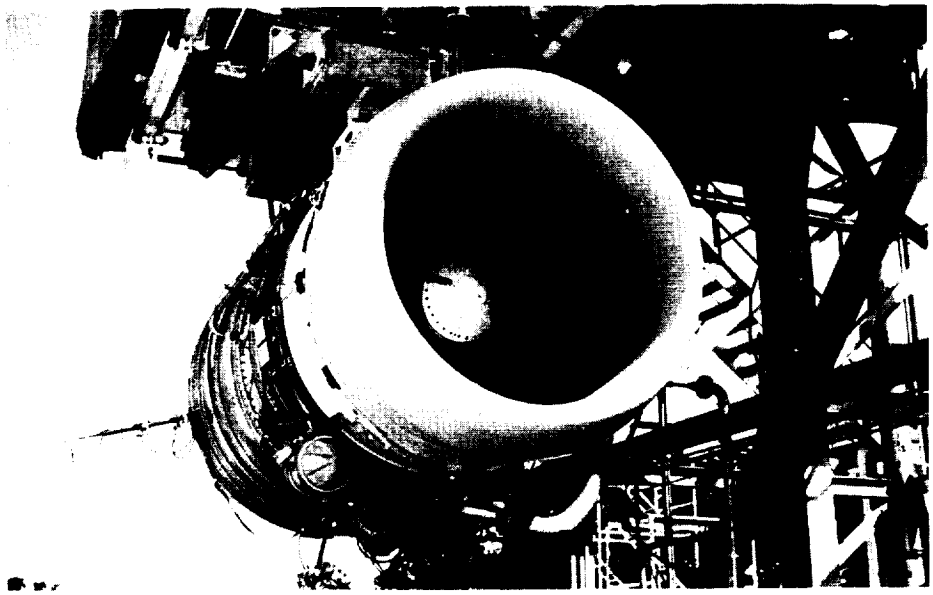

Figure VI-17

ENGINE A THIN LIP BLOW-IN DOOR INLET CONFIGURATION

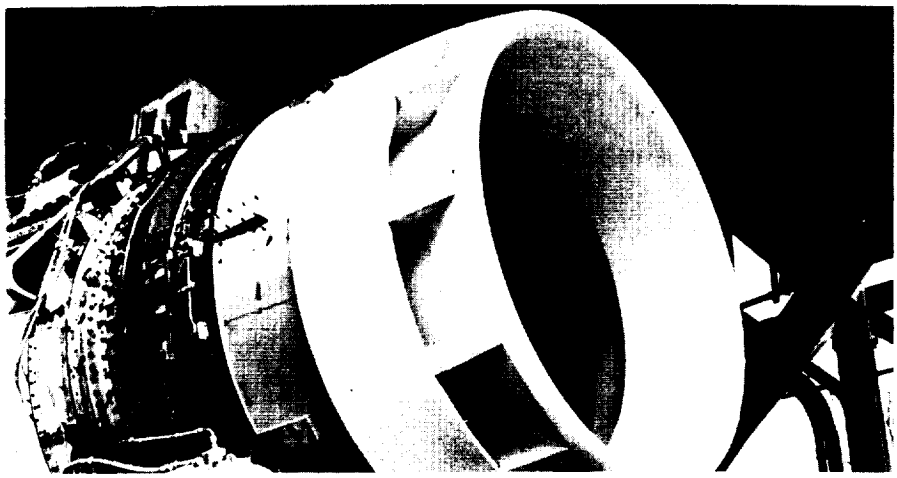

Figure VI-18

FAN C ROTOR ASSEMBLY

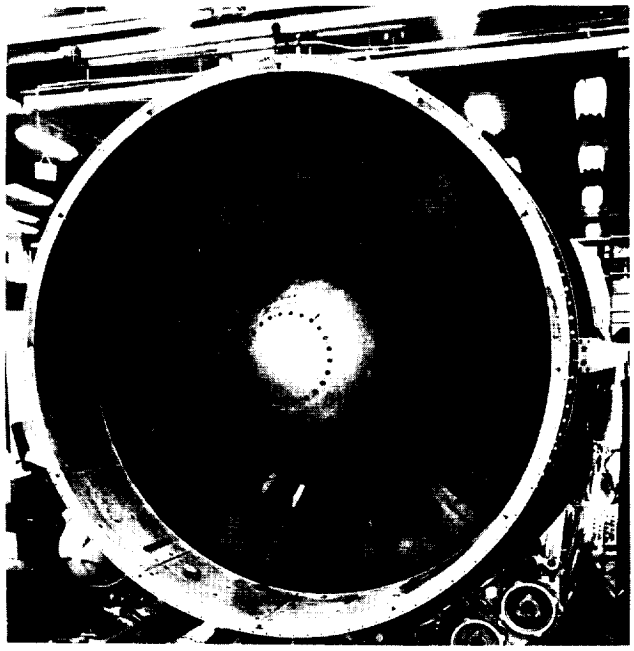

Figure VI-19

ACOUSTIC TREATED FAN C STATOR WITH BYPASS
AND TANDEM CORE OUTLET GUIDE VANES

Figure VI-20

TURBINE C MIDFRAME AND FIRST-STAGE LOW-PRESSURE NOZZLE DIAPHRAGM

Figure VI-21

TWO-STAGE LOW-PRESSURE TURBINE C ROTOR ASSEMBLY

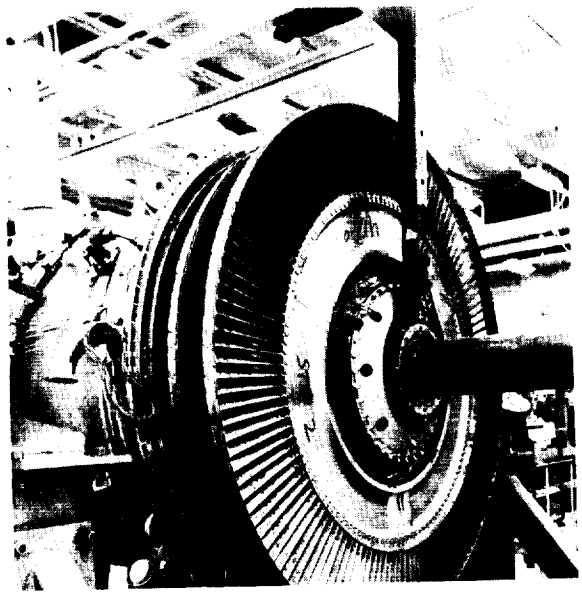

Figure VI-22

MAIN ENGINE C ASSEMBLY

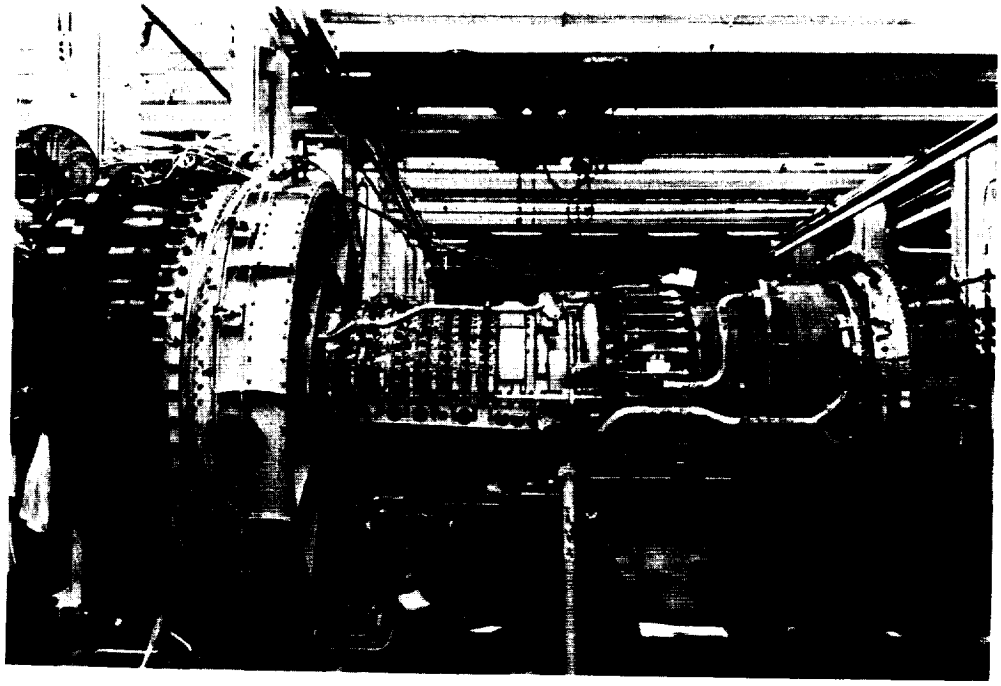

Figure VI-23

ENGINE C TEST STAND AT PEEBLES, OHIO

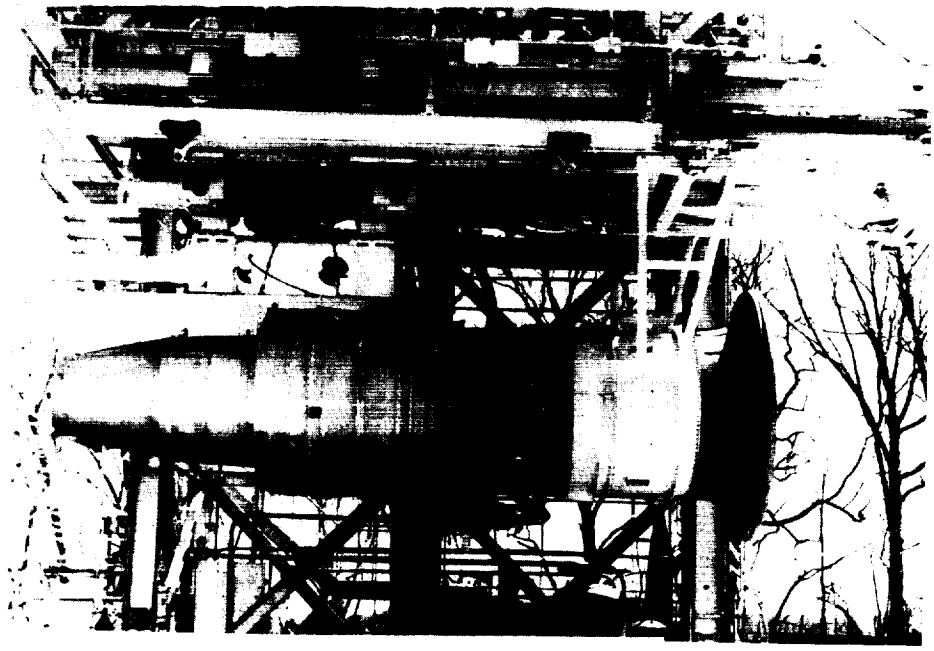

Figure VI-24

NASA-GE SIMULATED SUPERSUPPRESSED ENGINE INSTALLATIONS

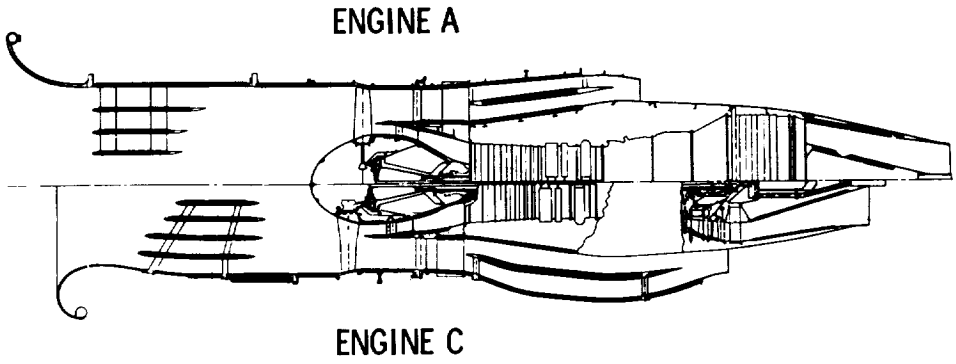

Figure VI-25

NASA-BOEING INLET WITH ACOUSTICALLY TREATED SPLITTERS

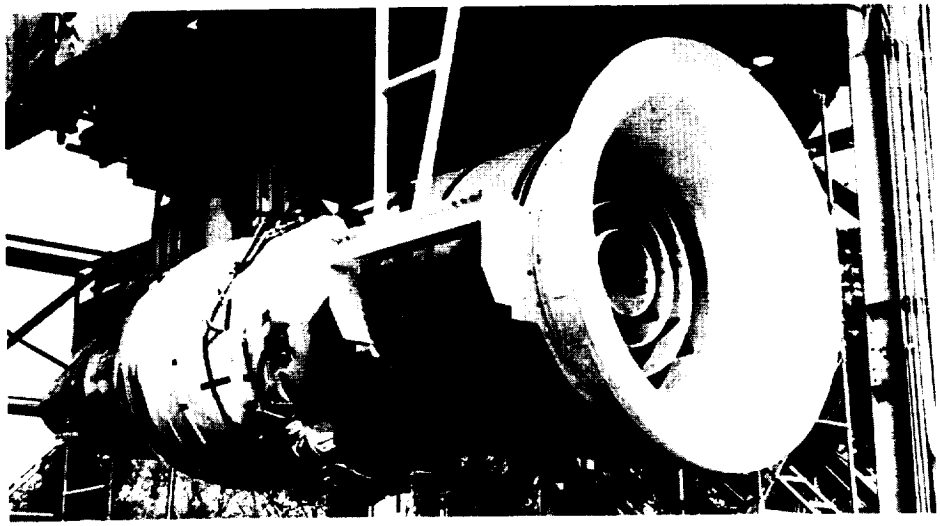

Figure VI-26

ENGINE A FAN EXHAUST DUCT SPLITTER WITH ACOUSTIC TREATMENT (INSTALLED)

Figure VI-27

ENGINE A CORE EXHAUST NOZZLE

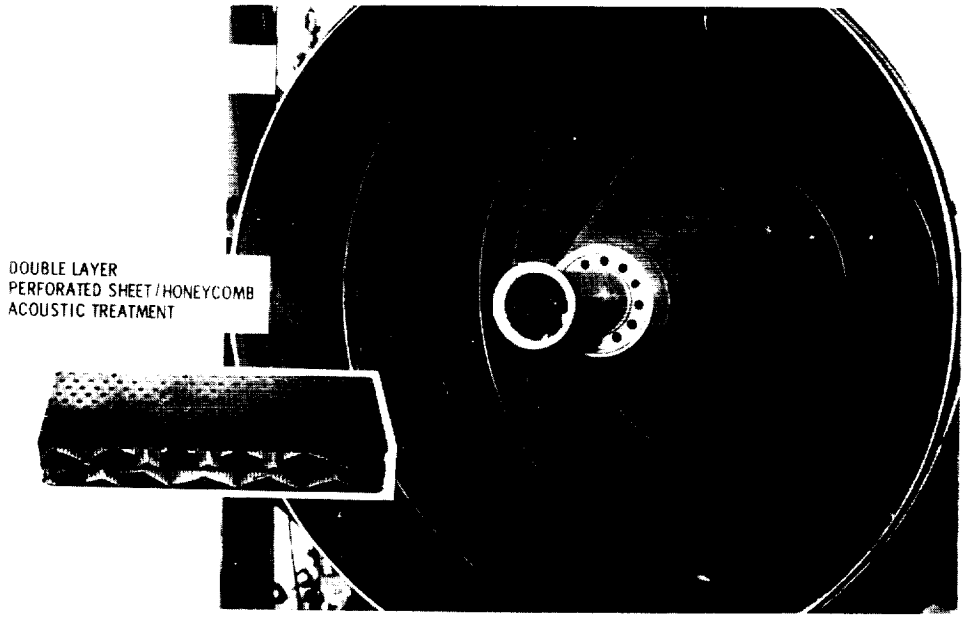

Figure VI-28

VII. QUIET ENGINE NACELLE DESIGN

M. Dean Nelsen*

For nearly 2 years the Boeing Company has been under contract to Lewis Research Center in a program of developmental design, fabrication, and testing of acoustic suppressors for the fans of high bypass ratio engines.

The quiet fans which have been under study are products of the NASA Quiet Engine Program. The Fan Noise Suppression Program is aimed at the further reduction of fan noise emanating from engines with fans which have been designed to minimize noise. Specifically, the fans studied in the suppression program have been the Lewis fan D and the General Electric Company fan A, both low tip speed fans. The program has been both technology and hardware oriented. Some of the specific objectives of this program include the development of the necessary technology and methodology for the design of inlets and fan ducts for the purpose of providing high fan noise attenuation. During 1969, the Douglas and Boeing companies flew nacelles designed to minimize the fan noise of existing JT3D engines during landing approach. The technology from this program was applicable to the two-stage fans of lower bypass ratio engines. In this case, the engine had not been designed to minimize noise. Thus, one of the objectives of the current Fan Noise Suppression Program is to adapt the technology generated during and since the previous flight test demonstrations and extend this technology to the modern Quiet Engine. Of concern in the suppression of noise from large single-stage quiet fans is the influence of the noise suppressor on fan aerodynamic performance and the resulting possibility of additional noise generation. Therefore, an important objective of the Fan Noise Suppression Program is to ascertain these effects based on actual measurements on full-scale hardware. Four nacelles have been conceptually designed during this program: two for an engine installation, and two for a full-scale fan rig test. Of these four, two have been detail designed for scheduled testing. A fan nacelle will be fabricated and delivered to Lewis in late 1972 for quiet

*The Boeing Company.

fan D full-scale fan rig tests. The second nacelle is the Quiet Engine nacelle now under test at Lewis. The remainder of this presentation is devoted to an overview of the Quiet Engine nacelle, some of its design features, new technology aspects, and the expected performance.

The Quiet Engine nacelle has four primary objectives. First, it is a nacelle which may be installed on the Quiet Engine for the purpose of ground tests to provide detail information on suppressor technology and the interrelations between the Quiet Engines and the nacelle. This Quiet Engine nacelle is designed with a goal of reducing peak fan noise by 15 PNdB (perceived noise decibels) in both the forward and aft quadrants. Although 15 PNdB cannot be measured on the Quiet Engine today because of jet and turbomachinery noise floors, the configuration is designed to provide long term flexibility such that noise floors can be studied and reduced without uncovering the fan noise. Finally, the nacelle must be representative of good aircraft nacelle design practices; that is, the nacelle must provide compatibility of internal and external aerodynamic lines. The inlet configuration must be chosen to provide the capability of being anti-iced and must not have adverse effects on the proper operation of the engine. Such things as influence of crosswind is an important consideration. The fan duct choice should again be compatible with proper operation of the engine and be realistic and representative of flight nacelles in the sense that additional hardware, such as thrust reversers, could be worked into the design.

The selected nacelle which has been designed and fabricated for the Quiet Engine is shown in figure VII-1. The nacelle excluding afterbody and pylon consists of a three-ring treated inlet, wrap cowl around the accessory section, and a single ring half-length treated fan duct. The nacelle design shown is intended for a pylon installation on an aircraft with a design cruise at Mach 0.82. The inlet rings and fixed treated centerbody are supported primarily from six forward radial struts and three aft stabilizing struts. The wrap cowl section covers the fan case mounted accessories. The fan duct provides for two possible concepts in fan reverser design and is designed to provide access to the engine. The nacelle is basically of glass fiber construction with aluminum supporting structure. The external cowling is necessary to preclude flanking noise paths from the engine case accessory and associated structures.

With a fan noise design objective of 15 PNdB, the relation of total inlet length to the number of acoustically treated circumferential rings in the inlet is indicated in figure VII-2. A flight inlet must provide internal diffusion for minimization of external aerodynamic drag during cruise plus providing for the necessary acoustic treatment to achieve the noise reduction. If the acoustic requirement were ignored, the inlet length which provides good balance between internal and external performance (with the absence of auxiliary "blow-in" doors) would provide an aerodynamic throat internally designed for the maximum corrected weight flow through the engine and approximately a 25-percent elliptical contraction between the highlight and the throat. Just downstream of the throat diffusion begins, and the contours at that station are critical. In order to prevent boundary layer separation under static operation, the angle θ must be very carefully controlled. If the hub-tip ratio of the Quiet Engine with fan A and the entrance flow angles to the fan are considered, the best aerodynamic design would be approximately 78 inches long. A "no-ring" inlet with peripheral treatment and a 15-PNdB noise reduction requirement would have astronomical length. The insertion of two acoustically treated rings would require approximately a 90-inch inlet; the three-ring inlet would be equal in length to the best aerodynamic design. A further increase in the number of acoustically treated rings would provide a longer inlet since the treatment thickness increases as flow passage size decreases. Consequently, to maintain the acceptable initial diffusion and maintain reasonable internal Mach numbers, a longer inlet is required. Thus, the selected three-ring design for the Quiet Engine inlet provides no compromise on inlet length and, consequently, no compromise in external aerodynamics.

In figure VII-3, the treated area required within the inlet is related to the number of acoustically treated rings. A two-ring inlet with an unlined centerbody requires approximately twice the treated area of a three-ring design. Treating the centerbody for the two-ring design has tremendous leverage in the reduction of the required treated area. For the three-ring design, a lined centerbody still provides a 25-percent reduction in treated area. The selected inlet design, then, requires 353 square feet of acoustic treatment to provide a 15-PNdB noise reduction. Treated area, of course, is wetted area in an inlet, and a wetted area is skin friction and weight.

Therefore, internally, the chosen design represents a substantial reduction in internal pressure losses over designs with fewer rings. A detailed anti-icing analysis of the three-ring design indicated marginally adequate capability within existing engine bleed availability. A further reduction in inlet treated area by the addition of a fourth ring would result in a design that probably could not be anti-iced.

The inlet acoustic treatment was designed realizing the severe effect that a boundary layer (or shear layer) has on lining attenuation. Figure VII-4 shows the theoretical relation of attenuation as a function of one-seventh power turbulent boundary layer thickness. The lower curve relates the dropoff in attenuation that one could expect for a lining design for the noted geometry and environmental conditions if the boundary layer thickness were ignored. Immersing a lining designed for the mean flow Mach number, in the absence of a boundary layer, could have disastrous results. A typical outer cowl inlet boundary layer near the fan face is of the order of 1.5 inches during takeoff conditions. In this case, a mean flow design would lose about 40 percent in theoretically available attenuation. This loss in expected attenuation has been observed in flow duct testing when one compares the test data with theory. The same phenomenon is not observed when the airflow and the acoustic energy are traveling in the same direction, such as in a fan duct. It has been shown theoretically in this program that, if the boundary layer is considered in the design of the inlet linings, a significant portion of the lost attenuation can be recovered by impedance adjustment. The upper curve on figure VII-4 indicates the theoretically achievable attenuation when the lining impedance is adjusted for the boundary layers indicated. Physically, the adjustment required is a reduction in resistive impedance with a corresponding increase in backing cavity depth. Thus, a key item of technology in inlet lining design is a thorough understanding of the boundary layer growth on all acoustically treated surfaces.

The configuration of the outer passage of the inlet is shown in figure VII-5. This passage is typical of all four of the flow channels in the inlet. The acoustic rings were located on streamlines. A boundary layer analysis was made to evaluate the stability of the boundary layer at the ring locations as well as to aid in the lining design. The required attenuation of fan noise is quite broadband since the quiet fan has relatively low blade passage tone

amplitudes with respect to the associated broadband noise. Three basic single degree of freedom linings were selected to provide the broadband attenuation for a noise reduction of 15 PNdB. The linings were tuned to the first, second, and third harmonics on the blade passage frequency at approach power fan speed. The linings on each wall of the channel were segmented as shown. Each lining is opposed by a like design on the opposite wall, thus allowing a configuration readily adaptable to theoretical analysis. Although there are only three basic linings in each channel, four sections of lining are provided in the outer channel in order to allow staggering of the linings on the treated rings. The staggering was accomplished to minimize the thickness of the rings and the associated aerodynamic performance losses. The next inward channel lining arrangement provides only three segments of lining, as can be seen on the inward side of the ring. The chosen face sheet material for the acoustic linings is a laminated glass fiber impregnated with a polyimide resin. The face sheet resistance is varied by the number of plies of glass fiber cloth in the laminate. The segments vary in length from 5 to 20 inches, and the backing cavity depth varies from 0.1 to nearly 0.75 inch. Since each segment of the lining requires a different acoustic impedance, both the face sheet resistance and backing cavity depth must be segmented.

In order to obtain a better idea of how a segmented lining, as shown in the previous figure, has been incorporated in the nacelle, a typical lining construction from the inlet is shown in figure VII-6. As mentioned previously, the lining facing sheets are constructed of many layers of polyimide impregnated glass cloth. The layers of glass cloth are arranged with angular orientation to provide uniformity in the permeability of the structure. As shown on this example, the transition between one segment of lining and another segment of lining provides a uniformly smooth aerodynamic surface with no loss in treated area. The 15 layers of cloth required for the thin lining must taper to the 7 plies for the thick lining. This transition can be accomplished in actual practice in approximately 0.5 inch. It is interesting to note that the thin lining facing sheet thickness is greater than the backing cavity depth. The polyimide facing sheet is bonded to a honeycomb cell structure and again bonded to an impervious backing sheet. This material was chosen for the nacelle design for numerous reasons. Some of these

reasons are as follows:

(1) The material has structural load carrying capability as it is used in the nacelle.

(2) The material has service test experience in airline usage.

(3) The material has a 400^{O} continuous operating temperature capability, thereby being compatible with engine compartment temperature.

(4) The most compelling reason is that glass cloth layup allows the segmentation of the acoustic linings with an uninterrupted structure. As seen from the photomicrograph (fig. VII-6), a uniform permeable structure results.

All the acoustic linings in the nacelle were designed analytically. Testing was accomplished, however, to determine the acoustic impedance properties of the materials which were considered. The special test setup used to determine the impedance properties under the environment of sound pressure level and grazing airflow is shown schematically in figure VII-7. This grazing flow impedance test apparatus was designed to accept acoustic panels on one wall of the test section. The testing section, with three walls unlined, has a 2 by 2 inch cross section to prevent the existence of acoustic modes other than the fundamental mode. Thus, the device is an acoustic wave guide. The airflow and sound are supplied in the same direction to minimize the effects of boundary layer on wave propagation. Within the test section, the wall opposite the test specimen is provided with a stationary flush-mounted microphone and a translating flush-mounted microphone. When the data from the two microphones are compared, the complex propagation constants in the axial direction can be ascertained from the resulting axial phase and attenuation rates. Knowing these constants and that only one mode exists makes it possible to compute the complex impedance.

Typical data obtained from this impedance rig are shown in figures VII-8 and VII-9. Figure VII-8 shows the resistive impedance of a 12-ply polyimide face sheet at 1500 hertz as a function of the test section Mach number and sound pressure level. It is interesting to note that the normalized resistance is both a strong function of Mach number and sound pressure level. Likewise, the reactance of the 12-ply face sheet as a function of Mach number and sound pressure level is shown in figure VII-9. Knowledge of such environmental effects on installed impedance, as noted in these last

two figures, is necessary in order to reliably predict attenuations analytically.

The theoretical prediction of the attenuation is shown in figure VII-10 as a function of frequency for the Quiet Engine nacelle inlet outer channel described in the previous figures. The theoretical prediction was made assuming no boundary layer in the inlet. The lining impedances had not been adjusted for boundary layer effects. The data scattered around the theoretical curve are test results from flow duct measurements for the actual lining design in the Quiet Engine inlet. Of course, the flow duct measurements include the effects of boundary layer. Since the linings tested were adjusted for the presence of realistic boundary layers, most of the attenuation that would normally be expected to be lost if the boundary layer in the design had been ignored is recovered.

The inlet rings and treated centerbody are shown prior to assembly in figure VII-11. The rings were fabricated in two halves and mechanically joined prior to assembly. The treated portion of the centerbody was fabricated as a continuous 360^{o} part.

The assembled inlet is shown in figure VII-12. The flight lip is removable to allow installation of a flight simulation bellmouth.

In figure VII-13 is a view of the inlet illustrating the relation of the inlet rings to the fixed centerbody and outer cowl. The six forward support struts incorporate provisions for acoustic and aerodynamic instrumentation probes.

Figure VII-14 shows the relation of the rings to the centerbody and cowl just upstream of the fan face. The fan A rotating spinner fits into the centerbody and is allowed to spin during engine operation. The Teflon rub seal is incorporated in the fixed centerbody to prevent a flanking noise path through the centerbody structure.

The fan duct lining configuration is shown in figure VII-15. In the same fashion as in the inlet design, the linings are segmented to provide the broadband attenuation. Likewise, the linings are staggered between the two channels to minimize thickness of the circumferential ring. A longer or thicker ring would severely affect the balance between internal and external aerodynamics. Thus, the low frequency lining, shown as number 2 on the diagram, was tuned to 2100 hertz, which is higher than the 1500-hertz first blade passage harmonic of the fan. Consequently, the fan duct design differs

in concept from the inlet design in that a 15-inch section of double degree of freedom lining is provided on the inner and outer walls of the fan duct but not on the ring. This lining is number 4 on the diagram. Double degree of freedom linings are designed for best performance at two frequencies. The two frequencies selected for the fan duct lining are the first and third blade passage harmonics (1500 and 4500 Hz). The double degree of freedom lining was opposed by a single degree of freedom lining on the ring designed for 4500 hertz. The opposing linings were thereby a matched pair at 4500 hertz. At 1500 hertz (the double degree of freedom lining design frequency), the opposing lining is extremely large; thus, the 1500-hertz impedance for the double degree of freedom lining was chosen as if the channel size was twice its actual size. The attenuation spectrum of this combination could then be analytically predicted by two separate analyses - one for low frequencies, one for high frequencies.

The resulting theoretical attenuation spectrum prediction for the combination is shown by the lower curve in figure VII-16. The triangle data points near the predicted curve are test data for the same lining configuration as measured in the flow duct. Note the 1500- and 4500-hertz tuning and associated broadbandness this powerful combination of linings gives. The theoretical prediction of the expected fan duct attenuation spectrum is shown by the upper curve. The flow duct test data are shown by the circles. The maximum attenuation predicted and measured occurs in the 2000- to 4000-hertz regime. The true attenuation could not be measured in this frequency range because of the flow duct noise floor. However, the data points in that portion of the spectra represent the actual measurements. The test data show that the theoretical predictions were too conservative at the high frequencies.

Figure VII-17 shows the fan duct ring and outer wall assembly looking in the flow direction. The ring is supported by thin struts from the outer wall only. Note the uninterrupted acoustic skins from the leading to trailing edge of the ring, a total of 5 feet.

The theoretical predictions of expected acoustic performance of the nacelle are shown in table VII-1. The predictions are made on both polar and sideline for both takeoff and approach power settings. The fan noise polar predictions are near the 15 PNdB design goal and are probably con-

TABLE VII-1. - ESTIMATED QUIET ENGINE A

NACELLE ACOUSTIC PERFORMANCE

Quadrant	Power setting	Peak noise reduction,[a] ΔPNdB			
		Fan noise		Complete engine	
		Polar	Sideline	Polar	Sideline
Forward	Approach	13	14	12	12
	Takeoff	15	14	11	10
Aft	Approach	16	14	7	6
	Takeoff	13	10	8	6

[a]Polar data, 200 ft. Sideline data: approach, 370 ft; takeoff, 1000 ft.

servative since they do not account for the influence of segmentation on lining performance, duct end impedance, and peak directivity indices greater than unity. The "Complete engine" columns are the predictions for the test stand. These predicted reductions are lower than for the fan by itself because of the influence of jet and turbomachinery noise floors.

Table VII-2 summarizes the predicted inlet and fan duct pressure losses

TABLE VII-2. - ESTIMATED QUIET ENGINE A

NACELLE PRESSURE LOSSES

Condition	Inlet pressure loss, percent		Fan duct pressure loss, percent	
	With treatment	Without treatment	With treatment	Without treatment
Cruise	2.0	0.4	4.7	1.5
Takeoff	1.6	.2	3.3	1.1

at takeoff and cruise for a nacelle without treatment and one with treatment. The pressure losses in the fan duct are higher than the inlet in either case: however, inlet pressure losses affect installed performance more than fan duct losses.

The predicted effects of the pressure losses on the installed Quiet Engine A performance are shown for the treated and untreated nacelles in table VII-3. The 15-PNdB fan noise reduction is expected to result in a

TABLE VII-3. - ESTIMATED QUIET ENGINE A

NACELLE PERFORMANCE

Condition	Thrust loss, percent		Takeoff specific fuel consumption increase, percent	
	With treatment	Without treatment	With treatment	Without treatment
Cruise	8.7	2.2	7.3	1.9
Takeoff	6.5	1.5	5.3	1.3

5-percent takeoff thrust loss and a 5.4-percent cruise specific fuel consumption increase.

The treated nacelle is shown in figure VII-18 on the Lewis test stand. The engine-nacelle combination is just beginning a series of comprehensive tests. Since the nacelle was designed both aerodynamically and acoustically from an analytical basis, the test program should provide direct comparisons between analysis and theory. In addition, the interactions between the nacelle and engine can be studied under laboratory conditions. Finally, the engine-nacelle combination provides an excellent test vehicle for the detail study and reduction of jet and turbomachinery noise.

QUIET ENGINE NACELLE

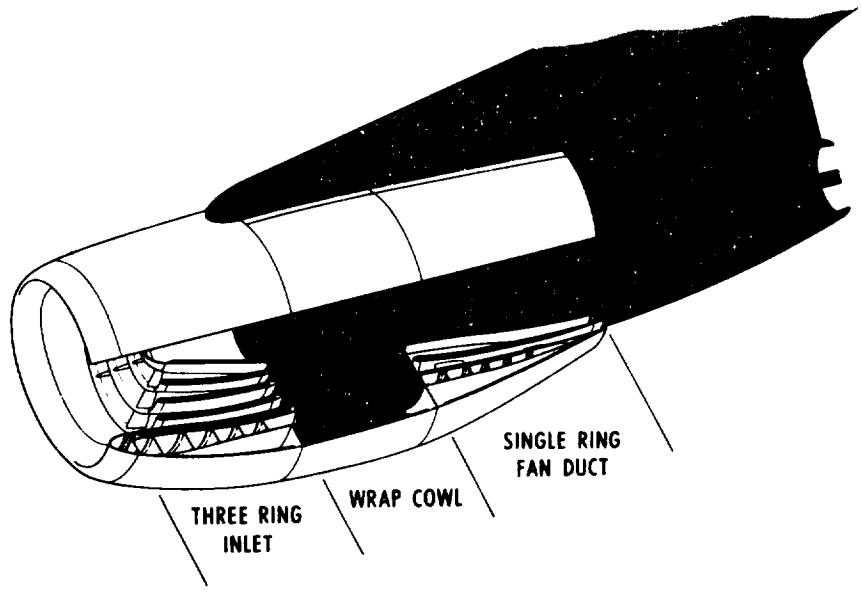

Figure VII-1

EFFECT OF NUMBER OF INLET ACOUSTIC RINGS ON TOTAL INLET LENGTH

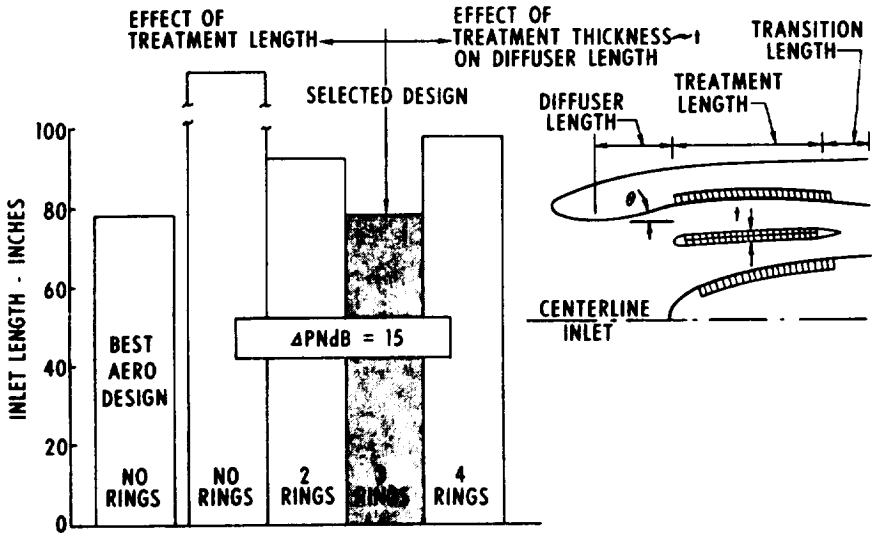

Figure VII-2

INLET CONFIGURATION TRADES

ΔPNdB = 15

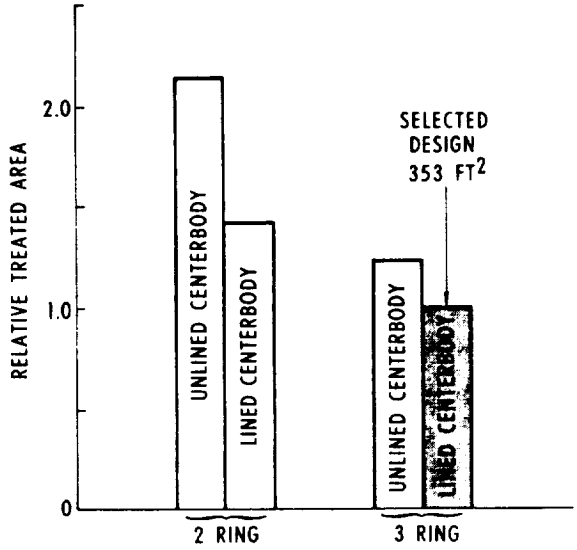

Figure VII-3

ATTENUATION RECOVERY WITH LINING OPTIMIZED FOR SHEARED FLOW

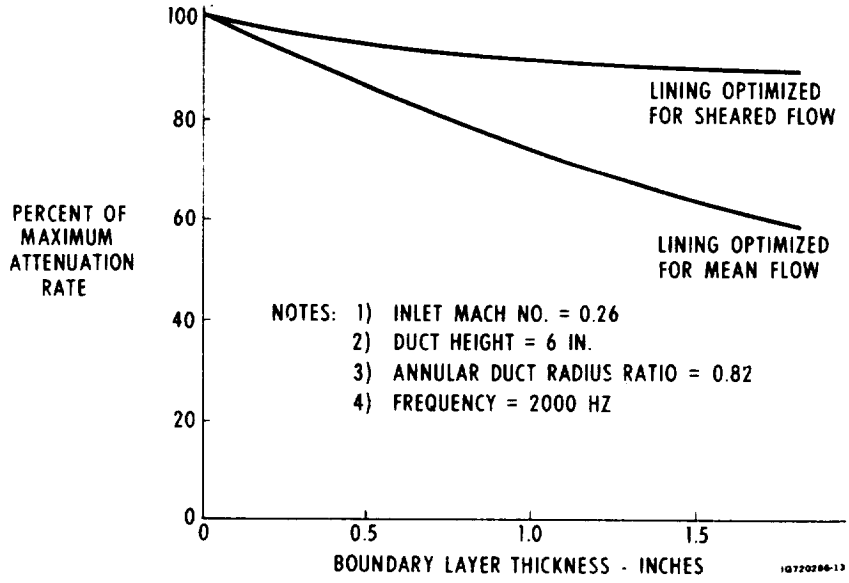

Figure VII-4

INLET ACOUSTIC LINING CONFIGURATION

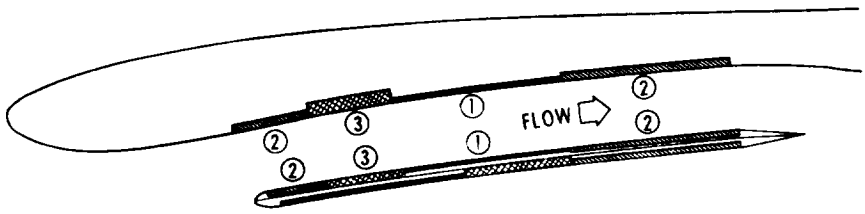

LINING NUMBER	NO. PLIES	CAVITY DEPTH (INCHES)	LENGTH (INCHES)	DESIGN FREQUENCY (HZ)
①	12	.08	20	4500
②	14	.19	RANGE 5 TO 10	3000
③	8	.74	8	1500

OUTER CHANNEL TYPICAL OF ALL CHANNELS

Figure VII-5

TYPICAL LINING CONSTRUCTION

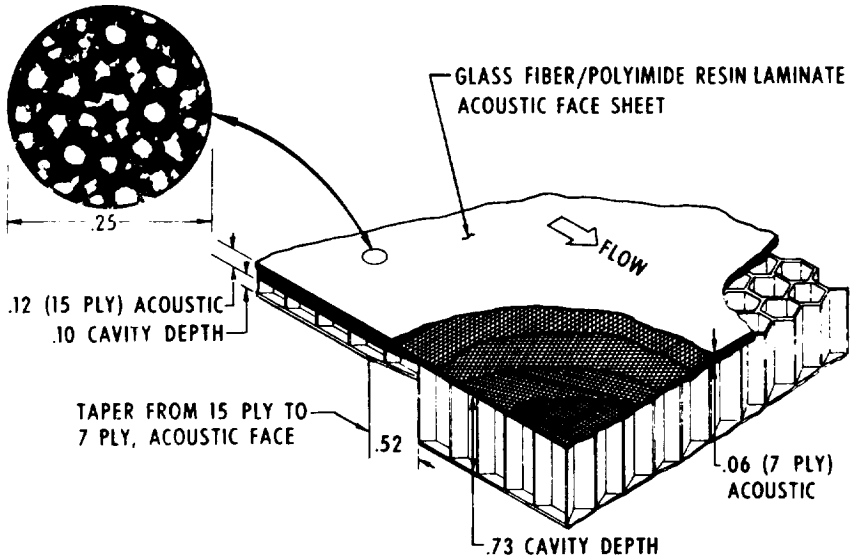

Figure VII-6

GRAZING FLOW IMPEDANCE TEST SECTION

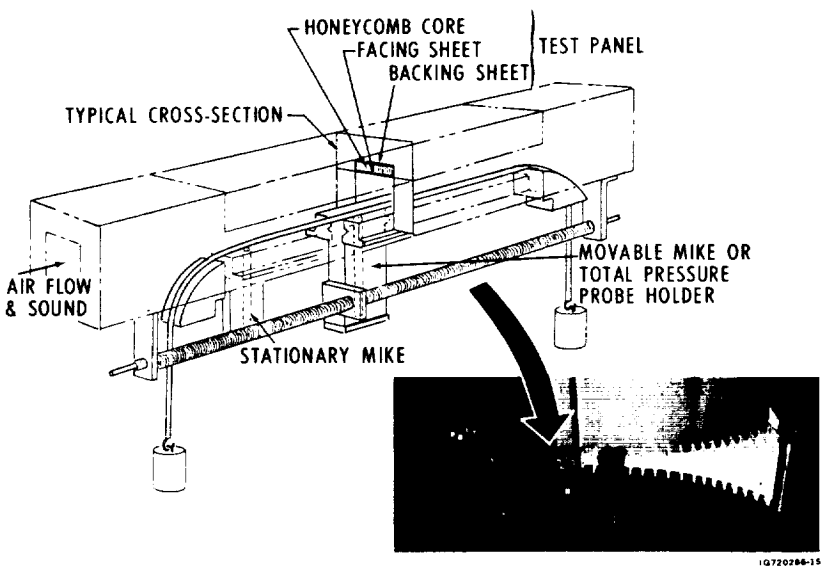

Figure VII-7

GRAZING FLOW IMPEDANCE DATA
12 PLY POLYIMIDE RESISTANCE

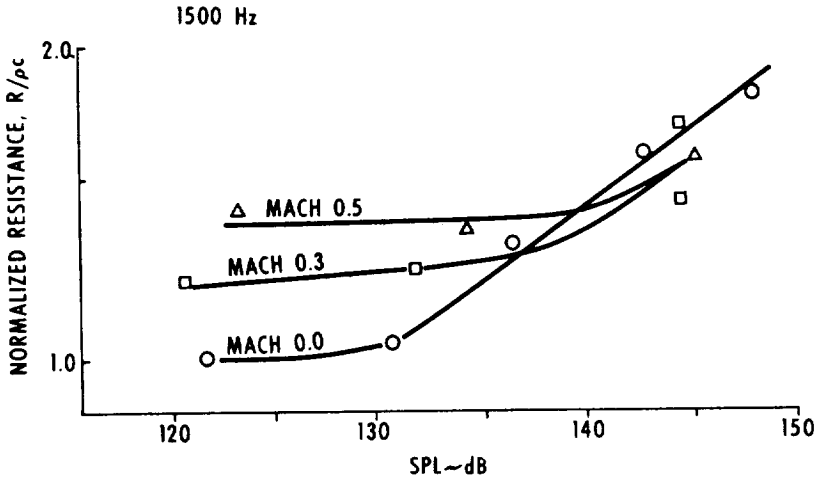

Figure VII-8

GRAZING FLOW IMPEDANCE DATA
12 PLY POLYIMIDE REACTANCE

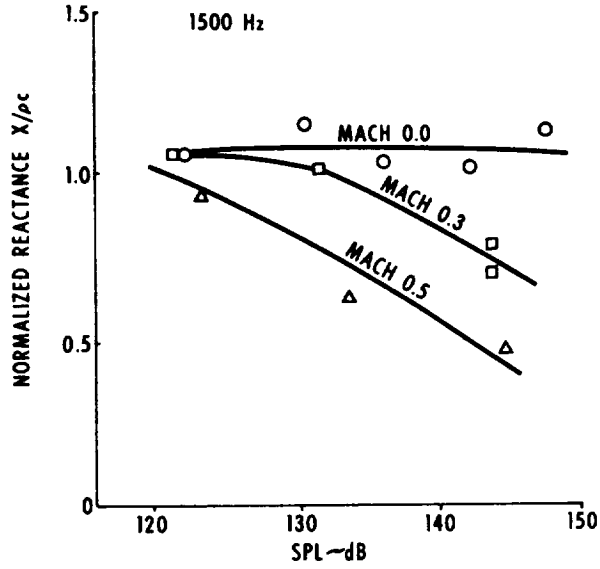

Figure VII-9

INLET OUTER CHANNEL LINING TEST RESULTS
QUIET ENGINE A NACELLE
APPROACH POWER

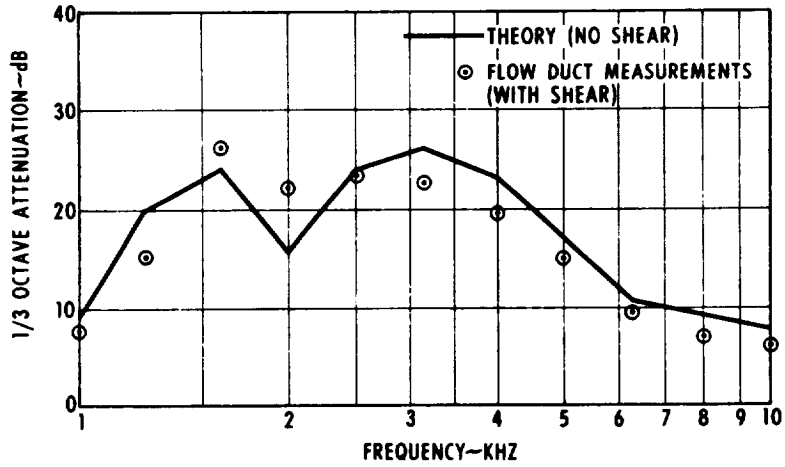

Figure VII-10

TREATED INLET COMPONENTS

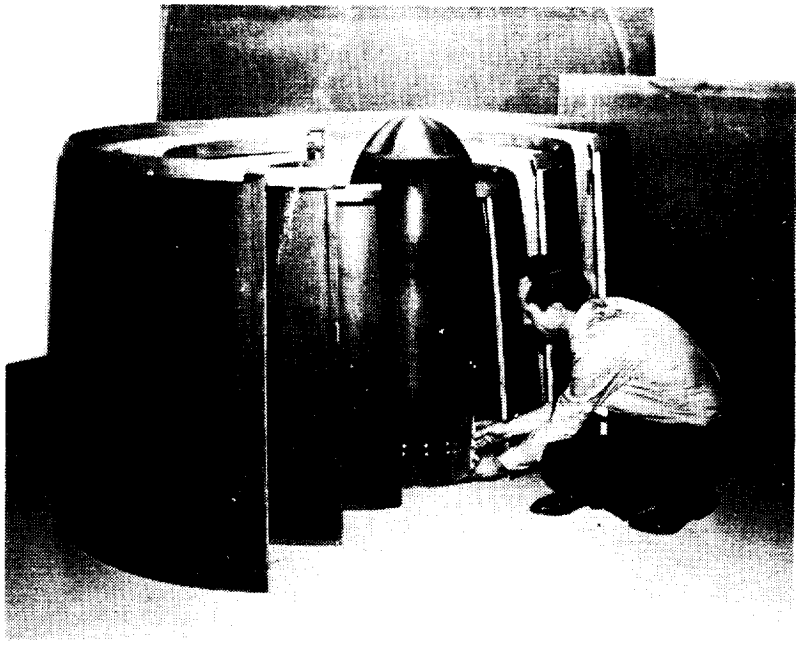

Figure VII-11

ASSEMBLED INLET

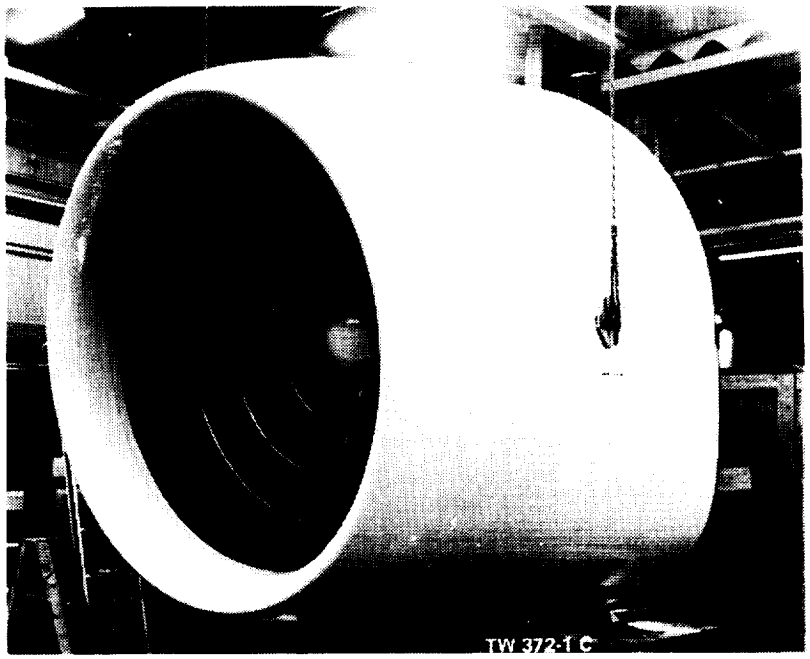

Figure VII-12

FRONT VIEW OF ASSEMBLED INLET

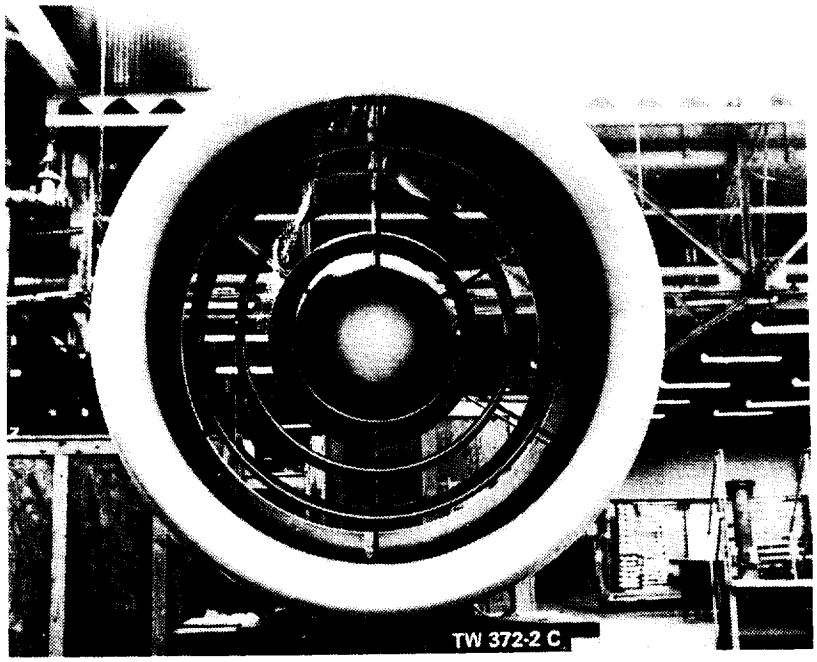

Figure VII-13

REAR VIEW OF ASSEMBLED INLET NEAR FAN FACE

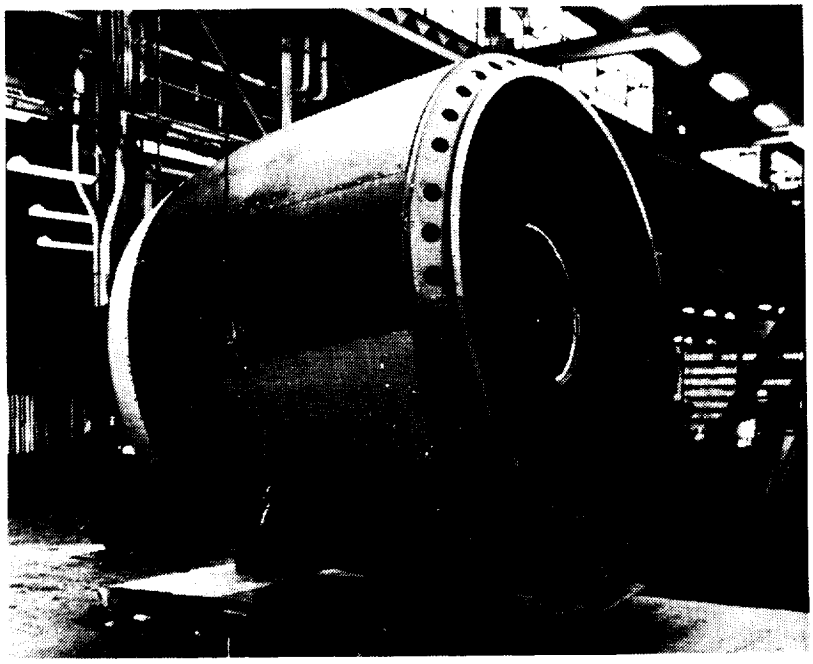

Figure VII-14

FAN DUCT ACOUSTIC LINING CONFIGURATION

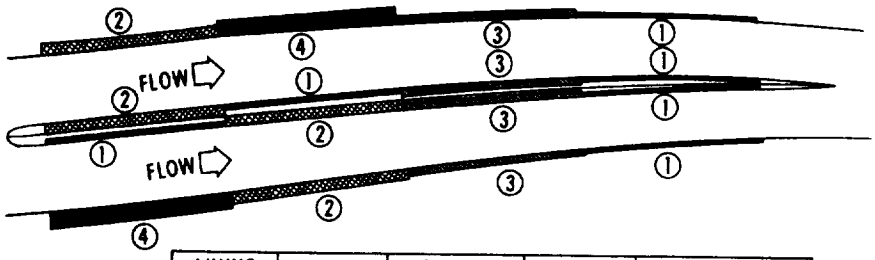

LINING NUMBER	NO. PLIES	DEPTH (INCHES)	LENGTH (INCHES)	DESIGN FREQUENCY (HZ)
①	7	.25 (AVG.)	15	4500
②	5	1.00	15	2100
③	6	.60	15	3000
④*	4 9	.5 .75	15	1500 4500

*DOUBLE DEGREE-OF-FREEDOM LINING (DDOF)

Figure VII-15

FAN DUCT LINING TEST RESULTS

QUIET ENGINE A NACELLE
APPROACH POWER

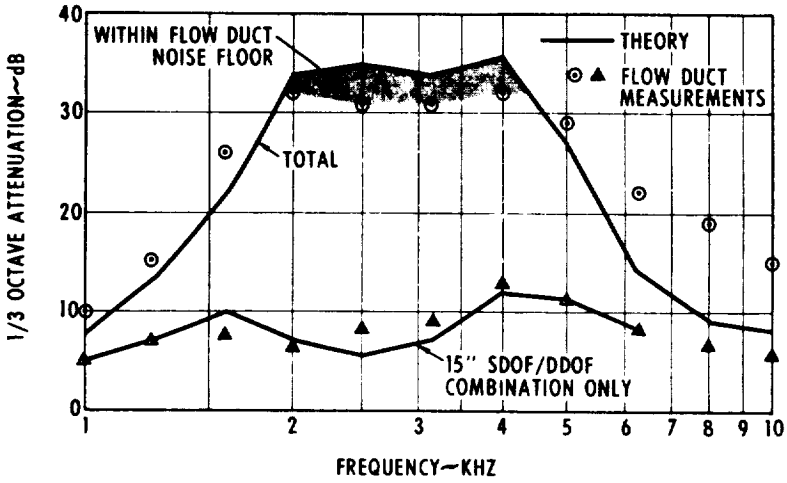

Figure VII-16

FAN DUCT RING AND OUTER WALL ASSEMBLY

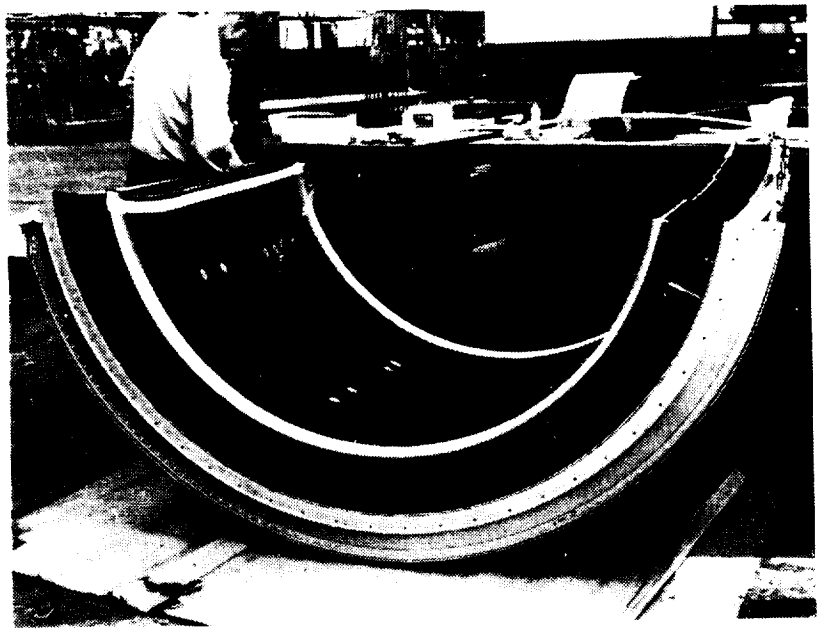

Figure VII-17

TREATED NACELLE ON LEWIS TEST STAND

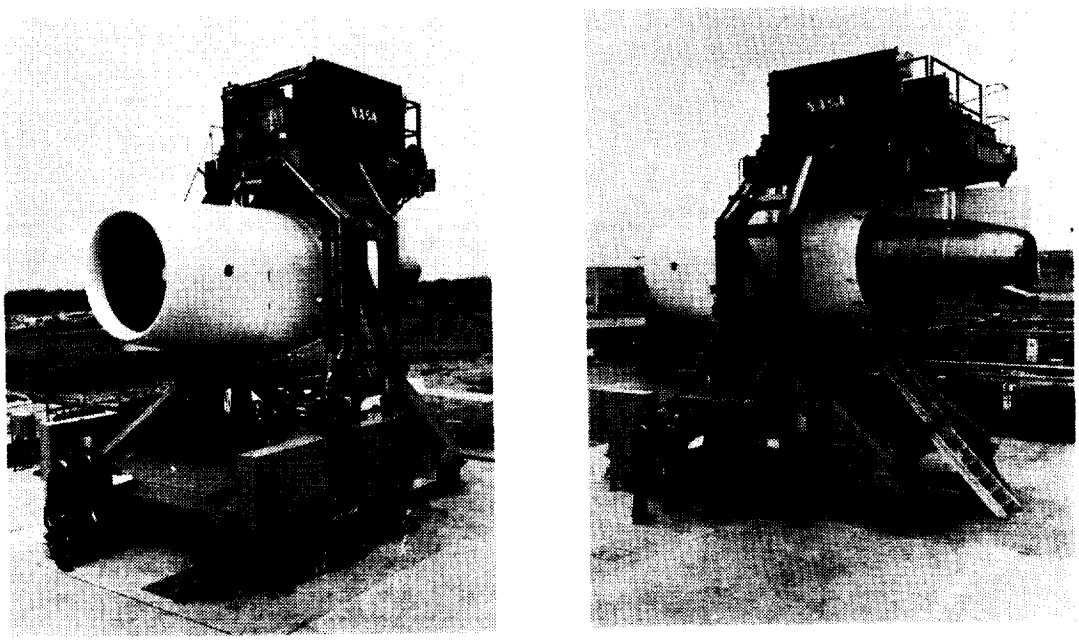

Figure VII-18

VIII. QUIET ENGINE TEST RESULTS

Carl C. Ciepluch, Frank J. Montegani,
Mike J. Benzakein,* and Steven B. Kazin*

The acoustic and aerodynamic test results obtained with the two NASA Quiet Engines are given in this presentation. Some of the test results obtained at the General Electric Company are reviewed first. This review includes the performance of the untreated or baseline Quiet Engines. In addition, test results are shown for various degrees and areas of engine acoustic treatment. Finally, the results obtained here at the Lewis Research Center when a flight-type, acoustically treated nacelle was added to one of the Quiet Engines is examined.

GENERAL ELECTRIC TEST FACILITY

The baseline Quiet Engines were initially tested at the General Electric Test Facility. Figure VIII-1 shows a schematic of the engine test facility at Peebles, Ohio. One of the primary functions of this facility is the measurement of engine noise. The field surrounding the engine is level and covered with a large aggregate crushed rock - a surface which is representative of an average between a hard reflecting surface and a completely absorbing surface. Placed around the engine are 16 microphone poles set at 10° increments on a 150-foot arc centered at the engine inlet centerline. The microphones are 40 feet above the ground while the engine centerline is $12\frac{1}{2}$ feet above the ground plane. This height was chosen because the resulting reflection pattern, caused by the interaction of the reflection from the ground and direct radiation to the microphone, is more representative of that which would be encountered in the actual flyover of the engine on an airplane.

The area behind the microphones is clear of obstructions for a sufficient distance so that no difficulties with reflections back to the microphones from behind will be encountered. The nearest structure being, in fact, the

*General Electric Company.

36-inch-diameter scale model facility, which is about 175 feet behind the microphone circle.

The signals from the individual microphones are lead underground to the control building on the left where they are recorded simultaneously on a multitrack high response tape recorder for later analysis.

Figure VIII-2 shows an aerial view of this same facility. The photograph is a view from right to left as related to the previously shown plat. The engine test stand is on the left.

The sound field for the engine pad extends from the lower left around to the center. The microphone stands at 40^{o}, 50^{o}, and 60^{o} from the inlet are in the position for data recording. The remainder of the microphone stands are lying down. The scale model facility is in the center with the control room and the General Electric crosswind facilities behind the scale model.

Also contained within this facility is sufficient measuring equipment to analyze the performance of the engines on test. These instruments are read in the control room and at the main plant in Evendale (Cincinnati) by means of telephone lines where a direct computer link provides online performance data.

ENGINE A AERODYNAMIC PERFORMANCE

A photograph of engine A on test at the General Electric Peebles Test Facility is shown in figure VIII-3. Engine A contains the 1160 foot per second, low tip speed fan; the fan is driven by a standard CF-6 engine core which has had one of the low pressure turbine stages removed. In table VIII-1 are presented some of the original NASA design requirements along with measured and estimated engine capability. It can be seen that engine A meets all the takeoff design requirements. The measured thrust and specific fuel consumption for the sea level static takeoff condition meet or exceed the design goals. The good specific fuel consumption noted results from the higher than expected efficiency of the low tip speed fan. For the Mach 0.25 takeoff flight condition the aircraft is in the vicinity of the standard FAA takeoff noise measuring station. Thus the design requirements shown for this condition are important parameters for limiting engine noise levels. Estimated performance values are shown which were extrapolated from sea level static

TABLE VIII-1. - ENGINE A PERFORMANCE

	Design requirement	Measured	Estimated
Takeoff (sea level static):			
Thrust, lb	22 000	22 000	-----
Specific fuel consumption, lb/hr-lb	0.360	0.356	-----
Takeoff (Mach 0.25, sea level):			
Fan tip speed, ft/sec	1030 (max.)	------	1020
Fan bypass airflow, lb/sec	----------	------	740
Core airflow, lb/sec	----------	------	124
Bypass jet velocity, ft/sec	900 (max.)	------	820
Core jet velocity, ft/sec	1275 (max.)	------	1180
Cruise (Mach 0.82; 35 000 ft):			
Thrust, lb	4900	------	4900
Fan tip speed, ft/sec	----------	------	1150
Fan bypass pressure ratio	1.5-1.6	------	1.5
Bypass ratio	5-6	------	6.1
Specific fuel consumption, lb/hr-lb	0.66	------	0.645
Turbine inlet temperature, ^{o}F	1775 (max.)	------	1920

data. It can be seen that engine A meets the fan tip speed, bypass jet, and core jet velocity requirements quite easily. The core jet velocity which is the dominant jet noise source is seen to be 1180 feet per second, or about 100 feet per second less than the design limit.

From the engine A cruise design requirements, which are also shown in table VIII-1, we can see that the fan tip speed at the cruise conditions is 1160 feet per second as previously indicated. The slightly higher than specified engine bypass ratio does not adversely affect the engine performance. The turbine inlet temperature, however, exceeded the design limit by some 145^{o}. Part of this problem resulted from a lower than predicted turbine inlet flow area. The turbine inlet temperature requirement was primarily established to operate the turbine at a conservative temperature level.

Since CF-6 turbine material and cooling technology have been certified for airline use at turbine inlet temperatures far in excess of 2000^{O} F, the engine is still operating at a relatively conservative temperature. No decrement in engine reliability is therefore expected because of the higher turbine inlet temperature.

ENGINE A BASELINE ACOUSTICS

For acoustic baseline testing of engine A, the configuration shown in figure VIII-4 was employed. The rotor and stator are spaced two true rotor chords apart; the rotor blades number 40 and the stator vanes number 90 for a vane-to-blade ratio of 2.25.

Acoustically absorbing panels were placed in the area of the fan and in the core engine inlet. The outer fan duct wall has 15.5 inches of treatment ahead of the rotor, 15 inches between the rotor and outlet guide vane, and 23 inches aft of the outlet guide vane. The treatment cross section is shown inset on the drawing. It is of a resonator type and is similar to the treatment which was flight qualified on the General Electric CF-6 engine. This type of material has demonstrated suppression over a relatively wide frequency band while displaying high flight reliability. The treatment is similar to the core inlet; however, it is tuned to reduce the higher frequency noise generally associated with the compressor.

As previously noted, the fan was first tested acoustically as a component here at the Lewis Research Center and then in the demonstrator engine at the General Electric Peebles test site. Figure VIII-5(a) shows a comparison of the approach speed perceived noise directivity for the fan and engine on a 370-foot sideline. The angle shown is measured such that 0^{O} is along the inlet axis and 180^{O} is along the exhaust jet axis. This sideline distance is representative of the altitude achieved by most aircraft on the landing approach when they pass over the FAA approach certification point. The two sets of data agree quite closely with the engine being slightly higher. This is as expected since the engine contains the core compressor, combustor, and turbine with their associated ducting as well, of course, as the core jet. The data indicate that the fan at this power setting is producing just about the same level at the forward peak at 40^{O} and the rear peak of 120^{O} while the

engine, because of its other noise sources, is slightly rear dominated.

The same type of data at takeoff thrust at a 1000-foot sideline is shown in figure VIII-5(b). This distance is representative of a typical altitude attained by a present-day four-engine aircraft on takeoff as the aircraft passes over the FAA certification point. The engine and fan component again are quite close. The difference between the two sets of data in the front angles, where the fan component is higher, is thought to be a result of the front end drive mechanism used at the Lewis Research Center. The engine core jet is now contributing significantly to the rear most angles (150^{o} and 160^{o}), which makes the engine data higher.

The part played by the core jet is clearly shown in figure VIII-6 on the 1/3-octave spectral comparison at 120^{o}. For the most part, the noise above 400 hertz follows the same trend for both vehicles. However, below 400 hertz and particularly around 160 hertz the low frequency core jet noise makes a significant contribution.

The two peaks in the spectrum at 2 and 4 kilohertz are the fan rotor's blade-passage frequency and its second harmonic. These two key noise components are very close for the two vehicles.

ENGINE C PERFORMANCE

Some results on engine C with the higher tip speed fan are now presented. In figure VIII-7, engine C is shown on test at Peebles. Some of the performance results obtained on that vehicle are shown in table VIII-2. It is apparent that the takeoff sea level static design requirement of thrust and specific fuel consumption were adequately met. Extrapolating those results to the takeoff Mach 0.25 requirements shows that the fan tip speed goal of 1400 feet per second (max.) was met. The bypass and core jet velocities were also well below the design requirements. As shown in table VIII-2, the design requirements for performance at cruise were again met. The specific fuel consumption for engine C is seen to be a little higher than what we previously had shown for engine A. This results from the lower efficiency of fan C.

TABLE VIII-2. - ENGINE C PERFORMANCE

	Design requirement	Measured	Estimated
Takeoff (sea level static):			
Thrust, lb	22 000	22 000	-----
Specific fuel consumption, lb/hr-lb	0.37	0.37	-----
Takeoff (Mach 0.25; sea level):			
Fan tip speed, ft/sec	1400 (max.)	------	1390
Fan bypass airflow, lb/sec	----------	------	695
Core airflow, lb/sec	----------	------	140
Bypass jet velocity, ft/sec	900 (max.)	------	900
Core jet velocity, ft/sec	1275 (max.)	------	850
Cruise (Mach 0.82; 35 000 ft):			
Thrust, lb	4900	------	4900
Fan tip speed, ft/sec	----------	------	1570
Fan bypass pressure ratio	1.5-1.6	------	1.66
Bypass ratio	4.5-6	------	5.1
Specific fuel consumption, lb/hr-lb	0.66	------	0.662
Turbine inlet temperature, ^{o}F	1775 (max.)	------	1840

TURBINE CHARACTERISTICS

Engines A and C, because of the large difference in the fan rotational speed, had two different low pressure turbine systems (fig. VIII-8). The aerodynamic characteristics of the two low pressure turbines are compared in table VIII-3.

Engine A incorporated essentially the first four stages of the CF6-6 low pressure turbine. The shaft work was 89.50 Btu per pound and was moderately low. The turbine loading which is defined as the enthalpy drop divided by the square of the blade speed at the mean radius was relatively low (0.764). The turbine efficiency, which was estimated prior to the test at 0.918, was measured at 0.902.

TABLE VIII-3. - LOW PRESSURE TURBINE

AERODYNAMIC CHARACTERISTICS

	Engine	
	A	B
Number of stages	4	2
Shaft work, Btu/lb	89.50	95.6
Loading, $gj\Delta H/2U^2_{pitch}$	0.764	1.035
Turbine efficiency predicted	0.918	0.903
Turbine efficiency measured	0.902	0.90

Engine C incorporated a new turbine. Taking advantage of the higher rotational speed of the fan and the advances made in turbine aerodynamic technology, the number of turbine stages was reduced to two with a relatively high loading coefficient of 1.035. The turbine diameter was also decreased by about 8 percent. These changes resulted in an appreciable weight saving in the turbine area. The shaft work is slightly up because of the higher fan pressure ratio on engine C. The turbine efficiency was predicted at 0.902 and was measured at 0.90.

ENGINE C BASELINE ACOUSTICS

Now some of the acoustic results obtained on baseline engine C are presented. In this engine configuration (fig. VIII-9) fan C has 26 blades, 60 vanes, and a two rotor-chord spacing between the rotor and the outlet guide vane.

As in engine A, the area around the fan and the engine core inlet was acoustically treated. The treatment along the outer wall being 15 inches ahead of the rotor, 20 inches between the rotor and stator, and 20 inches effective behind the stator. The treatment design is the same as was used in fan A.

A comparison of the approach speed perceived noise directivity at 370 feet between engines A and C is shown in figure VIII-10(a). Both the high and low speed fans produce the same noise level at most angles - the exception being at 120° where engine C is higher by about $1\frac{1}{2}$ perceived noise decibels (PNdB).

At takeoff speed (fig. VIII-10(b)) engine C is clearly noisier than engine A. On a maximum sideline noise basis, engine A peaks at 120° with a level of 98.5 PNdB, and engine C peaks at 50° with a level of 101.7 PNdB. However, the front maximum shows engine C to be dominant.

The 1/3-octave spectra at 50° (fig. VIII-11) shows the majority of the noise difference to be contained between 250 and 2000 hertz. This noise is commonly referred to as multiple pure tones or "buzz saw" noise and is characteristic of high tip speed fans. Although this noise is front radiated, it does, in fact, contribute to the rear maximum as well in this baseline configuration and largely accounts for the difference between engines A and C at 120°.

The solution to this high front end radiation problem on engine C is a major goal of the engine C test program now underway at Peebles.

ENGINE A WITH ACOUSTIC TREATMENT

In order to investigate the effect of fan acoustic treatment on the overall engine noise, a number of acoustic suppression configurations were tested on engine A (fig. VIII-12). In addition to the baseline acoustic treatment design described previously, two additional treatment configurations were tested.

First was the configuration labeled duct wall treatment, which incorporated 20 inches more acoustic treatment on the inlet duct outer wall and 35 inches more acoustic treatment on the exhaust duct inner and outer walls. This treatment was of the multiple degree of freedom type and was similar to the treatment incorporated in the baseline.

Second was the configuration labeled as fully suppressed. Here the treatment on the inlet wall was extended 58 inches, and three cylindrical rings acoustically treated on both sides were incorporated. All the additional inlet acoustic treatment was of the type as shown on the left side of

figure VIII-14. A photograph of the fully suppressed inlet is shown in figure VIII-13.

The fully suppressed configuration also incorporated an additional 37 inch long splitter in the exhaust duct. This splitter was treated on both sides with 1 inch thick polyurethane foam covered by a perforated plate.

Some of the results obtained using the preceding two treatment configurations are now summarized. Figure VIII-14(a) gives a comparison of the different configurations at the takeoff condition in terms of perceived noise levels as a function of angle. The duct wall treatment configuration provided a 3 to 4 PNdB decrease at the maximum front and aft angles compared to the baseline. The three-splitter inlet was quite effective in reducing the front quadrant noise (by an additional 7 PNdB), but the addition of the splitter in the exhaust duct provided only a 2 PNdB reduction in the aft quadrant.

Comparable results were obtained at the approach condition as shown in figure VIII-14(b). The three inlet splitters again provided an appreciable noise reduction while the exhaust duct splitter lowered the aft quadrant noise only by 2 to 3 PNdB.

It is interesting to examine the effectiveness of the three inlet splitters on the sound pressure level spectrum. Shown in figure VIII-15 is a plot of the third octave sound pressure level spectrum against frequency taken at 50° from the inlet axis at the approach condition. No reduction due to fan treatment from 0 to 500 hertz can be observed, the noise in those bands being controlled by core exhaust noise. However, the splitter provided an appreciable noise reduction not only at the fan blade passage frequency and its higher harmonics but across the whole fan noise spectrum. Inlet splitters are therefore quite effective in reducing front end noise.

When the fan has been suppressed as just shown, the next major item of concern is the turbomachinery noise emanating from the low pressure turbine. In view of this, a turbine suppressor was developed (fig. VIII-16) which covered both walls of the core nozzle with a double layer honeycomb resonator treatment. This design provides a sufficient suppression range to effectively reduce the relatively high frequency turbine noise. The treatment has an effective length of about 36 inches. The inset shows the design of this treatment which is constructed so as to withstand the high temperature environment in the nozzle.

The data shown in figure VIII-17 were obtained on the engine with and without the turbine treatment while the fan was fully suppressed at a speed equivalent to the landing approach on the 150 foot measuring arc at 120^{o} from the inlet. The data were analyzed with a 50-hertz narrowband pass filter. This method of analysis divides the spectrum into smaller elements and allows a more detailed analysis, particularly of the tone content. Indicated in the figure are the blade passage tones of the first, third, and fourth low pressure turbine stages. There is no indication in either spectrum of a second rotor tone.

Reduction due to the treatment at the third and fourth rotor fundamentals is clearly evident. However, a problem exists at the frequency band surrounding the first rotor blade passing frequency. The acoustic treatment has had almost no effect on this noise. Further investigation of this phenomenon is being pursued on the engine C program which is currently underway.

Fan A noise levels, shown previously, were reduced substantially by treatment of the fan inlet and exhaust ducts. It was felt that possibly with the fully suppressed configuration the noise radiating from the fan casing might make a contribution to the far-field acoustic signature. It was therefore decided to wrap the fan casing with a 2-inch-thick layer of polyurethane foam covered by a 1/8-inch-thick lead vinyl sheet to cut down casing radiation (fig. VIII-18). The engine was tested in a fully suppressed configuration with and without the muffled casing and showed, however, no noticeable changes in far-field noise at any speeds.

LEWIS RESEARCH CENTER TEST FACILITY

A significant milestone in the Quiet Engine Program was reached in December 1971 with the delivery of the low speed engine to Lewis for further testing. The major objective at Lewis was to determine how low a noise level could reasonably be reached when fan acoustic treatment is added to this engine. A flight-type, acoustically treated nacelle was built to make this evaluation. The nacelle acoustic treatment was tailored specifically to the low speed fan noise characteristics. Nacelle flow passages were carefully designed in order to keep performance losses low. This combination of Quiet Engine and acoustic nacelle is the best one tested to date considering

both acoustics and aerodynamic performance.

The Lewis engine noise test facility is shown schematically in figure VIII-19. The arrangement is very similar to the General Electric facility with microphones every 10^{o} on a 150 foot radius, but there are some differences. The Lewis microphones are at the same height as the engine centerline (13 ft) and they start on the inlet axis and go around to 160^{o}. Also, the reflecting plane is hard pavement. Engine operation is controlled from the flight research building where the noise instrumentation and anslysis equipment is located. The site is sufficiently far from the buildings so that reflections are no problem. A photograph of the site showing the engine in the thrust stand and some of the microphone poles is shown in figure VIII-20.

LEWIS RESEARCH CENTER QUIET ENGINE TESTS

So far the Lewis Quiet Engine has been tested in two basic configurations. The first, shown in figure VIII-21 is the baseline configuration, which is basically the same as that at Peebles. It has no acoustic treatment except what is built into the fan frame, and a bellmouth inlet is used.

The other configuration tested at Lewis was fully suppressed as shown in figure VIII-22. This consists of engine A mated with the Boeing acoustic nacelle. It has a flight inlet and also includes turbine acoustic treatment. This is the NASA Quiet Engine.

A cross section of this configuration is shown in figure VIII-23. The mating of the acoustic nacelle with the basic engine is shown. There is continuous treatment from inlet to exhaust in the fan duct outer wall, also from the inlet centerbody along the inner walls. There are three aerodynamically contoured splitters in the inlet duct and one in the exhaust duct. The turbine treatment is indicated. The areas and weights of the acoustic treatment in the nacelle are noted in the figure. The weights shown are for the test hardware and can possibly be reduced by as much as 50 percent for flight hardware.

It is generally conceded that noise results from different facilities vary because of different facility flow patterns, instrumentation techniques, and calculation procedures. This is one of the reasons for retesting the baseline configuration at Lewis. The sideline perceived noise levels for baseline

engine A from the Lewis and General Electric tests at takeoff are compared in figure VIII-24. In the rear quadrant the agreement is very good, but in the front quadrant there are some small differences which may be due to different inlet flow patterns. The Lewis baseline data, of course, provide the basis for assessing the performance of the acoustic nacelle.

In figure VIII-25 the baseline data and the nacelle data at takeoff are compared. These are static data. This means that the jet noise is higher than it would be in flight because there are no relative velocity effects. Two kinds of data are shown in figure VIII-25, predictions and engine test measurements. The predictions are based on the best information up to the time of the Lewis tests such as fan noise from the Lewis fan tests, jet noise and turbine noise from the General Electric tests, and nacelle performance predictions from Boeing. When the baseline measurements are compared with the predictions, the actual engine is about 5 PNdB lower in the front quadrant than predicted. In the front quadrant at this condition the predictions indicate that the noise is dominated by the fan so that the predicted data shown are essentially Lewis fan test results. It is assumed that the measured engine data shown here are fan dominated. It is felt that since the engine has an unusually unobstructed inlet for a test stand that the difference shown is due to the absence of inlet flow distortion.

The effect of the nacelle at 50^{o} on the measured data has been to reduce the noise (about 9 dB) to about 84 decibels. This 84-decibel level is considered to be a floor. The predictions indicate that the floor is made up of both the suppressed fan and jet noise. The fact that some measurements were lower than the predictions might be due to the absence of inlet flow distortion or it might be due to a misjudgment of the jet noise. Only further testing will explain the results.

The differences between measurements and predictions are not an indication of poor nacelle performance. The reduced level is most probably a floor. No fan noise reduction can be demonstrated below that floor. Since the engine started out lower than expected to begin with, the only difference that can be demonstrated is less than predicted.

In the rear quadrant the measurements and predictions agree quite well. It is believed that the suppressed data here represent a jet floor.

Figure VIII-26(a) shows spectra at the baseline front angle of 50^{o}. No suppression occurs below about 500 hertz which agrees with the understand-

ing that this region is controlled by jet noise. The baseline engine data have a strong peak in the 2000 hertz band which is due to the blade passage tone. The nacelle has removed all evidence of the tone from the spectrum. This means that the tone has been reduced well below the floor that remains. Otherwise, if the tone were reduced only to the floor, for example, it would combine with the floor noise and leave a bump in the spectrum. This is fairly clear evidence that the nacelle is working well. It is assumed that the remaining floor is jet noise.

The rear spectra are shown in figure VIII-26(b). A harmonic is evident in addition to the blade passage tone. Again the nacelle has removed all evidence of the tones. The general reductions are less than in the front quadrant because of reaching the floor, believed to be jet noise.

In figure VIII-27 is shown the perceived noise directivity at approach. Again in the front the measured values are something less than the predicted values. The difference is less, however, than for the case of takeoff. The fact that the difference is less here than at takeoff reinforces the belief that the reason is inlet flow distortion.

The floor reached by the nacelle in the front and rear agrees well with predictions. In the front the predictions indicate that both fan and jet noise are present. In the rear, fan, jet, and turbine noise are predicted to be contributing.

The spectra in the front at approach are very similar to those at takeoff and, consequently, are not shown. The rear at approach is very different, however, as shown in figure VIII-28. A strong tone in the 6300 hertz band is evident. The origin of this tone is not presently known, but it obviously needs to be identified so it can be reduced.

Some general conclusions can be drawn from these static data. First, the baseline engine is inherently quieter than originally believed, mainly because of reduced front end noise. Second, there is every evidence that the acoustic nacelle is functioning as planned. The actual nacelle performance will only come from detailed in-duct acoustic testing. Further measurements are also necessary to identify the origin of noise floors that emerge.

ACOUSTIC TREATMENT PENALTIES

In figure VIII-29 is presented the engine thrust penalty resulting from the addition of the acoustic treatment. Herein is plotted corrected engine thrust as a function of corrected fan speed. The upper curve was obtained from the data taken at the General Electric Company and represents the untreated engine A configuration. The lower curve represents engine A with the acoustically treated nacelle, and these data were obtained at Lewis. At the takeoff engine speed of 3260 rpm, the acoustic treatment reduces the engine thrust by about 5 percent. There are two primary reasons for this: one is a result of the additional wetted surface area introduced into the fan inlet and exhaust ducts due to the presence of the acoustic splitters, and the second is that the skin friction coefficient of the acoustic surface is higher than the usual smooth metal duct surface. The predicted thrust loss was 5 percent. The agreement here between measured and predicted values is quite good considering that the measured data were taken at two different facilities and that the differences are approaching measurement accuracies. In future testing at Lewis a more detailed evaluation of the thrust loss will be obtained. The specific fuel consumption increase at the takeoff speed was measured to be 6 percent. It is, therefore, apparent that the use of large amounts of acoustic treatment will penalize airplane economics due to both performance losses and weight increase.

QUIET ENGINE FLYOVER NOISE STUDIES

The static engine noise data tell only part of the story. To get the whole picture, the static data must be extrapolated to flight. This means taking into account relative velocity effects and discussing the results in terms of effective perceived noise decibels (EPNdB).

Some results of flyover studies for a four engine aircraft retrofitted with quiet engines and flying a path resulting from the retrofit are shown in figure VIII-30. The noise from individual sources associated with the engine is also presented.

Consider first takeoff. The first bar represents total engine noise computed from noise measurements at Lewis. The next bar shows the contribu-

tion made by the fan only. The unsuppressed fan level was deduced from the baseline engine measurements. The amount of suppression shown represents the predicted nacelle performance, which is not yet confirmed. This level then is the predicted fan noise contribution. The next bar is the jet noise derived from the General Electric engine tests and projected to flight. Turbine noise is not considered since it does not show up at takeoff.

The total engine results in a flyover noise of 90 EPNdB. This is contributed to principally by fan noise so that further reduction in engine noise can be achieved by better fan suppression. Such reductions can only be modest, however, since the jet noise floor is close to being reached. Reduction of jet noise to benefit from further fan noise reductions can only be accomplished by reducing the mean jet velocity such as with new cycle designs.

At approach it appears that better fan suppression will not reduce total engine noise unless something is done about what is calculated to be turbine noise. Jet noise is very low at approach.

The net potential impact of our results on the community noise problem is summarized in table VIII-4. A DC-8 airplane currently makes 116 and 118 EPNdB at takeoff and approach, respectively. These numbers compare with Federal Air Regulation 36 (FAR-36) limits of 104 and 106 for new aircraft of the same weight. Conservative extrapolation of the baseline Lewis tests to flight reduce these numbers to 97 and 98. Mating the engine with a tailored acoustic nacelle achieves values of 90 and 89, of the order of 15 EPNdB below current federal regulations.

TABLE VIII-4. - FLYOVER NOISE COMPARISON

FOR FOUR ENGINE AIRCRAFT

	Takeoff	Approach
	EPNdB	
DC-8	116	118
FAR-36	104	106
Baseline Quiet Engine A	97	98
Quiet Engine A with acoustic nacelle	90	89

CONCLUDING REMARKS

From this discussion of the Quiet Engine test results the following conclusions can be drawn. First, the low speed engine is basically a quieter engine than the high speed one in an untreated condition, primarily because it does not have the multiple pure tone noise content in the front end that is a characteristic of supersonic tip speed fan operation. But, this does not mean that the high speed engine can not be competitive from a noise standpoint, because additional fan acoustic treatment can be incorporated to reduce the high speed engine noise levels to that of the low speed engine. The additional treatment, however, introduces an engine performance and weight penalty that will reduce the basic weight advantage of the high speed engine. The extent of this penalty will be evaluated in future testing of the high speed engine and a final assessment of the merits of the high and low speed engines can then be made.

Using the low speed Quiet Engine technology without fan acoustic treatment on airplanes of the DC-8 class should result in an airplane that betters FAR-36 noise regulations by as much as 7 or 8 EPNdB. Furthermore, it is believed that noise levels approaching FAR-36 minus 15 decibels can be achieved when an acoustic nacelle incorporating splitters is added to the engine. However, the acoustic treatment will result in a penalty in airplane economics. It is important to note that the treated noise level is almost 30 EPNdB below that of the current DC-8 and 707 type aircraft and it, therefore, represents a substantial potential improvement in aircraft noise levels.

The question arises as to whether it is possible to reduce engine noise levels even further to perhaps FAR-36 minus 20 EPNdB. This will be a challenging task, especially if the impact on airplane economics must be minimized. New technology and changes in the engine cycle are needed to accomplish this. The fan is the component that needs attention first. It will be necessary to either reduce fan source noise or apply additional acoustic treatment. For the takeoff condition the jet noise floor will be encountered and this can be handled by increasing the engine bypass ratio in order to reduce jet velocities and the resulting jet noise floor. For the approach condition the aft turbomachinery noise floor needs to be suppressed.

In future Quiet Engine testing it is planned to investigate the turbomachinery noise problem and also to explore for other noise floors such as

combustion and flow scrubbing noises that may be encountered at very low engine noise levels.

GENERAL ELECTRIC PEEBLES ENGINE TEST FACILITY

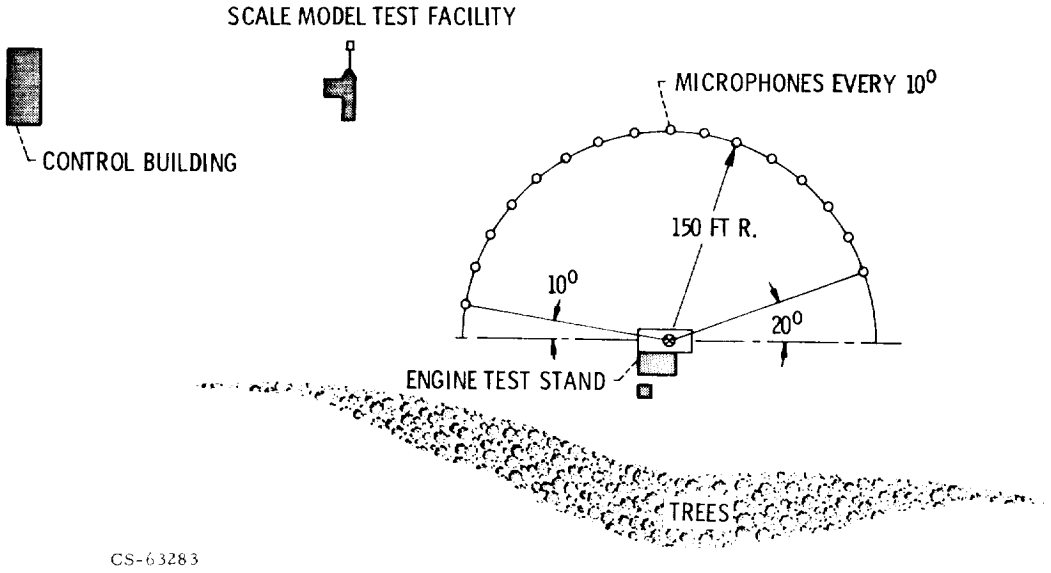

Figure VIII-1

AERIAL VIEW OF GENERAL ELECTRIC PEEBLES TEST FACILITY

CS-63381

Figure VIII-2

ENGINE A ON TEST

Figure VIII-3

QUIET ENGINE A BASELINE CONFIGURATION

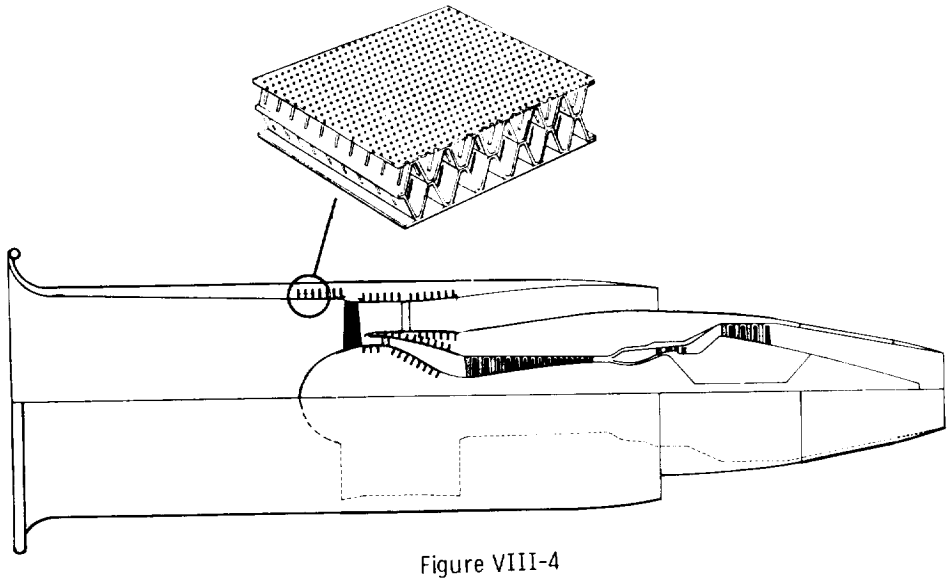

Figure VIII-4

CS-63322

ENGINE A AND FAN A
PERCEIVED NOISE DIRECTIVITY

(a) APPROACH SPEED, 370 FT SIDELINE

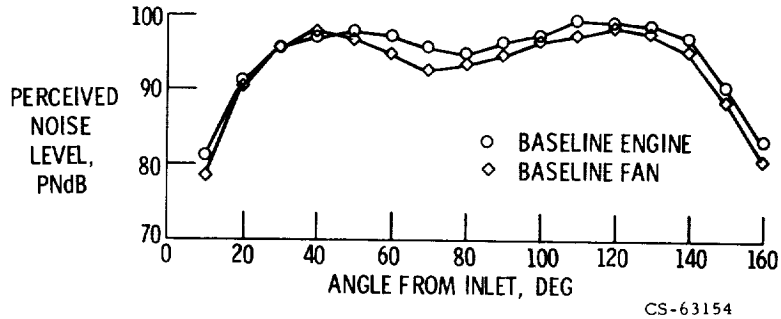

(b) TAKEOFF SPEED, 1000 FT SIDELINE

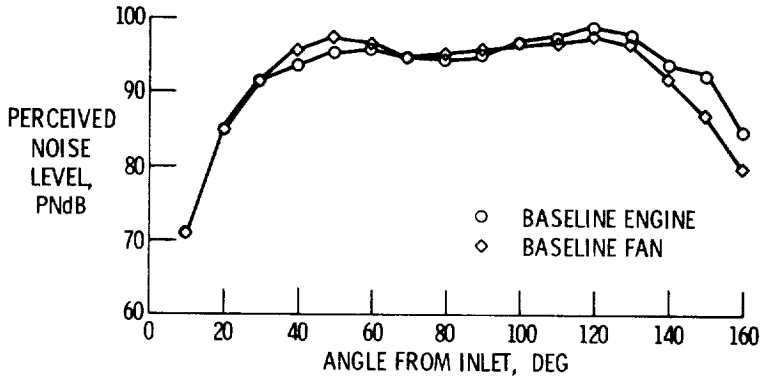

Figure VIII-5 CS-63148

ENGINE A AND FAN A $\frac{1}{3}$-OCTAVE BAND SPECTRA

TAKEOFF SPEED, 1000 FT SIDELINE

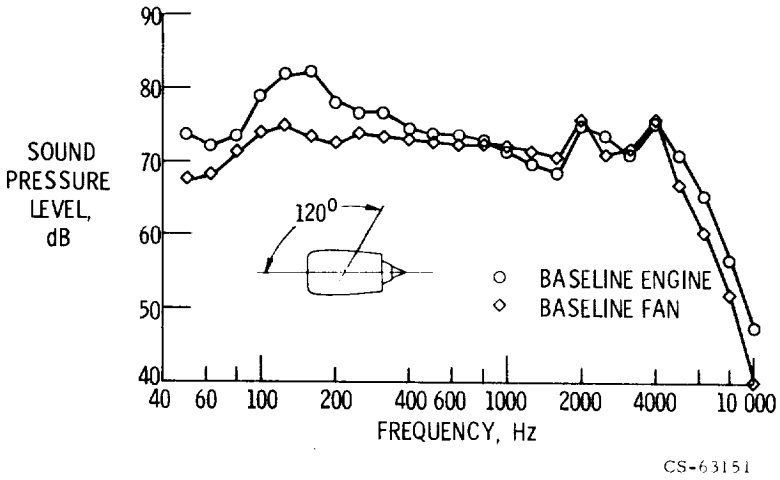

Figure VIII-6

ENGINE C ON TEST

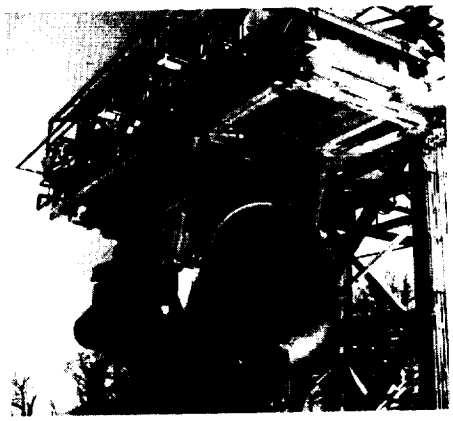

CS-63380

Figure VIII-7

LOW PRESSURE TURBINES

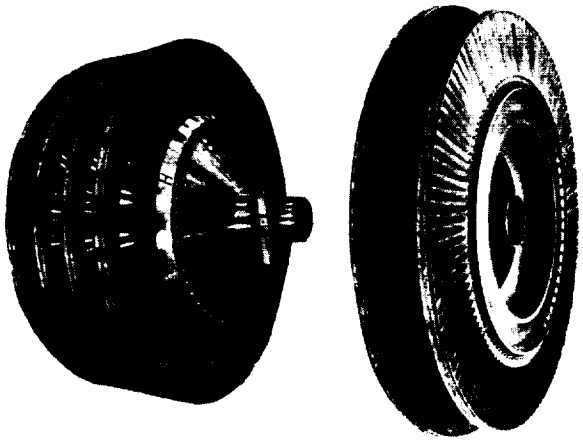

ENGINE A ENGINE C

CS-63378

Figure VIII-8

QUIET ENGINE C BASELINE CONFIGURATION

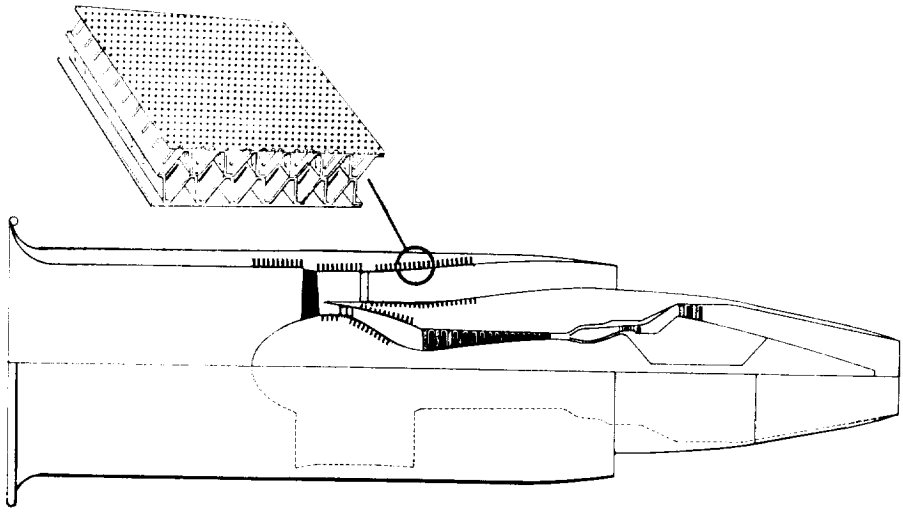

CS-63391

Figure VIII-9

BASELINE ENGINE PERCEIVED NOISE DIRECTIVITY

(a) APPROACH SPEED, 370 FT SIDELINE

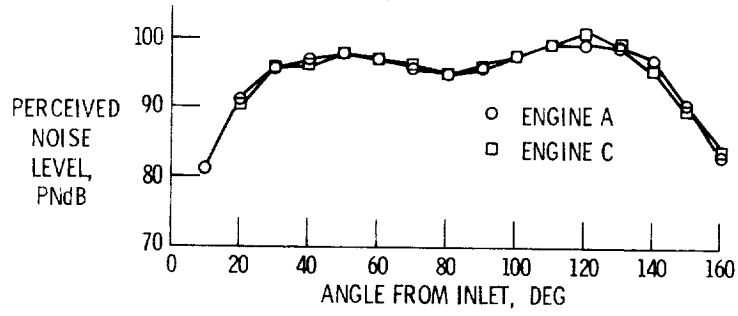

CS-63384

(b) TAKEOFF SPEED, 1000 FT SIDELINE

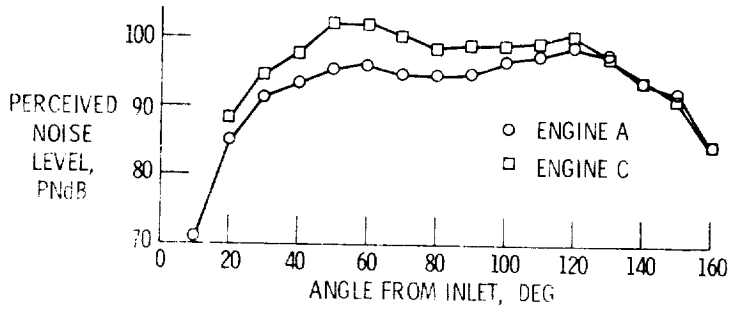

CS-63390

Figure VIII-10

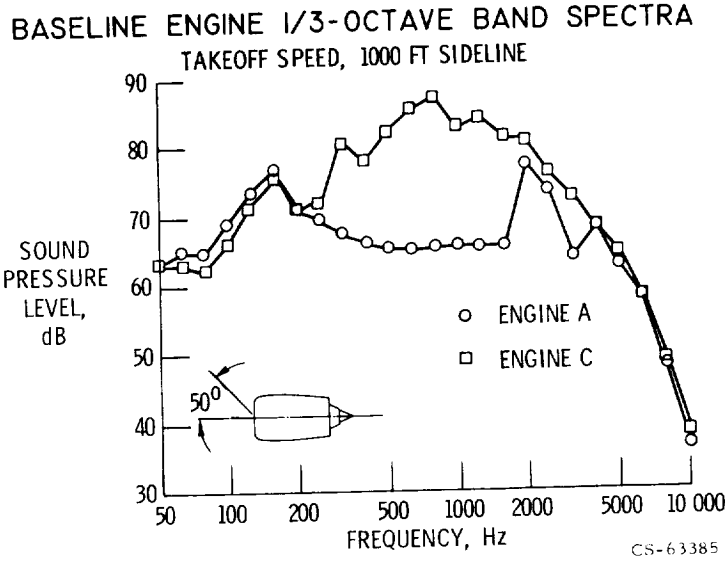

Figure VIII-11

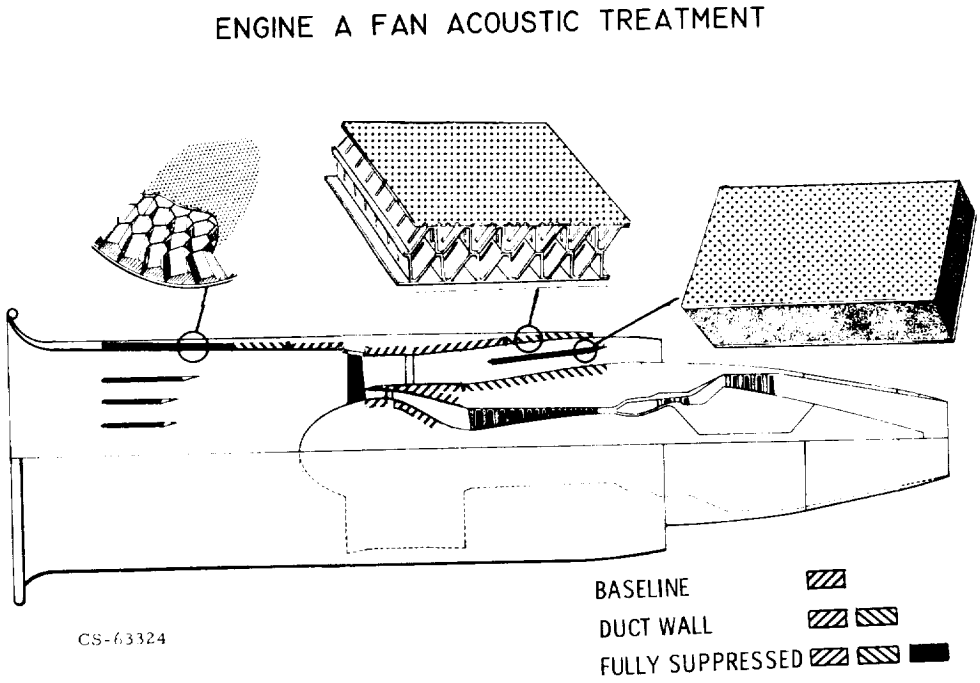

Figure VIII-12

TREATED INLET FOR ENGINE A

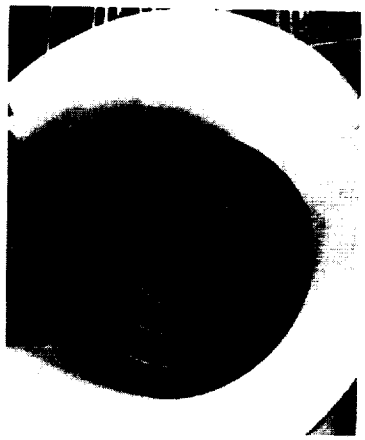

CS-63379

Figure VIII-13

ENGINE A PERCEIVED NOISE DIRECTIVITY

(a) TAKEOFF SPEED, 1000 FT SIDELINE

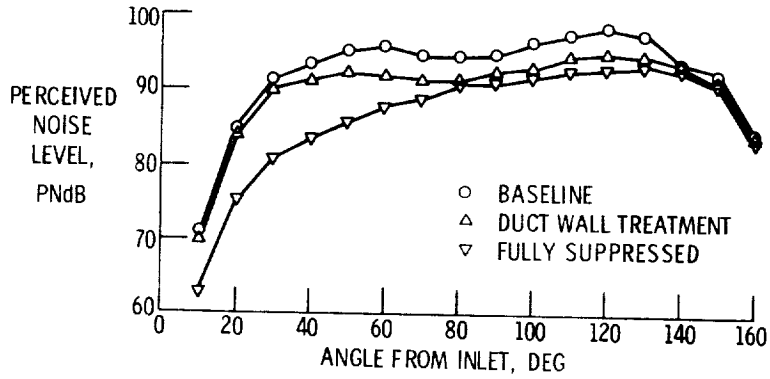

CS-63153

(b) APPROACH SPEED, 370 FT SIDELINE

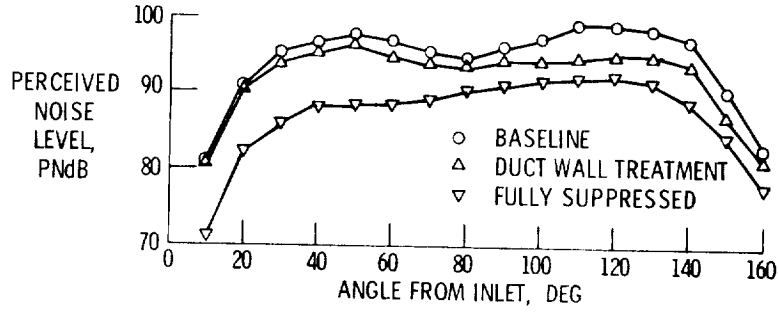

Figure VIII-14

CS-63147

ENGINE A $\frac{1}{3}$-OCTAVE BAND SPECTRA

APPROACH SPEED, 370 FT SIDELINE

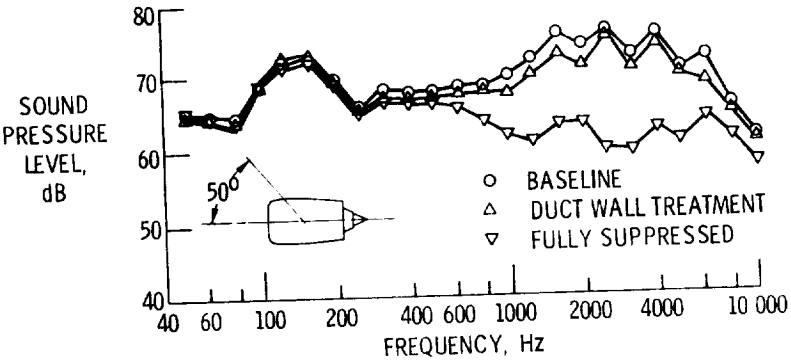

Figure VIII-15

CS-63149

ENGINE A WITH TURBINE TREATMENT

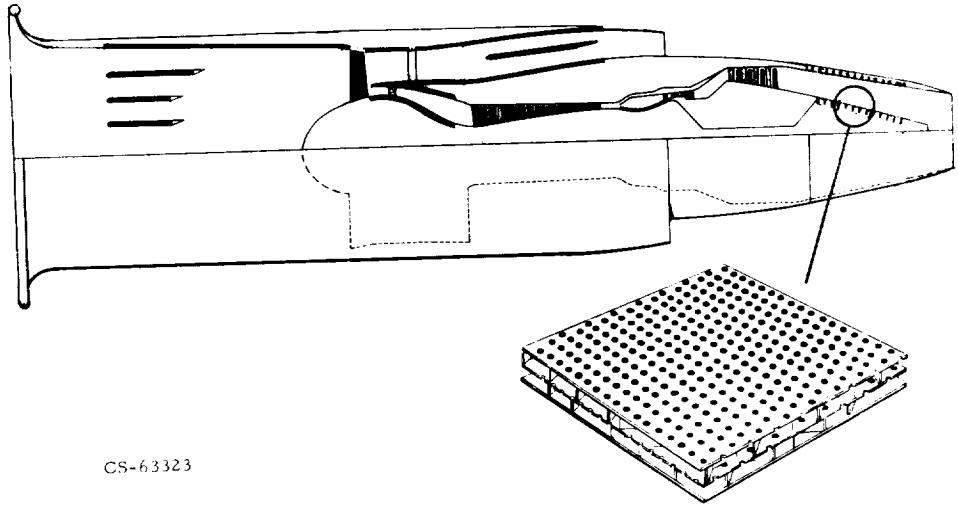

CS-63323

Figure VIII-16

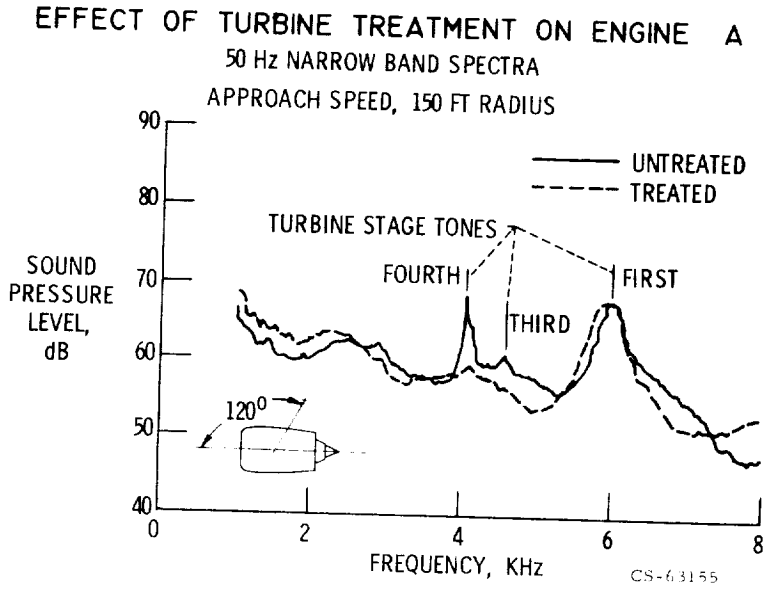

Figure VIII-17

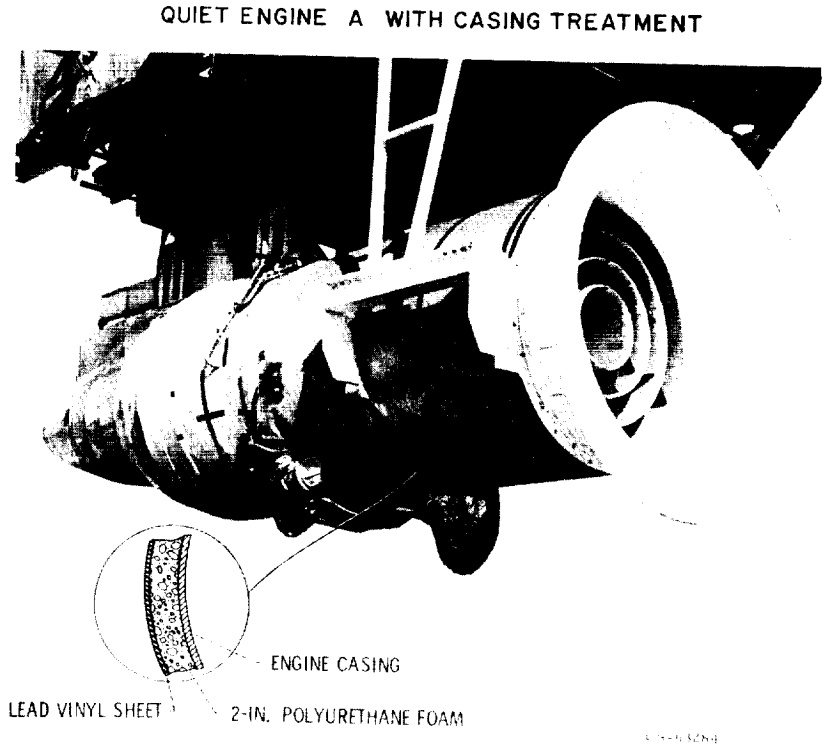

Figure VIII-18

LEWIS ENGINE ACOUSTIC TEST FACILITY

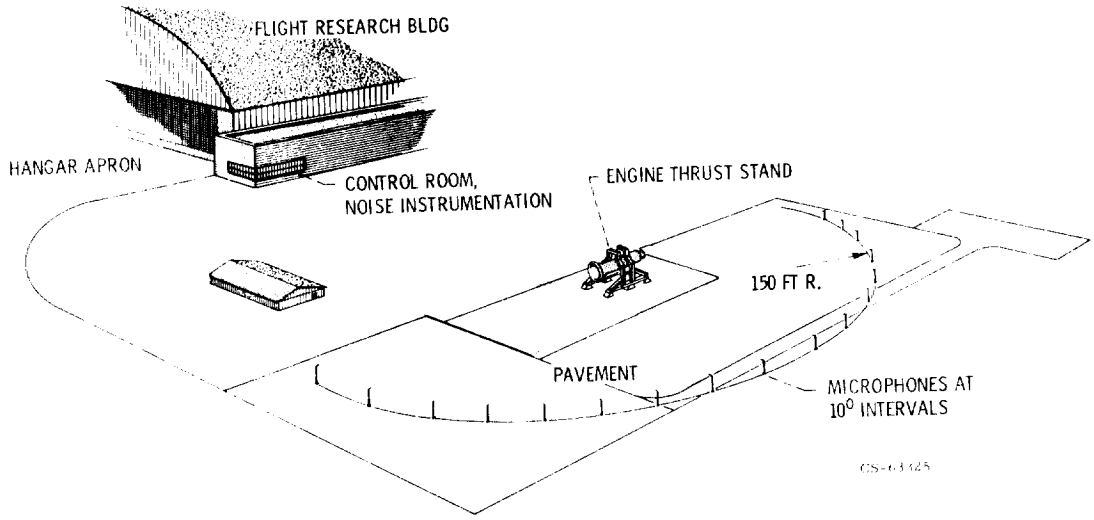

Figure VIII-19

LEWIS ENGINE ACOUSTIC TEST SITE

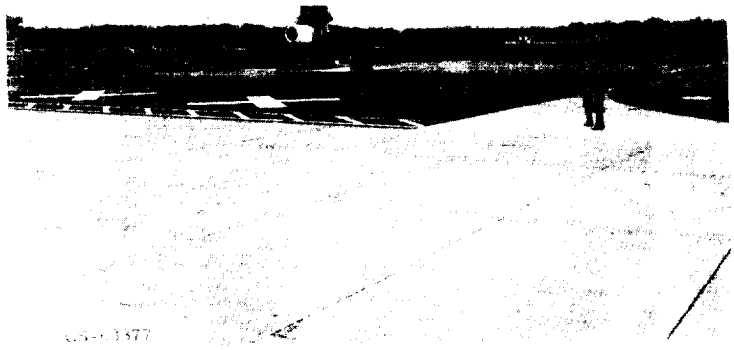

Figure VIII-20

BASELINE QUIET ENGINE A

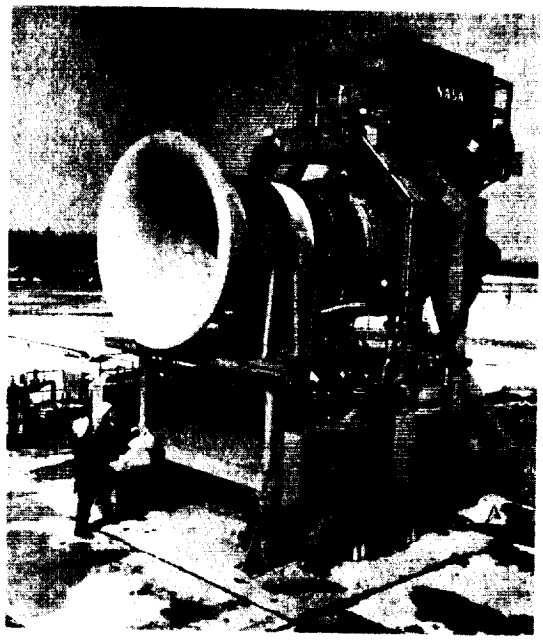

Figure VIII-21

QUIET ENGINE A WITH ACOUSTIC NACELLE

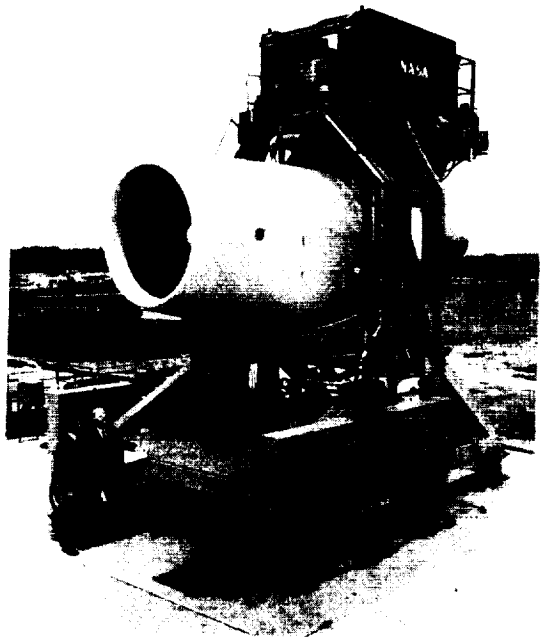

Figure VIII-22

QUIET ENGINE A WITH ACOUSTIC NACELLE

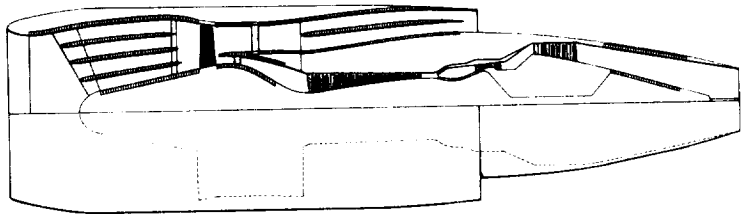

NACELLE ACOUSTIC TREATMENT

	INLET DUCT	EXHAUST DUCT
AREA, SQ FT	353	362
WEIGHT, LB	846	666

CS-63321

Figure VIII-23

BASELINE ENGINE A PERCEIVED NOISE DIRECTIVITY

TAKEOFF SPEED, 1000 FT SIDELINE

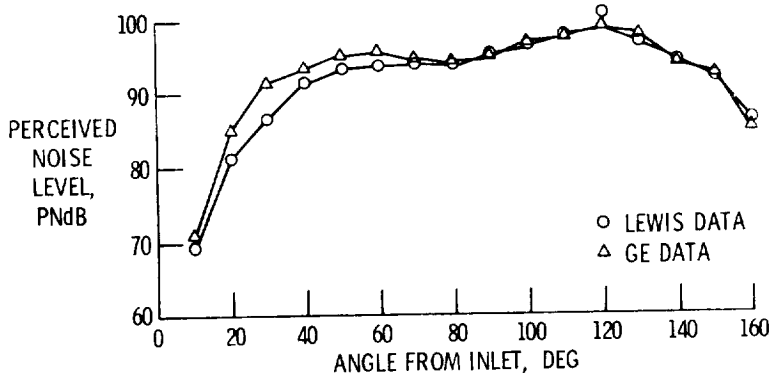

Figure VIII-24

CS-63382

QUIET ENGINE PERCEIVED NOISE DIRECTIVITY

TAKEOFF SPEED, 1000 FT SIDELINE

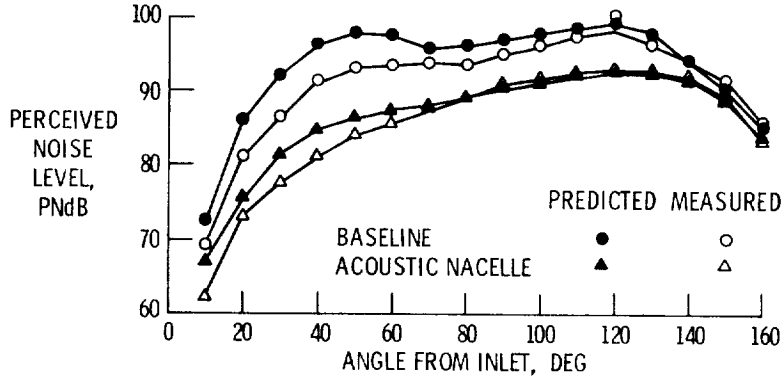

Figure VIII-25

CS-63282

QUIET ENGINE SOUND SPECTRA

(a) 1/3-OCTAVE BANDS; TAKEOFF SPEED, 1000 FT SIDELINE

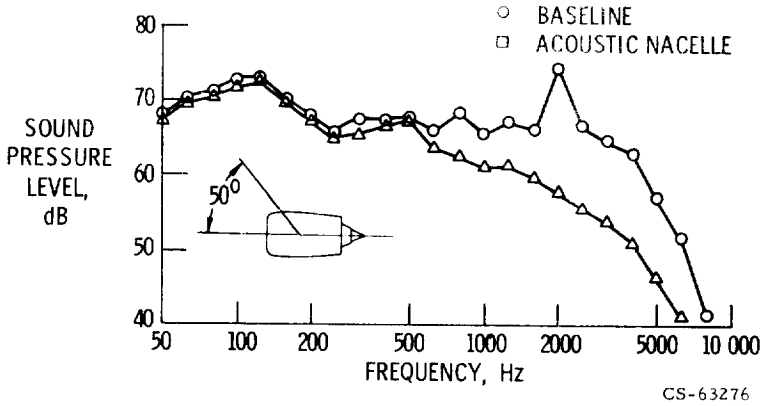

CS-63276

(b) 1/3-OCTAVE BANDS; TAKEOFF SPEED, 1000 FT SIDELINE

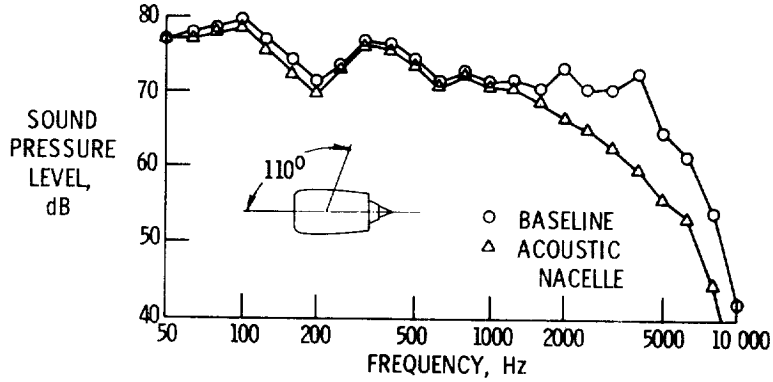

Figure VIII-26

CS-63281

QUIET ENGINE PERCEIVED NOISE DIRECTIVITY

APPROACH SPEED, 370 FT SIDELINE

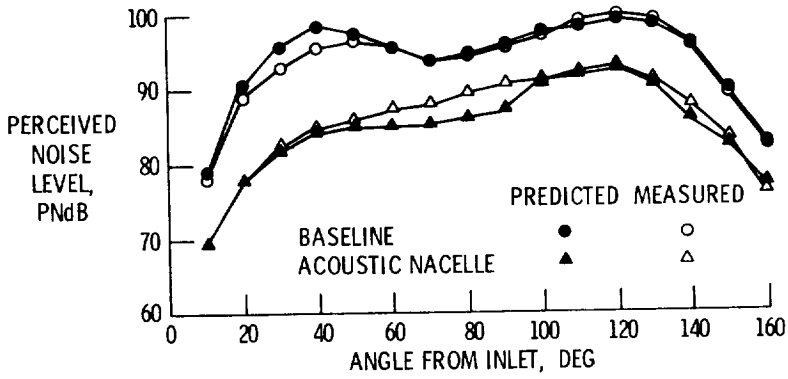

Figure VIII-27 CS-63280

QUIET ENGINE SOUND SPECTRA

1/3-OCTAVE BANDS; APPROACH SPEED, 370 FT SIDELINE

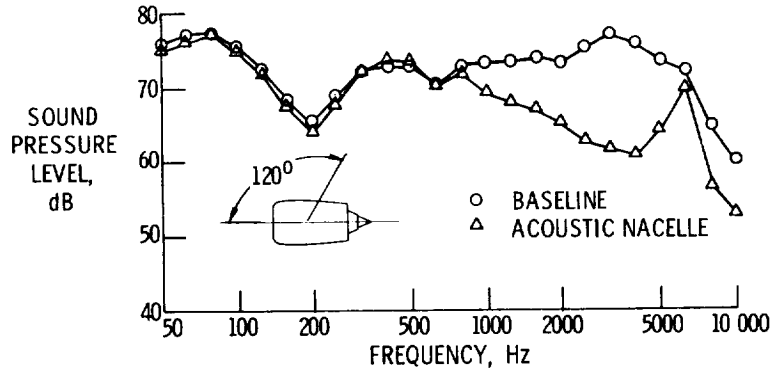

Figure VIII-28 CS-63279

EFFECT OF ACOUSTIC TREATMENT ON ENGINE A THRUST

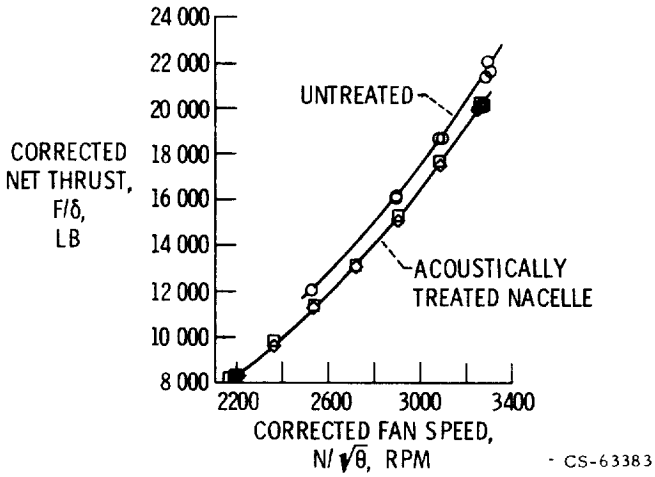

Figure VIII-29

QUIET ENGINE FLYOVER NOISE

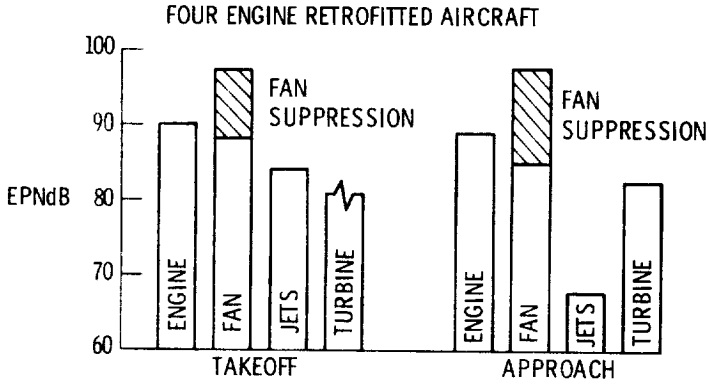

Figure VIII-30

CS-63278

IX. QUIET ENGINE DEMONSTRATION

Harry E. Bloomer

A demonstration was arranged for the conference attendees to compare the noise output of the Quiet Engine with treated nacelle to the noise output of the JT3D turbofan engine. (The design features of the Quiet Engine and Quiet Engine nacelle are presented in sections VI and VII. The test results are given in section VIII.)

The Quiet Engine is located on a test stand at the Lewis hangar apron as shown in figure IX-1. The attendees were initially positioned near the peak noise lobe of the forward quadrant to hear the fan noise and then in the rear quadrant to listen to the core jet and fan exhaust noise. The engine was operated at levels representing takeoff and approach. Attendees were visually informed of the noise levels for each position and operating condition.

Through the cooperation of the Air Force 4950th Test Wing under the command of Colonel James Walsh, Wright-Patterson Air Force Base, Ohio, a C-135 airplane fitted with the military counterpart of the JT3D engine was furnished to participate in the engine noise demonstration. The aircraft was parked next to the Quiet Engine site. One engine was operated alternately with the Quiet Engine in order to provide a direct evaluation of the engine noise reduction achieved by the Quiet Engine. The JT3D engine was also operated at takeoff and approach settings.

The physical differences of the two engines can be compared briefly by examining figures IX-2 and IX-3, which are sketches of the JT3D and the Quiet Engine, respectively. In addition, table IX-1 provides pertinent performance information for the two engines.

TABLE IX-1. - ENGINE COMPARISON

	JT3D/TF33	Quiet Engine
Takeoff:		
Thrust, lb	15 800	22 000
Bypass ratio	1.2	5.75
Core jet velocity, ft/sec	1618	1177
Fan jet velocity, ft/sec	1030	821
Approach:		
Thrust, lb	6000	8800
Bypass ratio	1.6	6.3
Core jet velocity, ft/sec	903	640
Fan jet velocity, ft/sec	766	505

QUIET ENGINE A WITH ACOUSTIC NACELLE

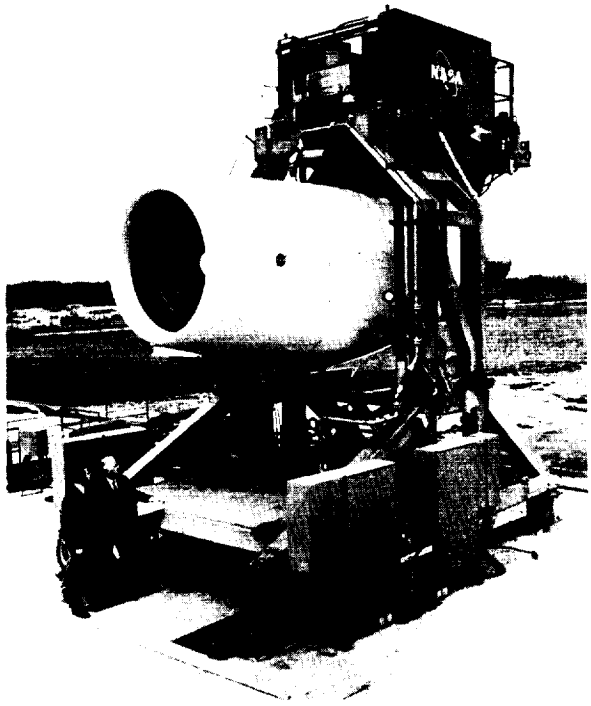

Figure IX-1

JT3D/TF33 ENGINE INSTALLED IN CONVENTIONAL UNTREATED NACELLE

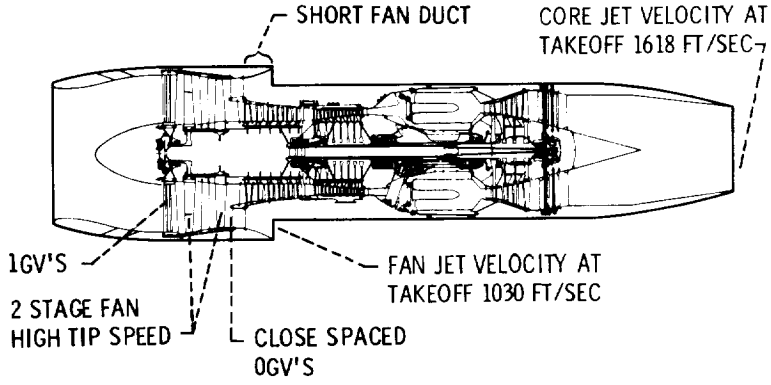

Figure IX-2

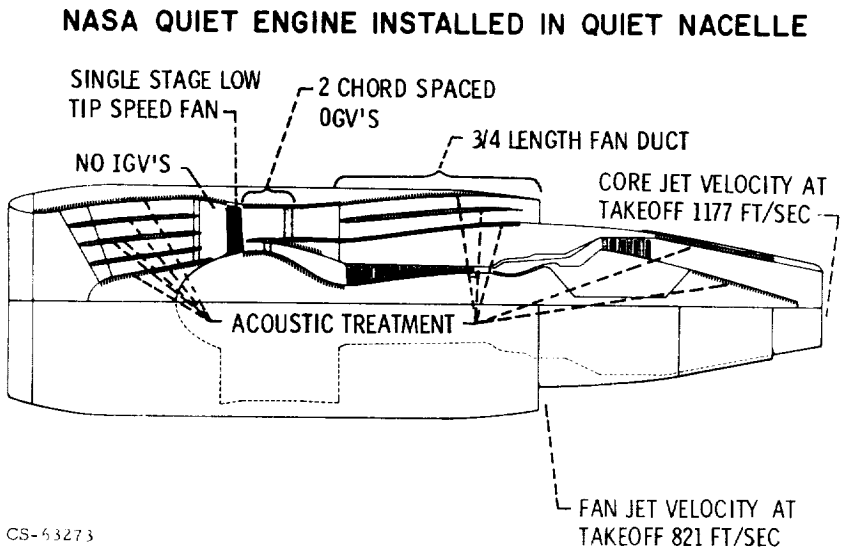
NASA QUIET ENGINE INSTALLED IN QUIET NACELLE
SINGLE STAGE LOW TIP SPEED FAN
2 CHORD SPACED OGV'S
3/4 LENGTH FAN DUCT
NO IGV'S
CORE JET VELOCITY AT TAKEOFF 1177 FT/SEC
ACOUSTIC TREATMENT
FAN JET VELOCITY AT TAKEOFF 821 FT/SEC
CS-53273

Figure IX-3

X. APPLICATIONS TO AIRCRAFT PROPULSION SYSTEMS

Newell D. Sanders, W. Harry Close,* Arthur A. Medeiros, and Richard J. Weber

Applications of the Quiet Engine technology to current and future airplanes are presented in this paper. The results of the Quiet Engine Program are briefly reviewed as follows. Most significantly, the goal of a 15- to 20-decibel reduction from Federal Air Regulation 36 (FAR-36) was exceeded. These noise levels were calculated for a four-engine airplane in the DC-8 and 707 class using the measured noise and performance of the Quiet Engine on the test stand. The noise reduction at takeoff is 26 decibels; 3.5 decibels of this comes from the improved airplane climb to a higher altitude over the judging point for takeoff noise. The noise reduction on approach is even more, 29 decibels. Another significant development is the elimination of the distinctive fan tones.

The FAR-36 noise levels for new aircraft similar to the DC-8 airplane are 104 decibels at takeoff and 106 decibels on approach. The new, large, wide-bodied jets now in service meet or better the FAR-36 levels. Starting with 116 decibels in the early 1960's, the first decade goal of a 10- to 15-decibel reduction has been achieved with these new airplanes. The experience with the Quiet Engine encourages us to believe that similar gains will be made in the next decade.

A comparison between the Quiet Engine and a modern new engine such as the JT9D, the CF6, or the RB211 is also of interest. A direct comparison is difficult because the flight engines have moderate amounts of sound suppression in the nacelles. Comparable flight tests with the Quiet Engine have not been made. It is estimated, however, that the bare engine A is 6 effective perceived noise decibels (EPNdB) quieter than the best of the new engines bare.

*Department of Transportation.

USES OF QUIET ENGINE TECHNOLOGY

The Quiet Engine as its exists today cannot be used on airliners; it is an experimental engine. The Quiet Engine uses a derated CF-6 engine core; the CF-6 engine produces twice the thrust of the Quiet Engine. Thus, the core is much oversized for the Quiet Engine, and this engine is much too heavy for airline use.

As part of the Quiet Engine Program, General Electric is making studies of engines that match the Quiet Engine fans to an advanced technology core. Figure X-1 shows cross sections of two engines: one using the low-speed fan A and the other using the high-speed fan C. Both engines have 22 000-pounds thrust at takeoff. The engine with fan A is longer than the one with fan C. It is larger in diameter, and has more turbine and booster stages.

Acoustic treatments for the two engines are shown in figure X-2. The upper half represents engine A and the lower half engine C. In both cases, acoustic treatment in the fan discharge duct matches the treatment that was used in the experimental Quiet Engine Program. It was pointed out in a previous section that the back end noise dominated the Quiet Engine and the front end noise was suppressed more than need be. The treatments shown here were selected to give a balanced noise from the front and the rear.

For fan A this balance is obtained without splitter rings; the inlet is lengthened and lined with acoustic absorbers as shown. Fan C was noisier, and simple lengthening of the inlet would not give the balanced noise between the front and the rear. Therefore, a splitter ring was added to the inlet. The inlet was shortened to give balanced noise from front to rear.

Significant characteristics of the engine installations are summarized in table X-1. Both engines produce 22 000 pounds of thrust at takeoff. Engine A has the low-speed fan operating at a tip speed of 1160 feet per second; the fan pressure ratio is 1.49, and the bypass ratio is 6.8. Engine C has the high-speed fan operating at a tip speed of 1550 feet per second; the fan pressure ratio is 1.55; and the bypass ratio is 6.4. Surprisingly, engine A is only a little larger in diameter even though it has a higher bypass ratio. Fan A, operates with a higher inflow velocity than does fan C; this higher

TABLE X-1. - QUIET ENGINES USING

ADVANCED CORES

	Engine	
	A	C
Takeoff thrust, lb	22 000	22 000
Fan tip speed (cruise), ft/sec	1160	1550
Fan pressure ratio (cruise)	1.49	1.55
Bypass ratio	6.8	6.4
Fan diameter, in.	68.7	68.3
Jet velocity (mixed), ft/sec	900	920
Engine weight, lb	3940	3500
Engine plus installation weight, lb	6900	6490
Relative specific fuel consumption, lb:		
Bare	0.981	1.000
Installed	0.986	1.009

inflow velocity produces almost exactly the flow increase required for the higher bypass ratio.

The combinations of fan pressure ratios and bypass ratios give the desired low jet velocities (900 and 920 ft/sec). These values assume that the primary and fan flows are mixed before being discharged as a jet. These velocities give noise floors well below the suppressed fan noises.

The weight of the low-speed engine A is 3940 pounds bare. It is heavier than engine C as might be expected because of the additional turbine and fan stages; the difference is 440 pounds.

When sound treatment is added, the differential between the two engines is slightly less because of the additional splitter in the inlet of engine C. Engine A with treatment weighs 6900 pounds, and engine C weighs 6490 pounds. The differential is reduced to 410 pounds per engine.

The specific fuel consumption of low-speed engine A is approximately 2 percent better than for high-speed engine C because of the higher fan effi-

ciency. The extra losses caused by the splitter in the inlet of engine C widens the efficiency gap slightly.

Until now, it has been assumed that the engines will be used in a DC-8 class airplane, but such a retrofit is costly. A more likely application is in new trijet and twin-jet airplanes. In the study of a trijet airplane powered by the Quiet Engine, the gross weight was 200 500 pounds. The corresponding FAR noise limits at takeoff and approach are 100 and 105 EPNdB, respectively. For engine A with suppression, the takeoff and approach noises are 91 and 92 EPNdB, respectively. These values are a little bit higher than values obtained with the experimental engine. The values are approximately 10 decibels below the FAR-36 levels. Engine C with the extra splitter in the inlet is 2 or 3 EPNdB noisier than engine A. It should be recalled that these noise levels are set by the aft end noise. The aft noise suppression, which was obtained in the experimental engine program, has been used, and the inlet suppression has been tailored to match. If future research lowers the back end noise another 5 decibels, the full end suppression that was demonstrated in the experimental engine program can then be used. In that event, the noise may decrease to 15 EPNdB below the FAR-36 level. In addition, distinctive fan tones will be suppressed completely.

The lower noise of engine A is obtained at extra initial cost and higher direct operating cost. Using the cost of one engine C and nacelle as the base for comparison, one engine A is expected to cost $73 000 more. This extra cost plus the net effects of the weight penalty, improved specific fuel consumption, extra maintenance, etc., are expected to cause the direct operating cost of aircraft powered with engine A to be 1.4 percent higher than for aircraft using engine C.

The discussion thus far has been directed toward methods of reducing the noise from future airplanes. As indicated earlier, fitting completely new Quiet Engines to existing airplanes will be extremely expensive. Some less expensive ways to obtain significant noise reductions for these airplanes are now discussed.

QUIETING OF EXISTING NARROW-BODIED AIRCRAFT

Noise reduction technology has been applied in the development of the new commercial aircraft, such as the DC-10, 747, and the L1011 and, of course, will be applied in newer aircraft. However, there are approximately 1700 existing domestic commercial aircraft that still have a long and economically useful life that create noise levels considerably in excess of the FAR-36 requirement for new aircraft of similar weight.

The aircraft in this category include the 707 and DC-8 powered by the JT3D engine and the 727, 737, and DC-9 powered by the JT8D engine.

There is no reason that existing noise technology cannot be applied to these aircraft to reduce significantly the overall aircraft noise problem more quickly than merely waiting for these aircraft to be retired.

In recognition of this, the Department of Transporation and NASA have initiated a joint program to reduce noise levels of these existing aircraft. Two approaches are being pursued: One requires no changes to the engines and uses a major amount of acoustic and jet suppression; the other involves engine modifications in addition to some degree of acoustic suppression. Both approaches are discussed.

FAA has contracted with the Boeing Company for the design, fabrication, and testing of a quiet nacelle for the 707. Shown in figure X-3 are cross-sectional views of the 707/JT3D production nacelle and of the FAA-Boeing retrofit nacelle. The two configurations indicate the approaches being taken to provide certifiable hardware that will greatly reduce the annoyance of the turbofan powered commercial fleet of 707 and DC-8 airplanes. The inlet cowl has been lengthened, and two inlet rings have been added to accommodate 70 square feet of acoustic treatment in the inlet. A new side cowl has been developed, and the fan ducts have been extended to three-quarters of the nacelle length to accommodate 171 square feet of acoustic treatment. These changes constitute the so-called "lower goal" configuration and are predicted to yield at least 15.5 EPNdB suppression on approach, 6 EPNdB at takeoff with cutback, and 4.5 EPNdB noise reduction on the sideline under FAR-36 procedures.

The plug nozzle shown in figure X-3 is also being added to gain an increment of jet noise suppression and is predicted to yield at least 3 EPNdB

additional suppression at takeoff and on the sideline. This configuration is known as the upper goal nacelle under the FAA contract terms. Ground tests of the noise reduction nacelle with jet suppression will be conducted in September 1972. Flight tests are planned for February 1973.

There are likely to be more than twice as many domestic aircraft powered by JT8D engines in the late 1970's and early 1980's as 707 and DC-8 aircraft powered by JT3D's. The 727, 737, and DC-9 aircraft that are powered by the JT8D are short-range aircraft, but they are used almost as many hours per day as the long-range airplanes and thereby generate many more takeoffs and landings per day, each of which is a noise event in some community. Figure X-4 illustrates the peak perceived noise level of a 727-200 airplane at a constant altitude of 370 feet for various thrust settings up to 100 percent takeoff thrust. The total noise level is indicated by the solid line; the constituents of this total noise level are indicated by the dashed lines. As with the JT3D engine, fan noise is the dominant noise source at approach thrust; however, the jet noise level is within 10 decibels of the total and is equal to the inlet noise level at approach power setting. As thrust is increased, it is evident that the jet noise continues to rise and rapidly becomes the dominant noise source for this engine. Therefore, the means to reduce the noise levels generated by JT8D engines are somewhat different from those considered for the JT3D. First, it is evident that 15 EPNdB of noise reduction at approach thrust is not possible with this engine unless a significant amount of jet suppression can be achieved at the low thrust setting. At the low jet velocities associated with approach thrust, significant amounts of jet suppression are unlikely to be achieved. However, at the higher exhaust velocities typical of the higher thrust settings, significant jet suppression can be anticipated and, in conjunction with inlet and fan-duct treatment, appreciable noise reduction can be affected.

In figure X-5 is illustrated a cross section of the 727/JT8D upper goal nacelle being developed by Boeing for the FAA under another contract. The upper portion of the figure portrays the full suppression mode, and the lower portion illustrates the cruise mode.

As with the JT3D, extensive inlet and fan-duct treatment has been added to attenuate the forward and aft radiated fan noise. Two polyimide honeycomb treated inlet rings have been added as well as lining material on the

outer wall and inner fairing. Perforated-plate treatment has been added to the existing long fan ducts, and the combined fan and core exhaust is channeled through a 20-lobe suppressor nozzle. Ambient air is entrained through the blow-in doors, and mixing is induced within the ejector shroud. Brazed perforated-plate - honeycomb lining material is strategically placed in the ejector shroud and on the plug to attenuate some of the mixing noise and to work on the fan noise that propagates out the fan duct.

To minimize the losses associated with the multilobe nozzle during cruise, the centerbody will be extended as shown in the lower portion of the figure. In this mode, the ejector doors are closed, the multilobe nozzle is not bounded in the central annulus of the flow, and a plug nozzle is now formed at the nacelle rear face.

This configuration will be flight tested later this year to verify the design.

The acoustic performance of these nacelle and jet-suppression configurations compared with the current production aircraft is shown in table X-2.

TABLE X-2. - ESTIMATED NOISE LEVELS AND NOISE EXPOSURE AREAS

Type of aircraft	Noise levels at FAR-36 conditions, EPNdB		Single takeoff and landing land area exposed to 90+ EPNdB, sq mile
	Takeoff	Approach	
707:			
Current	113	119.5	55.8
Nacelle-jet suppression retrofit	104	104	27.4
727:			
Current	101	109.5	29.4
Nacelle-jet suppression retrofit	96	99.5	6.6

Noise levels are shown for takeoff and approach conditions in accordance with procedures prescribed by FAR-36. As previously stated, the 707/JT3D nacelle and jet-suppression (or upper goal) configuration is anticipated to produce at least a 9-EPNdB noise reduction on takeoff and a $15\frac{1}{2}$-EPNdB noise suppression at the approach measuring point. A sideline noise reduction of $7\frac{1}{2}$ EPNdB or more is also expected for this configuration. The land area exposed to 90 EPNdB or greater during one takeoff and landing by the current aircraft is 55.8 square miles. The 707/JT3D nacelle and jet-suppression retrofit configuration is anticipated to expose only 27.4 square miles for one takeoff and one landing.

The 727/JT8D production aircraft and nacelle and jet-suppression configuration noise levels are also shown in table X-2. An approximately 5-EPNdB noise reduction is anticipated at takeoff and a 10-EPNdB noise reduction is expected for approach conditions. An 8-EPNdB sideline noise reduction is also expected as a result of the nacelle-jet-suppression configuration. These reductions in noise levels will reduce the 90 EPNdB contour for one takeoff and landing operation from the current 29.4 square miles to 6.6 square miles.

As mentioned earlier, another option to achieve noise reduction in JT3D and JT8D powered aircraft is to modify the engine by incorporating several noise reduction features in addition to some degree of acoustic suppression. This option is presently being studied by the Lewis Research Center in anticipation of establishing the required contracted effort.

A proposed modification for the JT3D engine is shown in figure X-6. The portion of the engine shown above the centerline is the current production version of the JT3D; that below the centerline is the proposed JT3D modification. Several noise reduction features are incorporated into the modification. Inlet guide vanes have been eliminated, the fan diameter has been increased to permit a higher bypass ratio, and a single-stage fan has replaced the original two-stage fan. The single-stage fan permits increased blade to vane spacing to about two rotor chord lengths without significantly increasing engine length. In addition, the blade vane ratio is acoustically optimized and swept-fan exit guide vanes are incorporated. Acoustic treatment is provided at the inner and outer wall of the fan inlet and on both surfaces of the two inlet rings. Acoustic treatment is also proposed at the inner

and outer wall of the fan discharge as well as both surfaces of the bypass splitter. This is not necessarily the optimum acoustic configuration and several with and without splitters and inlet rings will be investigated.

In order to minimize the number of changes and, hence, the cost of changes, a matching or booster stage would be used between the new fan and the existing core, so that the only change required to the core is a resetting of the last stage of the low-pressure turbine.

A comparison of some design parameters for the present and modified JT3D is shown in table X-3. The more significant parameters are an in-

TABLE X-3. - COMPARISON OF PRESENT AND MODIFIED JT3D

	Standard JT3D	New front fan JT3D
Fan tip diameter, in.	50.2	56.5
Sea level airflow, lb/sec	460	600
Bypass airflow, lb/sec	265	412
Bypass ratio	1.36	2.20
Fan pressure ratio	1.75	1.67
Core jet velocity at takeoff; ft/sec	1430	1285
Inlet guide vane	Yes	No
Fan stages	2	1
Fan tip speed, ft/sec:		
Takeoff	1423	1535
Cruise	1513	1600
Cycle temperature, ^{o}F	1703	1740

crease in fan diameter of 6.3 inches, an increase in bypass ratio of 0.84, and a reduction in core jet velocity of 145 feet per second.

The fan modifications, the resultant decrease in core jet velocity and the acoustic suppression can produce significant noise reduction while achieving

TABLE X-4. - ESTIMATED PERFORMANCE COMPARISONS

OF 707/JT3D

	Current	New front fan	Percent change
Installed takeoff thrust per engine, lb	15 430	17 300	12.2
Cruise thrust specific fuel consumption, (lb/hr)/lb	0.84	0.80	-4.4
Operating empty weight, lb	145 745	148 485	1.9
Maximum taxi weight, lb	333 600	333 600	0
FAR field length, ft	11 350	9950	-12.3
Range, n. mi.	4860	4830	-0.6

performance gains. The estimated performance changes for the modified JT3D engine installed in the 707 airplane are shown in table X-4. The higher bypass ratio for the modified engine results in an increased installed thrust and an improved cruise thrust specific fuel consumption of 12.2 and 4.4 percent, respectively. But the operating empty weight of the 707 is increased by 1.9 percent primarily because of the larger fan diameter and the weight of acoustic treatment.

There are several ways in which the performance improvement and weight increase can be traded off to achieve improved aircraft performance. In table X-4 it was assumed that the maximum taxi weight and the passenger and cargo payload were the same for both the current and modified aircraft. With this assumption the FAR field length is reduced by 12.3 percent by the modification, but the range is decreased by 0.6 percent. Further studies are required to determine the best use of the engine performance improvements.

The noise reduction goals deemed possible with the engine refanning are shown in figure X-7 for both approach and takeoff of the 707. At approach the noise level at the FAR-36 measuring station could be reduced by about 18 EPNdB below that of the current 707, which is about 5 EPNdB below the FAR-36 requirements for new aircraft in this weight class. Similarly, at

takeoff the noise level at the FAR-36 measuring station could be reduced about 15 EPNdB below that of the current 707, which is about 6 EPNdB below FAR-36 new aircraft requirements.

Another technique of presenting the noise reduction effect is to show the land area exposed to some given noise level. The land area exposed to 90 EPNdB or greater for both takeoff and landing is shown in figure X-8 for both the current and modified 707 aircraft. The refanned engine configuration reduces this area from 55.8 to 13.7 square miles, or a 75-percent reduction in affected land area. As mentioned previously, the corresponding land area for the 707 aircraft with the FAA nacelle is 27.4 square miles.

A similar approach can be used to reduce the noise produced by the JT8D engines; these engines power the three-engine 727, the two-engine 737, and the DC-8 aircrafts. Some of the pertinent design parameters for the current production JT8D and a JT8D refanned in a manner similar to JT3D are shown in table X-5.

TABLE X-5. - COMPARISON OF PRESENT AND MODIFIED JT8D

	Standard JT3D	New front fan JT3D
Fan tip diameter, in.	40.5	47.4
Sea level airflow, lb/sec	327	454
Bypass flow, lb/sec	158	288
Bypass ratio	0.934	1.73
Fan pressure ratio	2.04	1.73
Core jet velocity at takeoff, ft/sec	1816	1590
Inlet guide vanes	Yes	Yes
Fan stages	2	1
Fan tip speed, ft/sec:		
Takeoff	1470	1690
Cruise	1550	1820
Cycle temperature, ^{o}F	1960	1892

As was the case for the JT3D new front fan configuration, the bypass ratio is increased by the use of a larger diameter single-stage fan in place of the production two-stage fan. This particular new front fan design assumes minimum turbine modifications and retains the existing turbine shaft speed, which results in high fan tip speed. Under these conditions, inlet guide vanes are retained and fan noise treatment is required to minimize the fan noise. This aspect of the design is being explored further to evaluate several promising alternatives that may lower the fan tip speeds and eliminate the inlet guide vanes.

The primary objective, however, is to lower the core jet velocity by increasing the fan bypass flow. Installation restraints such as 727 center-duct maximum airflow and 737 ground clearance will be major factors in the final fan sizing. Costs associated with turbine modifications are the limiting factor on tip speed and they determine the practicality of eliminating the inlet guide vanes.

The noise benefit anticipated with the refanning of the JT8D is presented in figure X-9. Shown are 90-EPNdB contours for takeoff and landing of a 727 equipped with production JT8D's. All contours are for the maximum takeoff weight for which the 727 is certificated and for operation on a standard FAA day. As shown, the land area exposed to 90 EPNdB or greater is reduced by refanning from 29.4 to 3.9 square miles, an 87-percent reduction. The quiet nacelle previously described would reduce the exposed area to 6.6 square miles.

The pursuit of both the refanning configurations and the nacelle/jet suppressor configurations for the JT3D and JT8D engines will provide a broad range of avenues for retrofit decision making. Noise levels, performance, and nonrecurring and recurring costs must be evaluated and traded off to arrive at a final decision.

Some preliminary performance estimates that have been made of the nacelle and refan retrofit for the 707 and 727 aircraft are presented in table X-6. These early estimates indicate that both retrofit options reduce noise levels below FAR-36 requirements for aircraft of a similar weight class. The refan option provides improved performance and noise levels 3 to 6 EPNdB lower than the nacelle option; however, retrofit costs, which must also be considered, are higher for the refan option.

TABLE X-6. - PERFORMANCE AND NOISE COMPARISONS OF ACOUSTICALLY TREATED NACELLE AND NEW FRONT FAN RETROFIT

Type of aircraft	Performance change, percent					Noise level, EPNdB	
	Installed takeoff thrust	Cruise thrust sfc	Operating empty weight	FAR field length	Range	Takeoff	Approach
707/JT3D:							
Nacelle	-2.0	1.1	1.0	2.6	-4.4	104	104
New front fan	12.2	-4.4	1.9	-12.3	-.6	98	101
727/JT8D:							
Nacelle	-3.0	3.4	1.0	6.3	-10.0	96	99.5
New front fan	13.0	-4.3	2.5	-19.7	-1.3	92	96

TABLE X-7. - RETROFIT COST ESTIMATES

Type of aircraft	Domestic aircraft inventory[a]	Kit cost estimates, millions of dollars per ship set		Domestic fleet retrofit cost estimate, millions of dollars	
		Nacelle and jet suppressor	New front fan and nacelle	Nacelle and jet suppressor	New front fan and nacelle
707 and DC-8	460	0.6 to 0.8	1.2 to 2.0	----------	----------
727	660	.6 to 0.8	1.0 to 1.8	----------	----------
737 and DC-9	450	.4 to 0.6	.8 to 1.4	----------	----------
	1570 total	---------	---------	860 to 1200	1600 to 2700

[a]Estimated for 1980.

Cost estimates of a very preliminary nature are shown in table X-7. The estimated cost per aircraft for the nacelle retrofit varies from $400 000 to $600 000, whereas the refan cost estimates vary from $800 000 to $2 000 000.

These costs, translated into figures for retrofitting the entire projected domestic air fleet, would be estimated at an average of about a billion dollars for the nacelle against an average of approximately 2.1 billion dollars for the refan option. The approximately two to one ratio refan to nacelle estimated direct costs could be outweighed by the tangible performance advantage of the refanning and the social benefit of the lower noise level provided by refanning.

It is premature at this time to arrive at any firm recommendation on the best type of retrofit. Performance and noise data must be obtained for both the nacelle retrofit and the engine refanning. Then these data can be used to perform the economic and system analyses necessary to permit sound conclusions based on a rational evaluation consistent with each airline's particular set of economic considerations.

The DOT/NASA program will pursue both options for all aircraft and will perform system economic studies that will support rule making and retrofit decisions.

FUTURE QUIET AIRCRAFT

In the future advances in aerodynamics, structures, and propulsion systems can be anticipated. The NASA Advanced Transport Technology Program was initiated about a year ago to determine the kinds of improvements most beneficial for commercial transportation and to start building up a data base of advanced technology for use in airplanes of the 1980 decade. To guide the program, comprehensive studies have been performed by Boeing, Convair, and Lockheed under contract to the Langley Research Center. Parallel studies of the propulsion system are being done for the Lewis Research Center by General Electric and Pratt & Whitney.

Figure X-10 illustrates a possible configuration for a 1980 airliner as suggested by these studies. One of the main features of the advanced plane

will probably be use of the supercritical wing concept developed by Whitcomb and his associates at Langley. The best way to capitalize on this and other advances is not yet determined. For example, the flight speed might be raised considerably higher than at present - perhaps nearly to Mach 1. Or the structural weight at lower speeds might be lowered. The most desirable mix of speed, range, and payload will be decided by the airplane companies and their customers. In any event, we can expect to face a continuing concern over environmental factors such as pollution and noise.

Figure X-11 shows the sideline noise produced by various turbofan engines of the type that might be suitable for high-speed airplanes. The cruise Mach number of 0.98 used for these data emphasizes the differences from the engines discussed previously. Increasing either fan pressure ratio or bypass ratio extracts energy from the core and so reduces the jet noise, which is predominately from the core. Eventually, however, a limit is reached as the bypass jet noise becomes more significant. Other factors not shown here have a large effect on the numerical results. For example, the higher turbine-inlet temperatures anticipated for the advanced engines require higher bypass ratios than those shown earlier for comparable noise goals.

Another difference between the advanced engines and those previously discussed is the fan pressure ratio. As will be seen later, higher pressure ratios become desirable at speeds near Mach 1. The dashed lines show that fan machinery noise must be suppressed to reduce the total engine noise below 100 decibels. A related problem is that these pressure ratios are in the region where we must choose between use of a one-stage or a two-stage fan. Making the proper tradeoffs between fan efficiency, required suppression treatment, and overall engine weight is an important question requiring more research.

Figure X-12 shows how the same two engine design parameters affect airplane performance. Relative gross weight for a fixed range and payload is given as a function of bypass ratio and fan pressure ratio. The lowest weight is obtained at the highest pressure ratio. The optimum bypass ratio is 6, but a somewhat higher value is required to get the jet noise down to the level probably needed for a future airplane, of the order of 80 to 85 decibels, perhaps.

The effect of compromises in engine design for the sake of quieting the airplane is summarized in figure X-13. To reflect the economic penalties of the compromises, airplane performance is presented in terms of percent of return on investment (ROI).

The left curve represents the performance level that would be achieved with today's engine technology. As a reference point, changes in ROI will be used as a measurement, starting from a current-technology point at FAR-36.

By 1985 improvements in engine technology should shift the noise-ROI curve to the right as shown. The improvements include better designs of the rotating components that reduce the generation of machinery noise, lighter weight, such as through the use of composite materials, and higher turbine-inlet temperatures with reduced penalties associated with turbine cooling. The overall improvement can be invested into gains in airplane economy or reductions in noise or both. At the upper right, for example, the ROI could be increased by some 7 percent over today's level by selecting a high-pressure ratio, low-bypass-ratio design. However, such an engine would be much too noisy. At the other extreme, engines could be obtained that approach 20 decibels below FAR-36 with no penalty in ROI. The dashed portion of the curve is intended to suggest uncertainty about the amount of machinery noise suppression that can be achieved in this time period without undue weight or pressure drop.

As a longer range goal, whose achievement is as yet unknown, the technology would be advanced sufficiently to provide a benefit in ROI together with a reduction in noise. This is indicated by the third curve in the lower right corner of the figure. This discussion has been limited to engine technology. In concluding this topic it should be noted that in the coming decades, improvements in airframe technologies and operating procedures such as curved approach paths will also help in reducing noise and increasing ROI.

Consider now a brief review of another type of future airplane. Figure X-14 shows an advanced supersonic commercial transport. Although it is not certain whether the United States will ever build this airplane, NASA, in order to keep the nation's options open, is preparing to start a program for advanced supersonic aircraft similar to the one for subsonic transports.

The goals of the program are generally the same: to assess the readiness of the various technologies needed, to identify profitable areas for further research, and to build up a data base for use if and when it is determined that it is desirable to develop such a vehicle. A basic premise of the program is that the country will not seriously contemplate developing a supersonic transport unless we can reasonably predict, not merely high speed, but also profitable operation coupled with public acceptance. A major problem that will receive attention in this program is that of excessive engine noise.

Figure X-15 presents some feeling for the magnitude of the problem. Relative range is plotted against sideline noise, which is the most troublesome point for a supersonic airplane. Engine noise is quite sensitive to the type of airframe considered. For this figure a high-wing-loading, fixed-wing configuration similar to the recent Boeing SST design was assumed. The upper right point represents an afterburning turbojet (ABTJ) engine of the type used in that Boeing design. Sideline noise is greatly in excess of the current FAR limit of 108 decibels. One way to quiet this type of engine is to increase its size. The additional thrust then available is not required for takeoff, so instead it can be throttled back during takeoff, which reduces the noise. However, the larger propulsion system is heavier, which then hurts the range. Significant reductions in noise using this technique cause unacceptable losses in airplane performance. It may be possible to reduce these losses to some extent by replacing the afterburning turbojet by another type of propulsion system. Depending on the particular estimates of relative engine weights, installation drags, and so forth, the figure suggests that there is a benefit available through use of either duct burning turbofans (DBTF) or nonafterburning turbojets (dry TJ). Detailed studies of the engines in conjunction with the particular airplane of interest are necessary to confirm these estimates. However, at best, it appears that the alternative engines and oversizing are apt to be a costly way to achieve low noise levels.

The dashed line represents another possibility for low noise. The variable-cycle engine would combine the quietness of a high-bypass-ratio turbofan at takeoff with the efficient supersonic operation of an afterburning turbojet. If there were no weight or drag penalties incurred by this convertible engine, we might even obtain an improvement in range due to the

better subsonic fuel consumption of the turbofan. However, at the present time, this line is more of a hope than a fact. Serious studies of variable-cycle concepts are just now being initiated.

A different approach to quieting of supersonic engines is shown in figure X-16. Again, relative range is plotted against sideline noise. The solid line repeats the curve for the nonafterburning turbojet from the previous figure. The possibility of installing mechanical noise suppression devices on the exhaust nozzle is now considered. The data points represent the reductions in noise that have been experimentally measured in the laboratory and also show the losses in range due to the penalties in thrust caused by the suppressors. It is assumed that the thrust loss is imposed only during the takeoff process and that the suppressors are retracted with no loss during climb and cruise. The data points are generally in the vicinity of the dashed line that corresponds to a 1-decibel reduction for each percent of thrust penalty. Suppressors with this level of performance are considerably better than the simple oversizing technique. However, suppression devices by themselves cannot yet offer as much quieting as is required. That is, for an advanced airplane such as this, it will probably not be sufficient to just meet FAR-36. Secondly, this figure gives a somewhat misleading picture of what has been accomplished to date with noise suppressors. The data points do not necessarily represent devices that are ready for flight application in terms of low weight, retractability, or durability. Furthermore, many of the points were measured only at sea-level static conditions and actual performance in flight could be worse.

Further research on jet noise suppressors, perhaps in combination with improved engine cycles, should lead to a solution for the engine noise problem of supersonic airplanes.

SUMMARY

Estimates of the prospects for quiet airplanes in the future are now summarized. Figure X-17 shows noise estimates for five classes of airplanes. The heavy dashed line across the figure represents the FAR-36 noise certification levels at appropriate gross weights and operating conditions.

The SST using afterburning turbojets and no sound suppression is estimated to produce 129 EPNdB on the sideline. Suppression devices and operating techniques can reduce this noise markedly. It is believed, however, that future noise certification levels for subsonic airplanes will be 10 decibels lower than the present FAR-36 level and that SST's will be required to meet that level. This means a noise level near 100 decibels, a 30-decibel reduction. A dual cycle engine, it is hoped, might meet this requirement.

The present fleet of 707's and DC-8's produces noises nearly as high as 120 decibels on approach. Combinations of sound absorbing devices and engine modifications are expected to give a noise near 100 decibels. This compares with a FAR-36 value of 106 decibels.

The new advanced technology transports (ATT) are being studied with two noise goals in mind: one is 10 decibels and the other is 20 decibels below the FAR level of 106 on takeoff. Initial estimates indicate that the 10-decibel down, or 95-EPNdB goal, can be met and that probably 90 EPNdB can be reached. Further reduction to 20 decibels down from FAR-36 (i.e., 85 dB) will require a further advance in technology.

New trijets using new Quiet Engines are expected to meet FAR-36 minus 10 (i.e., 90 EPNdB) using the demonstrated Quiet Engine technology. Modest improvement in technology are expected to lower the back end noise another 5 decibels and allow full use of the front end suppression demonstrated in the Quiet Engine project. This reduction gives a level of 85 EPNdB. Future advances in technology are expected to yield another 5 decibels to give noise levels of 80 EPNdB.

The STOL airplane has a noise goal of 95 EPNdB along a sideline 500 feet from the runway. To compare these numbers with other values in the figure, the goal has been converted to noise along a sideline at 1500 feet. The goal stated this way is 80 EPNdB. It is apparent that this value is below anything accomplished so far and that it is on the level with future expectations for the Quiet Engine.

This promising future for greatly reduced airplane noise results from a continuation of the present combined efforts of the airplane industry, the engine industry, and of the Government.

QUIET ENGINES WITH ADVANCED CORES

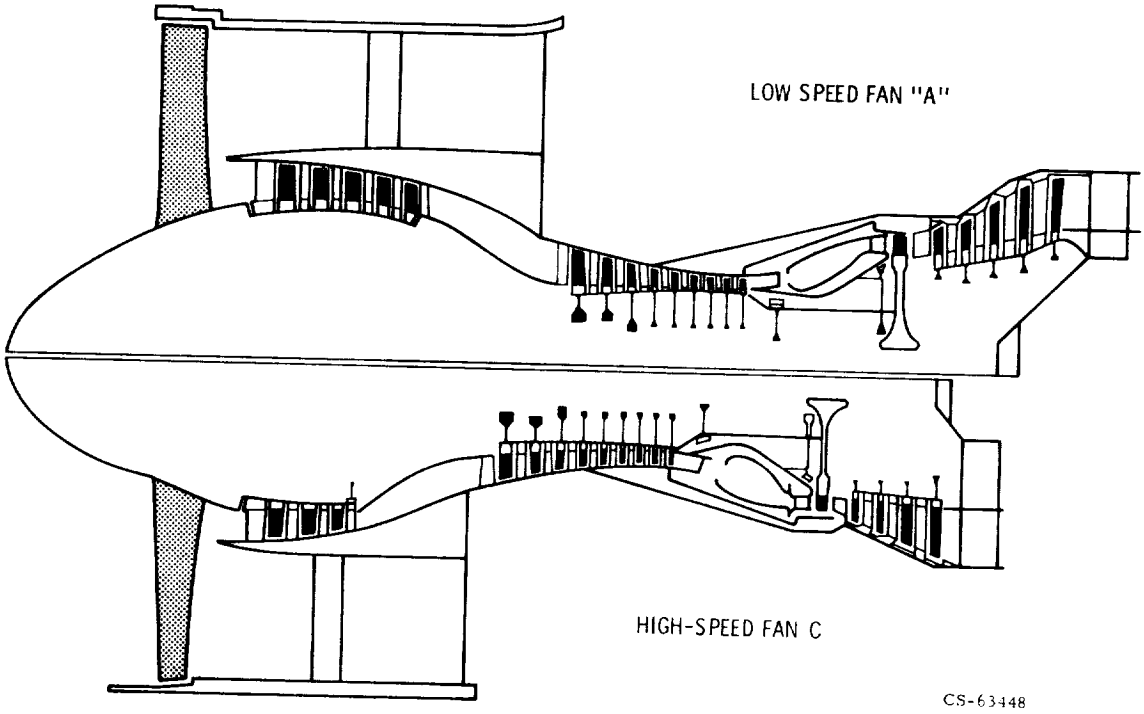

Figure X-1

ACOUSTIC TREATMENT FOR ENGINES A AND C

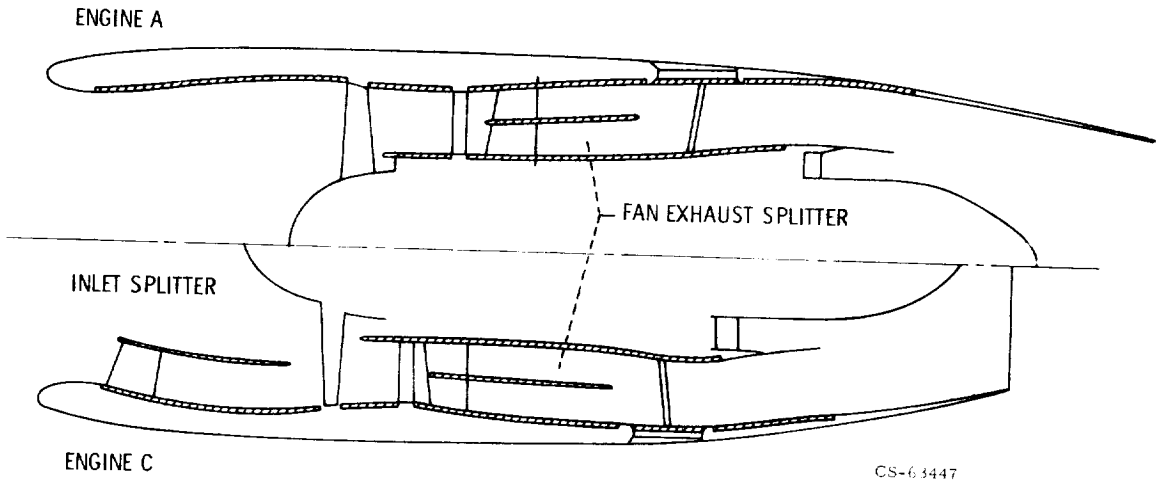

Figure X-2

707/JT3D NACELLE AND JET-SUPPRESSOR CONFIGURATION

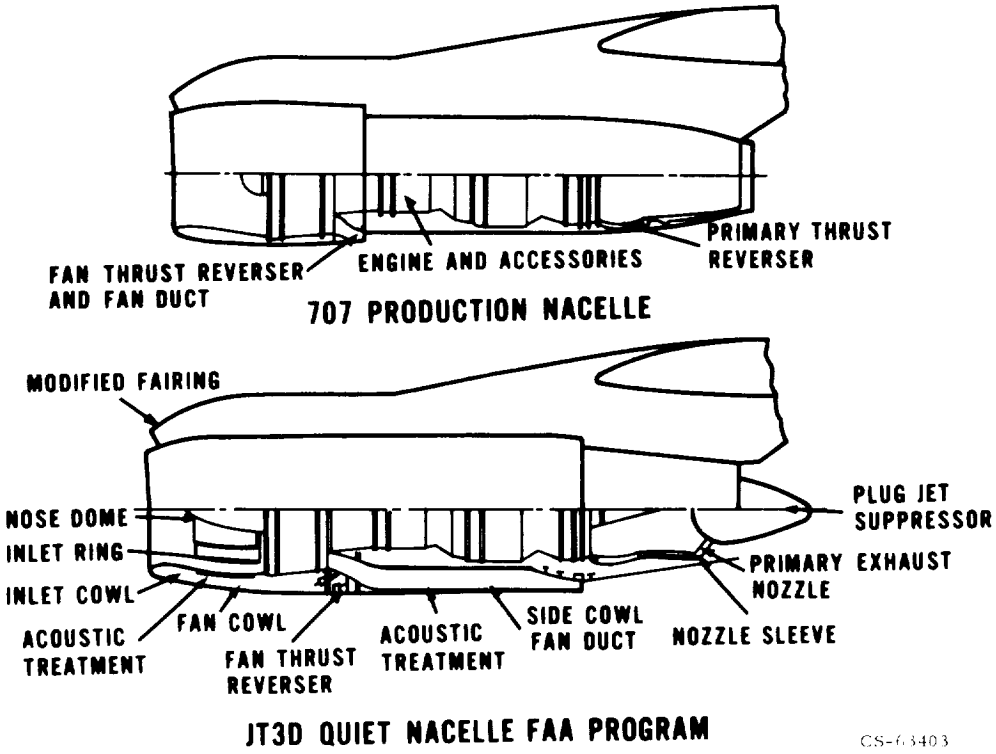

Figure X-3

PEAK PERCEIVED NOISE LEVEL–727–200 FLYOVER

370 FT ALTITUDE; THREE JT8D-7 ENGINES

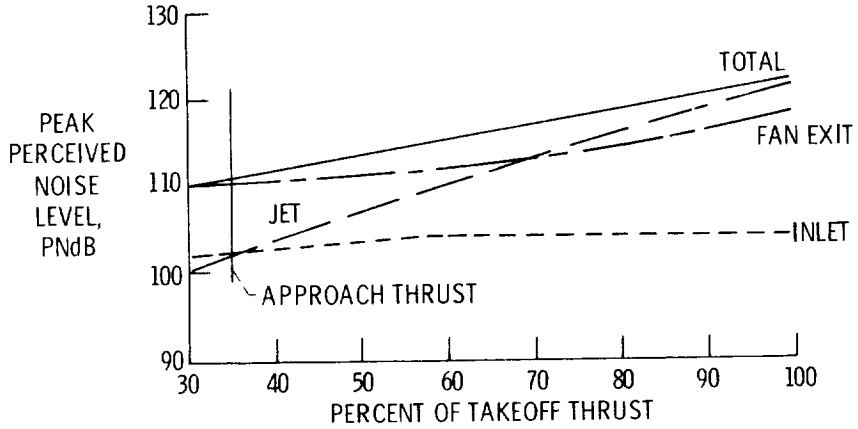

Figure X-4

CS-63647

727/JT8D NACELLE AND JET-SUPPRESSOR CONFIGURATION

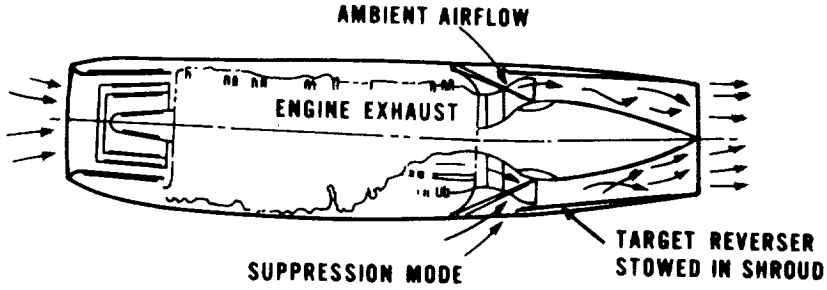

— INDICATES ACOUSTIC TREATMENT

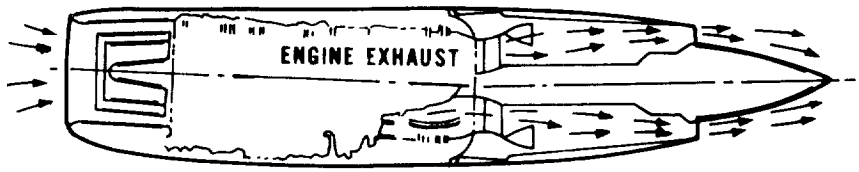

CRUISE MODE

CS-[illegible]402

Figure X-5

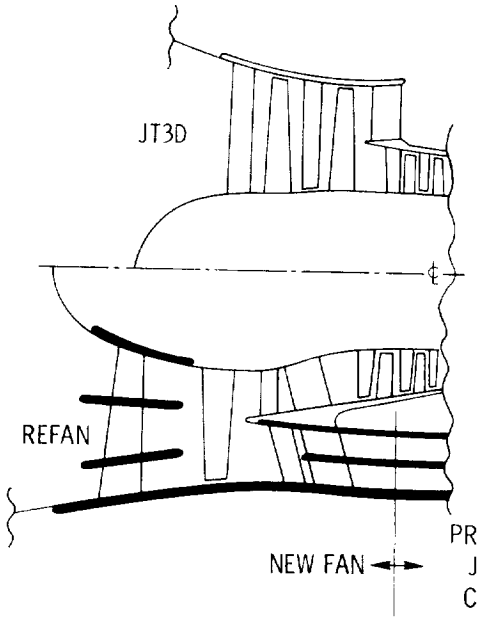

REFAN NOISE REDUCTION FEATURES

1. NO INLET GUIDE VANES
2. HIGH BYPASS RATIO
3. SINGLE-STAGE FAN
4. TWO INLET RINGS
5. SWEPT FAN EXIT GUIDE VANES
6. INCREASED BLADE VANE SPACING
7. OPTIMUM BLADE VANE NO.
8. BYPASS SPLITTER
9. ACOUSTIC WALL TREATMENT

CS-[illegible]3294

Figure X-6

NOISE REDUCTION GOAL FOR 707 REFAN RETROFIT

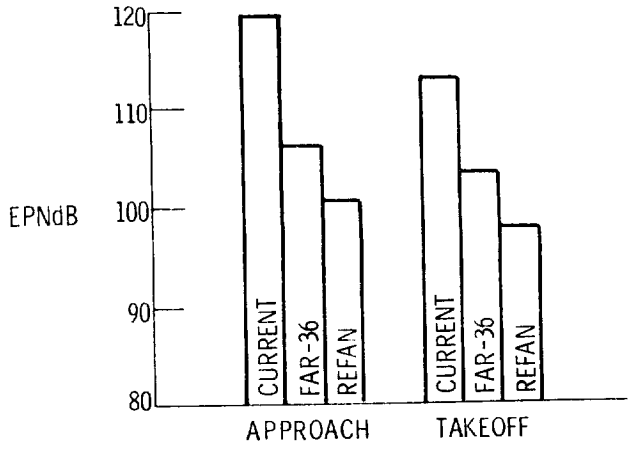

CS-63302

Figure X-7

90 EPNdB NOISE CONTOURS FOR 707

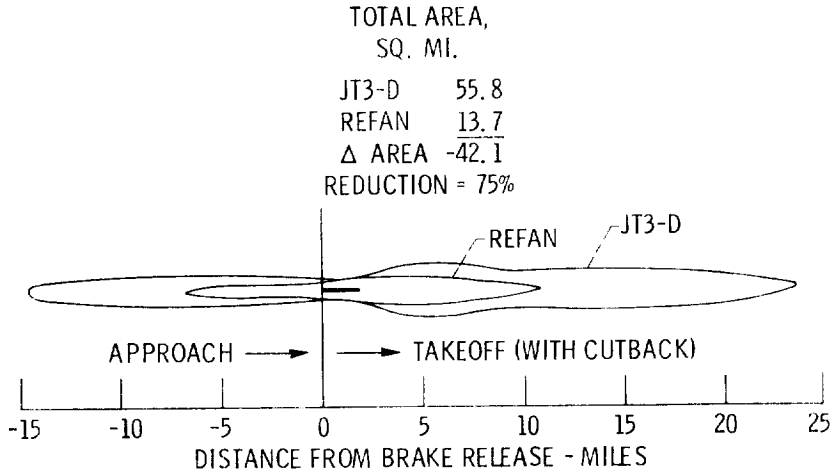

CS-63505

Figure X-8

90 EPNdB NOISE CONTOURS FOR 727

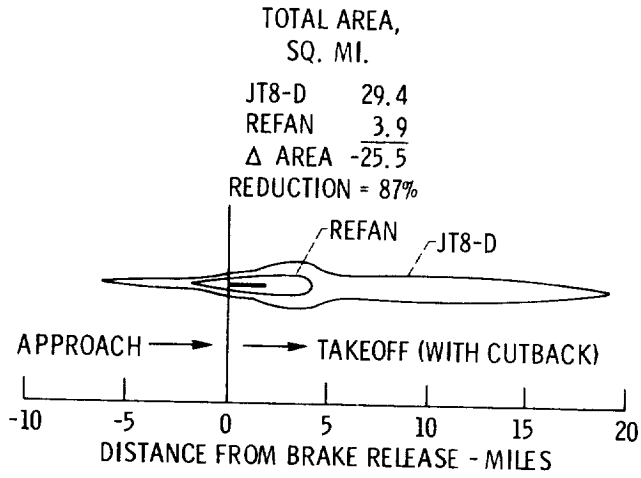

CS-63305

Figure X-9

ADVANCED TECHNOLOGY TRANSPORT

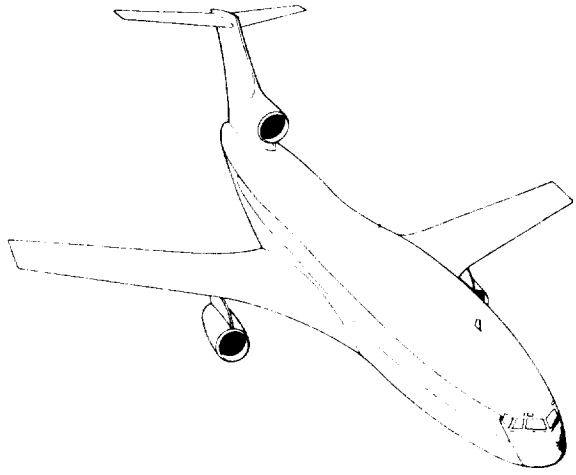

Figure X-10

CS-63294

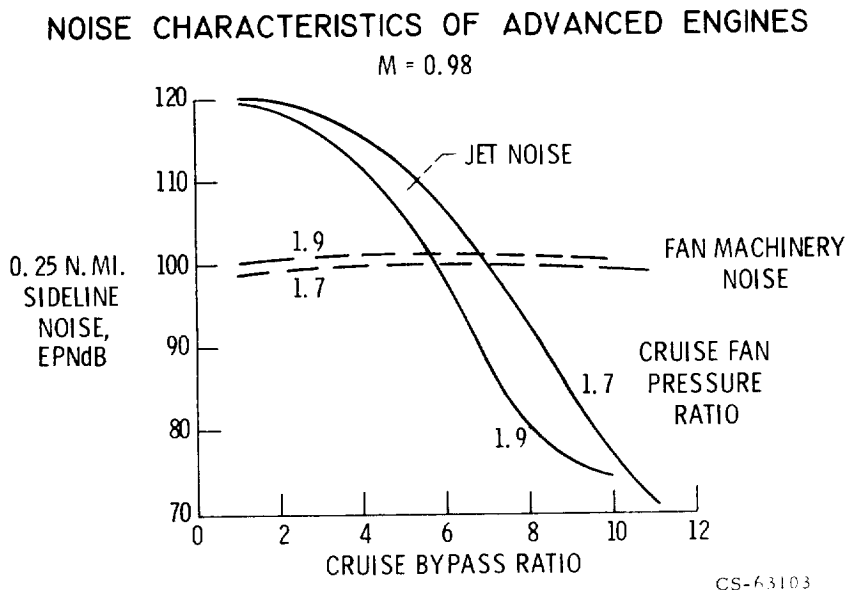

Figure X-11

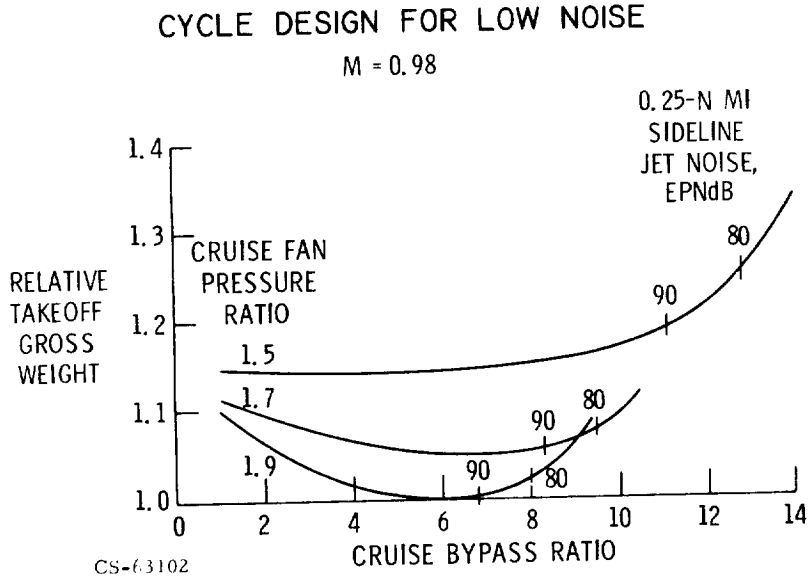

Figure X-12

BENEFIT OF ADVANCED ENGINE TECHNOLOGY

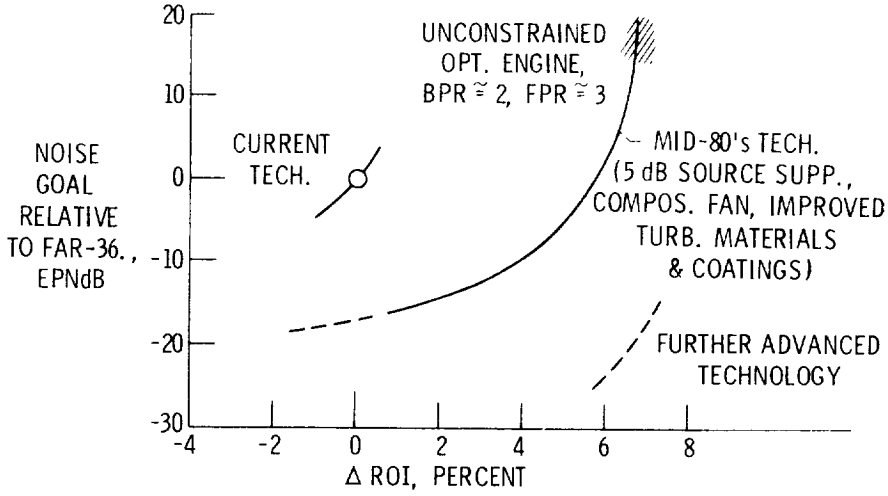

Figure X-13

CS-63104

ADVANCED SUPERSONIC TRANSPORT

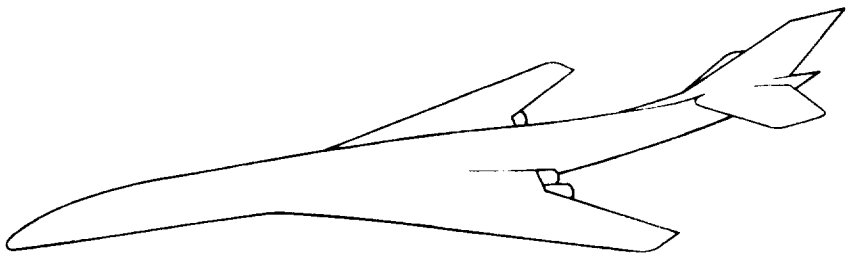

$2 < M_{CR} < 4$
230 TO 400 PASSENGERS
3500 TO 5500 N. MI.

Figure X-14

CS-63293

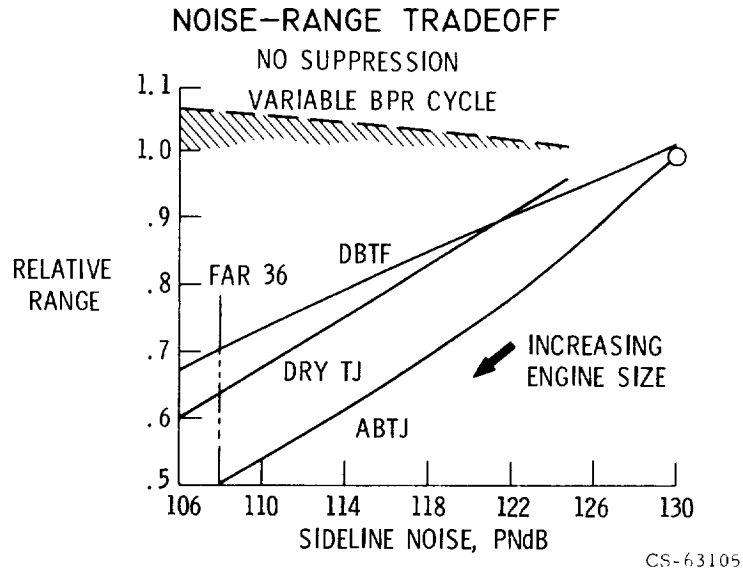

Figure X-15

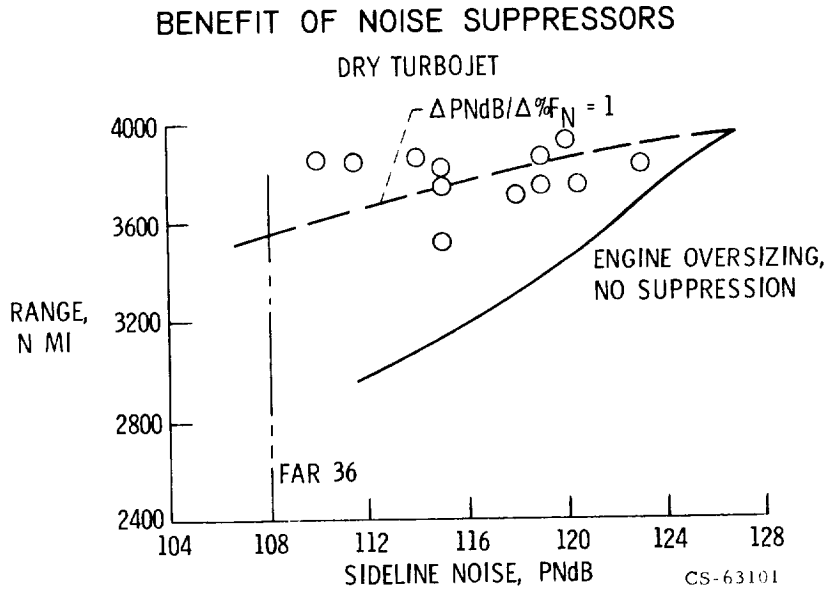

Figure X-16

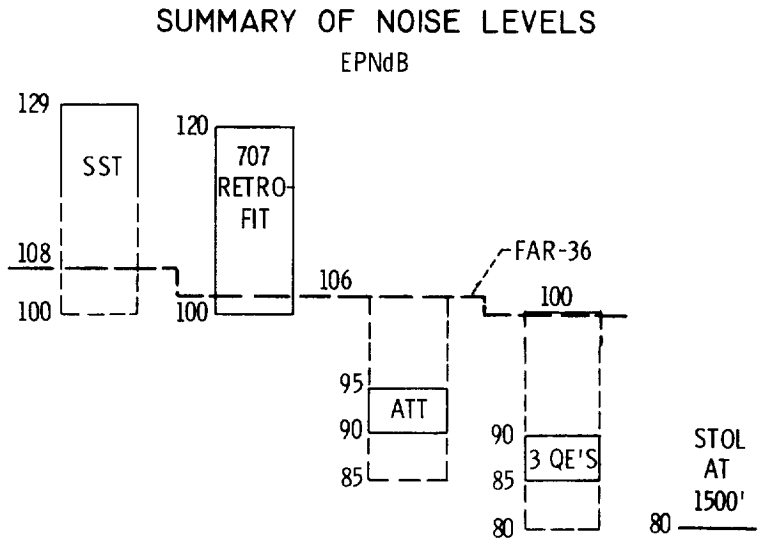

CS-63335

Figure X-17

XI. STOL NOISE SOURCES AND FAN NOISE TREATMENT

Raymond J. Rulis

So far the subject matter presented in this conference has been related to conventional takeoff and landing propulsion. Now we will turn to the effects of noise on short takeoff and landing systems. A viable STOL system will, by its nature, provide service out of heavily congested areas. As a consequence, the environmental specifications that will be imposed on these systems will be very severe. Extremely quiet and pollution-free operation will be demanded. Noise goals for these systems will require the initiation of major development efforts.

Current NASA activity in the STOL area has been initiated largely in response to the joint DOT-NASA card study, which was mentioned previously. The card study identified noise abatement and traffic congestion relief as the two highest priority needs in assessing national benefits related to aviation and aeronautic research and development. The propulsion programs that have been initiated at NASA in support of STOL are new when compared with the acitivity that is in support of CTOL systems. In fact, most of them have only been initiated in the last 1 to $1\frac{1}{2}$ years and are just beginning to yield results.

A very brief overview follows on STOL noise goals, noise sources, and their affect on engine design, and also a quick review of current NASA activities related to STOL systems.

No firm specifications exist at present for STOL systems that are comparable to Federal Air Regulation 36 (FAR-36). However, a much used figure-of-merit for STOL sideline noise is 95 perceived noise decibels (PNdB) at a 500-foot sideline (fig. XI-1). The figure presents a comparison of CTOL and STOL noise for a 150 000-pound-gross-weight aircraft. The allowable CTOL noise at a specification sideline of 2100 feet is 103 PNdB. Extrapolating this value to a 500-foot sideline results in an allowable noise value of approximately 124 PNdB, which is approximately 30 PNdB above the value of 95 PNdB for STOL.

Both the STOL noise goal and noise sources affect the propulsion sys-

tem design. As with CTOL systems, the noise sources are the same. They are engine machinery noise and jet exhaust noise. In addition, each STOL powered lift system generates an additional noise source peculiar to the lift system itself. For example, the externally blown flap lift system has flap impingement noise, the augmentor wing lift system has augmentor noise, and so on.

The blown-flap system (fig. XI-2) employs a turbofan engine whose total exhaust stream is directed against a large flap system that redirects the thrust vector. High lift coefficients are generated by the momentum change and by the induced supercirculation effect. The noise sources for this powered lift system are machinery noise, jet noise, and flap impingement noise.

Figure XI-2 also shows an upper surface blowing installation. In this case, the exhaust stream is directed along the top of the wing and is turned by the coanda effect along the flap surface. The noise sources of this powered lift system are machinery noise, jet noise, and wing and flap scrubbing noise.

The augmentor wing powered lift system (fig. XI-3) takes all or a good part of the total fan flow from a high-pressure-ratio fan and ducts the air through the wing onto the nozzle of the augmentor flap. Some of the air is also used for leading-edge blowing. Noise sources for this system are machinery noise, jet noise, and augmentor flap noise.

Jet noise and how it affects engine design is illustrated in figure XI-4. In order to meet the 95-PNdB STOL objective, an exhaust velocity, both fan and core, of approximately 850 feet per second is required. This corresponds to a high bypass fan design. Note the values of CTOL fan designs for comparison. In order to achieve the low STOL noise goal, the engine design is forced toward higher bypass fans than used in CTOL installations.

From the previous CTOL discussions it is apparent that the major machinery noise source is the fan (fig. XI-5). This is also the case for STOL. For STOL engine designs low-speed, single-stage fans are of interest for externally blown flap (EBF) powered lift systems, and the multistage fans are of interest for higher pressure ratio augmentor wing lift systems. The higher pressure ratios result in smaller internal ducting for the higher pressure ratio augmentor wing lift systems. To achieve a 95-PNdB sideline noise, substantial suppression is required for the EBF system and even greater amounts for the augmentor wing application. In addition to fan ma-

chinery noise, data indicate that the suppression of other machinery noises particularly in the turbine, will be required if the low STOL noise goals are to be achieved.

STOL powered lift systems also generate additional noise sources (fig. XI-6). For the EBF system, a jet with a velocity of 850 feet per second, which by itself results in less than 95 PNdB noise, reacting with a flap results in a noise level of approximately 105 PNdB for takeoff. If STOL system noise is to be controlled by basic engine design, a fan engine with very low pressure ratios is required.

The effect of noise goals on the physical design of a propulsion system is illustrated in figures XI-7 and XI-8. Shown are two schematics representative of EBF propulsion systems. Both have the same high-pressure-ratio core and are dimensionally scaled the same. The core jet has been designed to meet the STOL noise goal. The higher bypass engine has been configured with a sufficiently low-pressure-ratio fan to preclude the need for a velocity reducer. The other, a 1.35-pressure-ratio engine, does require a velocity reducer to lower EBF flap interaction noise. Note that the fans are designed for low noise; that is, rotor-to-stator spacing has been optimized. Both engines require substantial acoustic treatment as is shown in the inlet, fan exit, and core exit. For optimum cruise operation, variable-area nozzles are required. The high bypass engine also employs a booster stage. Without this stage, a low cruise thrust value results. With the high bypass fans, the engine thrust design point becomes the cruise point instead of the takeoff point.

The augmentor wing propulsive lift concept requires an engine design that supplies high-pressure fan air to the augmentor nozzle. The high-pressure air passing through the wing nozzle results in noise levels as shown in figure XI-9. Values of suppressed and unsuppressed flyover noise are shown. At high wing-slot pressure ratios, substantial noise reduction must take place to meet the STOL noise goals. Sideline noise, as shown, is not as severe as flyover noise.

A cutaway schematic of a two-stream engine suitable for augmentor wing powered lift systems is shown in figure XI-10. This engine does not look substantially different from conventional high-pressure-ratio fans except for the fan inlet and the discharge air duct work. The multistage fan has been configured for noise with proper rotor-stator spacings. The core exhaust jet is designed for low velocity, hence, low noise. Inasmuch as

substantial fan noise reduction is required, a variable-area acoustic inlet is shown. The inlet will provide near sonic flow conditions during takeoff and landing. Fan exit suppression is not required because the noise from fan-discharge air will be treated by the design of the augmentor wing proper.

A brief overview of two of the major NASA activities that have been initiated in support of STOL systems is now presented.

The first program is the QUESTOL Program. QUESTOL stands for quiet experimental STOL aircraft. In figure XI-11 is an artist's concept of an EBF-powered lift aircraft for the QUESTOL Program. Note that it is a high wing, multifan jet aircraft. The program objectives are as follows:

(1) Develop the technology base for turbofan STOL transport systems.

(2) Define the requirements and criteria for stability and control.

(3) Identify noise patterns.

(4) Develop data for operational criteria.

(5) Define guidance and navigational requirements.

(6) Investigate and validate promising powered lift concepts.

The QUESTOL Program will provide a test bed from which promising powered-lift concepts can be evaluated and, in addition, will provide the much needed system inputs required to enable the STOL system to become operational. The QUESTOL Program has one unique feature from a propulsion viewpoint, namely, the planned use of an existing powerplant for the first aircraft configuration. The task of quieting an existing propulsion system to the STOL noise goals will be great. A leading candidate for the EBF STOL is the TF-34 engine. It is a 6 to 1 bypass ratio engine with a thrust rating of approximately 9200 pounds.

An extensive test program is underway using a TF-34 engine as an acoustic test bed (see fig. XI-12). This engine requires large amounts of acoustic suppression for the fan and core. Tradeoffs of performance and noise will be evaluated. In addition, the velocity decayer shown will be evaluated with a large wing-flap system. The test program will permit a total system evaluation of noise to be made.

The second major program in support of STOL is the Quiet, Clean STOL Experimental Engine Program (QCSEE). While the QUESTOL Program provides the required aircraft technology background for STOL, the QCSEE

Program will provide the technology required to develop viable quiet, clean propulsion systems.

A substantial amount of component technology is being applied in the first phase of this engine. The QCSEE Program is summarized as follows:

(1) EBF development (fan pressure ratio, 1.15 to 1.35)
    (a) Small scale aerodynamics
    (b) Small scale acoustics
    (c) Large scale acoustics
    (d) Composite materials
(2) Augmentor wing fan development
    (a) Small scale aerodynamics
    (b) Larger scale aerodynamics and acoustics
(3) Propulsion system installation
    (a) Low-speed aerodynamics (fan pressure ratio, 1.15 to 1.5)
    (b) High-speed aerodynamics (fan pressure ratio, 1.15 to 1.5)
    (c) Sonic inlets
    (d) Thrust reversers
    (e) Externally blown fan wing interaction noise
    (f) Velocity decayers
    (g) Augmentor wing noise
(4) QCSEE studies
(5) Quiet turbofan STOL aircraft studies
(6) QCSEE development

You can readily see that we are concentrating heavily in the fan noise suppression area. The two powered-lift systems discussed require fans covering a very large range of pressure ratios. These fans must be efficient, quiet, and able to tolerate severe airflow distortions. In addition to the fan technology, a substantial effort is being put forth to resolve the STOL propulsion installation problems.

STOL and CTOL aircraft operate differently. STOL aircraft will approach and take off with much higher angles of attack. In addition, runway layout will probably require that the STOL propulsion system have greater tolerance to crosswinds. In the overall program installation effects for both cruise and low-speed flight conditions will be covered.

Two study programs are included in the QCSEE Program. One is in direct support of the engine program. In it we shall be examining a variety of

propulsion systems covering a wide range of fan pressure ratios (from 1.15 to 3.0). Results from parametric studies will be used to define and optimize the physical layouts of the more promising systems. The second study will cover the entire STOL system, with a sizeable effort going toward optimizing aircraft configurations. The two studies are being conducted in parallel and are closely integrated. Results from one are fed into the other, so that in the end we shall have a very good understanding of the propulsion needs for STOL.

It is expected that the study programs and the component technology effort should enable us to begin the hardware development phase of the QCSEE Program by mid 1973.

In summary, the pronounced effect that the 95-PNdB sideline noise goal has on the design of the entire STOL system can easily by recognized - both for the propulsion system and the aircraft. Most of the problem areas associated with STOL propulsion systems have been defined and the required research begun to provide answers to the problems.

There is a great need for the two major programs QUESTOL and QCSEE to move forward rapidly to provide the technology base needed in order to permit the initiation of a viable and environmentally acceptable STOL system.

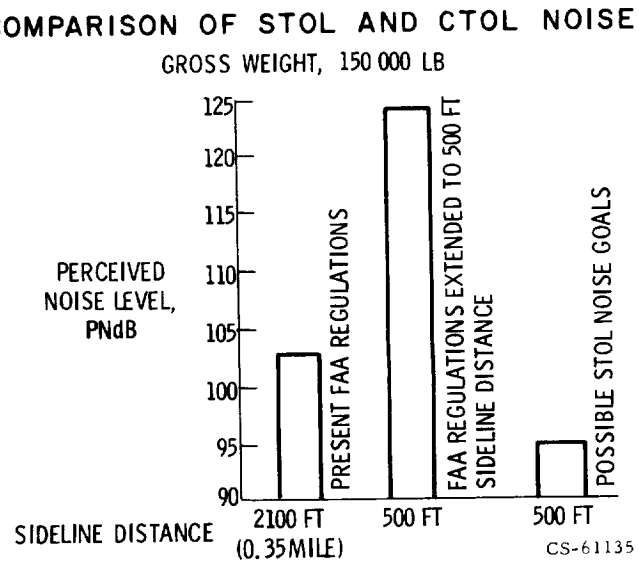

Figure XI-1

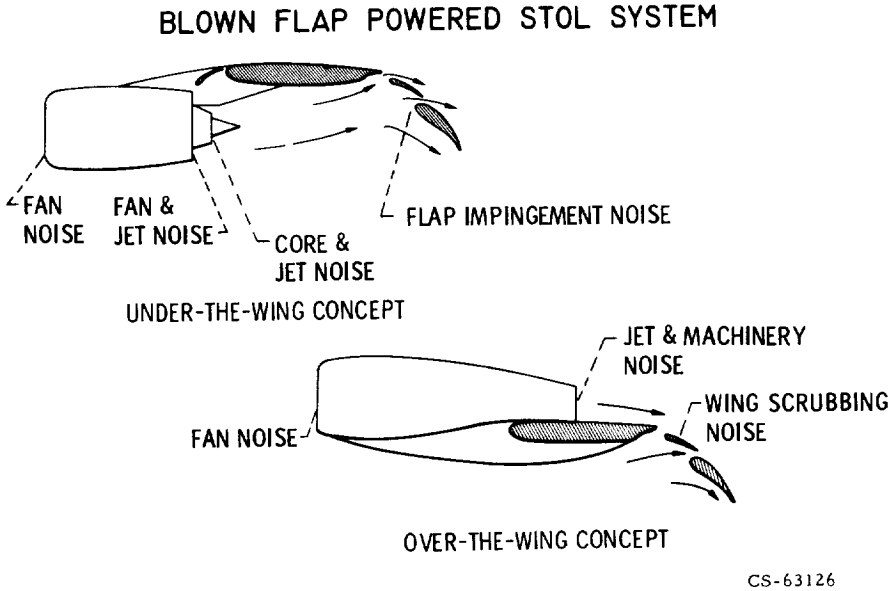

Figure XI-2

AUGMENTOR WING PROPULSION SYSTEM

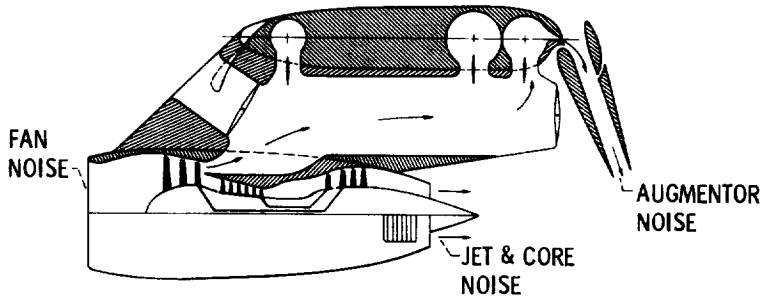

Figure XI-3

CS-63128

JET NOISE GOAL EFFECT ON PROPULSION DESIGN

500-FT FLYOVER

TOTAL THRUST, 97 000 LB; FOUR ENGINES

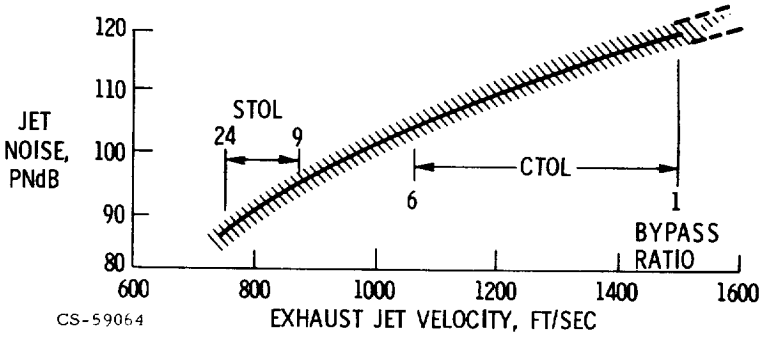

CS-59064

Figure XI-4

UNSUPPRESSED FAN NOISE

FOUR ENGINES - 90 000-LB TAKE-OFF THRUST; 500 FT SIDELINE

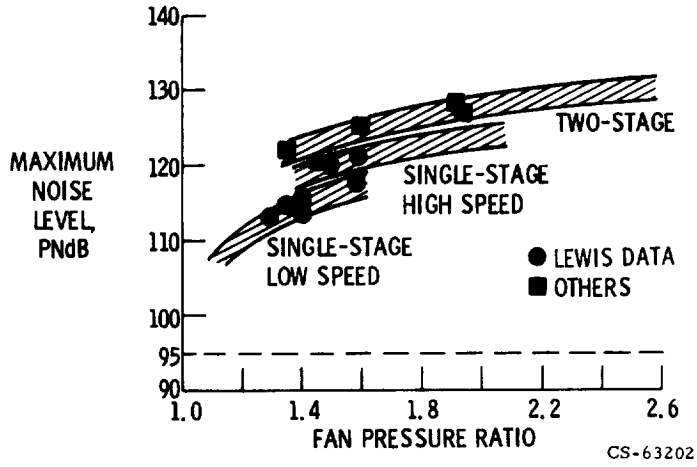

Figure XI-5

ESTIMATE OF MAXIMUM 500-FT SIDELINE FLAP NOISE DURING TAKEOFF

170 000-LB GROSS WEIGHT AIRPLANE; 94 000-LB THRUST (FOUR ENGINES); 15° CLIMB ANGLE

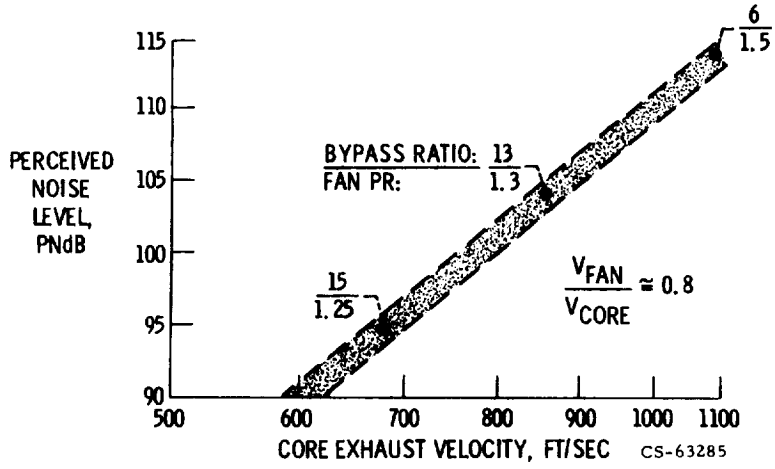

Figure XI-6

EXTERNALLY BLOWN FLAP PROPULSION SYSTEM

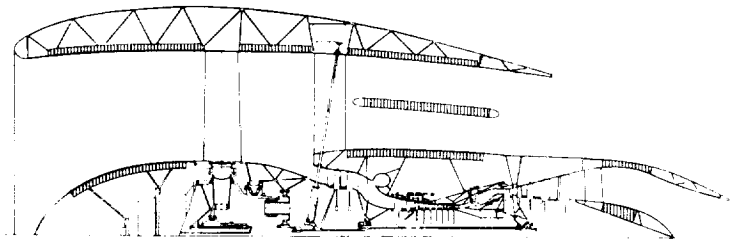

	UNBOOSTED	BOOSTED
FAN PRESSURE RATIO	1.15	1.15
BYPASS RATIO	24.3	23.5
TAKEOFF THRUST, LB		
WITHOUT BLEED		
WITH BLEED	25 600	33 900
CRUISE THRUST (UNINSTALLED)	23 500	33 000
(25 000 FT, M = .75)	3860	5000
CORE JET VELOCITY, FT/SEC	840	
FAN JET VELOCITY, FT/SEC	500	

Figure XI-7

EXTERNALLY BLOWN FLAP PROPULSION SYSTEM

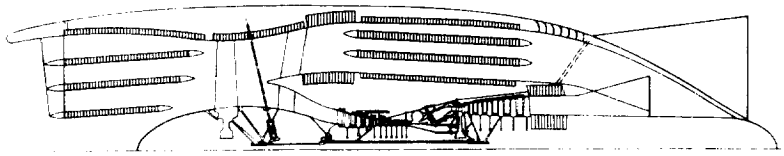

FAN PRESSURE RATIO	1.35
TAKEOFF THRUST (LB)	21 000
BYPASS RATIO	11.2
CRUISE THRUST (25 000 FT, M = .75)	4420
CORE JET VELOCITY, FT/SEC	740
FAN JET VELOCITY, FT/SEC	710

CS-63297

Figure XI-8

EFFECT OF PRESSURE RATIO ON AUGMENTOR WING NOISE

GROSS WEIGHT, 170 000 LB; FOUR-ENGINES

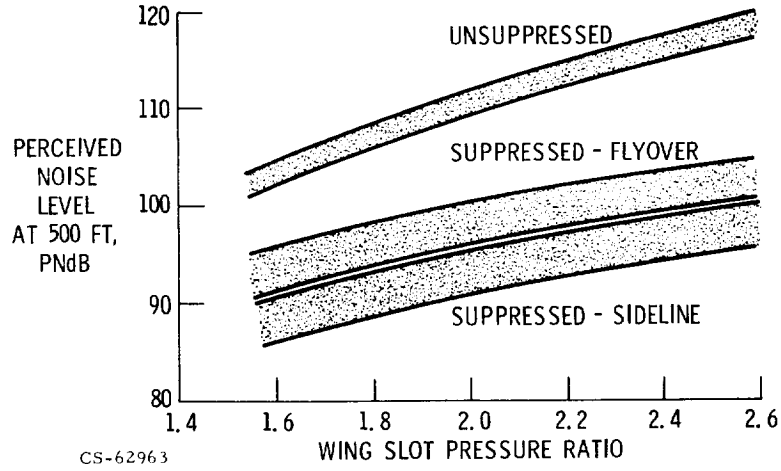

Figure XI-9

AUGMENTOR WING PROPULSION SYSTEM

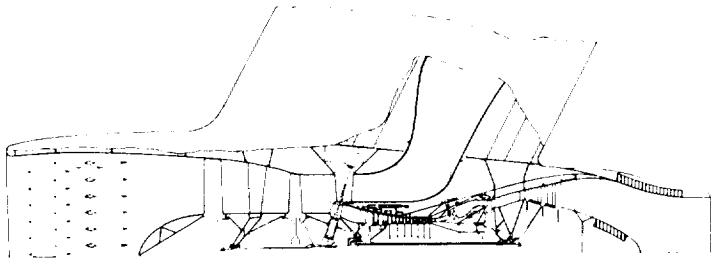

FAN PRESSURE RATIO	2.4
TAKEOFF THRUST (LB)[a]	17,900
THRUST SPLIT WING/EXHAUST	83/17
CRUISE THRUST (25 000 FT, M = .75)	5150
CORE JET VELOCITY, FT/SEC	820

[a]INCLUDES 15% DUCT LOSS TO WING.

CS-63295

Figure XI-10

ARTIST'S CONCEPT OF EXTERNALLY BLOWN FLAP POWERED AIRCRAFT

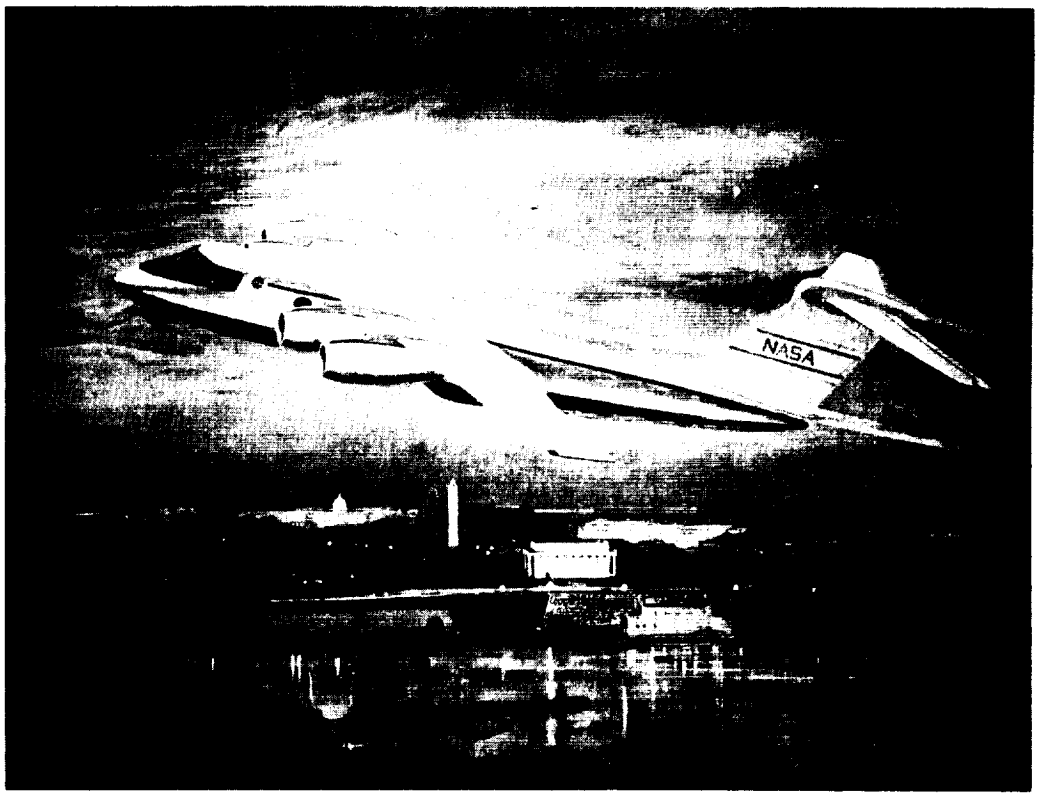

Figure XI-11

TF-34 ACOUSTIC TEST ENGINE

CS-63203

Figure XI-12

XII. FLAP NOISE

Robert G. Dorsch, Paul L. Lasagna,* Domenic J. Maglieri,**
and William A. Olsen

This paper reports the progress of NASA in-house research on the noise created by externally-blown-flap STOL airplanes, specifically, the noise associated with the powered lift obtained by flap blowing. The major part of the report concerns flap noise associated with lower-surface blowing. This portion is followed by a brief discussion of the flap noise related to upper-surface blowing.

LOWER-SURFACE BLOWING

An externally-blown-flap STOL airplane with the engines located below the wing employs lower-surface flap blowing (fig. XII-1). Lift augmentation is obtained by lowering the flaps directly into the fan-jet exhaust. The flap interaction noise data presented herein are for a double-slotted flap system similar to the type shown in figure XII-1.

In the Lewis tests (fig. XII-2) the exhaust of a 10 000-pound-force-thrust fan-jet engine with a bypass ratio of 6 was simulated by a 1/2-scale model of its bypass nozzle assembly supplied with pressurized ambient-temperature air. The nozzle assembly was pylon-mounted on a wing section having a 7-foot chord length and large double-slotted flaps for lift augmentation. The span of the wing section was 9 feet. The core nozzle was 8 inches in diameter, and the outer diameter of the annular nozzle was approximately 23 inches.

Similar noise tests (fig. XII-3) were conducted at the NASA Flight Research Center (FRC) with a test facility which used a modified F-111B wing-and-flap system blown by the exhaust from a CF-700 turbofan engine. The

*NASA Flight Research Center

**NASA Langley Research Center

engine had a 12-foot-long acoustically treated inlet to suppress fan noise. A 9-foot-long acoustically treated tailpipe was installed aft of the engine to remove machinery noise from the engine exhaust. The mixed fan and core stream exhausted from the tailpipe through a 22-inch-diameter convergent nozzle and was directed at the flap system. The wing was mounted on an X-Y table that could be actuated in either the longitudinal or transverse directions in order to vary the relative positions of the exhaust nozzle and flap system.

The noise tests at both Centers were conducted over a range of nozzle exhaust velocities and flap deflection angles.

Typical noise radiation patterns obtained from the Lewis 1/2-scale model are shown in figure XII-4. The exhaust velocity for the core was 765 feet per second and that for the fan was 582 feet per second. Overall sound pressure level is given for three flap position settings and for the nozzle alone. The innermost set of data points represents the sound level for the nozzle alone. The triangular symbols give the sound level when the nozzle is installed below the wing with the flaps in the retracted position. This arrangement is considerably louder at most angles than the nozzle alone. The increased noise is caused by reflection of the nozzle noise and impingement of the jet on the retracted flap system. When the flaps are lowered to the 10°-20° position, the sound level (square symbols) increases further as a result of greater impingement. And finally, the outermost set of data points (circular symbols) is the sound level with the flaps in the 30°-60° position. It is clear that there is a large increase in noise below the wing as the flaps are lowered into the jet exhaust. For example, directly below the wing at 90° from the engine inlet there is a 10-decibel increase in noise level when the flaps are lowered from the retracted to the 30°-60° position.

Similar trends can be seen in the sound pressure level 1/3-octave spectra (fig. XII-5). Here the sound pressure level against frequency at 85° from the inlet is shown for the same exhaust velocities. The flap noise spectra are broadband and similar to jet noise spectra. The strong increase in noise as the flaps are lowered is again readily apparent. At the 30°-60° setting the flap interaction noise completely dominates the nozzle noise.

The results with the FRC blown flap test facility were generally very similar to the Lewis results. The higher mixed exhaust temperature of the

CF-700 engine did not have a significant effect on the flap noise radiation pattern.

Noise Scaling Laws

Noise scaling laws are needed to scale the flap noise data up to the full-size blown-flap systems of STOL airplanes. Special blown-flap noise tests were conducted to establish the scaling laws.

For these tests the bypass nozzle assembly used on the 1/2-scale Lewis model was replaced by a 13-inch-diameter round convergent nozzle (fig. XII-6). In addition, a geometrically scaled small version of the 1/2-scale model was constructed. The small model (fig. XII-7) had a 2-inch-diameter nozzle and a wing chord length of 13 inches. The geometric scale factor was 6.5. This means that all 1/2-scale model dimensions are divided by 6.5. The 1/2-scale and the 1/13-scale models were tested at the same nozzle pressure ratios and inlet temperatures. Thus, two sets of flap noise data were obtained that could be compared at the same exhaust velocities. The data were taken at microphone radii of 50 feet for the large model and 10 feet for the small model.

The noise radiation patterns for the two models with 30°-60° flap settings are compared in figure XII-8 for three nozzle pressure ratios. At each nozzle pressure ratio the 1/2-scale data points are shown by the solid squares. The 1/13-scale data are shown as open circles. The small-model overall sound pressure level data were scaled up to the large-model data as follows: The noise level was assumed to be proportional to the square of the 6.5 scale factor. The difference in microphone distance was accounted for by using the inverse square law. This resulted in a 2.3-decibel correction, which was added to the 1/13-scale data. The comparison shows that nearly identical radiation patterns were obtained with the geometrically similar models.

The 1/3-octave spectra for the two models are compared at 85° from the inlet at a nozzle pressure ratio of 1.7 in figure XII-9. In order to make this comparison it is necessary to scale the frequency of the flap noise as well as the level. The 1/13-scale model spectra were scaled up to the 1/2-scale model data as follows: The frequencies were divided by the 6.5 scale

factor. And, the 2.3-decibel power level and microphone distance correction was added to the sound pressure levels at each scaled frequency. The spectra shown are corrected for ground effects. Again, the agreement between the data from the two different-sized models is excellent.

The effect of nozzle exhaust velocity on flap noise below the wing is shown at 80° from the inlet in figure XII-10. Data are shown for the 1/2-scale model as solid symbols and for the 1/13-scale model as open symbols. The data are shown for the three flap positions and for the nozzle alone. The nozzle-alone data for both diameter nozzles show the well-established eighth-power velocity dependence. In contrast, the overall sound pressure levels for the flap noise vary with the sixth power of the velocity for both models.

The results shown in figures XII-8 to XII-10 indicate that noise measurements from geometrically similar acoustic test models can be used to predict the flap noise for full-size externally-blown-flap systems.

Preliminary noise estimates for a full-scale externally-blown-flap system that differs significantly from the preceding acoustic test model become more difficult. To assist in this type of scaling, research is being conducted on the effects of geometric variations and differences in engine exhaust velocity profiles.

As an example, consider the problem of comparing the 1/2-scale Lewis flap noise data with the FRC data. Because of the different kinds of nozzle air supplies, the nozzle exhaust velocity profiles and decay rates were not the same. However, the data can be scaled by using the impingement velocity profiles measured with aerodynamic rakes at the flap stations. As an example (fig. XII-11), consider two profiles having nearly the same peak velocity (775 ft/sec) at the 60° trailing flap station for the test conditions shown. The FRC flap impingement velocity profile is approximately 1.6 times the width of the Lewis profile. The FRC 60° trailing flap chord length is 1.5 times the length of the Lewis flap. This is nearly the same ratio. Thus, an approximate scale factor of 1.5 can be used to scale the Lewis data to the FRC data.

The flap noise spectra for the two tests are compared at 40° from the engine inlet in figure XII-12. With a 60° flap deflection, the flap interaction noise peaks near this microphone location. The Lewis data have been scaled up to the FRC data by using the 1.5 scale factor and by accounting for the

differences in microphone distance by the inverse square law. At frequencies above 500 hertz the agreement is very good. These are the frequencies which are important in determining the perceived noise level of an externally-blown-flap airplane. The data below 500 hertz were affected by ground reflections, causing the dips and peaks. When ground-effect corrections were applied, the low-frequency data were in much better agreement. Both sets of data would give very similar noise estimates for full-scale airplane flap noise.

Now consider a geometric variation in which the nozzle diameter is changed but the wing-flap size is kept the same. Results from small-scale tests, where the peak impingement velocity is fixed at 700 feet per second, are shown in figure XII-13. The variation in overall sound pressure level is given for nozzle diameters between 1 and 3 inches. The noise level is noted to vary directly as the first power of nozzle diameter rather than as diameter squared, which would be the case for geometric similarity.

Next consider the effect of changing engine nozzle location on the noise radiation patterns (fig. XII-14), all other parameters being held constant. Overall sound pressure levels are plotted as a function of angle from the inlet for three positions of the nozzle. The angles of most interest are those positions directly under the aircraft, that is, 70° to 100°. The solid circular symbols are for the normal position of the nozzle. Moving the nozzle towards the flaps, as represented by the square symbols, increases the noise below the wing because of the higher impingement velocities. Similarly, moving the nozzle up to the position represented by the triangular symbols increases the noise even more because of the impingement on the wing leading edge and increased scrubbing area.

Noise Sources

The externally-blown-flap noise sources are now discussed in more detail (fig. XII-15). It is apparent that the externally blown flap with the engine under the wing can generate more noise than the engine alone. The engine alone generates internal noise and jet mixing noise. The internal noise comes from the engine machinery, such as the fan. Impingement of the engine exhaust jet upon the surfaces of the wing and flaps generates additional

noise: scrubbing noise, leading-edge noise, and trailing-edge noise.

It is difficult to separately investigate all these noise sources. These sources, therefore, are discussed in terms of the results of a simple experiment (fig. XII-16). The jet from a 2-inch nozzle was directed at three vastly different surface shapes, in turn. These surfaces were a large flat board, a wing with flaps, and finally a slotless wing that followed the inner boundary of the wing with flaps. At a given nozzle exhaust velocity the peak impingement velocity would be the same for each surface. The impingement area and impingement angle were also nearly the same so far as noise generation was concerned. The only major difference was the surface shape.

The results of the experiment are summarized in table XII-1. The

TABLE XII-1. - EFFECT OF SURFACE SHAPE ON NOISE

Surface	Source of noise				Power law
	Jet mixing	Scrubbing	Trailing edge	Leading edge	
Nozzle alone	X				V_j^8
Large flat board	X	X			V_i^8
Slotless wing	X	X	X		V_i^6 to V_i^8
Wing with flaps	X	X	X	X	V_i^6

nozzle alone has only jet mixing noise because there is no internal noise in this experiment. The flat board has the nozzle jet mixing noise and, in addition, there is scrubbing noise, which is associated with air flowing along a large surface. The flat board is so large that air leaving the edges of the board is of very low velocity. Therefore the board will have no trailing-edge noise. Further, with no leading edges it, of course, has no leading-edge noise. The slotless wing also has jet mixing noise and scrubbing noise. In addition, trailing-edge noise now becomes important, because the exhaust velocity off this small surface is high. Again there are no leading edges

exposed to the flow. The wing with flaps has small surfaces and flap leading edges, therefore it has all the noise sources.

The noise below the "wing," for the three surfaces, is shown in figure XII-17. This figure illustrates the relative noise level from each noise source. The noise level is plotted as a function of nozzle exhaust velocity; however, it could also have been plotted as a function of the peak impingement velocity for the surfaces. As indicated previously, the noise below the aircraft follows the sixth power of velocity for the small surfaces that make up the wing with flaps. However, the board, with its large surface, follows a much higher power law. These power laws are followed by these two surfaces at all angles measured from the inlet. The slotless wing follows power laws somewhere in between these two limits, depending on the angle. Below the aircraft the slotless wing is quieter than the wing with flaps at low velocity, because it has no leading edges. For all three surfaces the noise from the nozzle jet is small compared to the noise generated by jet impingement.

The noise spectra for the three surfaces are compared at two velocities in figure XII-18. The normalized power spectral density in this figure is plotted as a function of a Strouhal number. The spectra are normalized to take out the variations in the overall noise level which are caused by variations of surface shape and velocity. Only spectral variations can show up on this type of plot. The spectral shapes for all three surfaces are very similar, in spite of the different noise characteristics of the surfaces.

Noise Levels for STOL Aircraft

Estimates based on the 1/2-scale model data have been made of the flap noise during takeoff of a four-engine 170 000-pound externally-blown-flap airplane having 94 000 pounds total thrust (fig. XII-19). The maximum 500-foot-sideline perceived noise level during a 15^{o} climb is given as a function of core exhaust velocity. The fan exhaust velocity was assumed to be approximately 0.8 of the core velocity. An airplane having engines with a bypass ratio of 6 and a fan pressure ratio of 1.5 would have a perceived noise level of 114 PNdB at the 500-foot sideline. This is an unacceptably high noise level for commercial STOL airplanes. Fortunately, the estimates

show that there is a very large decrease in noise as the engine exhaust velocities are decreased. An airplane having engines with a very high bypass ratio of 15 would have a maximum sideline noise of only 95 PNdB. For core velocities above 700 feet per second, some form of flap noise suppression will be required in order to get the flap noise down to acceptable levels.

Noise Suppression

A possible means of noise suppression is to reduce the flap impingement velocity. For the conventional fan jet nozzle, the potential core flow extends back almost to the flap assembly (fig. XII-20). In this case the impingement velocity is nearly equal to the nozzle exhaust velocity.

To reduce the impingement velocity a multitube mixer nozzle can be used. The mixer nozzle (fig. XII-21) takes advantage of the fact that the potential core length is proportional to the diameter of the tube. The short potential core causes good mixing up to the point where the individual jets coalesce into a single larger jet.

Calculations show that in order to obtain the needed flap noise reduction the nozzle should be designed so that the impingement velocity is approximately equal to one-half the nozzle exhaust velocity.

Instead of round tubes, a multilobed, or daisy, nozzle can be used to get the same type of effect.

Flap noise suppression tests (fig. XII-22) were run with the Lewis 1/2-scale model by replacing the bypass nozzle assembly with a seven-lobed mixer nozzle placed at the core exhaust position. Similar tests were run on the FRC externally-blown-flap test facility by replacing the conical nozzle with a daisy mixer nozzle (fig. XII-23).

Results of the Lewis tests are shown in figure XII-24 for a flap angle of 30°-60°, which is a landing flap setting. The nozzle exhaust velocity is 773 feet per second. The mixer nozzle overall sound pressure level data are shown by the inner curve. For comparison, data taken using a round convergent nozzle having the same throat area are shown by the outer curve. At all angles the mixer nozzle was quieter than the convergent nozzle. For example, there is a 6-decibel suppression at 70° from the inlet. The 70° angle gives the maximum flyover noise during landing. This is just about

the amount of noise suppression that would be predicted from the reduction in impingement velocity when the change in exhaust width is accounted for.

Tests at the 10^{o}-20^{o} flap angle used during takeoff showed that the mixer nozzle did not reduce the overall sound pressure level. Actually, the perceived noise level was slightly higher. This is because the higher frequency characteristic of the mixer nozzle itself plays a much more important role since the flap interaction noise is smaller at low flap angles. The increase in perceived noise level caused by the increase in high-frequency noise was found to cancel out all benefits of velocity reduction.

The daisy mixer nozzle tests at the Flight Research Center gave very similar results for both landing and takeoff flap angle settings.

Means of reducing mixer nozzle high-frequency noise are presently being studied. One method might be to use a thin layer of low-velocity secondary airflow surrounding each lobe. Another means might be to use an acoustically lined ejector shroud around the nozzle.

In addition to the use of mixer nozzles, other methods of flap noise suppression, which try to reduce the flap noise at the source, are being examined and tests are being run. They include compliant and porous flap surface treatment and the use of air injection next to the surface near the flap trailing edge.

Another approach to obtaining acceptable flap noise levels is to develop engines with very high bypass ratios and low exhaust velocities (see fig. XII-19). As an example, consider the 170 000-pound airplane equipped with engines having a bypass ratio of 15.5. The fan design pressure ratio is 1.25; the area ratio is 7.25. The takeoff thrust at 100 knots is 23 500 pounds force. The exhaust velocities for takeoff and approach are as follows:

Exhaust velocity, ft/sec	Takeoff	Approach
Core	687	496
Fan	529	434

The fan duct inlet is treated to give 9.2-PNdB suppression at the 500-foot sideline. The exhaust duct is treated to give 22.5-PNdB suppression. The fan exhaust duct requires more acoustic treatment because the blade passage frequency tones are louder in the rearward direction and because the 120° maximum lobe occurs at nearly the same angle as the flap noise maximum during takeoff.

The perceived noise level contours for a four-engine STOL airplane equipped with these high-bypass-ratio engines are shown in figure XII-25. The contours were estimated from flap noise data and from estimates of the suppressed fan noise spectra. The inner boundary of each contour is determined solely by the flap noise. The outer boundary was obtained by adding the suppressed fan noise spectra to the flap noise spectra at each point on the ground. The height above the runway is given by the upper curves for approach and takeoff. The noise "footprint" shows that this would be a very quiet STOL airplane, considering that powered lift is being employed by external lower-surface flap blowing. The 95-PNdB contour for example extends out to approximately the 500-foot-sideline distance and closes within 4000 feet on takeoff.

UPPER-SURFACE BLOWING

Another means of obtaining lift augmentation from an externally-blown-flap system is to place the engine above the wing and make provision for the exhaust flow to attach to the upper surface of the wing and flaps. Such an arrangement might look like the artist's conception shown in figure XII-26. For this aircraft all the primary and bypass flows from the engine are mixed and exhausted from a slot or D-nozzle over the wing. The flow attaches to the wing and is turned downward over the flap. From a noise standpoint this engine-wing arrangement could be very favorable because the wing flap system can shield the community from some of the noise. The data that are presented for upper-surface blowing configurations are preliminary small-scale data taken at the Lewis Research Center. Additional noise tests are being run at the Langley Research Center. The aerodynamic performance of these configurations is presently being evaluated.

There are several ways by which lift augmentation can be achieved by means of exhaust flow attachment. Three possible methods are shown in figure XII-27. In the first arrangement, shown at the top of the figure, the engine is mounted above the wing and the exhaust jet is turned downward to the wing by a deflector. Another way is to cant the engine or its exhaust nozzle so that the flow is directed downward to the wing. The flow is not turned downward during cruise for either of these methods. The last method shown uses a slot or D-nozzle on top of the wing rather than a circular jet. The jet flow attaches to the wing upper surface immediately upon exhausting from the nozzle.

The noise characteristics below an aircraft employing the upper-surface blowing arrangements described in the preceding paragraph depend on which noise-producing mechanisms dominate. For purpose of discussion let us examine the various noise sources associated with the deflector configuration (fig. XII-28). The usual engine-alone noises - the internal noise from the engine turbomachinery and the jet mixing noise - are still there. The presence of the deflector in the jet exhaust flow also generates noise. Scrubbing noise also arises because the deflected exhaust flow strikes the upper surfaces of the wing-flap system. Finally, there is the noise associated with the exhaust flow over the trailing edge of the flap. In this sketch it is assumed that the gaps between the wing and slots are closed. If these were opened, leading-edge noise and the leakage of noise through the slots would have to be considered.

The small-scale deflector configuration model that was tested is shown in figure XII-29. This model has a 2-inch-diameter circular nozzle and deflector on top of a 13-inch-chord slotless wing. The wing has a 60° trailing flap.

The noise radiation pattern in the flyover plane for this model is plotted in figure XII-30 (open symbols) for an exhaust velocity of 585 feet per second. These conditions are typical of landing. For comparison, the equivalent engine-under-the-wing configuration is also given (solid symbols). Significantly lower overall noise levels occur below the engine-above-the-wing configuration.

It is also important to examine the noise spectra below the model aircraft using a deflector at these same test conditions (fig. XII-31) in order to obtain an idea of the magnitude of the noise sources. The three curves

shown in this figure represent the spectra for the nozzle alone, the nozzle with the deflector, and the nozzle with deflector above a slotless wing. When the deflector is added to the nozzle, the noise level increases over the nozzle-alone case at all frequencies and particularly at the higher frequencies. When the wing is added, a significant change in the spectrum occurs. The high frequencies are effectively shielded by the wing surface; however, considerable low-frequency trailing-edge noise is generated as the flow exhausts at the trailing edge. The perceived noise level is primarily influenced by the high-frequency part of the spectrum when these model data are scaled up to a full-sized aircraft. The low-frequency noise must also be considered because of its effect on aircraft and community structures.

Upper-surface-blowing noise data for the canted nozzle configuration is shown in figure XII-32. The nozzle is canted downward, with the nozzle exhaust directed toward the slotless wing in such a way that the flow attaches. The noise spectrum below this model wing section is plotted as solid square symbols for conditions typical of takeoff. For takeoff the exhaust velocity from the circular nozzle is 750 feet per second, and the trailing flap has been set at 20°. The spectrum for the deflector arrangement at the same conditions is also plotted on this figure as open circular symbols. The spectra for each of these attached-flow cases is about the same. As a further comparison the nozzle was blown over the slotless wing with no attachment. This spectrum is shown by the diamond symbols. The two attached-flow cases have additional low-frequency trailing-edge noise. For the conditions noted in this figure the spectra for all the wing cases come together at high frequency, regardless of the degree of attachment. Of interest also is that the noise below the model wing is less than the noise from the nozzle alone at high frequency, because of shielding.

Noise measurements (fig. XII-33) have also been obtained on the upper-surface flow arrangement consisting of a slot nozzle placed immediately adjacent to the wing upper surface. Noise spectra below the model aircraft are shown here for slot nozzles having slot-width-to-height ratios of 5:1 and 10:1. The exhaust areas of the rectangular nozzles are equivalent to a circular nozzle of 2-inch diameter. The nozzles exhausted over slotless wings having 60° trailing flaps and flap-length-to-slot-height ratios of 17, 28, and 58.

All the spectra have significant low-frequency trailing-edge noise. Increases in the flap-length-to-slot-height ratio generally result in lower noise levels at high frequency because of improved shielding. The quietest arrangement was the 10:1 slot with a 58:1 flap-length-to-slot-height ratio. This arrangement would actually be more typical of the conventional jet flap, where air is supplied from a fan stage through internal wing ducts. The other two configurations shown might possibly be employed with external upper-surface blowing. As a matter of interest, the noise spectrum below the model of the 5:1 slot nozzle is nearly the same as the previously shown circular nozzle with deflector.

Noise radiation patterns, for the same test conditions, are shown in figure XII-34 for the above-the-wing arrangement using the 5:1 and 10:1 slot nozzles. Also shown for comparison is the noise radiation pattern for the equivalent engine under the wing. It should be noted that the upper-surface slot-flap arrangements produce significantly less noise than the engine-under-the-wing configuration.

There is some miscellaneous information that can be mentioned about the upper-surface blowing configurations. All the upper-surface blowing data shown were for slotless wing-flap combinations. Open slots will raise the noise level below the aircraft a few decibels. If the circular nozzle of the previous examples is replaced by a mixer nozzle in either the canted-nozzle or deflector configurations, such an arrangement is somewhat quieter. The noise level below the aircraft also proved to be sensitive to the nozzle location and orientation for all the upper-surface blowing arrangements.

In addition to the shielding of aerodynamic noise, the upper-surface blowing arrangements should also provide shielding of internal engine noise; such as the noise from the compressor, fan, and turbine. In other words, with the engine above the wing, the wing and flaps can shield the community below from some of the internal noise that passes through the nozzle. The results presented in figure XII-35 show the amount of internal noise reduction, or shielding, in the sideline and flyover planes. The data are for the model wing section using a 2-inch nozzle with deflector above a slotless wing with a 60° trailing flap. For this data, internal machinery noise was simulated by placing an orifice upstream of the exhaust nozzle. Noise reductions of 4 to 10 decibels were observed directly below the wing. This result is probably conservative. It suggests that less exhaust duct treatment would

be required to reduce the internal engine noise below STOL aircraft with the engines located over the wing.

From strictly a noise standpoint, the small-model tests indicate that the engine-over-the-wing externally-blown-flap configuration may have important advantages over the engine-below-the-wing configuration. However, the embodiment of this upper-surface blowing concept into a practical airplane requires consideration of other factors, such as the low- and high-speed aerodynamic performance of engine-over-the-wing airplanes. Also the internal performance of slot and other noncircular exhaust nozzles must be considered. Although the work completed to date does not indicate serious problems in these areas, considerable investigation and refinement will be required to define a complete upper-surface blowing configuration.

SUMMARY

This progress report on externally-blown-flap noise research can be summarized by the following remarks: With lower-surface blowing, the sources of the flap noise are beginning to be understood and the noise scaling laws have been established. Further, progress has been made on suppressing the flap interaction noise at the large flap deflections used during landing. More work is needed to solve the flap noise problem at the low flap deflections used during takeoff. Recent small-scale noise tests of configurations using external upper-surface blowing indicate that engine-over-the-wing configurations may be promising; however, large-scale noise tests are needed to determine the noise scaling laws and to better assess the potential of this externally-blown-flap configuration.

EXTERNALLY-BLOWN-FLAP STOL AIRPLANE

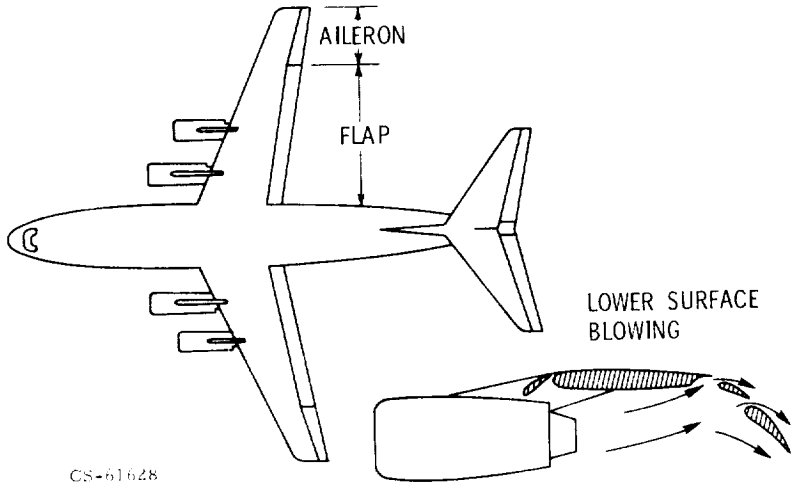

Figure XII-1

ONE-HALF SCALE EXTERNALLY BLOWN FLAP MODEL

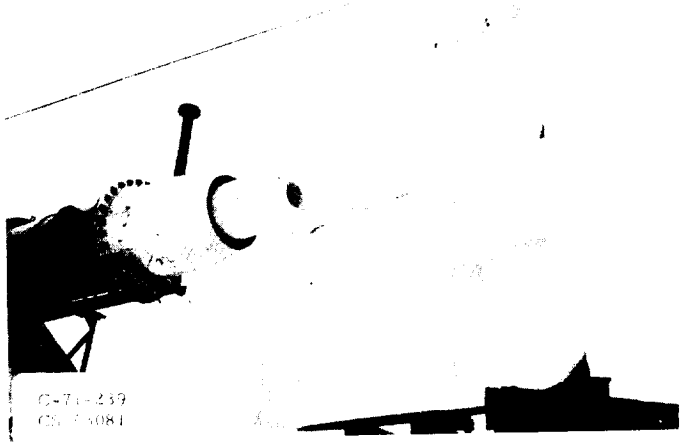

Figure XII-2

EXTERNALLY BLOWN FLAP TEST FACILITY

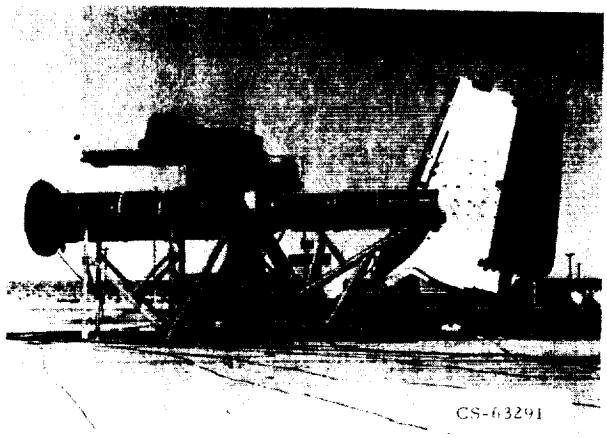

Figure XII-3

RADIATION PATTERNS AT 50 FT

EXHAUST VELOCITY: CORE, 765 FT/SEC; FAN, 582 FT/SEC

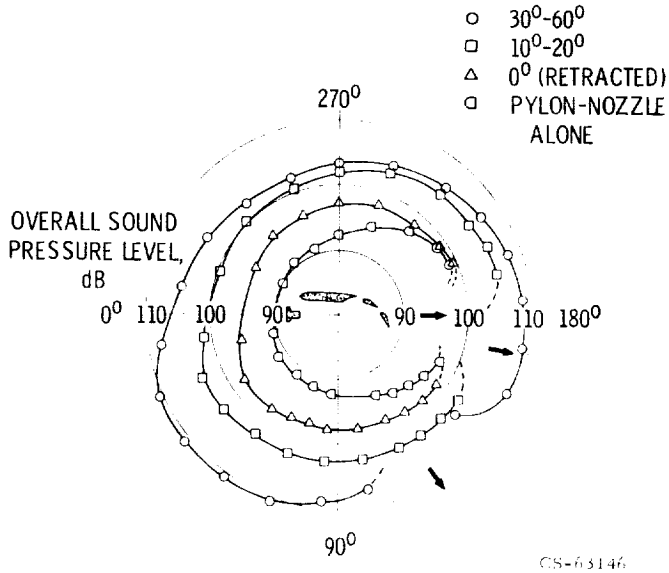

Figure XII-4

1/3-OCTAVE SPECTRA AT 50 FT

EXHAUST VELOCITY: CORE, 765 FT/SEC; FAN, 582 FT/SEC

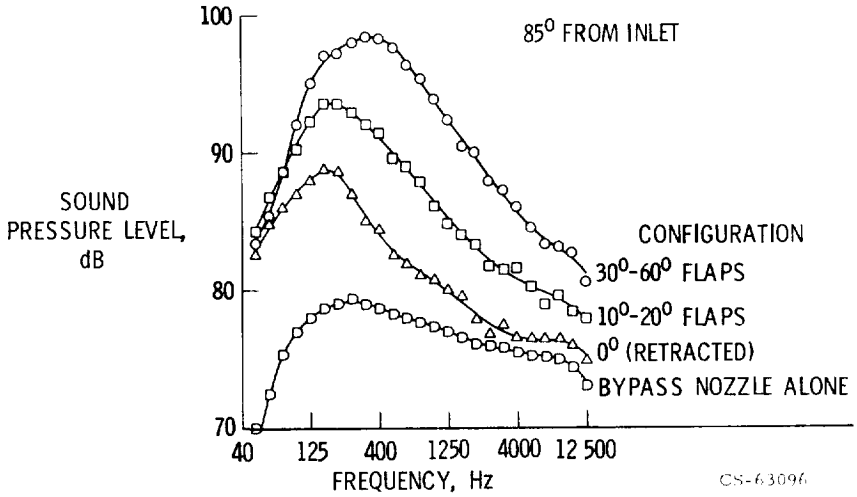

Figure XII-5

1/2-SCALE EXTERNALLY BLOWN FLAP MODEL

13-IN. DIAMETER NOZZLE

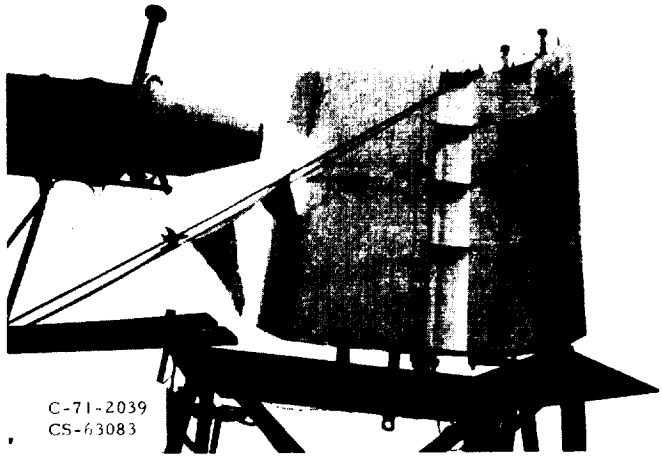

Figure XII-6

1/13-SCALE EXTERNALLY BLOWN FLAP MODEL

2-IN. DIAMETER NOZZLE

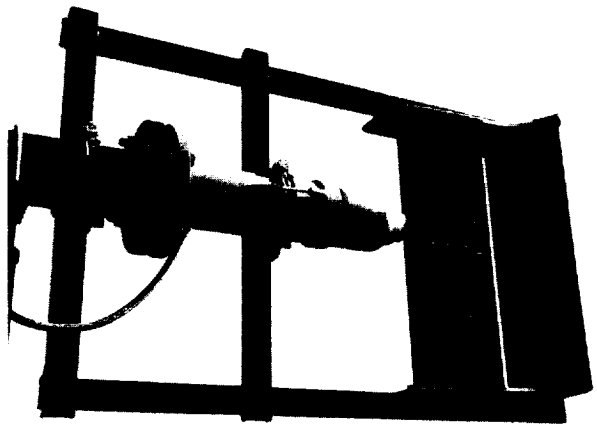

Figure XII-7

C-71-657
CS-63080

COMPARISON OF LARGE- AND SMALL-MODEL DATA AT 50 FT

FLAP ANGLE, 30^0-60^0

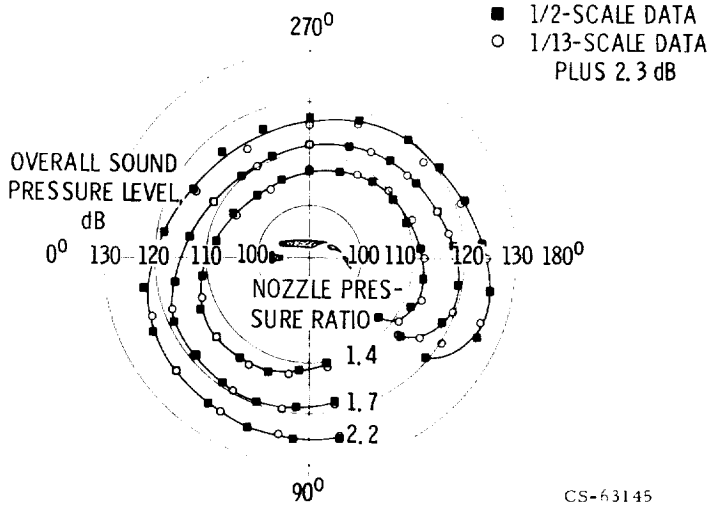

CS-63145

Figure XII-8

COMPARISON OF LARGE- AND SMALL-MODEL SPECTRA AT 50 FT

FLAP ANGLE, 30^0-60^0; NOZZLE PRESSURE RATIO 1.7; 85^0 FROM INLET

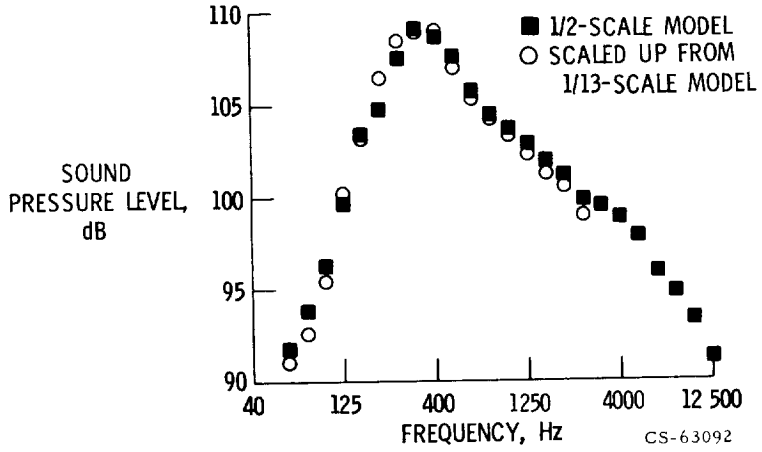

Figure XII-9

EFFECT OF VELOCITY ON FLAP NOISE LEVEL AT 50 FT

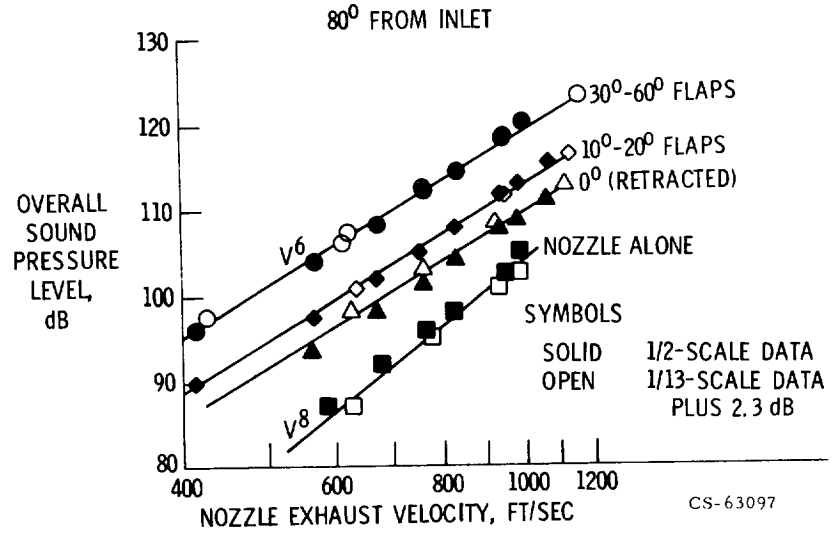

Figure XII-10

COMPARISON OF IMPINGEMENT VELOCITY PROFILES

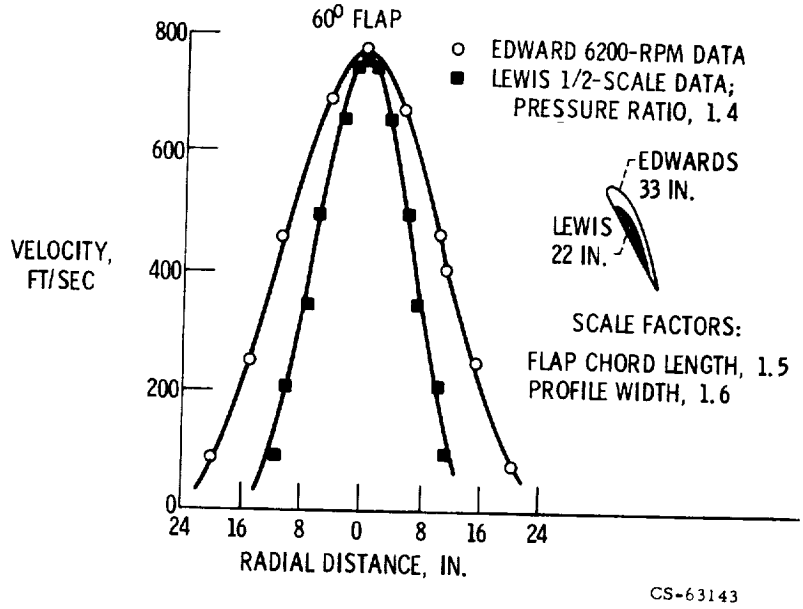

Figure XII-11

COMPARISON OF LARGE-SCALE MODEL EXTERNALLY-BLOWN-FLAP SPECTRA AT 100 FT

40° FROM INLET; 60° TRAILING FLAP; IMPINGEMENT VELOCITY, 775 FT/SEC

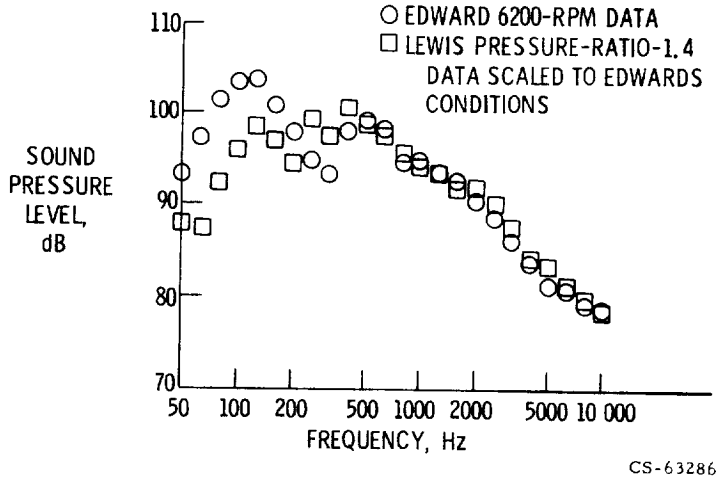

Figure XII-12

EFFECT OF NOZZLE DIAMETER ON NOISE AT 10 FT

IMPINGEMENT VELOCITY, 700 FT/SEC; 30^0-60^0 FLAP; 80^0 FROM INLET

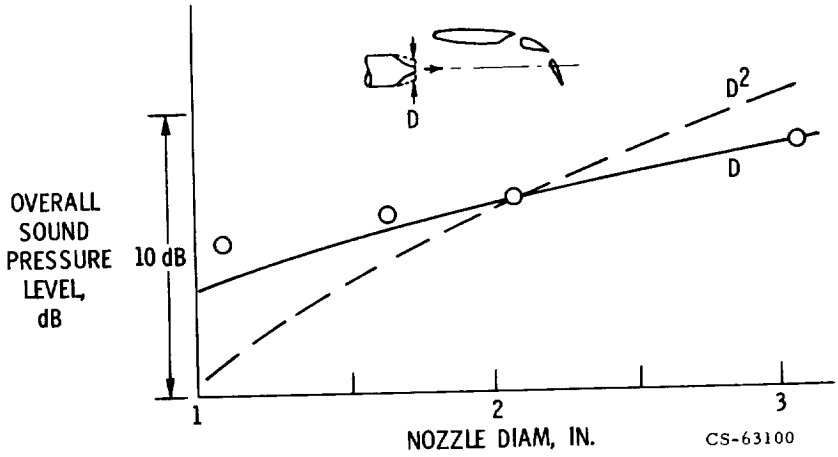

Figure XII-13

EFFECT OF MOVING NOZZLE WITH RESPECT TO WING

EXHAUST VELOCITY, 965 FT/SEC; NOZZLE DIAM, 2.06 IN.; 30^0-60^0 FLAP

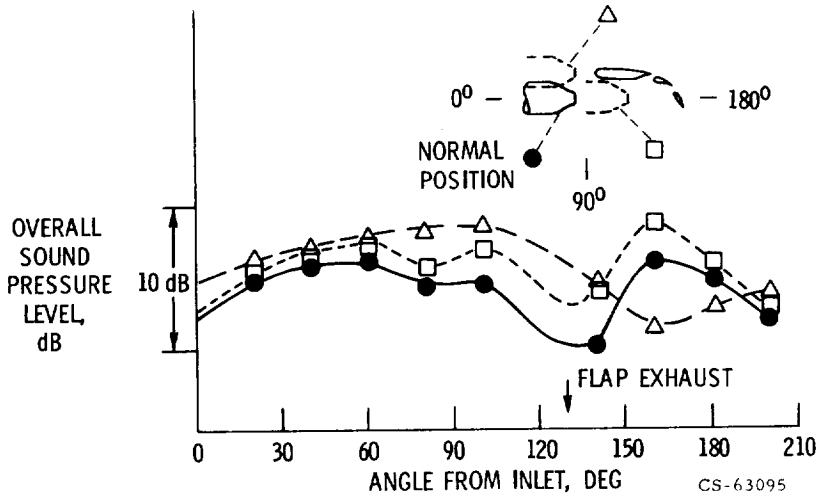

Figure XII-14

EXTERNALLY-BLOWN-FLAP NOISE SOURCES

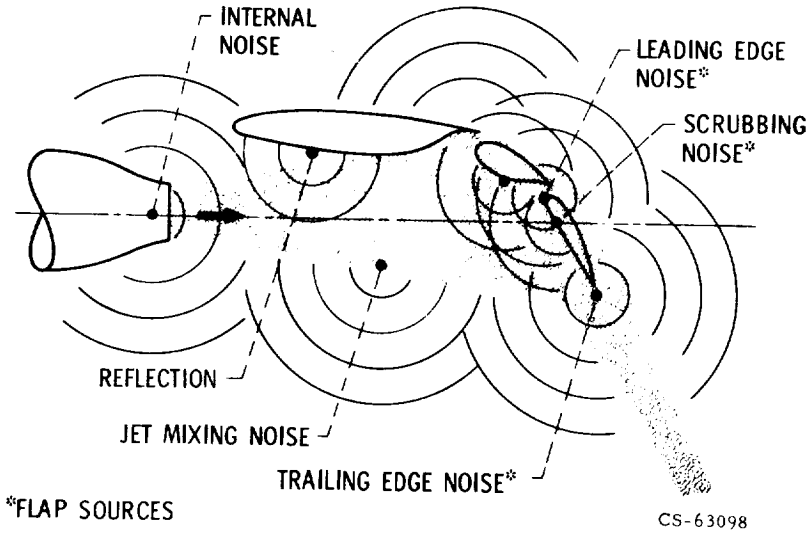

Figure XII-15

SURFACE–SHAPE NOISE TESTS

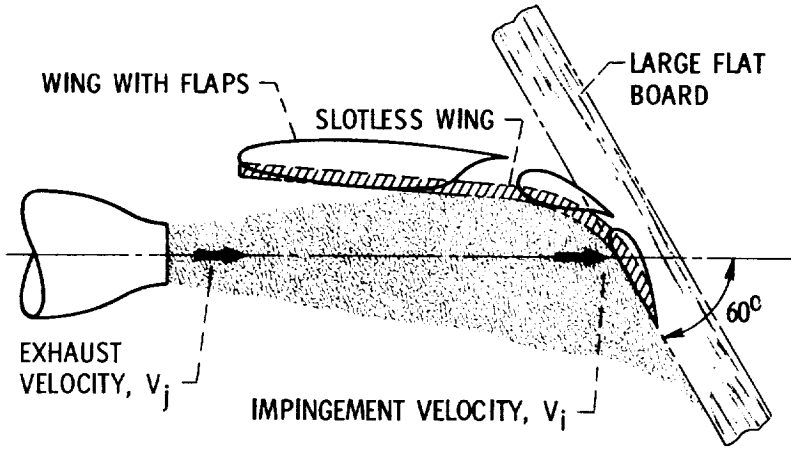

Figure XII-16

EFFECT OF SURFACE SHAPE ON NOISE AT 10 FT

NOZZLE DIAMETER, 2.06 IN.; IMPINGEMENT ANGLE, 60^0; 80^0 FROM INLET

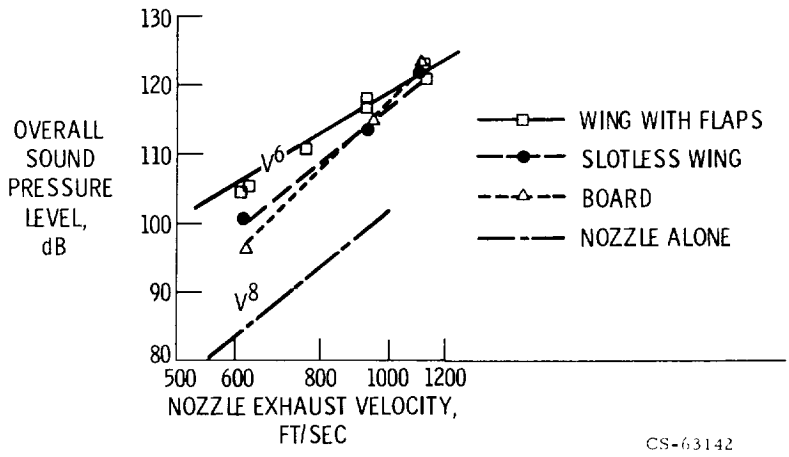

Figure XII-17

EFFECT OF SURFACE SHAPE ON NOISE SPECTRA

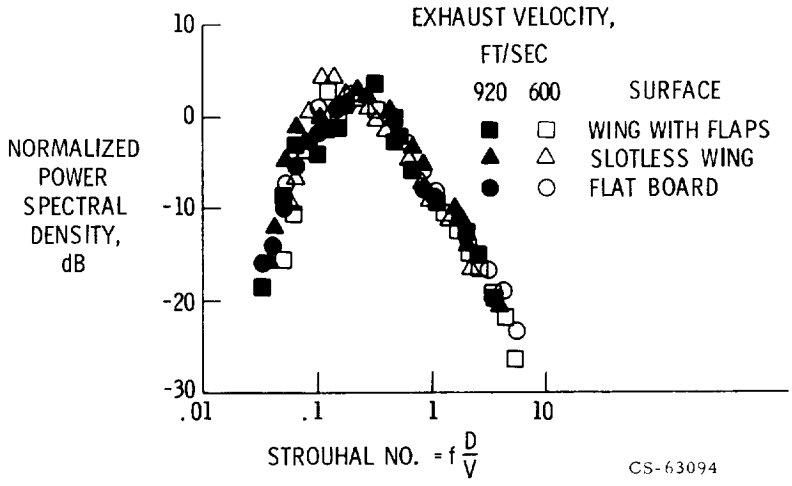

Figure XII-18

ESTIMATE OF MAXIMUM 500-FT-SIDELINE FLAP NOISE DURING TAKEOFF

170,000 LB GROSS WEIGHT AIRPLANE; 94,000 LB THRUST (4 ENGINES); 15^0 CLIMB ANGLE

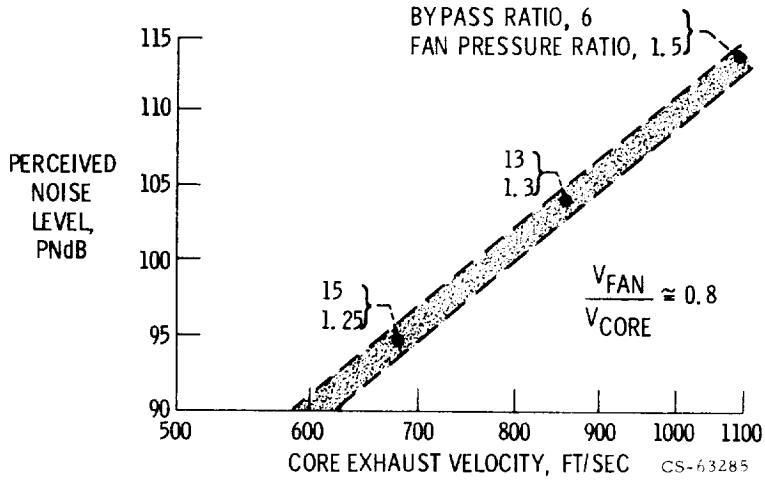

Figure XII-19

EXHAUST VELOCITY DECAY

CONVENTIONAL FAN-JET NOZZLE

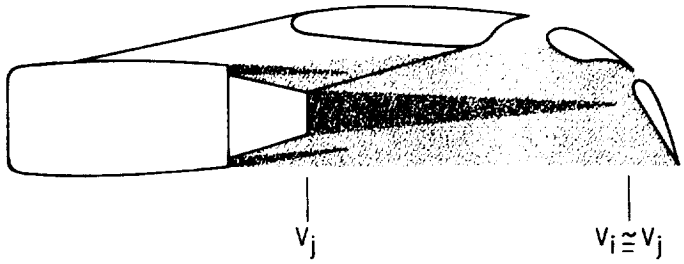

Figure XII-20

CS-63088

EXHAUST VELOCITY DECAY

MULTITUBE MIXER NOZZLE

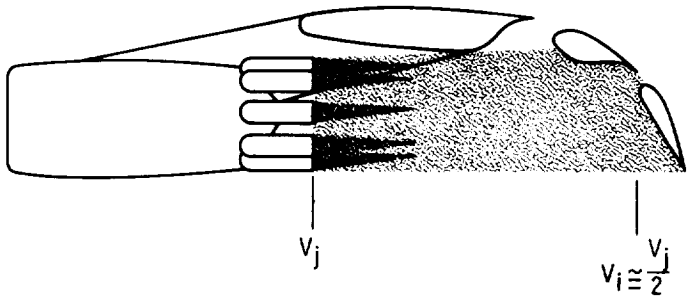

Figure XII-21

CS-63087

1/2-SCALE MODEL WITH MIXER NOZZLE

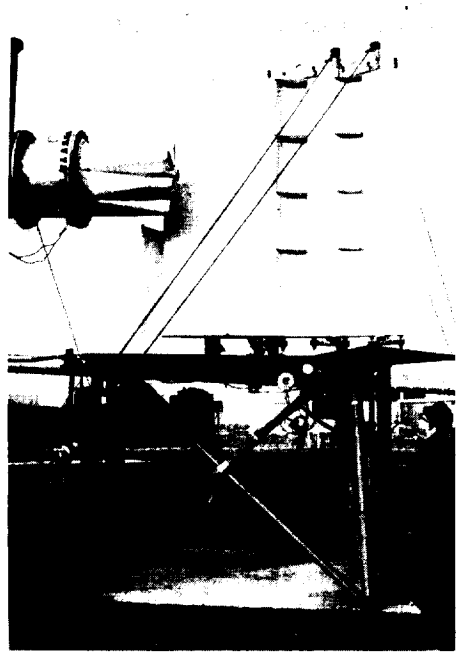

C-71-3984
CS-63082

Figure XII-22

DAISY MIXER NOZZLE TEST

CS-63292

Figure XII-23

COMPARISON OF RADIATION PATTERNS AT 50 FT

EXHAUST VELOCITY, 773 FT/SEC; FLAP ANGLE, 30°-60°

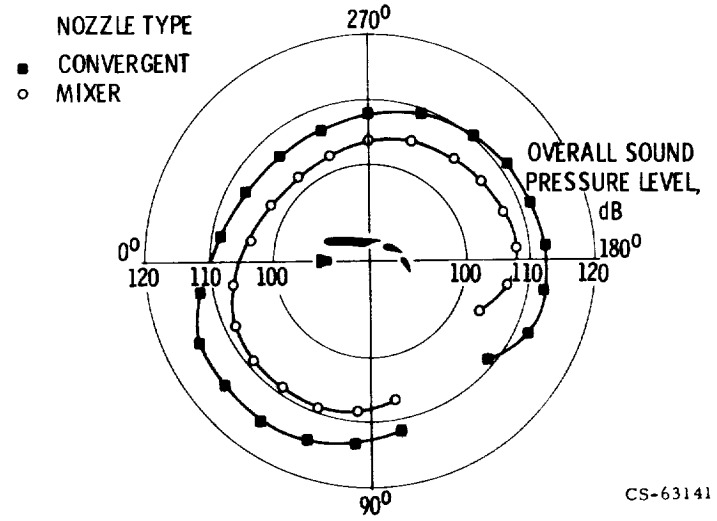

Figure XII-24

PERCEIVED NOISE LEVEL CONTOURS

170 000-LB-GROSS-WEIGHT STOL AIRPLANE

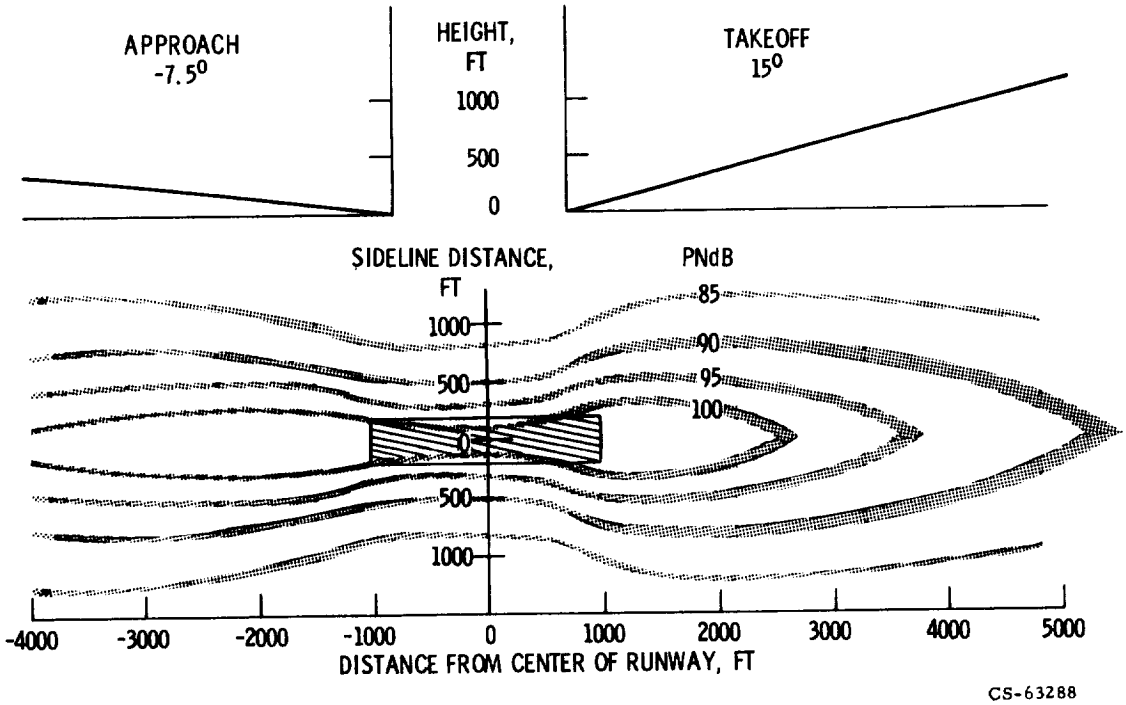

CS-63288

Figure XII-25

EXTERNALLY BLOWN FLAP AIRPLANE

UPPER SURFACE BLOWING

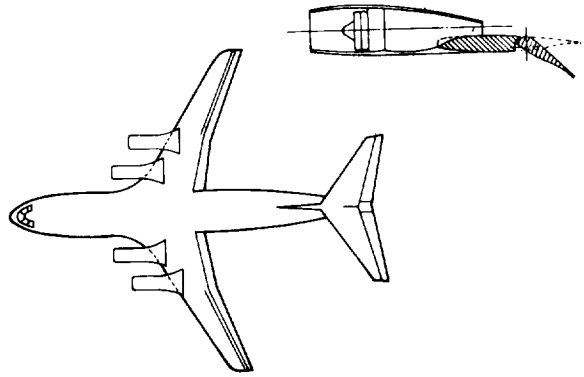

Figure XII-26 CS-63139

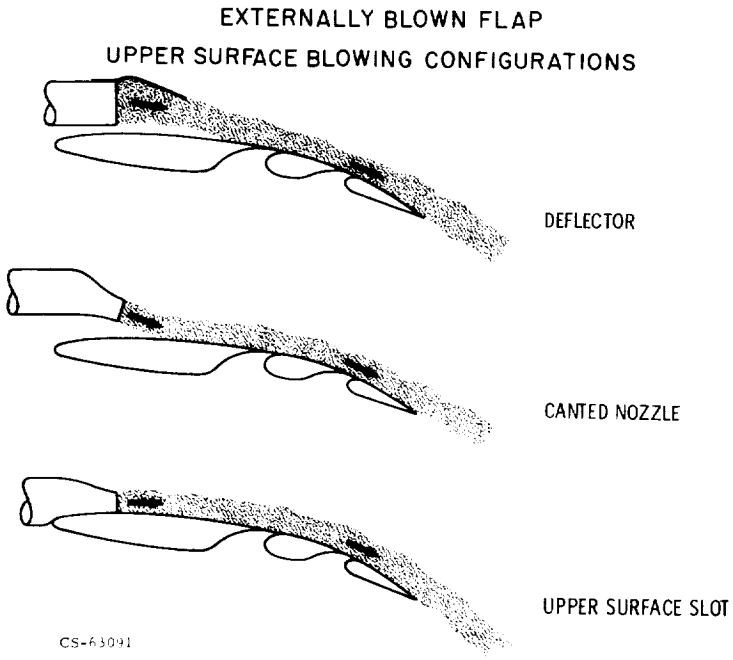

Figure XII-27

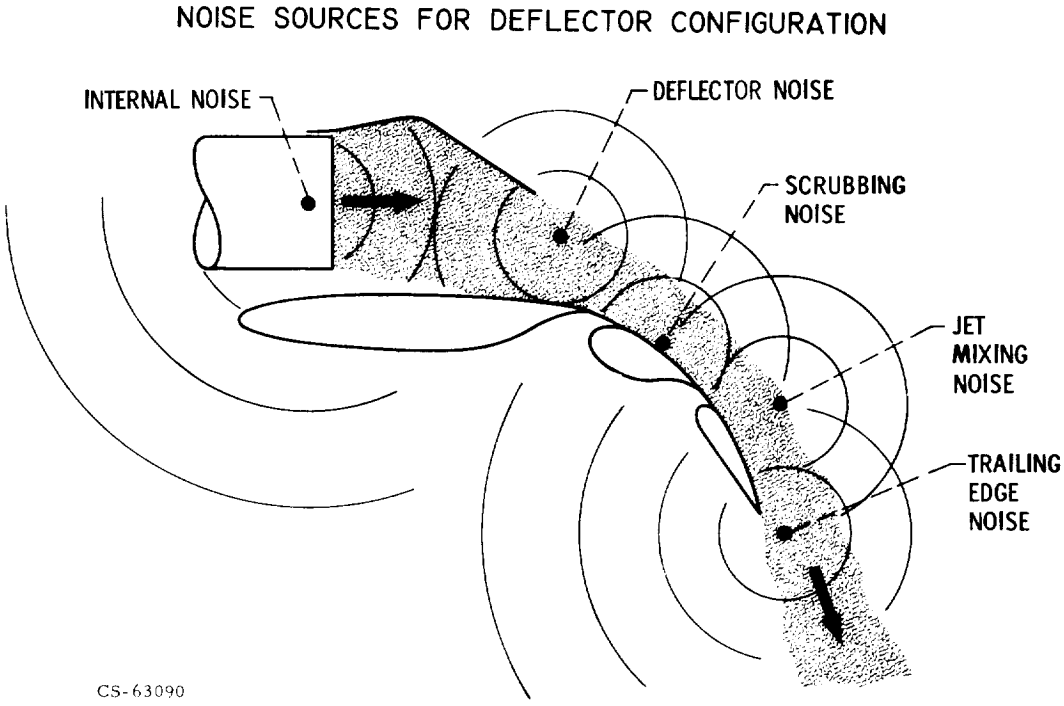

Figure XII-28

EXTERNALLY BLOWN FLAP MODEL WITH UPPER SURFACE BLOWING

2-IN. DIAMETER NOZZLE WITH DEFLECTOR

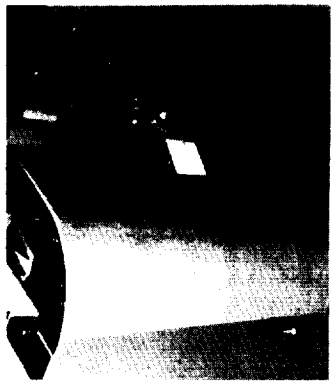

CS-63290

Figure XII-29

COMPARISON OF NOISE PATTERNS FOR EXTERNALLY BLOWN FLAPS AT 10 FT

EXHAUST VELOCITY, 585 FT/SEC; NOZZLE DIAMETER, 2.06 IN.; 60° TRAILING FLAP

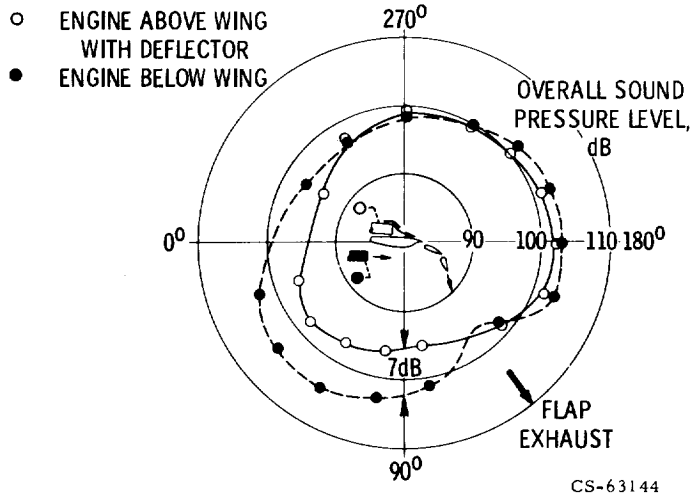

Figure XII-30

NOISE SPECTRA FOR DEFLECTOR CONFIGURATION WITH ROUND NOZZLE AT 10 FT

EXHAUST VELOCITY, 585 FT/SEC; NOZZLE DIAMETER, 2 IN.; SLOTLESS WING CHORD, 13 IN.; 60^0 FLAP ANGLE; 80^0 FROM INLET

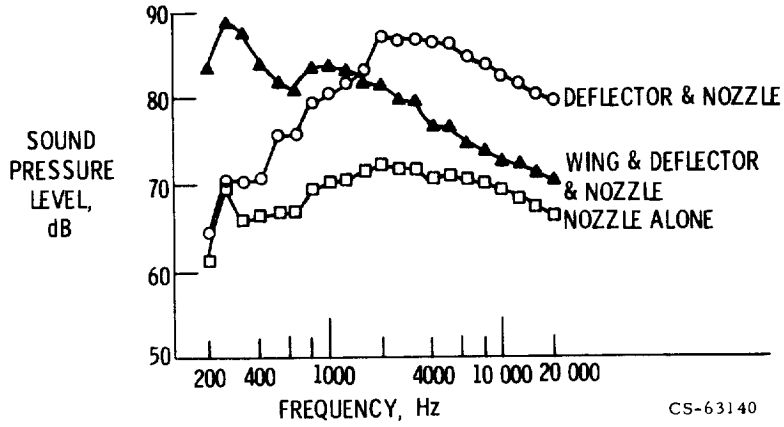

Figure XII-31

COMPARISON OF NOISE SPECTRA AT 10 FT

ROUND NOZZLE DIAM, 2 IN.; EXHAUST VELOCITY, 750 FT/SEC; SLOTLESS WING WITH 20^0 FLAP; 120^0 FROM ENGINE INLET

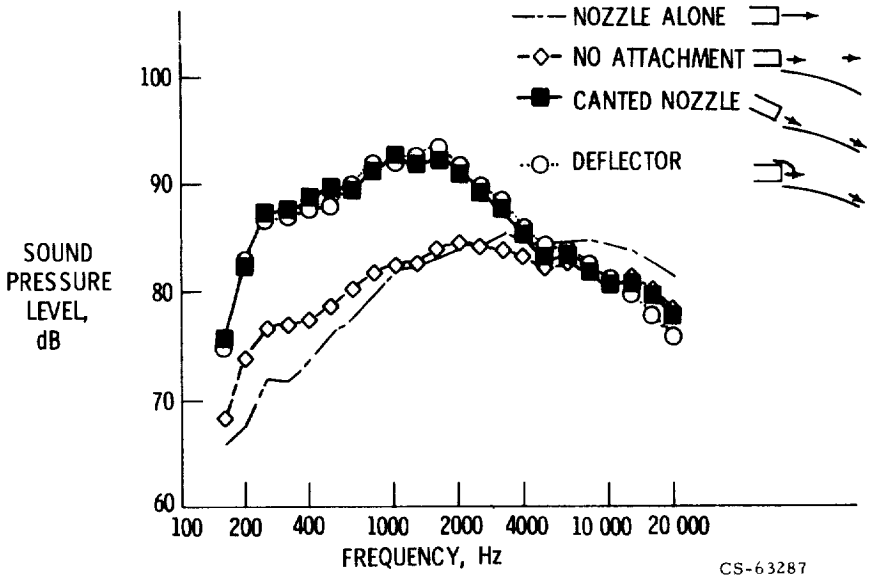

Figure XII-32

EFFECT OF FLAP LENGTH AND SLOT NOZZLE ASPECT RATIO

EXHAUST VELOCITY, 590 FT/SEC; SLOT AREA, 3.4 IN.^{2}; 60^0 TRAILING FLAP; MICROPHONE AT 10 FT; 80^0 FROM INLET

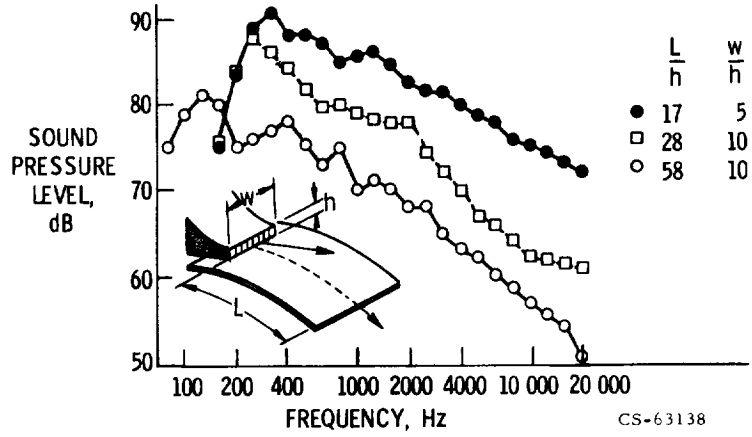

Figure XII-33

COMPARISON OF NOISE PATTERNS FOR EXTERNALLY BLOWN FLAP MODELS AT 10 FT

EXHAUST VELOCITY, 590 FT/SEC, NOZZLE AREA, 3.4 IN.^{2}, TRAILING FLAP, 60^0

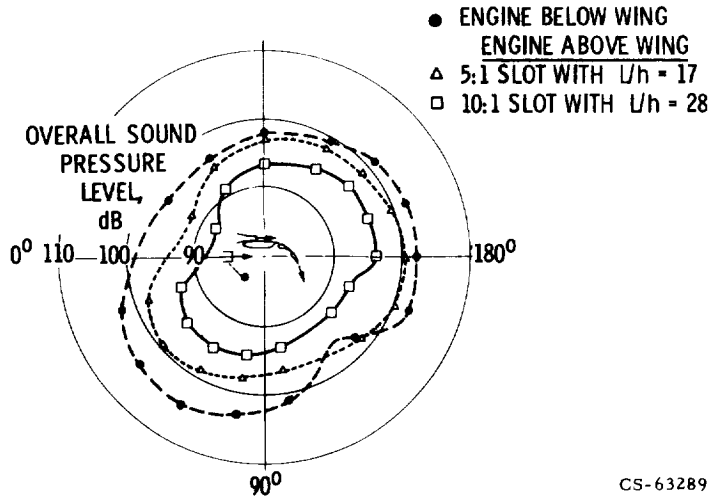

Figure XII-34

SHIELDING OF INTERNAL NOISE BY SLOTLESS WING

DEFLECTOR CONFIGURATION

WING CHORD, 13 IN.; 60^0 FLAP ANGLE;

NOZZLE PRESSURE RATIO, 1.25

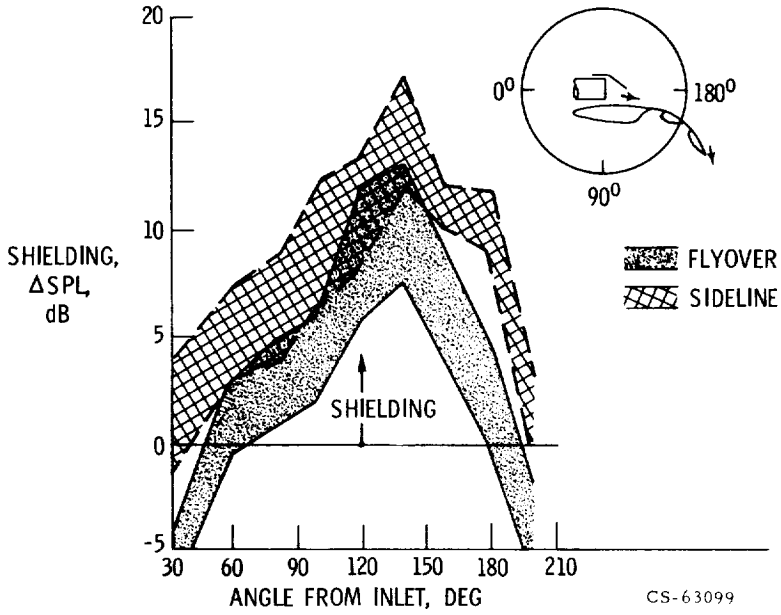

Figure XII-35

XIII. DESIGN INTEGRATION AND NOISE STUDY FOR A LARGE STOL AUGMENTOR WING TRANSPORT

Jack V. O'Keefe*

The major noise components of an augmentor wing STOL airplane engine are forward arc radiated inlet noise, rear arc radiated jet noise, and augmentor noise, which is directed immediately under the aircraft on a flyover (fig. XIII-1). The beam patterns of these components are separated sufficiently by directivity that they are nonadditive for peak perceived noise level predictions. The required reductions are plotted in the figure.

Primary jet velocity is the governing parameter for jet noise levels through engine cycle selection. A two-stream engine installation with all the fan air being routed to the wing to provide an 80/20 percent thrust split is shown in figure XIII-2. Internal flow turning duct wall acoustic lining eliminates aft arc fan noise. Inlet noise reduction using a sonic inlet is the subject of the paper by F. Klujber.

The objective of this NASA-Ames - Boeing augmentor program is to develop through analysis, design, experimental static testing, wind-tunnel testing, and design integration studies an augmentor wing jet flap configuration for a jet STOL transport aircraft having maximum propulsion and aerodynamic performance with minimum noise generation. The program has three basic elements: (1) static testing of a scale wing section to demonstrate augmentor performance and noise characteristics, (2) two-dimensional wind-tunnel testing to determine flight-speed effects on performance, and (3) system design and evaluation that optimizes the complete system and ensures that the design is compatible with the requirements for a large STOL transport having a 500-foot sideline noise of 95 perceived noise decibels (PNdB) or less.

All performance and acoustic tests were performed at the Boeing North Field Mechanical Laboratories, Seattle, Washington. The laboratories have a facility designed for large-scale combined acoustic and thrust performance

*The Boeing Company.

test programs. The augmentor thrust is measured with a six-component, platform balance bridged with high-pressure air; the noise can be measured in a 180^{o} arc in an acoustic arena (fig. XIII-3). The thrust stand accurately measures model forces using either hot (300^{o} F) or ambient-temperature air. Nozzle flow rates are determined with precision using ASME venturi flowmeters calibrated against a Boeing standard nozzle. An acoustically treated muffler plenum, located on the balance platform upstream of the test nozzle plenum, prevents any noise generated by the air supply lines and control valves from reaching the test nozzles. A flap system is shown installed on the test stand in figure XIII-4.

Initial static testing included slot nozzles with aspect ratios between 50 and 400, a convergent-divergent nozzle, and various multielement nozzles with lobe and tube shapes. A representative array of nozzles is shown in figure XIII-5. Subsequent static testing included improved nozzles in full augmentor systems. The results presented in this paper show how the noise and performance objectives are met with the augmentor.

The static testing included multirow tube and lobe nozzles of array area ratios varying from 4 to 8. Array area ratio is defined as the ratio of total array area to nozzle exit area. Several configurations of augmentor geometries with internal design variations were investigated with a range of acoustically tuned linings. Combinations of flap and shroud lengths were tested for their thrust augmentation and noise characteristics. The best configurations for performance and noise used high array area ratio multielement nozzles in augmentors with symmetrical internal contours.

The achievement of the large noise suppression required to meet the 95-PNdB (perceived noise decibels) noise level depends on a series of carefully integrated design steps. These are shown starting with a high-aspect-ratio unaugmented slot nozzle and progressing through an augmentor with acoustically tuned lining.

A peak level of 116 PNdB would be measured on the 500-foot sideline at takeoff of a jet STOL aircraft employing a high-aspect-ratio slot nozzle for bypass thrust and a nozzle pressure ratio of 2.6. A suppression of 21 PNdB, relative to such a slot nozzle, is required to achieve the goal of this task. This suppression is equivalent to a reduction of annoyance by a factor of 4 to 5. The noy-weighted spectrum (fig. XIII-6) of the slot nozzle identifies the

problem area as the mid- and high-frequency range of the spectrum. The annoyance levels in the 2- to 4-kilohertz bands (to which the human ear is most sensitive) are particulary prominent. While a large array area ratio (AAR) multirow lobe nozzle alone alleviates the midfrequency band level problem (fig. XIII-6), the effect in the critical high-frequency bands is only enough to deliver a suppression of 8 PNdB for the nozzle alone.

Adding an unlined augmentor to the lobe nozzle reduces the noise level in high-frequency bands, but it increases noise in the low-frequency bands and provides a net noise suppression of 10 PNdB (fig. XIII-7). Additional reductions of noise in higher frequency bands are achieved by screech suppression and by using acoustically tuned lining in the augmentor.

The aerodynamically induced jet screech produced by the multirow lobe nozzle is eliminated by extending one side of each lobe six lobe widths (fig. XIII-8).

The basic nozzle suppression with unlined augmentors increases to 12 PNdB, and the tuned lining suppression (relative to unlined augmentor) increases from 3.5 PNdB without screech shielding to 7PNdB when the screech shields are used, resulting in a 19-PNdB suppression relative to the slot nozzle. Matching the core depths of the tuned lining to the frequency distribution along the jet axis and also installing a baffle at the lower secondary air gap results in a total suppression of 21 PNdB (fig. XIII-9).

In summary, the noise suppression available from one of the best configurations is illustrated in figure XIII-10. The noise objective of 95 PNdB at the 500-foot sideline is met by this configuration and the static thrust augmentation level (total thrust vector; flaps on/flaps off) is above 1.42 at takeoff flap setting.

An important element in obtaining the 21 PNdB noise suppression is the proper design and application of tuned lining for the augmentor surfaces. This was accomplished by testing a matrix of seven linings. The results confirm the design procedure. The best lining was in the eye of the matrix and achieved a 7-PNdB suppression relative to the unlined augmentor. The sound pressure level spectrum for this is shown in figure XIII-11.

Although the lining designs are successful, the initial suppression was below the 6 PNdB predicted. The effectiveness of the acoustic lining was initially masked by nozzle screech. Consequently, an investigation was

made to develop an effective screech suppressor for the primary nozzles. The screech shield was devised and applied to the AAR = 6, 172-lobe primary nozzle. The same tuned lining reduced the noise by 7 PNdB relative to the unlined augmentor.

The spectrum and beam patterns of the best lined augmentor tested are shown in figures XIII-12 and XIII-13. The primary nozzle has screech shields; the augmentor has mixed single-layer lining and a lower gap baffle. The sound pressure level spectrum is based on the same data as the noy-weighted spectrum of figure XIII-10, and it is compared with a basic slot nozzle. The suppressed spectrum is flat with no pure tones and varies less than 10 decibels through the frequency range. The maximum perceived noise level is reduced by 21 PNdB relative to the slot nozzle. The beam pattern of the suppressor is highly directional, providing additional advantages with respect to the time duration effects for this noise component.

High static thrust augmentation is developed with multirow lobe nozzles of large array height operating with a relatively short augmentor system. The multielement nozzles in augmentors demonstrate high static thrust augmentation through 45° of internal flow turning without the need for special boundary-layer control slots on the flap or other devices for energizing the boundary layer.

The relation among the achievable augmentation ratios, nozzle array area ratios, and nozzle ventilation is illustrated in figure XIII-14. As the nozzles increase in length, in array area ratio, and in the number of elements (and nozzle perimeter), the augmentation ratio increases from 1.2 to 1.48.

Since thrust augmentation does not include nozzle internal loss effects, these must be identified to evaluate total airplane performance. The small penalties for nozzles with large numbers of elements are predictable. For example, the 172-lobe nozzle has a velocity coefficient of 0.95 at a design nozzle pressure ratio of 2.6. Suppressor nozzles tested correlate well as a function of hydraulic diameter.

Compromises were made in order to satisfy airplane installation requirements. One of the most important factors in augmentor wing airplane designs is the trade-off in augmentor system length. Although increasing the nozzle length significantly improves augmentation (fig. XIII-14), no

change in noise suppression was measured. Increasing the flap length, however, provides both acoustic and augmentation improvement (fig. XIII-15). Within the range of lengths considered, it is important to use as long an augmentor as possible.

Figure XIII-16 is a review of the major acoustic predictions, data, and configuration milestones of the program. The objective of future tasks is to improve the noise suppression by 5 PNdB and the thrust augmentation ratio by five counts. The acoustic improvement lies primarily in the area of the application of multielement acoustic linings, while the thrust improvement lies in the area of better mixing primary nozzles, improved nozzle ventilation, and refinements in internal augmentor contours.

The projected peak 500-foot sideline noise of the 1978 augmentor wing airplane is 90 PNdB. The airplane takeoff noise "footprint" generated by the 1978 augmentor at maximum STOL takeoff weight is given in figure XIII-17. The 90-PNdB closure point directly under the flight path is located at 7200 feet from brake release. The total takeoff noise area encompassed by the 90-PNdB isocontour is approximately 100 acres. This type of footprint should be acceptable for a large majority of STOL ports, especially since the noise spectrum will not contain sharp, pure tones. A 90-PNdB short-duration transportation noise level will blend with many community ambient noise levels and result in little or no annoyance.

AUGMENTOR WING STOL AIRPLANE FLYOVER NOISE (PREDICTED)

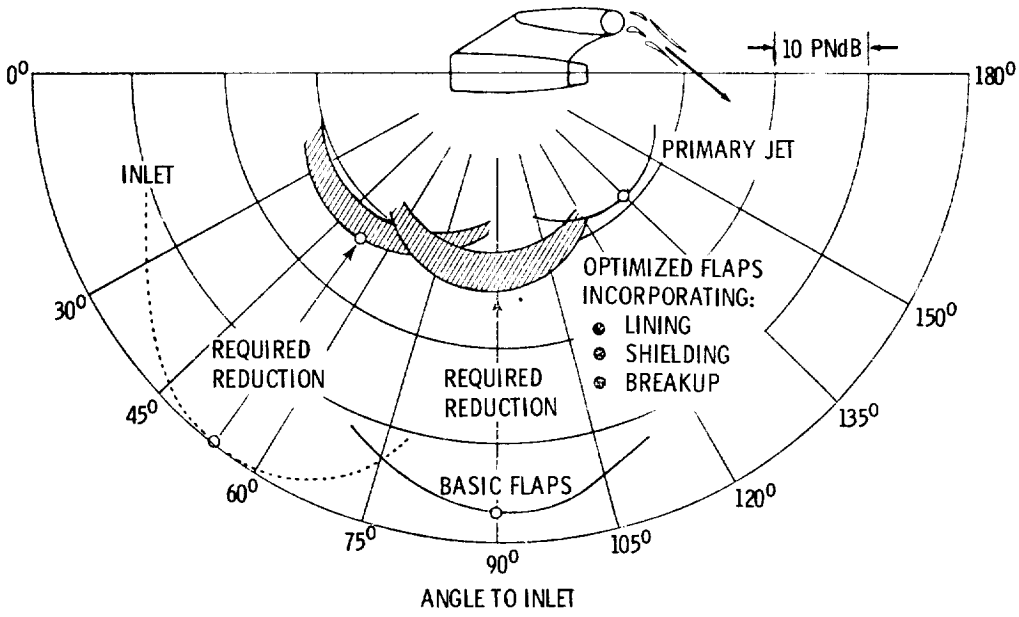

Figure XIII-1

AUGMENTOR WING PROPULSION SYSTEM

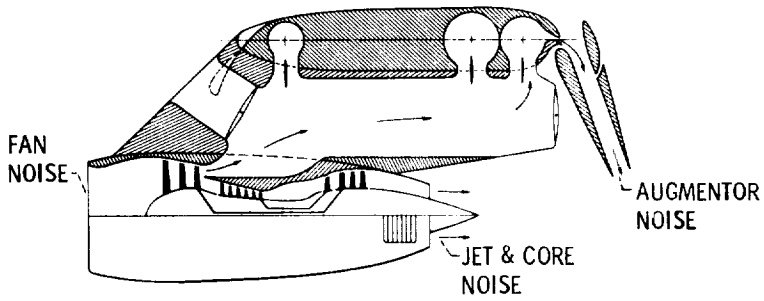

Figure XIII-2

CS-63128

MICROPHONE ARRAY NOISE FACILITY

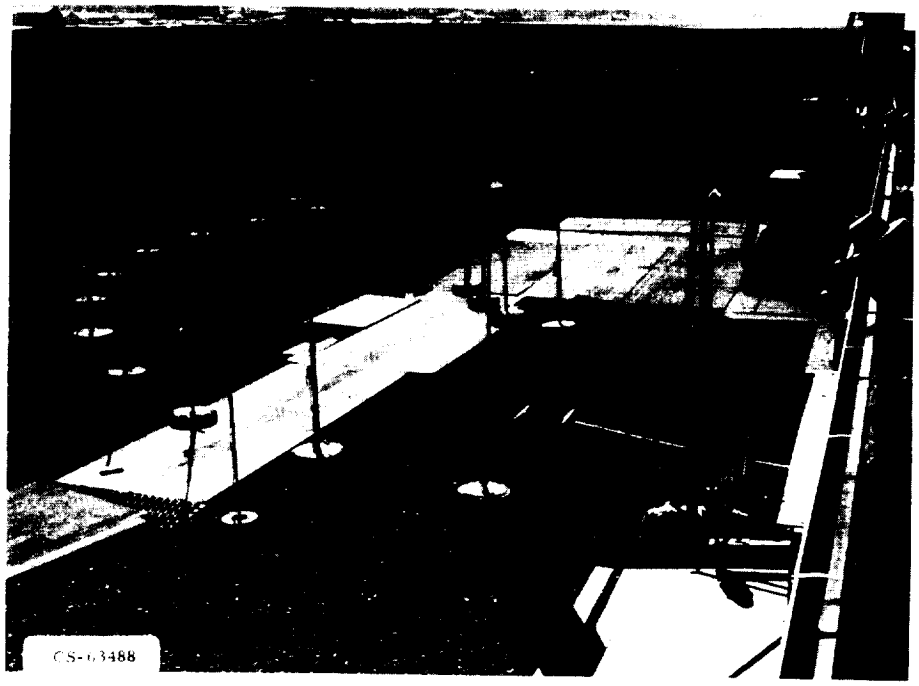

Figure XIII-3

NOZZLE FLAP SYSTEM ON NOISE TEST FACILITY

Figure XIII-4

TYPICAL NOZZLE TEST SPECIMENS

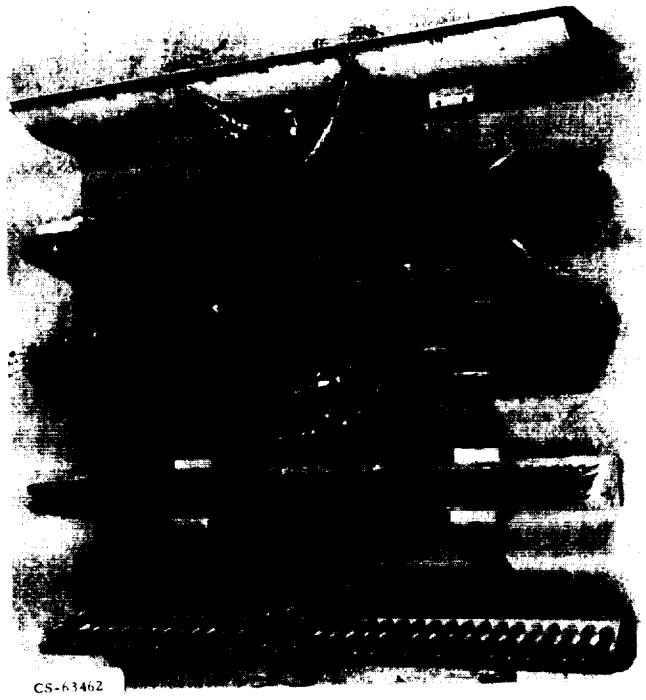

Figure XIII-5

TAKEOFF PERCEIVED NOISE LEVELS WITHOUT AUGMENTOR

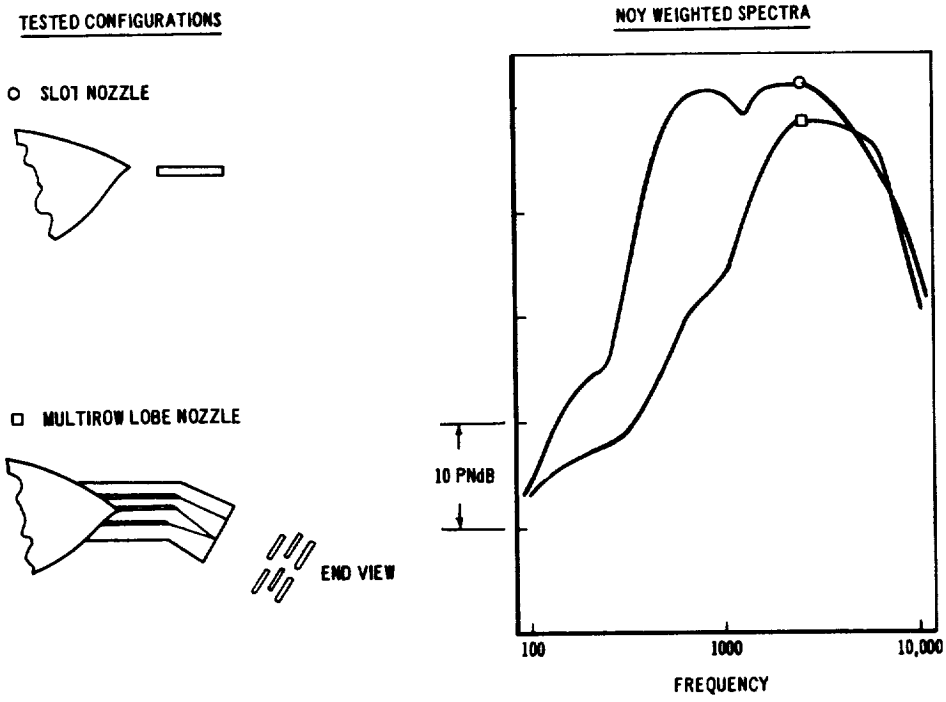

Figure XIII-6

TAKEOFF PERCEIVED NOISE LEVELS WITH AUGMENTOR

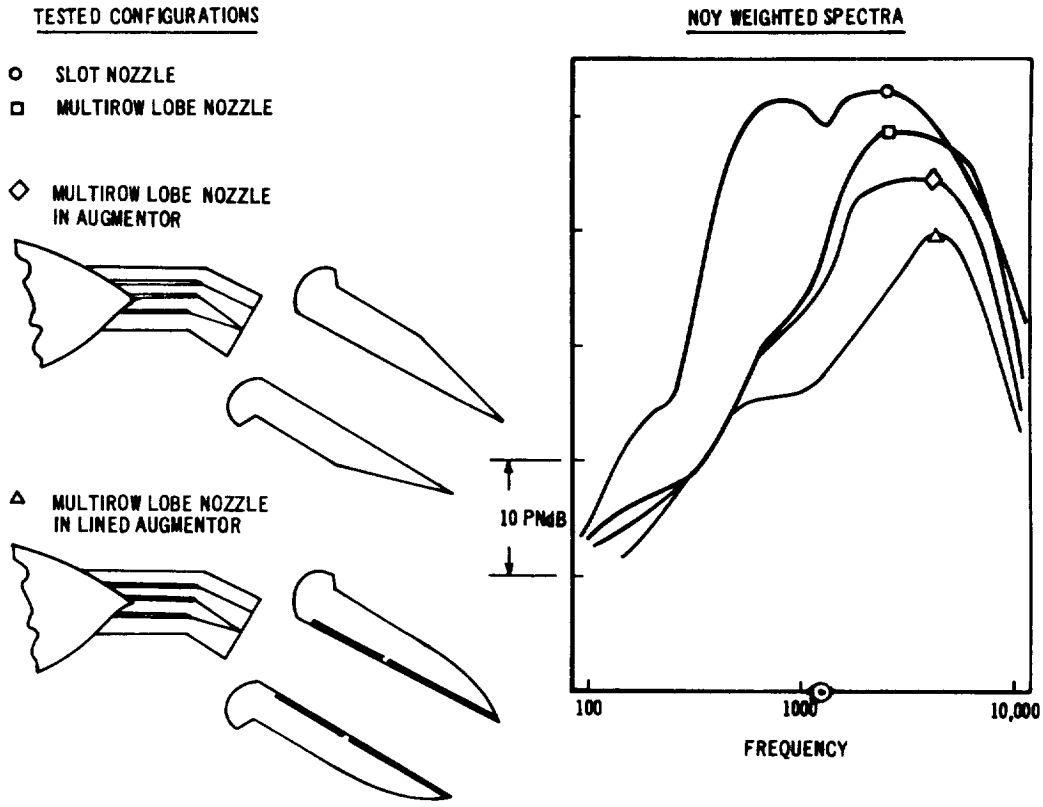

Figure XIII-7

NOZZLE SCREECH SUPPRESSORS (SCREECH SHIELDS)

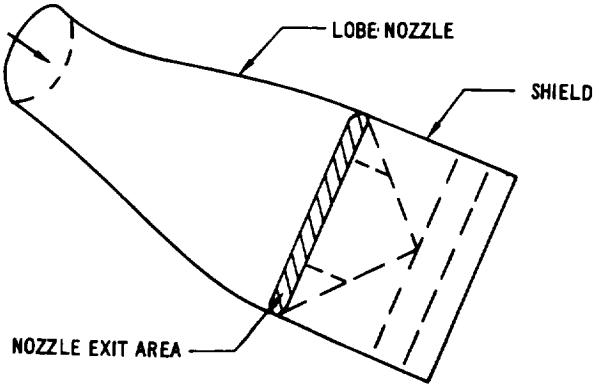

Figure XIII-8

TAKEOFF PERCEIVED NOISE LEVEL WITH LINED AUGMENTOR, SCREECH SHIELD AND BAFFLE

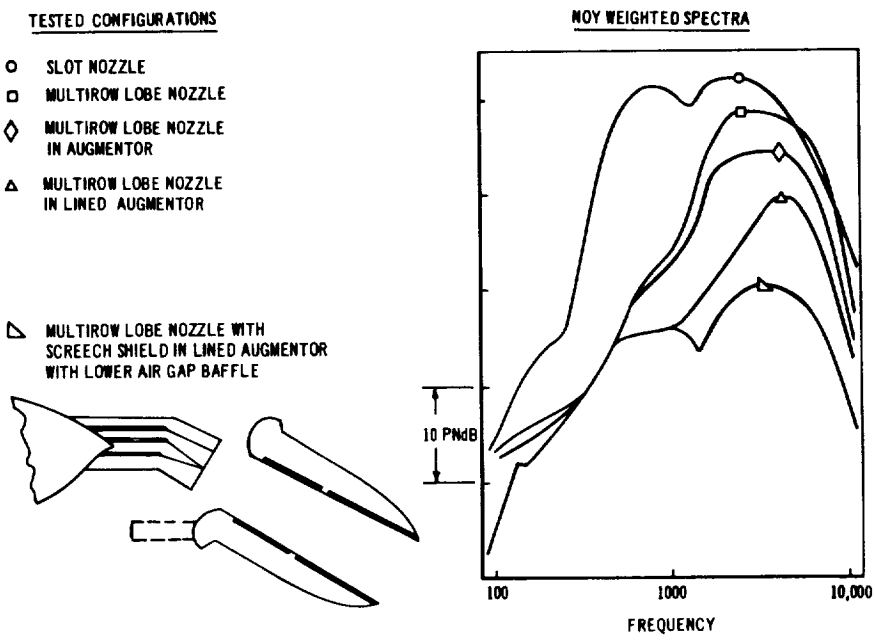

Figure XIII-9

TAKEOFF PERCEIVED NOISE LEVELS

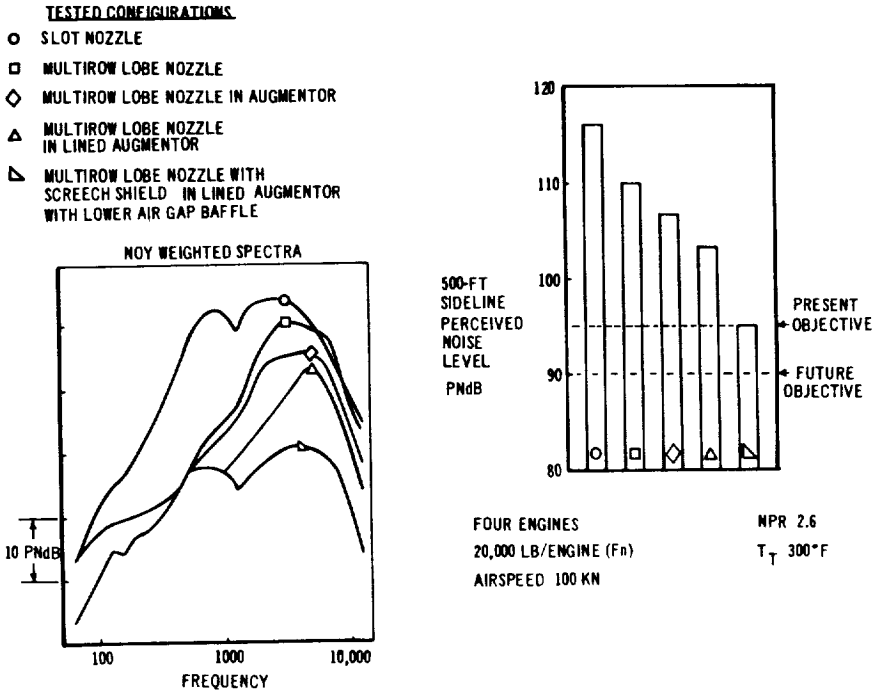

Figure XIII-10

COMPARISON OF NOISE SPECTRA

UNLINED VS LINED AUGMENTOR, AS MEASURED MODEL SCALE (172 LOBE NOZZLE WITH SCREECH SHIELDS, MIXED LINING

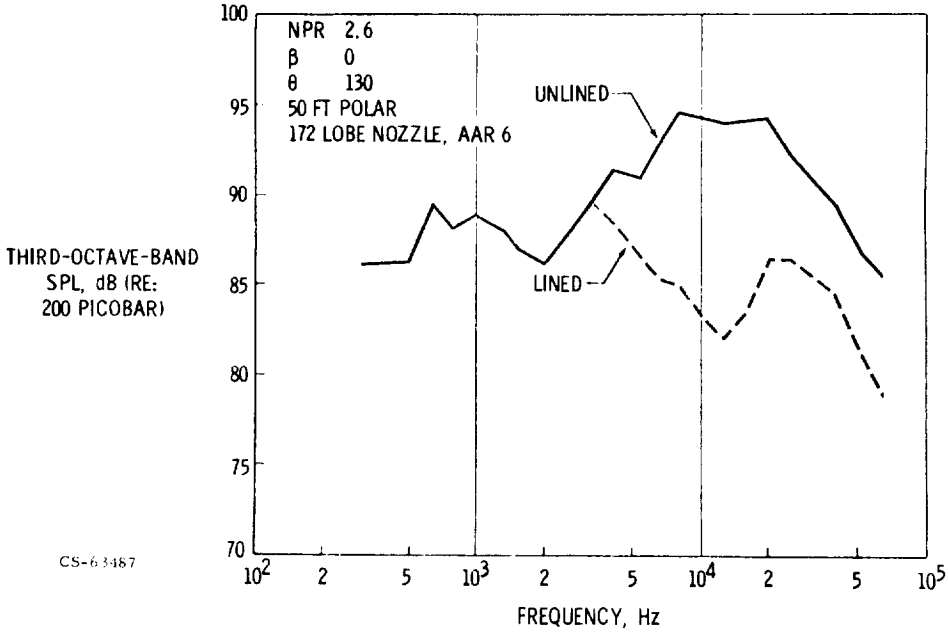

Figure XIII-11

21-PNdB SUPPRESSOR SPECTRA AND BEAM PATTERNS

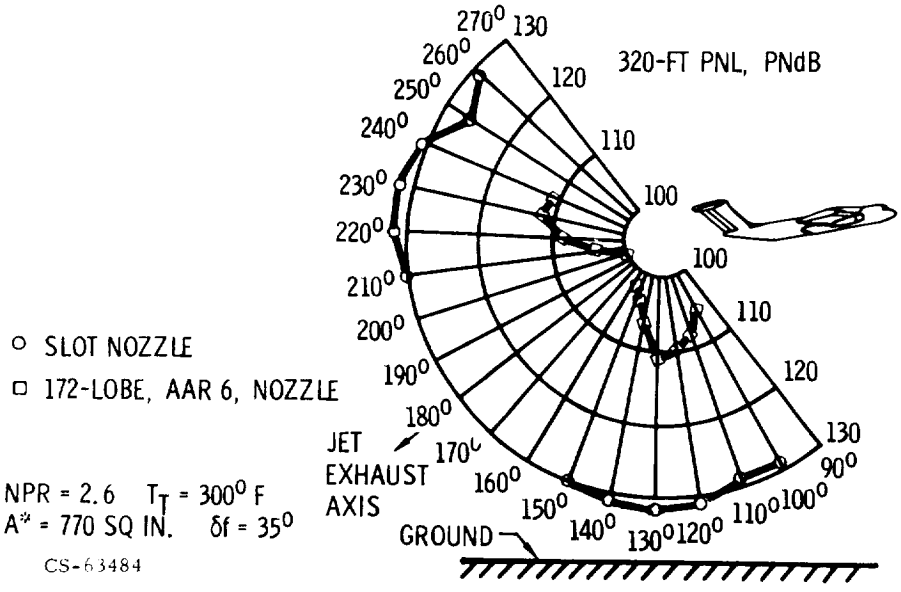

Figure XIII-12

21-PNdB SUPPRESSOR SPECTRA AND BEAM PATTERNS

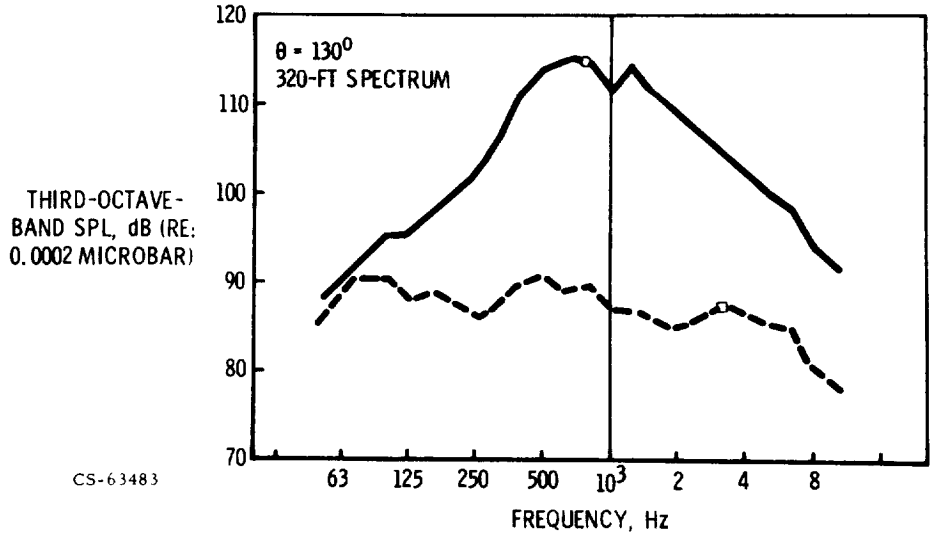

Figure XIII-13

PRIMARY NOZZLE GEOMETRY EFFECTS

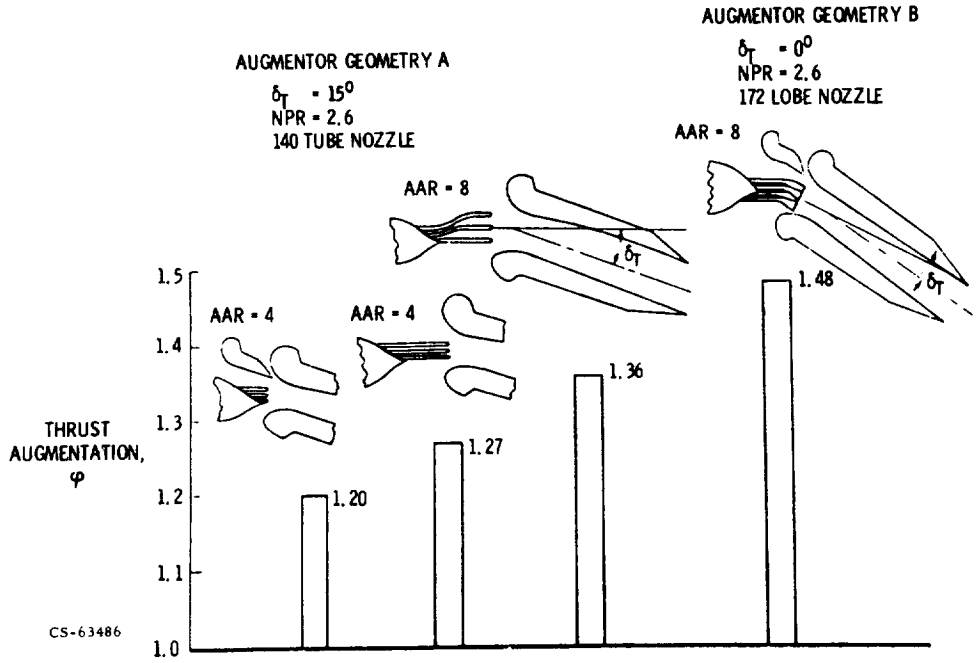

Figure XIII-14

AUGMENTOR LENGTH EFFECTS

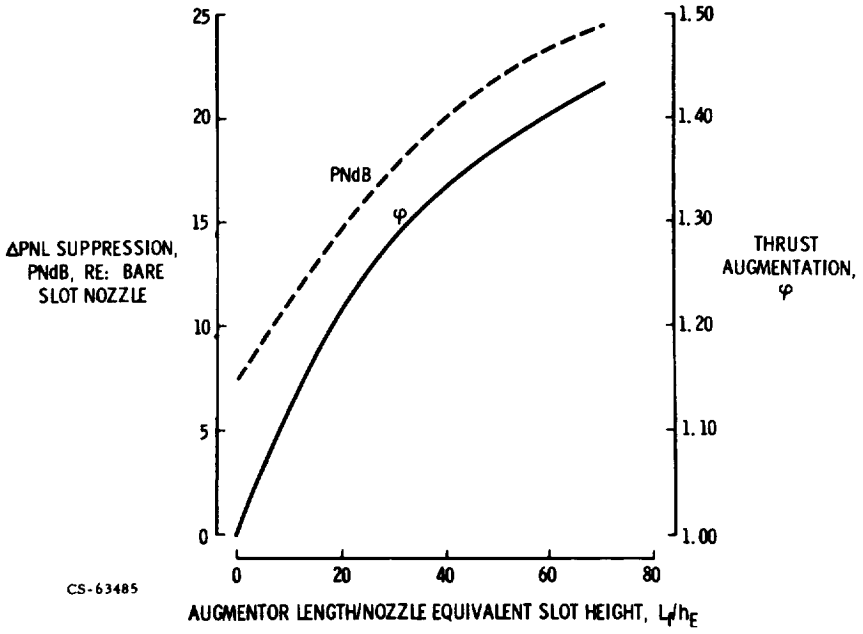

Figure XIII-15

AUGMENTOR WING NOISE LEVELS

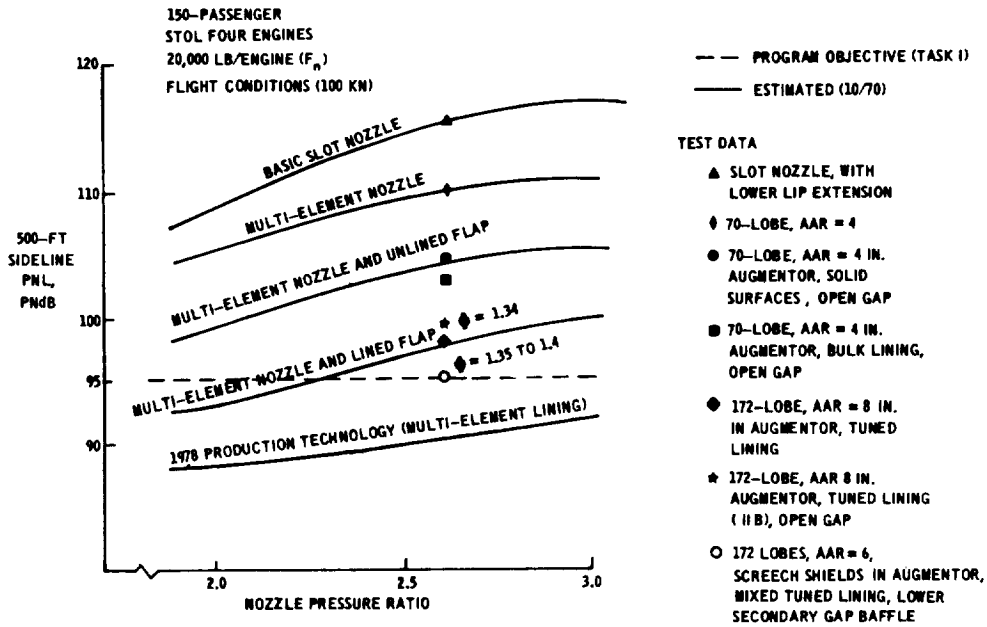

Figure XIII-16

TAKEOFF FOOTPRINTS FOR TWO-STREAM AUGMENTOR WING AIRPLANE

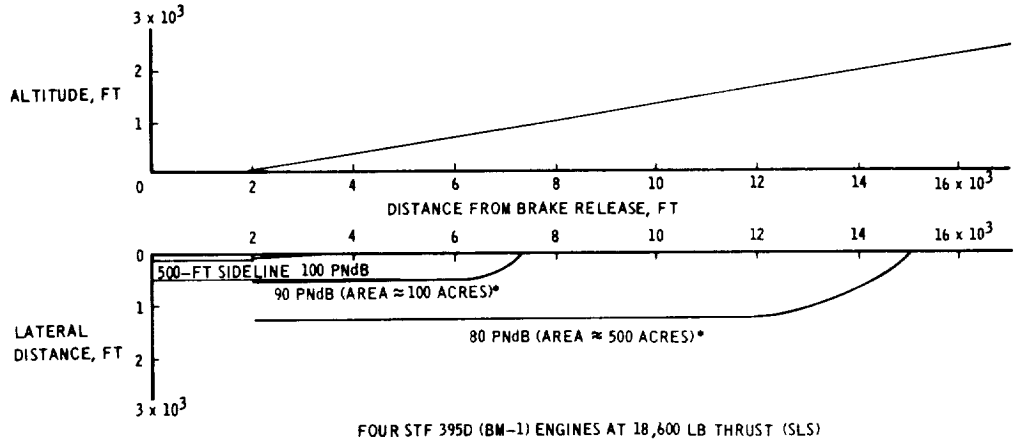

FOUR STF 395D (BM-1) ENGINES AT 18,600 LB THRUST (SLS)
AVERAGE GRADIENT 0.149
AVERAGE AIRSPEED 91 KTAS

*AREA MEASURED FROM BRAKE RELEASE

Figure XIII-17

XIV. SONIC INLET DEVELOPMENT FOR TURBOFAN ENGINES

Frank Klujber*

STOL propulsion installation requires substantial inlet noise reduction to satisfy anticipated airplane noise requirements. Depending on the engine and airplane configuration chosen, a 15 to 30 perceived noise decibel (PNdB) inlet noise suppression is required to match other reduced noise source levels.

As indicated in figure XIV-1, the augmentor wing airplane requires an inlet noise suppression of 25 to 30 PNdB. For such high levels of inlet noise suppression, sonic or high Mach number inlets become attractive candidates. In addition to the augmentor wing propulsion system, a broad range of applications of sonic or high Mach number inlets is foreseen for future propulsion systems.

Suppression of engine inlet noise by use of a sonic throat has been under consideration for a number of years. A limited amount of testing has been conducted by NASA, the Boeing Company, and others. However, there has been a need for a systematic investigation of fundamental noise suppression characteristics, evaluation of the several candidate configurations, and a study of the design and operational characteristics required for practical flight installations. Such a program was undertaken in January 1972 by the Boeing Company under contract to the Lewis Research Center.

The basic acoustic principle of sonic inlet operation is that sound waves are attenuated while traveling upstream in a high Mach number flow stream. The limit case is achieved when a complete sonic plane is generated. In this case, theoretically, no sound waves can travel past the sonic plane (fig. XIV-2). The aerodynamic principle of operation is that the flow is accelerated to produce a high velocity throat and then is diffused to provide acceptable flow velocities to the engine.

There are two basic airplane operating conditions under which low noise

*The Boeing Company.

(i.e., choked inlet mode) is desired for community noise reduction - takeoff and landing approach. Since the engine power settings for these two conditions are different, the area must be variable for maximum noise reduction.

Based on the flow area requirements for the critical operating conditions, one can establish the basic requirements for the design of a sonic inlet:

(1) Provide throat area reduction in the inlet to produce sonic or near sonic flow conditions.

(2) Provide a diffuser beyond the throat to reduce flow velocity to the engine inlet.

(3) Provide area variability for takeoff, approach, and cruise.

In order to arrive at an optimum choice for an operationally and economically viable inlet, the merits of each design must be determined by the amount of noise reduction balanced against other technical requirements. The following are the most important of these requirements:

(1) Minimization of inlet flow recovery losses

(2) Minimization of flow distortion

(3) Minimization of external drag

(4) Minimization of weight

(5) Mechanical feasibility

An added requirement for the best sonic inlet choice would be to satisfy these performance requirements under actual operating conditions of angle of attack and crosswind.

Many sonic inlet configurations could satisfy the previous design requirements. These inlets fall in two basic categories, namely, single passage and multiple passage types. Examples of single passage inlets are the following:

(1) Translating centerbody

(2) Expanding centerbody

(3) Contracting cowl wall

Multiple passage inlet types include the following:

(1) Movable concentric rings

(2) Movable radial vanes, etc.

Boeing is currently conducting a program under an NASA Lewis contract for sonic inlet configuration selection and design technology development

(fig. XIV-3). The first phase of the current program consists of designing and testing different inlet models in order to select the most promising concepts for further development (fig. XIV-3). After these initial screening tests two concepts will be further refined and optimized.

The test program is being conducted in an anechoic chamber (fig. XIV-4) where inlet noise is separated from other fan noise sources and background noise is minimized. This arrangement allows evaluation of the actual noise reduction potential of sonic inlets. Detailed state-of-the-art aerodynamic design and instrumentation also allowthe comparison of different inlets in terms of their noise reduction potential and aerodynamic performance (i.e., pressure recovery and flow distortion).

A baseline inlet (fig. XIV-5) has been tested in the program to study the near field noise attenuation characteristics of sonic inlets. This inlet was designed with adequate length to ensure good aerodynamic performance and boundary layer separation free operation. Instrumentation included a line of wall static pressures, boundary layer rakes, and inlet wall kulite probes for noise measurement (fig. XIV-5). Total pressure rakes were traversed at the exit plane of the inlet to obtain recovery and flow distortion data. This instrumentation is typical for all test models.

The baseline inlet has been probed in the near field with a specially constructed probe for continuous measurement of noise and static pressure inside the inlet (fig. XIV-6). The probe is mounted on an X-Y traverse mechanism to enable continuous recording in both axial and radial planes.

Typical Mach number and blade passage frequency noise contours are shown based on the axial traverses at various radial positions (fig. XIV-7). The data show that the noise level at the fan face is greatly dependent on radial position. The hub noise levels are the lowest, and the highest values are measured at the tip. In the throat region rapid noise reduction takes place when the Mach number exceeds 0.7 with the minimum noise measured at the throat. Radial noise gradients disappear at the throat.

Specific attention was centered on the attenuation of shock waves and multiple pure tones by sonic inlets at supersonic fan tip speeds. Noise measurements were taken near the fan face, downstream of the throat, and in the throat. The spectrum comparisons for these measuring points indicate that all pure tones were effectively attenuated by the sonic inlet (fig. XIV-8).

Another point of interest is the possible noise generated by the sonic plane itself. Therefore, measurements were also taken ahead of the shock plane (fig. XIV-9). The comparisons indicate that no significant noise increase was experienced because of noise generation by the sonic plane for the test conditions investigated.

Testing to date has been completed on several inlet models. Single passage inlet test results show (fig. XIV-10) that a 28 to 30 PNdB inlet noise reduction at approach engine power setting can be achieved by sonic inlets with 0.97 inlet recovery within acceptable inlet distortion limits. The test data show that sonic inlets within realistic length limits (L/D = 1) can be designed to achieve high noise reduction and acceptable aerodynamic performance on a static performance basis. Takeoff configuration tests have shown similarly good results for approach on the static tests (fig. XIV-11). The measured single-passage-fan face total-pressure distortion levels are shown for a range of Mach number conditions (fig. XIV-12). With the exception of the last test condition shown, no flow separation is indicated by these measurements. A further investigation of the flow separation phenomenon at a high Mach number and low recovery operation is planned to extend the range of operating envelope of these inlets.

One multipassage sonic inlet has been tested to date. This inlet was a radial-vane-type sonic inlet with 36 retractable radial vanes forming the sonic plane. Acoustic and aerodynamic data from this test are shown in comparison to the L/D = 1 centerbody inlet on figure XIV-13. The multipassage inlet produced lower noise reduction with significantly lower pressure recovery.

In spite of the poorer static performance of the multipassage inlet, interest will be continued in these configurations until wind tunnel evaluation of the different concepts can be made. Multipassage inlets are believed to be less sensitive to angle of attack and crosswind conditions.

Spectral comparison of the noise for the baseline and sonic inlet indicates that some dependence of attenuation effectiveness exists as a function of frequency (fig. XIV-14). Pure tones of high frequency and high frequency broadband noise are more effectively attenuated than the tones of low frequency noise. This phenomenon seems to be Mach number dependent, indicating that flow velocity effects may interact with the direction of noise

propagation. Thus, plane waves (low frequency noise) traveling in the axial direction will propagate from the inlet at high flow Mach numbers, while traversely propagating modes (high frequency) get reflected at lower inlet flow velocities. Further analytical work is required to fully understand and quantify these relations.

Noise directivity measurements taken in the acoustic chamber with adequate inlet sidewall insulation and other noise sources minimized (fig. XIV-15) indicate that the noise is effectively reduced at all angles in the forward arc. This result helps to clarify some questions with regard to sideline (90^{o}) effectiveness of sonic inlets.

In summary, the static program has shown to date that very large noise reductions can be achieved by the sonic inlet concept with realistic inlet length and good aerodynamic performance. It is also shown that different inlet concepts produce substantially different results. It should be emphasized that the conclusions drawn here are based on static performance evaluation necessitated by the current status of the program. Therefore, adequate caution must be exercised until distortion and angle of attack effects are fully determined on the performance of these inlets.

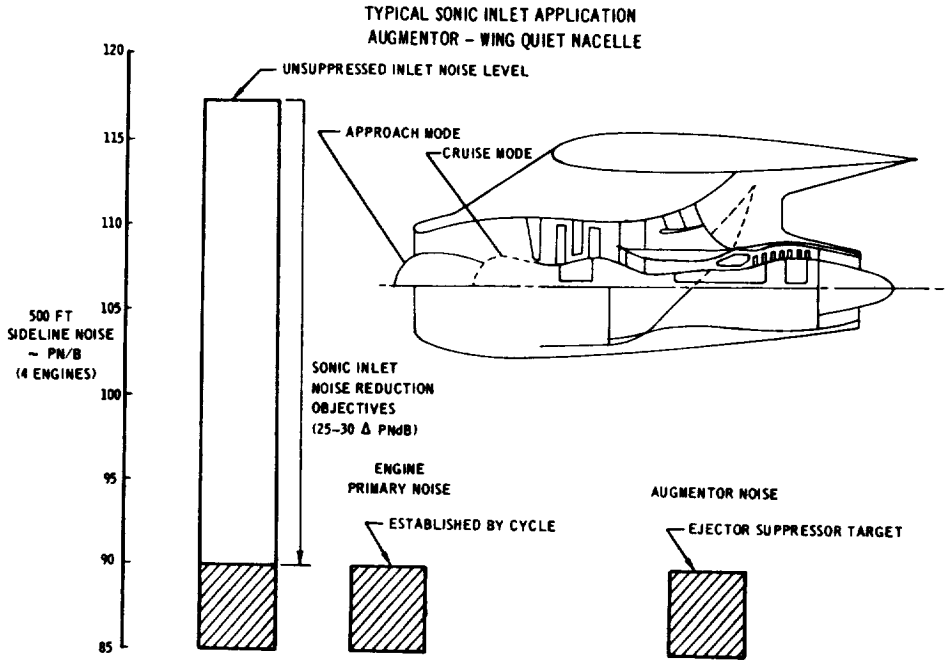

Figure XIV-1

SONIC INLET OPERATIONAL REQUIREMENTS
AND
DESIGN CONSIDERATIONS

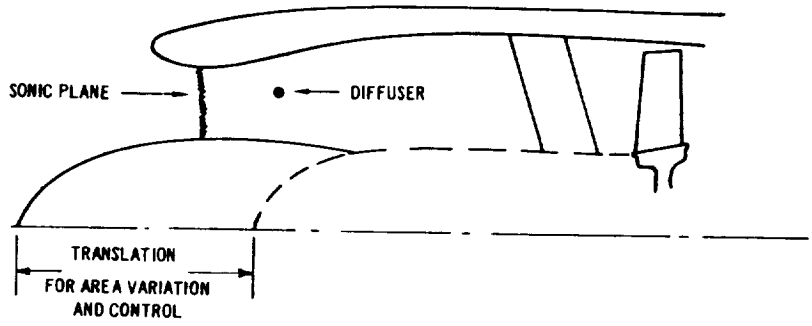

MAIN DESIGN CONSIDERATIONS :

- MINIMUM LOSS
  MINIMUM FLOW DISTORTION
- LIGHT WEIGHT
- MECHANICAL FEASIBILITY AND SIMPLICITY

Figure XIV-2

NASA/BOEING SCALE MODEL SONIC INLET PROGRAM

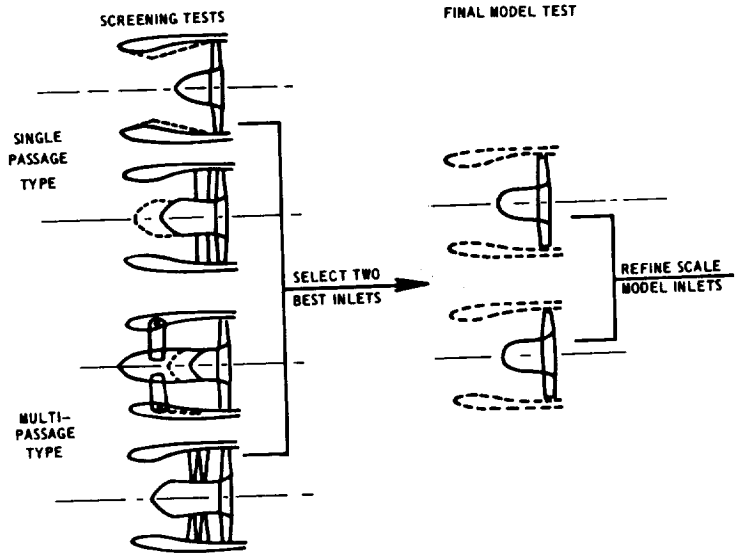

Figure XIV-3

12-INCH RIG MICROPHONE ARRAY

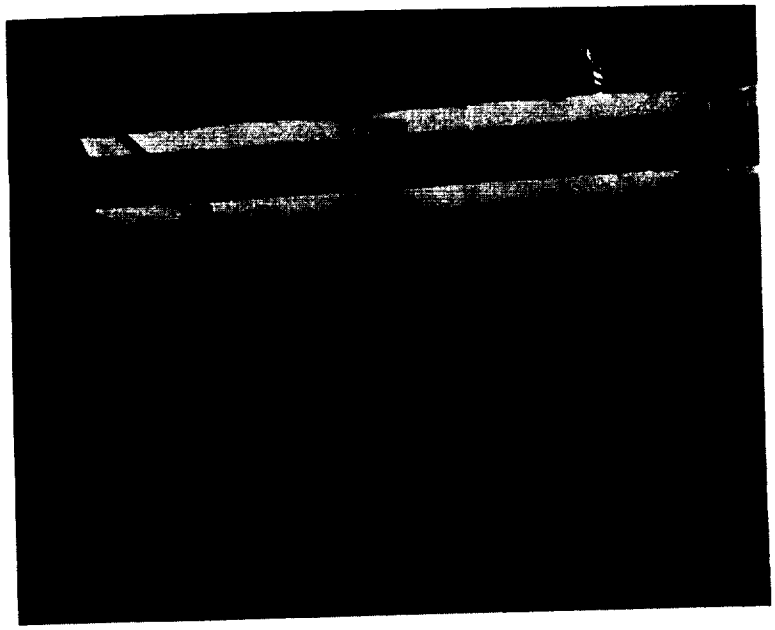

Figure XIV-4

SONIC INLET NOISE MECHANISMS
TEST INSTRUMENTATION

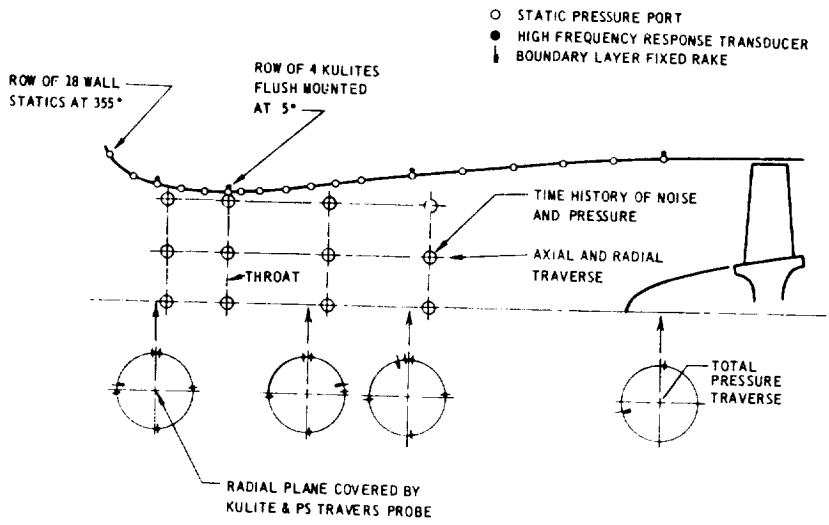

Figure XIV-5

12-INCH FAN RIG SYSTEM

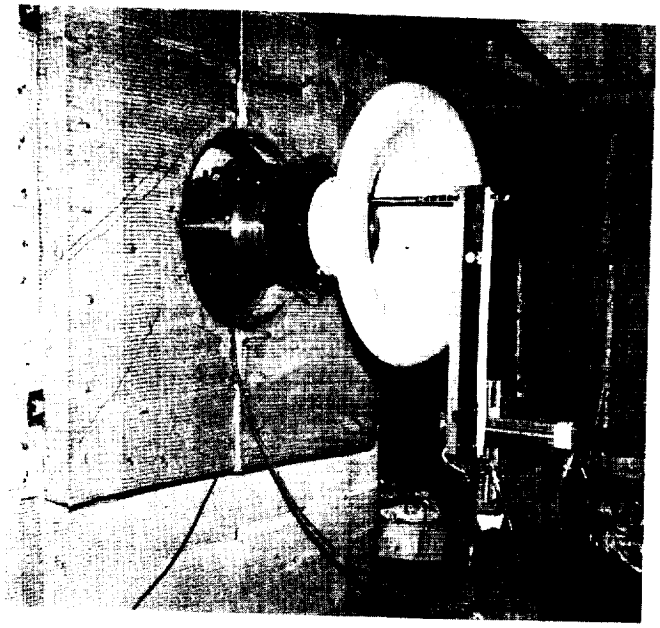

Figure XIV-6

EFFECT OF RADIAL AND AXIAL LOCATION ON FAN TONE LEVEL

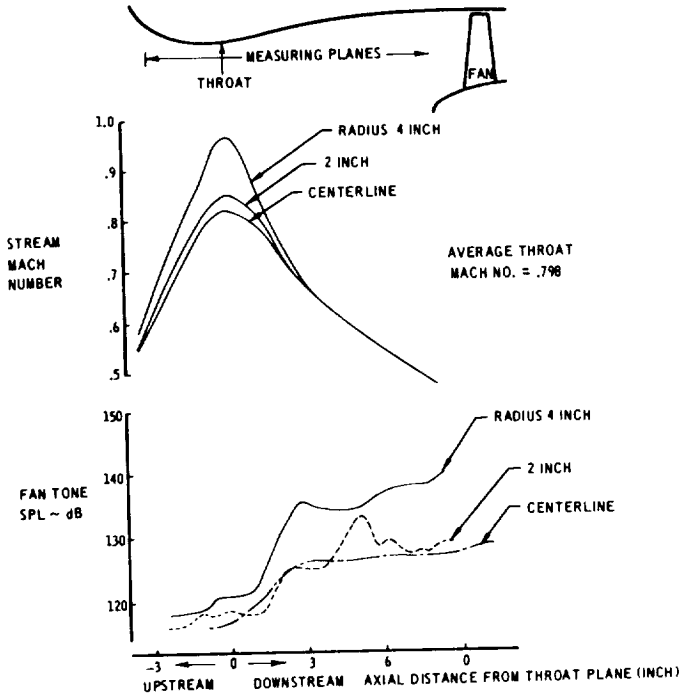

Figure XIV-7

NOISE SPECTRUM COMPARISON BEHIND A SONIC INLET

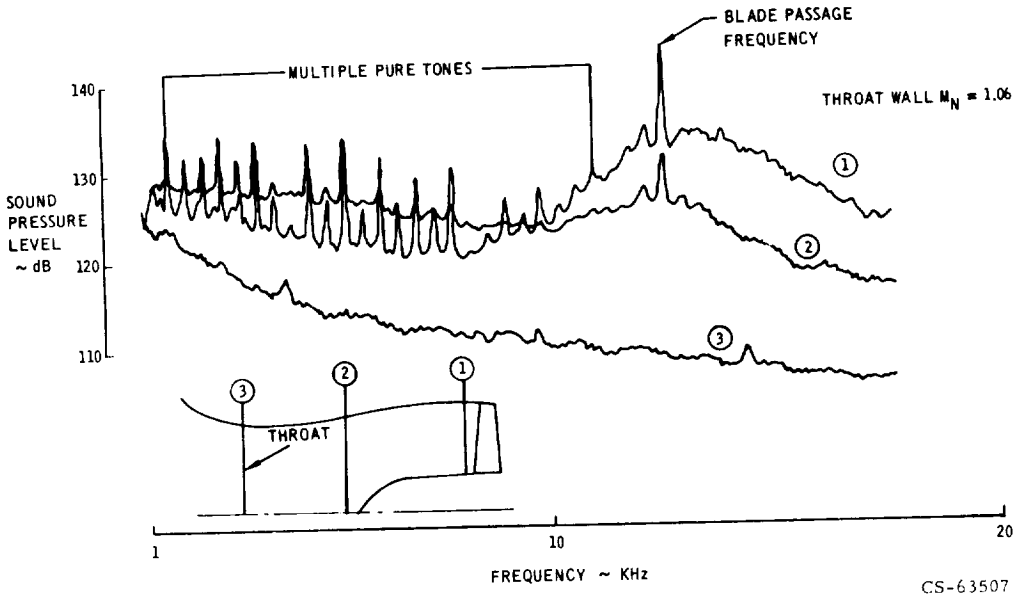

Figure XIV-8

NOISE SPECTRUM COMPARISON AHEAD OF A SONIC INLET

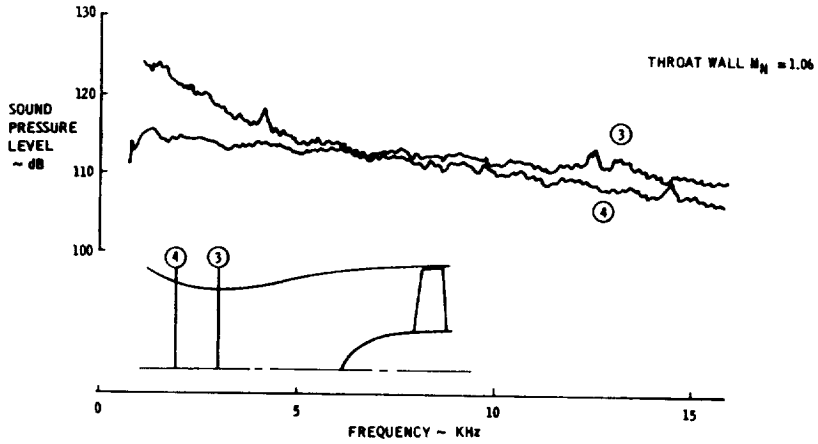

Figure XIV-9

SONIC INLET PERFORMANCE - APPROACH

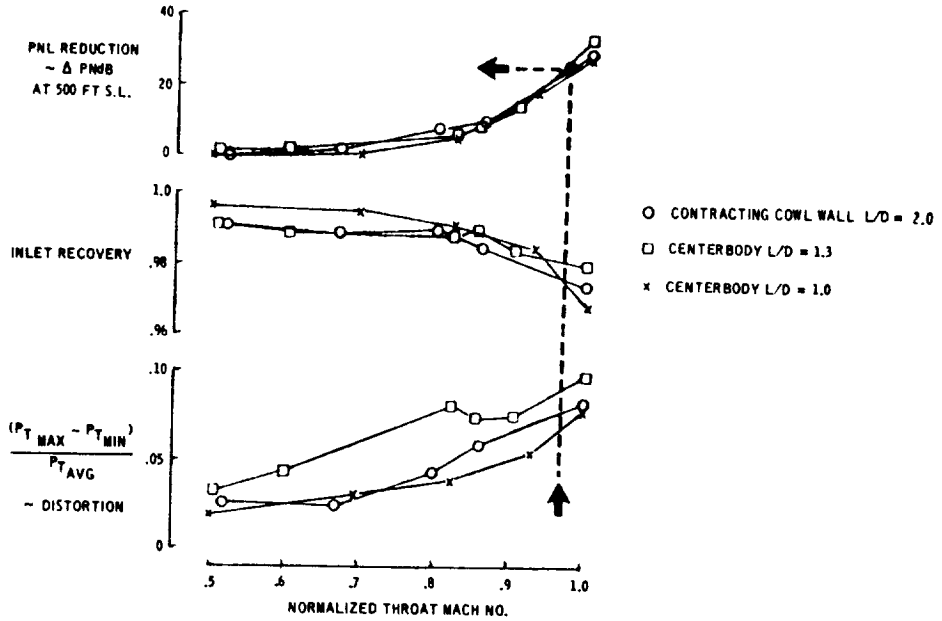

Figure XIV-10

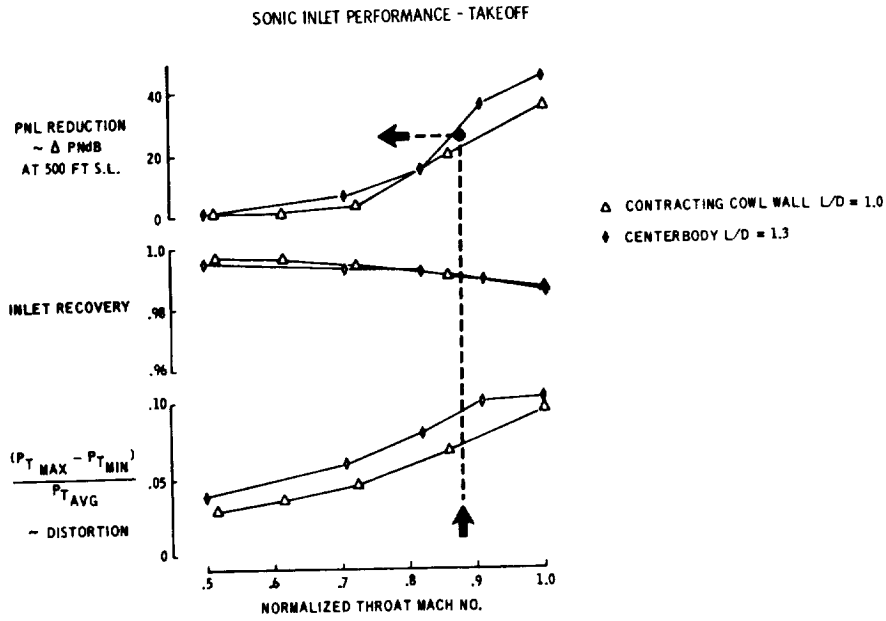

Figure XIV-11

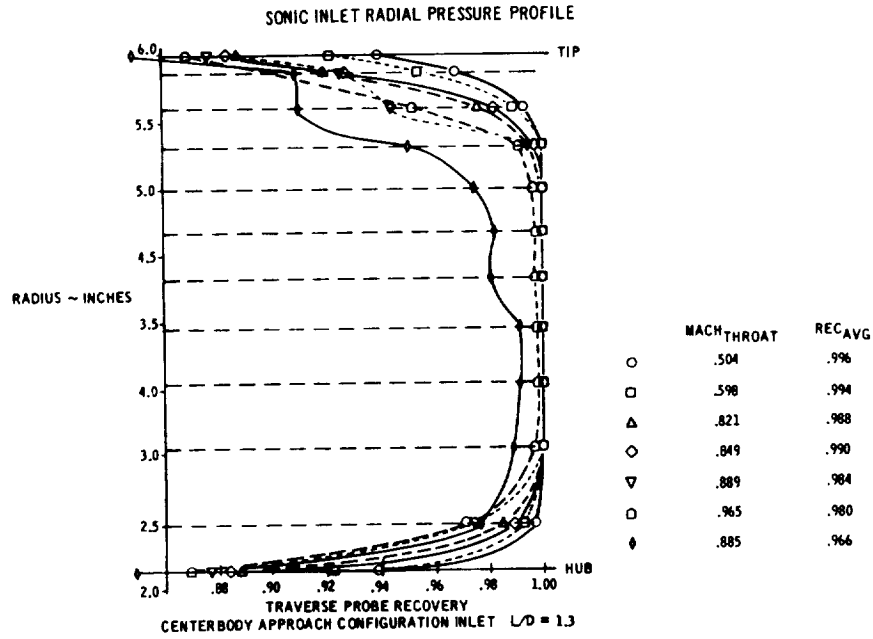

Figure XIV-12

PERFORMANCE COMPARISON OF SINGLE AND MULTIPASSAGE SONIC INLETS - APPROACH

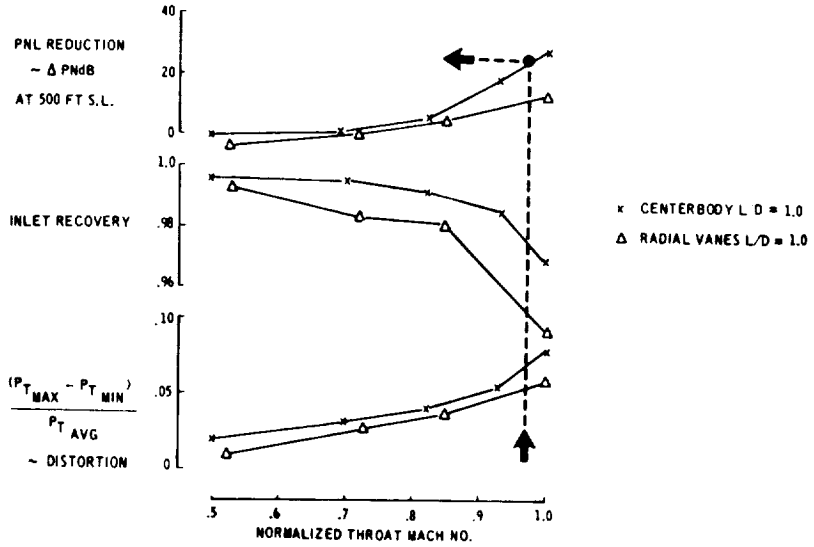

Figure XIV-13

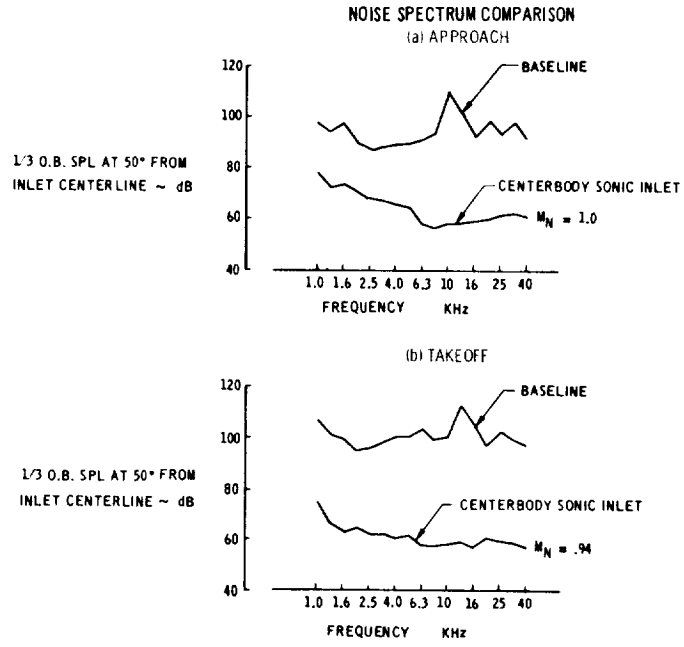

Figure XIV-14

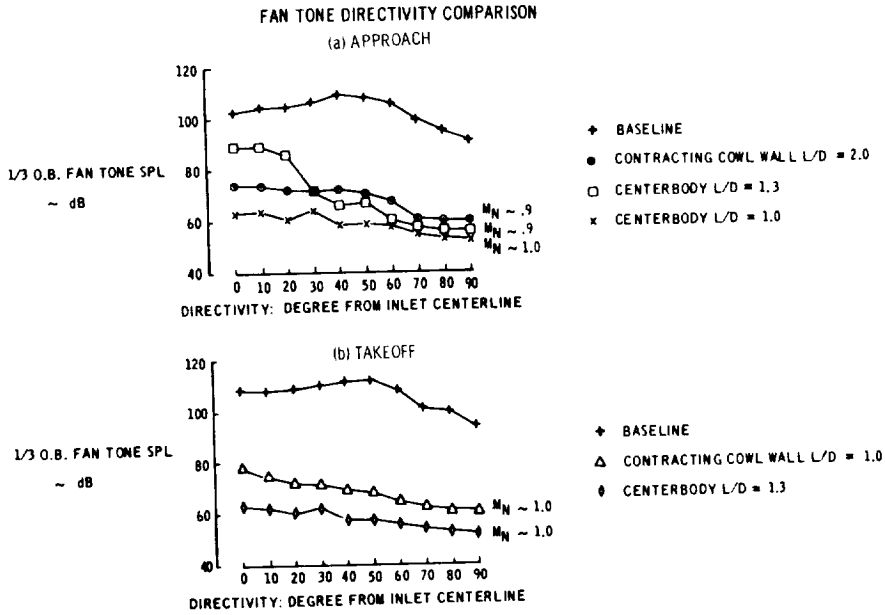

Figure XIV-15